Analytical and numerical investigation of two-phase flows

Dissertation
zur Erlangung des akademischen Grades

doctor rerum naturalium
(Dr. rer. nat.)

genehmigt durch die Fakultät für Mathematik
der Otto-von-Guericke Universität Magdeburg

von **Dipl.-Math. Nikolai Andrianov**
geb. am 20. April 1974 in Leningrad, Rußland

Gutachter:
Prof. Dr. Gerald Warnecke
Prof. Dr. Rémi Abgrall
Prof. Dr. Richard Saurel

Abstract

We consider a generic homogenized model of two-phase flows, obtained by averaging of balance laws for single phases. The resulting system of equations is non-strictly hyperbolic and non-conservative, i.e. it cannot be written in divergence form. This poses serious difficulties for the theoretical investigation of this system, as well as for its numerical solution.

We use a physically motivated principle in order to obtain a discretization of the non-conservative terms in the generic model and propose a numerical method on its basis. We show its accuracy and robustness on a number of test problems, and through the comparison with experimental data.

Further, we study several submodels of the generic model, characterized by the different choice of the interface parameters. In particular, we consider the model for a deflagration-to-detonation transition (DDT) in gas-permeable, reactive granular materials. For the homogeneous part of the model, we study a simple initial-value problem, the Riemann problem. We note that the non-conservative terms act only along one wave in the solution to the Riemann problem. This alows us to define a weak solution to the Riemann problem as a composition of weak solutions to conservation laws in sectors. Then, we give a physical interpretation to the situations when some waves in the solution to the Riemann problem coincide. Also, we construct the exact solution to Riemann problems and implement in a software package. With its help, we propose a number of test problems, which are intended to assess the perfomance of numerical methods for a certain type of non-conservative systems.

It appears that the solution across one wave in the Riemann problem is not unique. To deal with this, we adopt a physically motivated criterion, the evolutionarity condition. We argue that the well-known discontinuities arising in the solution of conservation laws must be evolutionary. For the classical case of strictly hyperbolic conservation laws, we show that the usual conditions on these discontinuities are equivalent to the evolutionarity criterion.

Under certain assumptions, the generic model of two-phase flows reveals the well-known Euler equations in a duct of variable cross-section. Since this system is much simpler than the generic model, its study provides deeper insight into the structure of the generic model. For the Euler equations in a duct, we show that the solution to the Riemann problem is not unique. We study the conditions, which lead to the non-uniqueness, as well as the conditions for a unique solution. In order to decide, which solution is physically relevant, we carry out 2D computations in a duct of corresponding geometry. Then, we compare the 1D solution to the Riemann problem with the averaged 2D computations. It appears that the 1D solution, picked out by the 2D computations, satisfies a kind of entropy rate admissibility criterion.

The system of the Euler equations in a duct belongs to the class of resonant non-strictly hyperbolic systems. Such systems have been studied in the literature, and it is known that one wave in the solution to the Riemann problem is not unique. To deal with it, an admissibility criterion has been proposed. We show that this criterion is actually a particular case of the evolutionarity criterion.

Finally, we solve the Riemann problem for the Euler equations in a duct exactly and propose a Godunov-type method on its basis. It employs the idea that the non-conservative terms act only along cell boundaries, so we are left with a conservation law inside a cell. The numerical experiments show excellent accuracy of the scheme.

Zusammenfassung

Wir betrachten das generische homogenisierte Modell für Zweiphasenströmungen. Dieses Modell ist hergeleitet durch die Mittelung der Bilanzgleichungen für die einzelne Phasen. Das entsprechende Gleichungssystem ist nicht-strikt hyperbolisch und nicht-konservativ, d.h. es ist nicht darstellbar in Divergenzform. Dies führt zu Schwierigkeiten sowohl bei der mathematischen Untersuchung, als auch für die numerische Lösung.

Wir benutzen ein physikalisch motiviertes Prinzip zum Gewinnen einer Diskretisierung von nicht-konservativen Termen, und schlagen ein numerisches Verfahren aufgrund dieser Diskretisierung vor. Wir beweisen die Genauigkeit und Robustheit des Verfahrens durch Vergleich mit einigen Test-Problemen und experimentellen Untersuchungen.

Weiterhin, untersuchen wir einige Variationen des generischen Modells, die man durch gewisse Ansätze für die Grenzfläche-Parameter bestimmt. Insbesondere, betrachten wir ein Modell für den Deflagration-zur-Detonation-Übergang (DDT) in gasdurchlässigen, reaktiven Stoffe. Für den homogenen Teil des Modells, untersuchen wir ein einfaches Anfangswertproblem, das Riemann-Problem. Wir merken, daß die nicht-konservativen Terme nur entlang einer Welle in der Lösung des Riemann-Problems wirken. Dies ermöglicht es uns, die schwache Lösung des Riemann-Rroblems als eine Zusammensetzung der schwachen Lösungen für Erhaltungsgleichungen in Sektoren zu definieren. Wir geben die physikalische Deutung für die Situationen, in denen einige Wellen in der Lösung des Riemann-Problems miteinander übereinstimmen. Außerdem, konstruieren wir exakte Lösungen des Riemann-Problems und setzen sie in Form eines Programmpakets um. Mit Hilfe von diesem Programmpaket schlagen wir eine Reihe von Test-Problemen vor, die zur Bewertung von numerischen Methoden für bestimmte nicht-konservative Systeme dienen können.

Es kommt vor, daß die Lösung über eine Welle im Riemann-Problem nicht eindeutig ist. Um dieses Problem zu bewältigen, nehmen wir ein physikalisches Kriterium, die evolutionäre Bedingung, zu Hilfe. Wir argumentieren, daß die wohlbekannte Unstetigkeiten von Erhaltungsgleichungen evolutionär seien sollen. Für den klassischen Fall von strikt hyperbolischen Systemen zeigen wir die Äquivalenz zwischen den üblichen Beziehungen für diese Unstetigkeiten und der evolutionären Beziehung.

Unter bestimmten Annahmen, lässt sich das generische Modell für Zweiphasenströmungen zu den wohlbekannten Euler-Gleichungen in einem Kanal mit variablem Durchschnitt reduzieren. Da dieses System viel einfacher als das generische Modell ist, kann man durch seine Untersuchung die Struktur des generischen Modells besser verstehen. Für die Euler-Gleichungen in einem Kanal stellen wir fest, daß die Lösung des Riemann-Problems nicht eindeutig lösbar ist. Wir untersuchen die Bedingungen, die zu dieser Nichteindeutigkeit führen, und die Voraussetzungen für eine eindeutige Lösung. Um eine Entscheidung zu treffen, welche der Lösungen physikalisch relevant ist, führen wir 2D-Berechnungen in einem Kanal der entsprechenden Geometrie durch. Dann, vergleichen wir die 1D-Lösungen des Riemann-Problems mit gemittelten 2D-Lösung. Die 1D-Lösung, die auf diese Weise ausgewählt wird, genügt einer Art von Entropie-Raten-Zulässigkeits-Kriterium.

Zum Abschluß, lösen wir das Riemann-Problem für die Euler-Gleichungen in einem Kanal exakt und schlagen eine Methode vom Godunov-Typ aufgrund dieser Lösung vor. Die Methode beruht auf der Idee, daß die nicht-konservativen Terme nur entlang des Zellenrandes wirken. Deshalb hat man eine Erhaltungsgleichung innerhalb eine Zelle. Die numerische Experimente zeigen die ausgezeichnete Genauigkeit der Methode.

Acknowledgements

I am very grateful to my advisor Prof. Gerald Warnecke for providing me an interesting topic of research. I have enjoyed numerous discussions with him, which revealed beautiful and often unexpected relationships between seemingly completely different ideas.

I would like to express my sincere gratitude to Prof. Richard Saurel. A single A4 sheet of paper where he sketched the idea of a numerical method at CEM-RACS'2000 strongly influenced my further work. It was also the starting point for my interest in Riemann problems for non-conservative systems.

I am grateful to my present and former colleagues at IAN. My special thanks go to Dr. Matthias Kunik for his interest in my work and for numerous critical comments on it.

This work would be unthinkable without my family, which gives me an immense support and encouragement, no matter how far away we are from each other.

Contents

Chapter 1

Introduction

1.1 Overview

Two-phase flows which occur in nature can differ significantly in phase materials, flow configuration, and the scale of interactions. According to phase materials, the two-phase flows can be subdivided into three categories: Gas-liquid flows (bubbly flows, separated flows, gas-droplet flows), gas-solid flows (gas-particle flows, fluidized beds), liquid-solid flows (slurry flows, sediment transport).

The second classification is based on the interfacial structures of the phases, namely separated, transitional, and dispersed flows. It is far more complicated, since these structures can change continuously. Following Ishii [46], we can represent the variety of flows in Table 1.1.

All kinds of the two-phase flows are characterized by the *interface*, which separates the phases. The correct mathematical and numerical treatment of interfaces is the central problem in the theory of two-phase flows. Depending on the way we represent it, one can distinguish several big classes of models.

The most straight-forward approach would be to have the interface between the phases explicitly in the model. One can refer to this class of models as the *interface models*. Inside this class, the *sharp-interface models* treat the interface as a free boundary in the flow. This formulation results in a free-boundary problem. However, physically this interface is not a surface of discontinuity, but has certain thickness, usually of the order of few Ångströms (1 Å $= 10^{-10}$ m). In some situations one wishes to account for the internal structure of the interface, e.g. when the physical phenomena have a length scale comparable with the thickness of the interfacial region, or when considering flows involving large interface deformations (breakup of fluid jets, merging of bubbles). These are the situations when the *diffuse-interface models* come into play. For both models one has separate regions occupied by one phase only. There we are left with the single-phase flow equations (Euler or Navier-Stokes). For compressible flows, the system of equations is closed by appropriate *equations of state* (EOS). The phase
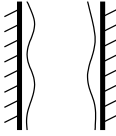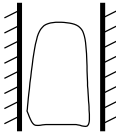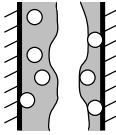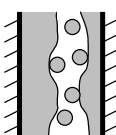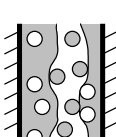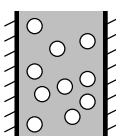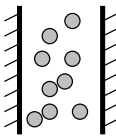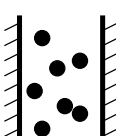
Class	Typical regimes	Geometry	Configuration	Examples
Separated flows	Film flow		• Liquid film in gas • Gas film in liquid	• Film cooling • Film boiling
	Annular flow		• Liquid core and gas film • Gas core and liquid film	• Film boiling • Condensers
	Jet flow		• Liquid jet in gas • Gas jet in liquid	• Atomization • Jet condenser
Transitional flows	Slug flow		• Liquid film in gas • Gas film in liquid	• Film cooling • Film boiling
	Bubbly annular flow		• Gas bubbles in liquid with gas core	• Evaporators with wall nucleation
	Droplet annular flow		• Gas core with droplets and liquid film	• Steam generator
	Bubbly droplet annular flow		• Gas core with droplets and liquid film with gas bubbles	• Nuclear reactor channel
Dispersed flows	Bubbly flow		• Gas bubbles in liquid	• Chemical reactors
	Droplet flow		• Liquid droplets in gas	• Spray cooling
	Particulate flow		• Solid particles in gas or liquid	• Transportation of wheat

Table 1.1. Classification of two-phase flows according to Ishii [46].

transition can be incorporated directly into the EOS, or be described by corresponding source terms. Since it is not our goal to give a complete description of different interface models here, we refer to more general reviews of interfacial fluid flows by Scardovelli and Zaleski [77], Tryggvason *et al.* [92], Hou *et al.* [43], Osher and Fedkiw [70], Abgrall and Karni [2], Anderson *et al.* [4].

Another class of two-phase models consists of the Lagrangian models for dispersed flows (droplets, bubbles, or particles). Here one usually has the Euler or Navier-Stokes equations for the carrier phase, augmented by the Lagrangian equations describing the position, velocity, temperature, and mass of single particles. The phase transition (evaporation or condensation) is described by the source terms on the right-hand side of these Lagrangian equations. See e.g. Crowe, Sommerfeld, and Tsuji [23] for an extensive review.

Often the detailed knowledge of the positions of phase interfaces is not necessary, or it is too expensive to get it computationally. In particular, this applies to the dispersed flows with a large number of droplets, bubbles, or particles. Then, the so-called *homogenized* or *averaged mixture models* are the better alternative to the interface methods described above. In this thesis, we will concern ourselves exclusively with this kind of models. The system of governing equations for such models is obtained by volume and time averaging of the single phase equations. This approach dates back to the works of Ishii [46] and Nigmatulin [69] in the mid-70s. Since then, much has been done for a better understanding of the system of governing equations, see e.g. [28, 83].

Nowadays, the more or less established model includes the two continuity, two momentum, and two energy equations for both phases. The averaging of the single phase equations results in additional terms, which describe the interaction between the phases. These are the mass transfer terms for the continuity equations, the momentum exchange terms for the momentum equations, and the energy exchange terms for the energy equations. The exact expressions for the transfer terms are usually unknown and one has to use some additional considerations (experimental data, simplified models etc.) to formulate them. All in all, the resulting system looks similar to the two sets of the single phase equations, coupled by the transfer terms. Note that at each point of the physical domain the presence of both phases is allowed: We are not restricted to interface problems. The derivation of this model was carried out by many researchers. We mention here the works of Lahey and Drew [54], Crowe, Sommerfeld, and Tsuji [23], Drew and Passman [28].

In what follows, we will refer this model to as the *generic model* of two-phase flows. Note that the system of governing equations for it is underdetermined: We need some assumptions for the phase interactions terms. Using different assumptions for the these terms, we arrive to different *submodels* of the generic model. In this thesis, we will deal with three such submodels:

(i) The Saurel–Abgrall (SA) model for multiphase mixtures [75].

(ii) The Baer–Nunziato (BN) model for the deflagration-to-detonation transition (DDT) in gas-permeable, reactive granular materials [10].

(iii) The Euler equations in a duct of varying cross-section, derivation in e.g. Zucrow and Hoffman [97].

Note that although physically, the last submodel has actually nothing to do with two-phase flows, mathematically the structure of the system of governing equations is the same as for the generic model. Considering the Euler equations in a duct as a submodel of the generic model of two-phase flows helps greatly to gain understanding of the generic model.

The relationships between the submodels and the generic model are as follows. The results for the generic model apply for all its submodels. The SA and BN models are equivalent only for the case of pure phases or a mixture in velocity and pressure equilibrium. The Euler equations in a duct is a submodel of the BN model. In this thesis, we will intensively use this hierarchy of the models.

1.2   Results

In this thesis, we are concerned with analytical and numerical investigation of several systems of equations, arising in the theory of two-phase flows. The main difficulty in their investigation lies in the fact that they are *non-conservative*, i.e. cannot be written in divergence form. Therefore, the results of the theory of *conservation laws*, developed in past decades, cannot be largely used here. This applies equally to the mathematical and numerical analysis of non-conservative systems.

We start with the generic model of two-phase flows and propose a method for its numerical solution, provided we are given some assumptions for the phase interaction terms. This method is a combination of two schemes, widely used for conservation laws, namely the Godunov method [39], and the Roe method [73]. We solve Riemann problems at cell interfaces as in Roe's method, and calculate the numerical flux function as in Godunov's method. This idea has been proposed by Gallouët and Masella [33] in context of conservation laws. To extend the method to non-conservative systems we follow the approach of Saurel and Abgrall [75]. They use a physically motivated criterion due to Abgrall [1], in order to get a discretization for non-conservative terms. However, the approximate Riemann solver used in [75] is too dissipative, which results in poor accuracy of the method. With the approximate Riemann solver of Gallouët and Masella [33], we avoid this drawback, and get much more transparent discretization of non-conservative terms. Numerous numerical experiments show better resolution of the flow, compared to the method of [75]. Also, the method is simple in use and robust.

Next, we turn to investigate the mathematical properties of the submodels of the generic model. For the SA model [75], we establish that the system of governing equations is non-strictly hyperbolic. However, further analysis appears to be very complicated. This results from the fact that the assumptions for the phase interaction terms are quite sophisticated. On the other hand, these assumptions allow for solution of a wide range of physical two-phase problems, see [75].

For the next submodel, the BN model [10], the characteristic analysis was carried out by Embid and Baer [31]. They show that the system of governing equation is also non-strictly hyperbolic. In order to get deeper understanding of this system, we study a simple initial-value problem for it, the *Riemann problem.* We notice that the solution across one wave in the Riemann problem is not unique. To pick out the physically admissible wave, we adopt a fundamental principle of hyperbolic systems arising from continuum physics, the *evolutionarity criterion.* It states that in order for a discontinuity in a physical flow to be determined, the number of unknowns at this discontinuity should be equal to the number of conditions on them. From the standpoint of this criterion, we discuss the classical discontinuities of conservation laws, namely the Lax shock [57] and the contact discontinuity.

Further, we present a procedure for constructing the exact solution to the Riemann problem, and implement it in an interactive software package CONSTRUCT [5]. Since the system of Euler equations in a duct of variable cross-section is a submodel of the BN model, we can use CONSTRUCT for this system as well. With CONSTRUCT, we are able to achieve two goals. Firstly, we propose a number of test cases which intend to assess the performance of numerical methods for non-conservative systems. Our idea is that interested researchers may try their methods on either the BN model [10], or the Euler equations in a duct, and compare the results with the exact solution, obtained with CONSTRUCT [5]. Secondly, this package is a convenient tool to study the properties of the Riemann solution.

Since the system of governing equiations for the BN model is non-strictly hyperbolic, the wave configurations for the Riemann problem can be quite complicated. We establish some properties of the Riemann solution, in particular when some of the waves coincide. Our numerical experiments show that numerical methods can have hard time for such configurations.

Next, we notice that in the special case of a Riemann problem, the system of (non-conservative) governing equations is equivalent to some system of conservation equations locally. This allows us to introduce a notion of a weak solution to the non-conservative Riemann problem, composed of local weak solutions to conservation equations. Although there exists a definition of a weak solution for general non-conservative systems due to Dal Maso, LeFloch, and Murat [26], our definition might be helpful e.g. for constructing efficient numerical schemes for the non-conservative systems of certain type.

To get deeper insight into the structure of the Riemann solution to the BN model, we study the Riemann problem for its submodel, the Euler equations in a duct of varying cross-section. This system belongs to the class of so-called *resonant systems* of hyperbolic balance laws. The Riemann problem for such systems was investigated by Isaacson and Temple [44]. They establish that the solution across one wave is not unique, and propose an admissibility criterion to pick out the relevant wave. We show that their criterion is a particular case of the evolutionarity criterion discussed above.

Analogously to the case of the BN model, we introduce a notion of a weak solution to the Riemann problem for the Euler equations in a duct. It appears that the solution to the Riemann problem for this system is not unique. Since the Euler equations in a duct can be formally obtained from the BN model, the same will be the case for the BN model as well.

The non-uniqueness of the Riemann solution is a consequence of the fact that the system of governing equations is non-strictly hyperbolic and non-conservative. Namely, for certain initial data, several *wave configurations*, i.e. the mutual positions of the waves in the Riemann solution, are possible. We study the structure of the Riemann solution, and point out the initial data which may lead to non-uniqueness. Also, we show that under certain conditions the solution to the Riemann problem in form of a certain configuration is unique.

To decide which solution is physically relevant, we carry out 2D calculations of the usual Euler equations in a duct of corresponding geometry. Then we compare the averaged 2D results with the 1D exact solution, obtained with CONSTRUCT. It appears that the 1D solution chosen in such way, satisfies a kind of the *entropy rate admissibility criterion*, proposed by Dafermos [24] for conservation laws.

Finally, we solve the Riemann problem for Euler equations in a duct exactly. The problem reduces to the solution of the nonlinear algebraic system of 6 equations. Using this exact Riemann solver, we present a Godunov-type method for the numerical solution of the Euler equations in a duct. Here we use the fact that the non-conservative terms act only along the boundaries of computational cells, and inside of a cell we have a conservation law. It is remarkable that it is a *conservative* method for the *non-conservative* system.

1.3   Outline

The contents of this thesis are organized as follows:

In Chapter 2 we present the mathematical formulation of the homogenized model for the two-phase flows. Further, we introduce several possible equations of state, which are often used for the thermodynamical closure of the problem. However, unlike in the classical theory of conservation laws, they are not enough to close the overall system of equations. We discuss a number of possible closure relations, which are widely used in the literature. Since the homogenized model

is obtained by averaging of the conservation equations for each phase, we present some basic facts from the theory of conservation laws. Then we carry out the mathematical analysis of the system of governing equations for the homogenized generic model, and its submodels.

In Chapter 3, we are concerned with the numerical solution of the generic two-phase model. First, along with some other methods, we introduce a finite volume method based on an approximate Riemann solver for the conservation laws. In this Riemann solver, we account for all waves in the solution of the local linearized Riemann problem, which ensures high accuracy. We extend the method for the generic non-conservative model by looking for a suitable discretization of the non-conservative terms. In doing so, we follow the universal principle that a moving contact discontinuity should be preserved. Posing of this constraint on the design of the scheme gives us the desired discretization. We solve several test problems and observe good resolution of the flow.

Chapter 4 is devoted to the analysis of the Riemann problem for the homogeneous Baer-Nunziato model [10]. Here, we first present the procedure of constructing the exact solution to this problem, and its implementation in the software package CONSTRUCT [5]. Using the exact solution, we construct several test cases, which are intended to assess the perfomance of numerical methods on the problems, typical for non-conservative systems. Then, we discuss the properties of one wave in the solution of the Riemann problem: The solid contact discontinuity. This wave is intrinsic to the two-phase model we consider and does not have a counterpart in single-phase flows; only across it, the volume fraction of the phases may change. It appears that the solution across the solid contact is non-unique. We propose that the admissible solid contact should be an evolutionary discontinuity. It appears that only due to the presence of this wave in the Riemann solution, we cannot define a weak solution in a way how it is done in the theory of conservation laws. However, we show that the system of (non-conservative) governing equations is equivalent to some system of conservation equations locally. This allows us to introduce a notion of a weak solution to the non-conservative Riemann problem, composed of local weak solutions to conservation equations.

In Chapter 5 we study the well-known system of single-phase Euler equations in a duct with variable cross-section. On the one hand, it can be viewed as a submodel of the BN model of two-phase flows, so the above analysis applies for this system as well. On the other side, the system of Euler equations in a duct belongs to the class of resonant systems of hyperbolic balance laws, studied by Isaacson and Temple [44, 45]. Analogously to the case of the BN model, the solution across one wave in the Riemann problem here is not unique. To pick out the single solution, Isaacson and Temple [44] proposed an admissibility criterion. We prove that this admissibility criterion is actually a particular case of the evolutionarity condition, introduced in Chapter 4.

It appears that the solution to the Riemann problem for the Euler equations

in a duct is in general not unique. We study different wave configurations and prove several uniqueness criteria. Further, we provide 2D computations of the Euler equations in a duct, and compare it with the exact 1D solutions. Then the 1D solutions, picked out by the 2D computations, possess higher entropy production than the other. This can be viewed as a kind od the entropy rate admissibility criterion due to Dafermos [24].

Finally, we describe a procedure for finding the exact solution to the Riemann problem and introduce a Godunov-type method for the numerical solution of the Euler equations in a duct with variable cross-section on its basis. To assess the perfomance of this method, we solve several test problems and compare the results with those of the method introduced in Chapter 3. For certain tests, e.g. with slow waves in the solution, the Godunov-type method behaves considerably better.

Parts of Chapters 3 to 4 have been published before. Chapter 3 has appeared as

- N. Andrianov, R. Saurel, and G. Warnecke, A simple method for compressible multiphase mixtures and interfaces, *Int. J. Numer. Meth. Fluids* **41**, 109-131 (2003).

Chapter 4 will appear as

- N. Andrianov and G. Warnecke, The Riemann problem for the Baer-Nunziato model of two-phase flows, submitted for publication, 2002. Also available as preprint at
  http://www.math.ntnu.no/conservation/2002/048.html.

A condensed form will appear as

- N. Andrianov, R. Saurel and G. Warnecke, The Riemann problem for a model of two-phase flows, to appear in *Proc. of 9th Int. Conf. on Hyperbolic Problems*, Pasadena, California, March 25-29, 2002.

A part of Chapter 5 will appear as

- N. Andrianov and G. Warnecke, On the solution to the Riemann problem for the compressible duct flow, submitted for publication, 2003. Also available as preprint at
  http://www.math.ntnu.no/conservation/2003/019.html.

Chapter 2

Mathematical modeling of the two-phase flows

2.1 Generic model

In this work, we consider only non-viscous flows without mass exchange, heat transfer and wall friction. Moreover, we restrict outselves to one-dimensional flow. Then, the generic model for the two-phase flow will have the following form

$$
\begin{aligned}
\frac{\partial \alpha_a \rho_a}{\partial t} + \frac{\partial \alpha_a \rho_a u_a}{\partial x} &= 0 \\
\frac{\partial \alpha_a \rho_a u_a}{\partial t} + \frac{\partial (\alpha_a \rho_a u_a^2 + \alpha_a p_a)}{\partial x} &= +P \frac{\partial \alpha_a}{\partial x} + \mathcal{M} \\
\frac{\partial \alpha_a \rho_a E_a}{\partial t} + \frac{\partial \alpha_a u_a (\rho_a E_a + p_a)}{\partial x} &= -P \frac{\partial \alpha_a}{\partial t} + \mathcal{E} \\
\frac{\partial \alpha_b \rho_b}{\partial t} + \frac{\partial \alpha_b \rho_b u_b}{\partial x} &= 0 \\
\frac{\partial \alpha_b \rho_b u_b}{\partial t} + \frac{\partial (\alpha_b \rho_b u_b^2 + \alpha_b p_b)}{\partial x} &= -P \frac{\partial \alpha_a}{\partial x} - \mathcal{M} \\
\frac{\partial \alpha_b \rho_b E_b}{\partial t} + \frac{\partial \alpha_b u_b (\rho_b E_b + p_b)}{\partial x} &= +P \frac{\partial \alpha_a}{\partial t} - \mathcal{E}.
\end{aligned}
\tag{2.1}
$$

For derivation, see e.g. Lahey and Drew [54], Crowe, Sommerfeld, and Tsuji [23], Drew and Passman [28]. Here, the two phases are denoted with subscripts a and b, respectively. The notations are classical: ρ_k is the density, u_k the velocity, p_k the pressure, $E_k = e_k + \frac{u^2}{2}$ the total specific energy, and α_k the volume fraction of the phase $k = a, b$. The terms $\mathcal{M}$ and $\mathcal{E}$ express the interchange of momentum and energy between the phases. Note that for the case $\alpha_a = $ const, the system decouples into two sets of Euler equations for the phases a and b. For the mixture, one can get the balance equations by summing the corresponding single-phase equations.

2.2   Closure problem

There are 11 independent variables in the system (2.1),

$$\alpha_k, \rho_k, u_k, p_k, E_k, P, \quad k = a, b.$$

The source terms of the system, i.e. the non-differential terms on the right-hand side of (2.1), are the functions of these variables. Note that there are only 6 equations in the system (2.1). Consequently, one needs to augment the system with 5 additional equations.

One of these is obviously the *saturation constraint*

$$\alpha_a + \alpha_b = 1.$$

Another two are the equations of state (EOS) for the each phase $k = a, b$. We will consider several EOS in Section 2.2.1.

Now, one has to either add some other equations, or to reduce the number of unknowns. Below we will discuss both methods.

2.2.1   Equation of state

A system in thermodynamical equilibrium is completely described by two physical variables. One popular choice for them is the pressure p and the density ρ. One can relate these variables to the temperature via the *thermal equation of state*

$$T = T(p, \rho) \tag{2.2}$$

and the internal energy via the *caloric equation of state*

$$e = e(p, \rho). \tag{2.3}$$

Since the temperature T does not explicitly appear in the system (2.1), we will be interested only in the second one. For more information on the foundations of thermodynamics and different EOS, we refer to [22, 38, 89].

Ideal gas EOS

For the calorically ideal gas the relation (2.3) has the simple form

$$e = \frac{p}{\rho(\gamma - 1)}, \tag{2.4}$$

where $\gamma > 0$ is a constant that depends on the particular gas under consideration. For the ideal gas, the local speed of sound is

$$c = \sqrt{\left.\frac{\partial p}{\partial \rho}\right|_{\eta=\text{const}}} = \sqrt{\frac{\gamma p}{\rho}},$$

and the isentrope $\eta = \text{const}$ is

$$\eta = \frac{p}{\rho^\gamma} = \text{const.}$$

Tait's EOS

This equation of state is used to describe a liquid, in particular water. Unlike gases, in liquids the pressure may be considered as a function of density alone,

$$p = A \left(\frac{\rho}{\rho_0} \right)^\gamma - B,$$

where A, B, γ are constants, specific for the particular liquid, and ρ_0 is the reference density. For water,

$$A, B \approx 3 \cdot 10^8 \text{ Pa}, \quad \gamma = 7, \quad \rho_0 = 1000 \text{ kg/m}^3.$$

The speed of sound is

$$c = \sqrt{\frac{dp}{d\rho}} = \sqrt{\frac{\gamma(p+B)}{\rho}}.$$

Stiffened gas EOS

This equation of state is based on the stiffened equation of Grüneisen type, see Menikoff and Plohr [66]. It has the form

$$e = \frac{p + \gamma \pi}{\rho(\gamma - 1)}, \tag{2.5}$$

where $\gamma, \pi > 0$ are material specific constants. Note that (2.5) reduces to the ideal gas EOS (2.4) if $\pi = 0$. Modifying γ, π, one is able to describe a wide range of materials, see e.g. Saurel and Abgrall [75] for some examples. The expressions for the sound speed c and the isentrope $\eta = $ const are obtained from the second law of thermodynamics,

$$\begin{aligned}
0 = T d\eta &= de + pd\left(\frac{1}{\rho}\right) = \left.\frac{\partial e}{\partial p}\right|_\rho dp + \left.\frac{\partial e}{\partial \rho}\right|_p d\rho - \frac{p}{\rho^2} d\rho \\
&= \frac{dp}{\rho(\gamma - 1)} - \frac{\gamma(p + \pi)}{\rho^2(\gamma - 1)} d\rho.
\end{aligned} \tag{2.6}$$

From (2.6), we obtain the sound speed

$$c = \sqrt{\left.\frac{\partial p}{\partial \rho}\right|_{\eta = \text{const}}} = \sqrt{\frac{\gamma(p + \pi)}{\rho}}.$$

Integrating (2.6), we get the expression for the isentrope,

$$\eta = \text{const} \iff \frac{p + \pi}{\rho^\gamma} = \text{const}.$$

Everywhere in this thesis, we will use exclusively the stiffened gas EOS (2.5) for the thermodynamical closure of the system (2.1).

2.2.2   Different approaches towards achieving closure

Equal pressure model

One of the most common procedures to close the system (2.1) is to postulate a local pressure equilibrium between the phases, i.e. to set

$$P := p_a := p_b = p$$

in the system (2.1). Then the number of unknowns (13) is equal to the number of equations, and the system is closed. However, it suffers from a serious mathematical difficulty: It appears to be ill-posed, see Stewart and Wendroff [83]. It has several consequences:

- The model does not correctly describe pressure wave propagation phenomena

- Instabilities may grow in the numerical solution

- Numerical techniques which make explicit use of the hyperbolic character of the flow equations cannot be used.

There are two distinct ways to address these problems. One approach is to introduce a numerical viscosity into the numerical algorithm, to dampen out the instabilities. This has been used in a number of industrial two-phase codes, e.g. TRAC [91], RELAP5 [79]. The other method is to try to gain back hyperbolicity in the system (2.1). In the case when the two phases are gas and liquid, one can consider so-called virtual mass force, which is due to acceleration of the gaseous phase relative to the liquid phase. Then, the inclusion of this term into the system (2.1) results in hyperbolicity. In the literature, different expressions for this force can be found, see e.g. [13, 53, 79, 82, 88, 91].

Evolutionary equation

A more physical way of closing the system (2.1) would be not to cancel some variables there, but to add an additional equation. There are a number of authors, who proposed to augment the system with an evolutionary equation for some physical variable.

Already Ishii, who wrote his classical text [46] in 1975, closed the system of governing equations in such a way [46, p. 187]:

> Finally we should have a constitutive equation for the surface area concetration $1/L_s$. In general it should have the form of the balance equation
>
> $$\frac{\partial}{\partial t}\left(\frac{1}{L_s}\right) + \nabla \cdot \left(\frac{1}{L_s}\mathbf{v}_i\right) = \Phi_L,$$
>
> where Φ_L is the source term [..], and $\mathbf{v}_i$ is the average interface velocity.
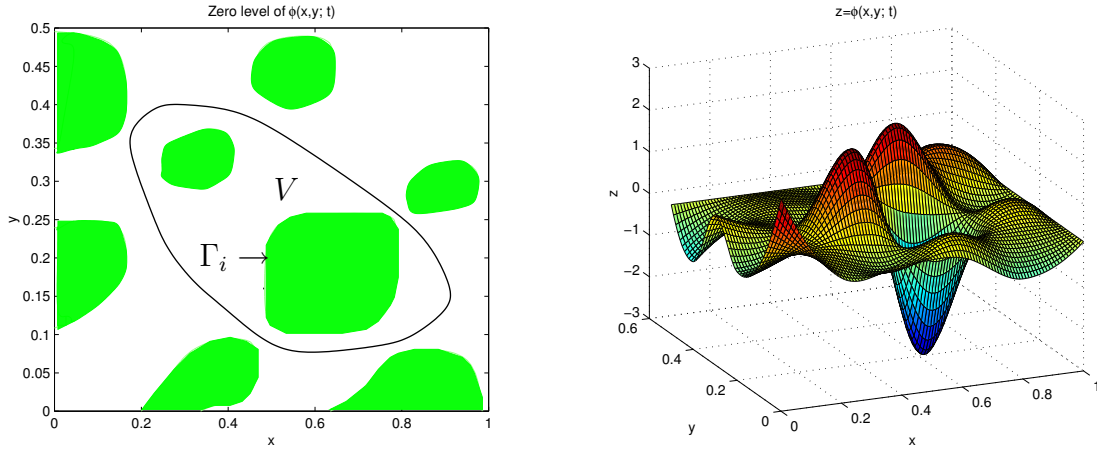
Fig. 2.1. Left: In the Lagrangian volume V, the propagating interfaces Γ_i separate the phase a (shaded) and phase b. Right: The corresponding level set function $z = \phi(x, y; t)$.

Unfortunately, no theoretical justification of this statement is given.

In their paper [10], Baer and Nunziato introduce a transport equation [10, p. 867]:

> Here we write an additional evolutionary equation for the volume fraction of each constituent a:
> $$\frac{\partial \alpha_a}{\partial t} + v_a \frac{\partial \alpha_a}{\partial x} = f_a.$$
> These equations permit us to account for the compressibility of constituents. [Here v_a is the velocity of phase a, f_a is the source term.]

Again, no rigorous derivation is given.

Motivated by the uncertainty mentioned above, we propose here yet another derivation of the evolutionary equation for the volume fraction. Consider the control volume V, filled with phases a and b. Microscopically, we can always separate these phases. Assume that at each time instant t, the phase a is separated from the phase b by the interface

$$\Gamma(t) = \bigcup_{i=1}^{N} \Gamma_i, \tag{2.7}$$

see Fig. 2.1. In the course of time, the interfaces Γ_i can change topology, break or merge. To describe the motion of the interfaces Γ_i, the level set approach [80] may be used. For simplicity, we use here the 2D description, the 3D version is obtained without any significant changes.

Consider a function

$$z = \phi(x, y; t), \qquad \phi : \mathbb{R}^2 \times \mathbb{R} \to \mathbb{R}$$

such that the zero level of $\phi(x, y; t)$ coincides with the interface (2.7), i.e.,

$$\Gamma(t) = \{(x, y) : \phi(x, y; t) = 0\}.$$

Consider a particular point (x, y) on the curve $\Gamma(t)$. Then, by definition of $\Gamma(t)$,

$$\phi(x(t), y(t); t) = 0.$$

By the chain rule,

$$\frac{\partial \phi}{\partial t} + \nabla \phi \cdot \mathbf{x}'(t) = 0, \qquad \mathbf{x} = (x, y). \tag{2.8}$$

Here $\mathbf{x}'(t)$ is the velocity of the point $(x, y) \in \Gamma(t)$, i.e. it is the velocity of the interface,

$$\mathbf{v}_i = \mathbf{x}'(t).$$

Following Sethian [80], the initial data for (2.8) are specified as follows. Given the initial position of the interface

$$\Gamma(t = 0) = \{(x, y) : \phi(x, y; t = 0) = 0\},$$

we define

$$\phi(x, y; t = 0) := \pm d, \tag{2.9}$$

where d is the distance from (x, y) to $\Gamma(t = 0)$ and the plus(minus) sign is chosen if the point (x, y) is outside(inside) the initial curve $\Gamma(t = 0)$.

For each t, the graph of the solution $\phi(x, y; t)$ of the differential equation (2.8) is a surface in $\mathbb{R}^3$. The temporal evolution of the interface $\Gamma(t)$ is then given by the zero level of $\phi(x, y; t)$ at each time instant t.

There are several difficulties concerning the application of the level set method for the description of the propagation of the interfaces.

- The interface velocity $\mathbf{v}_i$ is in general a function of the other flow variables, e.g. phase velocities, and cannot assumed to be given.

- The solution of (2.8) is in general not differentiable and a weak solution must be constructed to continue the solution. For certain $\mathbf{v}_i$, the equation (2.8) is a Hamilton-Jacobi equation. The notion of a weak solution for the Hamilton-Jacobi equations was introduced by Crandall and Lions [20], see also Crandall, Evans, and Lions [21].

- For given $\mathbf{v}_i$, the solution of the problem (2.8)-(2.9) with multiple interfaces Γ_i is a complicated task, see Sethian [80].

Fortunately, we do not have to solve this complicated problem on the macroscopic level, since we are interested only in the change of the local *area* (*volume* in 3D case) of each phase in the course of time. Consider again Fig. 2.1. Let V_k be the area of the phase k, $k = a, b$, and V the area of the control volume. Let now V be a *Lagrangian* volume, such that there is no flow of area of the phase k, $k = a, b$ through its boundary. Denote the speed of V by $\mathbf{U}$. Then, a change of area of the phases will occur only due to production(annihilation) inside of V. Note that although V and V_k will change in time, the relation

$$V_a + V_b = V$$

will always hold. Consequently,

$$\alpha_a + \alpha_b = 1, \quad \alpha_k = \frac{V_k}{V}, \quad k = a, b,$$

where α_k is the volume fraction of the phase k.

Let us introduce the substantial derivative D/Dt, following the Lagrangian volume V,

$$\frac{D}{Dt} = \frac{\partial}{\partial t} + \mathbf{U} \cdot \nabla. \tag{2.10}$$

The time rate of change of α_k in the Lagrangian volume V is

$$\frac{D\alpha_k}{Dt} = \mathcal{S}_k, \tag{2.11}$$

where $\mathcal{S}_k$ is the production rate of the volume fraction of the phase k. Obviously,

$$\mathcal{S}_a = -\mathcal{S}_b.$$

Combining (2.10) and (2.11), we get the evolution equation for the volume fraction of the phase k,

$$\frac{\partial \alpha_k}{\partial t} + \mathbf{U} \cdot \nabla \alpha_k = \mathcal{S}_k. \tag{2.12}$$

We use the 1D version of the equation (2.12) to augment the system of governing

equations for the generic model (2.1) as follows,

$$
\begin{aligned}
\frac{\partial \alpha_a}{\partial t} + U\frac{\partial \alpha_a}{\partial x} &= \mathcal{S}_a \\
\frac{\partial \alpha_a \rho_a}{\partial t} + \frac{\partial \alpha_a \rho_a u_a}{\partial x} &= 0 \\
\frac{\partial \alpha_a \rho_a u_a}{\partial t} + \frac{\partial (\alpha_a \rho_a u_a^2 + \alpha_a p_a)}{\partial x} &= +P\frac{\partial \alpha_a}{\partial x} + \mathcal{M} \\
\frac{\partial \alpha_a \rho_a E_a}{\partial t} + \frac{\partial \alpha_a u_a(\rho_a E_a + p_a)}{\partial x} &= +PU\frac{\partial \alpha_a}{\partial x} + \mathcal{E} \\
\frac{\partial \alpha_b \rho_b}{\partial t} + \frac{\partial \alpha_b \rho_b u_b}{\partial x} &= 0 \\
\frac{\partial \alpha_b \rho_b u_b}{\partial t} + \frac{\partial (\alpha_b \rho_b u_b^2 + \alpha_b p_b)}{\partial x} &= -P\frac{\partial \alpha_a}{\partial x} - \mathcal{M} \\
\frac{\partial \alpha_b \rho_b E_b}{\partial t} + \frac{\partial \alpha_b u_b(\rho_b E_b + p_b)}{\partial x} &= -PU\frac{\partial \alpha_a}{\partial x} - \mathcal{E}.
\end{aligned}
\tag{2.13}
$$

To close this system, one needs expressions for the parameters U and P. It is common to call them *interface* velocity and pressure, although they are just some averaged velocity and pressure, see the derivation of the evolutionary equation above. Since the exact expressions for U and P are known only in particular cases, it is a usual practice to introduce some ansatz for them. Of course, for different types of flows, it should be different. In the rest of this chapter, we will introduce several *submodels* of the generic model (2.13). They are determined by the the choice of the interface parameters U and P. We order them by increasing simplicity of this choice.

2.3   Submodels of the generic model

2.3.1   Saurel–Abgrall model

In 1999, Saurel and Abgrall [75] have proposed the following ansatz,

$$
U = \frac{\alpha_a \rho_a u_a + \alpha_b \rho_b u_b}{\alpha_a \rho_a + \alpha_b \rho_b}, \qquad P = \alpha_a p_a + \alpha_b p_b.
\tag{2.14}
$$

The expression for U is the mass-averaged velocity of the phases. Since the model (2.13) assumes that in each point of the physical domain the velocities of the phases are in general different, there is a relaxation mechanism which drives the phase velocities to an equilibrium. Then, the expression for U in (2.14) corresponds to the instantaneous velocity relaxation, see [75] for details. The expression for P in (2.14) is the mixture pressure. Since U and P depend on the variables of both phases, they should approximate the averaged interface velocity and pressure, respectively. Indeed, this model is able to describe a wide range of

applications, e.g. shock waves in solid mixtures, cavitation in fluids, and interface resolution, see [76, 75]. In what follows, we will refer this model to as the *SA model*.

2.3.2 Baer–Nunziato model

One of the most established models in the theory of two-phase flows was proposed in 1986 by Baer and Nunziato [10], see also Bdzil *et al.* [12], Kapila *et al.* [47, 48], Embid and Baer [31]. It describes the flame spread and the deflagration-to-detonation transition (DDT) in gas-permeable, reactive granular materials. The two phases in this model are the solid grains and the hot gases, so when discussing this model, we will often call the phase *a solid*, and phase *b gas*. This model can be obtained formally from (2.13) by setting

$$U = u_a, \qquad P = p_b. \tag{2.15}$$

In what follows, we will refer to the model of Baer and Nunziato [10] as the *BN model*.

2.3.3 Euler equations in a duct of variable cross-section

If we set

$$P = p_b, \quad u_a = U = \mathcal{S} = \mathcal{M} = \mathcal{E} = 0 \tag{2.16}$$

in the governing equations for the generic model (2.13), we obtain the following system of equations

$$\frac{\partial \alpha_b}{\partial t} = 0 \tag{2.17a}$$

$$\frac{\partial \alpha_a p_a}{\partial x} = p_b \frac{\partial \alpha_a}{\partial x} \tag{2.17b}$$

$$\frac{\partial \alpha_b \rho_b}{\partial t} + \frac{\partial \alpha_b \rho_b u_b}{\partial x} = 0 \tag{2.17c}$$

$$\frac{\partial \alpha_b \rho_b u_b}{\partial t} + \frac{\partial (\alpha_b \rho_b u_b^2 + \alpha_b p_b)}{\partial x} = p_b \frac{\partial \alpha_b}{\partial x} \tag{2.17d}$$

$$\frac{\partial \alpha_b \rho_b E_b}{\partial t} + \frac{\partial \alpha_b u_b (\rho_b E_b + p_b)}{\partial x} = 0. \tag{2.17e}$$

Note that the continuity and energy equations for the phase *a* in the system (2.13) will give $\rho_a = \rho_a(x)$, $p_a = p_a(x)$ under assumptions (2.16).

On the other hand, consider the system of Euler equations in a duct of variable

cross section $A = A(x)$,

$$
\begin{aligned}
\frac{\partial A\rho}{\partial t} + \frac{\partial A\rho v}{\partial x} &= 0 \\
\frac{\partial A\rho v}{\partial t} + \frac{\partial A(\rho v^2 + p)}{\partial x} &= p\frac{\partial A}{\partial x} \\
\frac{\partial A\rho E}{\partial t} + \frac{\partial Av(\rho E + p)}{\partial x} &= 0.
\end{aligned}
\tag{2.18}
$$

For the derivation, see e.g. Zucrow and Hoffman [97]. Usually, the cross-section $A = A(x)$ is assumed to be given *a priori*. However, we can consider it as an additional unknown, and supply the trivial equation $A_t = 0$ for determining it. Thus, the system (2.18) becomes

$$
\begin{aligned}
\frac{\partial A}{\partial t} &= 0 \\
\frac{\partial A\rho}{\partial t} + \frac{\partial A\rho v}{\partial x} &= 0 \\
\frac{\partial A\rho v}{\partial t} + \frac{\partial A(\rho v^2 + p)}{\partial x} &= p\frac{\partial A}{\partial x} \\
\frac{\partial A\rho E}{\partial t} + \frac{\partial Av(\rho E + p)}{\partial x} &= 0.
\end{aligned}
\tag{2.19}
$$

We can easily make analogies between this system and the equations (2.17a), (2.17c), (2.17d), (2.17e), if we use the correspondence

$$
(\alpha_b, \rho_b, u_b, p_b, E_b) \longleftrightarrow (A, \rho, v, p, E),
\tag{2.20}
$$

i.e., the volume fraction of the phase b plays the role of the variable cross-section A, and the density, velocity, pressure, and energy of the phase b have the corresponding meanings for the gas flow in a duct of variable cross-section. The equation (2.17b) decouples from the rest of the system (2.17).

2.3.4 Hierarchy of the submodels

In the subsequent chapters, we will investigate the properties of the submodels introduced above. The goal of this section is to establish the subordinate relations between the submodels. Then, one will be able to transfer the results for one particular submodel to another.

SA model vs. BN model

For the SA model, the interface velocity U and pressure P are given by (2.14), and for the BN model by (2.15). The models are equivalent, if U and P are the same for both models, i.e.

$$
\frac{\alpha_a \rho_a u_a + \alpha_b \rho_b u_b}{\alpha_a \rho_a + \alpha_b \rho_b} = u_a, \qquad \alpha_a p_a + \alpha_b p_b = p_b.
$$
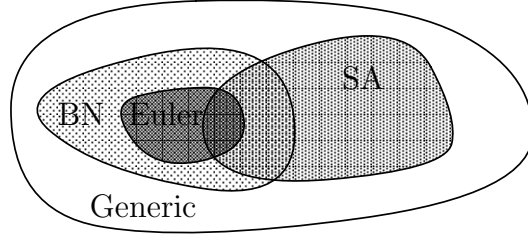
Fig. 2.2. Hierarchy of the submodels of the generic model. The BN model and the Euler in a duct are equivalent to the SA model only for the pure phases, or the mixture with equal velocities and pressures.

Since $\alpha_a + \alpha_b = 1$, these equations can be rewritten as follows,

$$\left\{ \begin{array}{l} \alpha_b \rho_b (u_a - u_b) = 0 \\ \alpha_a (p_a - p_b) = 0. \end{array} \right. \qquad (2.21)$$

The system (2.21) has three solutions, namely

1. Pure phase a: $\alpha_b = 0$, $\alpha_a = 1$, $p_a = p_b$, for all u_a, u_b.

2. Phase mixture in velocity and pressure equilibrium: $\alpha_b \neq 0$, $\alpha_a \neq 1$, $u_a = u_b$, $p_a = p_b$.

3. Pure phase b: $\alpha_a = 0$, $\alpha_b = 1$, $u_a = u_b$, for all p_a, p_b.

For the case of pure phase a or b, both SA and BN models, as well as the generic model (2.13), reduce to the usual single-phase Euler equations for the corresponding phase.

In case of the phase mixture in velocity and pressure equilibrium, i.e.

$$u_a = u_b =: u, \qquad p_a = p_b =: p,$$

the system of governing equations (2.13) becomes overdetermined. To obtain a closed system, we can sum the corresponding momentum and energy single-phase equations. Then the two-phase mixture model reads as

$$
\begin{aligned}
\frac{\partial \alpha_a}{\partial t} + u \frac{\partial \alpha_a}{\partial x} &= 0 \\
\frac{\partial \alpha_a \rho_a}{\partial t} + \frac{\partial \alpha_a \rho_a u}{\partial x} &= 0 \\
\frac{\partial \alpha_b \rho_b}{\partial t} + \frac{\partial \alpha_b \rho_b u}{\partial x} &= 0 \qquad (2.22) \\
\frac{\partial (\alpha_a \rho_a + \alpha_b \rho_b) u}{\partial t} + \frac{\partial ((\alpha_a \rho_a + \alpha_b \rho_b) u^2 + p)}{\partial x} &= 0 \\
\frac{\partial (\alpha_a \rho_a E_a + \alpha_b \rho_b E_b)}{\partial t} + \frac{\partial u(\alpha_a \rho_a E_a + \alpha_b \rho_b E_b + p)}{\partial x} &= 0.
\end{aligned}
$$

The system (2.22) describes a flow of two phases, which possess the same velocity u and pressure p. In particular, the equality of pressures and velocities is valid for a mixture of gases, unless they have significantly different molecular weights. Therefore, the models of this kind are widely used to this end, see e.g. Abgrall and Karni [2] for a review. However, in this thesis, we are concerned with two-phase flows with essentially different phase variables. Thus, the mixture model (2.22) will be not interesting for us.

To summarize, the SA and BN models are equivalent to each other only in trivial cases: Single-phase flow, described with the usual Euler equations, or the mixture model (2.22).

Euler in a duct vs. BN model

Exactly as in Section 2.3.3, we can show that under the assumptions (2.16) the BN model reduces to the Euler equations in a duct of variable cross-section. In other words, the Euler equations in a duct is the submodel of the BN model. Since the intersection of the BN and SA models is trivial, the same can be said about the intersection of the Euler in a duct and the SA model. In fact, this will be either a stationary single-phase flow, or the stationary mixture in pressure equilibrium. Graphically, we represent the hierarchy of the models in Fig. 2.2.

2.4   Basic facts on conservation laws

We have seen that the two-phase flow equations (2.13) are obtained from the balance laws of mass, momentum, and energy for the both phases. Mathematically, these laws are described by a system of partial differential equations in divergence form, called *conservation laws.* To make the exposition self-contained, we present a brief outline of the theory below. The references we have used here include Smoller [81], LeVeque [59], Godlewski and Raviart [38], Dafermos [25], and Serre [78]. We refer to these authors for details on the theory of conservation laws and related issues.

2.4.1   Weak solution

Consider a system of conservation laws

$$\mathbf{u}_t + \mathbf{f}(\mathbf{u})_x = 0 \tag{2.23}$$

with the initial data

$$\mathbf{u}(x,0) = \mathbf{u}_0(x). \tag{2.24}$$

Here $\mathbf{u} \in \mathbb{R}^p$, $x \in \mathbb{R}$, $t > 0$ and $\mathbf{f} : \mathbb{R}^p \to \mathbb{R}^p$ is a smooth function. The system is called *strictly hyperbolic* if the Jacobian matrix $\mathbf{A}(\mathbf{u}) = \mathbf{f}'(\mathbf{u})$ has p distinct real

eigenvalues

$$\lambda_1 < \lambda_2 < \cdots < \lambda_p \tag{2.25}$$

and therefore a complete set of eigenvectors. If the eigenvalues are not distinct, i.e.

$$\lambda_1 \leq \lambda_2 \leq \cdots \leq \lambda_p \tag{2.26}$$

but there is still a complete set of eigenvectors, then the system (2.23) is called *non-strictly hyperbolic*. On the other hand, if some eigenvectors become linearly dependent, then the system (2.23) is called *parabolic degenerate*.

An essential issue for the Cauchy problem (2.23), (2.24) is that in general, its solution may become discontinuous beyond some finite time interval, even if the initial data $\mathbf{u}_0$ is smooth, see e.g. Smoller [81] for an example. Then, the differentiation in (2.23) is not determined in the classical sense. To deal with this difficulty, one can define a *weak solution* to (2.23), (2.24) as follows. The function $\mathbf{u} \in L_{loc}^\infty(\mathbb{R} \times [0, \infty[)^p$ is called a weak solution of (2.23), (2.24) if

$$\int_0^\infty \int_{-\infty}^\infty [\boldsymbol{\phi}_t \cdot \mathbf{u} + \boldsymbol{\phi}_x \cdot \mathbf{f}(\mathbf{u})]dxdt + \int_{-\infty}^\infty \boldsymbol{\phi}(x, 0) \cdot \mathbf{u}(x, 0)dx = 0, \tag{2.27}$$

for all *test functions* $\boldsymbol{\phi} \in C_0^1(\mathbb{R} \times [0, \infty[)^p$. Note that $\boldsymbol{\phi}$ is a vector-valued function. By choosing $\boldsymbol{\phi} = (0, \ldots, 0, \phi_i, 0, \ldots, 0)$ with $\phi_i \in C_0^1(\mathbb{R})$ and $i = 1, \ldots, p$, the equation (2.27) defines a weak solution for a i-th component of the Cauchy problem (2.23), (2.24).

Now a weak solution $\mathbf{u}$ to (2.23), (2.24) can be discontinuous. However, not every discontinuity is permissible; a direct consequence of (2.27) is that across a curve of discontinuity, the *Rankine–Hugoniot conditions* must hold

$$\sigma[\mathbf{u}] = [\mathbf{f}(\mathbf{u})], \tag{2.28}$$

where σ is the propagation speed of the discontinuity, see e.g. Smoller [81]. Discontinuities which satisfy (2.28) are called *shocks*. This terminology comes from gas dynamics; there, the shocks are necessarily *compressive*, i.e. pressure and density of a gas particle increase on crossing the shock, see e.g. Courant and Friedrichs [22].

Remark 2.1. Consider the homogeneous part of the system of the generic model for two-phase flows (2.13), i.e., without the non-differential source terms on the right-hand side of it. Note that this homogeneous system *cannot* be written in divergence form, i.e. it is *not* a conservation law of the form (2.23). In what follows, we will call such systems the *non-conservative systems*, to distinguish them from the conservation laws (2.23), which by definition are in divergence form.

Obviously we cannot use the definitions of a weak solution and a shock introduced above in the context of conservations laws, for non-conservative systems.

This is in fact one of the main difficulties in dealing with such systems and is currently an area of active research. A definition for general non-conservative systems was given by Dal Maso, LeFloch, and Murat [26]. In this thesis, we propose a definition of a weak solution to a special class of initial-value problems for certain non-conservative systems, see Sections 4.6 and 5.3. These systems include the Baer–Nunziato model [10], and the Euler equations in a duct of variable cross-section, see Section 2.3.

It is well known that in general, a weak solution of (2.23), (2.24) is not unique, see again Smoller [81] for several examples. Hence, we need some criterion that enables us to choose the "physically relevant" solution among all weak solutions of (2.23), (2.24). Observe that all systems of balance laws from continuum physics are endowed with an additional inequality, which expesses the second law of thermodynamics. This gives rise to the following definition.

One says that a strictly convex function $U(\mathbf{u})$ is a (mathematical) *entropy* of the system (2.23), if there exist a function $F(\mathbf{u})$, called *entropy flux*, such that

$$U'(\mathbf{u})\mathbf{f}'(\mathbf{u}) = F'(\mathbf{u}).$$

Here $U'(\mathbf{u})$ and $F'(\mathbf{u})$ are the row vectors

$$U'(\mathbf{u}) = \left(\frac{\partial U}{\partial u_1}, \ldots, \frac{\partial U}{\partial u_p}\right), \quad F'(\mathbf{u}) = \left(\frac{\partial F}{\partial u_1}, \ldots, \frac{\partial F}{\partial u_p}\right).$$

Then (U, F) is called an *entropy pair* for the system (2.23). A weak solution $\mathbf{u}$ is an *entropy solution* if $\mathbf{u}$ satisfies, for all entropy functions U, the *entropy condition*

$$\frac{\partial U(\mathbf{u})}{\partial t} + \frac{\partial F(\mathbf{u})}{\partial x} \leq 0 \tag{2.29}$$

in the sense of distributions, that is

$$\int_0^\infty \int_{-\infty}^\infty [\phi_t U(\mathbf{u}) + \phi_x F(\mathbf{u})]dxdt + \int_{-\infty}^\infty \phi(x,0)U(\mathbf{u}(x,0))dx \geq 0, \tag{2.30}$$

for all $\phi \in C_0^1(\mathbb{R} \times [0, \infty[)$, $\phi \geq 0$. Across a discontinuity, propagating with the speed σ, the condition (2.30) is equivalent to

$$\sigma[U(\mathbf{u})] \geq [F(\mathbf{u})]. \tag{2.31}$$

The condition (2.31) is used to pick out a physically relevant, or *admissible* shock among all others. There are several other shock admissibility criteria, see Dafermos [24] for an excellent review. We mention here only the classical criterion due to Lax [57]: An i-shock of speed σ is called admissible, if

$$\lambda_i(\mathbf{u}_-) \geq \sigma \geq \lambda_i(\mathbf{u}_+), \tag{2.32}$$

where λ_i is an eigenvalue of the Jacobian matrix $\mathbf{A}(\mathbf{u}) = \mathbf{f}'(\mathbf{u})$, and $\mathbf{u}_\mp$ are the states to the left on the right of the shock, respectively. In particular, when both parts of (2.32) hold as equalities, the shock is called an *i-contact discontinuity*. It can be proven, that for sufficiently weak shocks the Lax criterion (2.32) is equivalent to the condition (2.31).

Since for hyperbolic systems information propagates along characteristics, the criterion (2.32) implies that the information from the past, carried by the k-characteristic, is absorbed and lost into admissible shocks.

Remark 2.2. Consider the single-phase Euler equations

$$\mathbf{u}_t + \mathbf{f}(\mathbf{u})_x = 0, \tag{2.33}$$

where $\mathbf{u}$ and $\mathbf{f}(\mathbf{u})$ are given as

$$\mathbf{u} = \begin{bmatrix} \rho \\ \rho v \\ \rho E \end{bmatrix}, \quad \mathbf{f}(\mathbf{u}) = \begin{bmatrix} \rho v \\ \rho v^2 + p \\ v(\rho E + p) \end{bmatrix}. \tag{2.34}$$

Let us close (2.33) with the ideal gas EOS (2.4), i.e.

$$e = \frac{p}{\rho(\gamma - 1)}.$$

Assume also that the gas obeys the ideal thermal EOS in the form

$$e = c_v T,$$

where the specific heat capacity c_v is constant. From the second law of thermodynamics we obtain the following expression for the entropy,

$$\eta = c_v \ln \left(\frac{p}{\rho^\gamma} \right) + C_0,$$

where C_0 is a constant, see e.g. Godlewski and Raviart [38]. Then, one can prove that

$$U(\mathbf{u}) = -\rho\eta, \quad F(\mathbf{u}) = -\rho\eta u$$

is an entropy pair for the Euler equations (2.33). But now the condition (2.29) corresponds to the second law of thermodynamics, which states that the physical entropy can only increase,

$$\frac{d\eta}{dt} \geq 0.$$

Thus the entropy condition (2.29) reflects the physical reality.

2.4.2   Characteristic fields

Consider the system of quasilinear hyperbolic equations

$$\mathbf{u}_t + \mathbf{A}(\mathbf{u})\mathbf{u}_x = 0, \tag{2.35}$$

where $\mathbf{u} \in \mathbb{R}^p$ and $\mathbf{A}(\mathbf{u})$ is a $p \times p$ matrix. Further, let $\lambda_i \in \mathbb{R}$ be the eigenvalues and $\mathbf{r}_i$ the corresponding eigenvectors of $\mathbf{A}(\mathbf{u})$ for $i = 1, \ldots, p$. In what follows, we will be particularly interested in situations when some of the eigenvalues can coincide, i.e. $\lambda_i = \lambda_j$ for $i \neq j$, since in fact this will be the case for the generic model of two-phase flows (2.13).

Each characteristic speed λ_i determines a *characteristic field*, also called the *i-field*. The solution of (2.35), corresponding to a certain *i*-characteristic field, is called an *i-wave*. Depending on the type of the particular characteristic field, the corresponding wave exhibits very different properties. The two types of characteristic fields are the following.

Definition 2.3 (Linearly degenerate field). *An i-characteristic field is said to be **linearly dependent** at the state $\mathbf{u} \in \mathbb{R}^p$, if there*

$$\nabla_{\mathbf{u}} \lambda_i(\mathbf{u}) \cdot \mathbf{r}_i(\mathbf{u}) = 0.$$

Definition 2.4 (Genuinely nonlinear field). *An i-characteristic field is said to be **genuinely nonlinear** at the state $\mathbf{u} \in \mathbb{R}^p$, if there*

$$\nabla_{\mathbf{u}} \lambda_i(\mathbf{u}) \cdot \mathbf{r}_i(\mathbf{u}) \neq 0.$$

Definition 2.5 (*i*-Riemann invariant). *A smooth function $\psi : \mathbb{R}^p \to \mathbb{R}$ is called an i-**Riemann invariant** if*

$$\nabla_{\mathbf{u}} \psi(\mathbf{u}) \cdot \mathbf{r}_i(\mathbf{u}) = 0$$

for all $\mathbf{u} \in \mathbb{R}^p$.

We stress that the above definitions are valid also for the case when the system (2.35) *cannot be written in divergence form*, i.e. when $\mathbf{A}(\mathbf{u})$ is not the differential of some flux function $\mathbf{f}(\mathbf{u})$. This observation is crucial for us, since the system of governing equations for two-phase flows (2.13), which we are interested in, cannot be written in divergence form.

In this thesis, we will always assume that all characteristic fields are either linearly degenerate, or genuinely nonlinear for all $\mathbf{u} \in \mathbb{R}^p$. This is in fact true for the most of submodels of the generic model (2.13), if we use the equation of state (2.5). The case when a certain field can change its type is much more complicated. We refer to Menikoff and Plohr [66] and to a recent book of LeFloch [58] for details.

Next, we state the following results which will be used intensively in this thesis.

Theorem 2.6. *Consider the system of quasilinear hyperbolic equations* (2.35). *If some eigenvalue λ_k has constant multiplicity $a(\lambda_k)$ and $a(\lambda_k) \geq 2$, then the following statements are true.*

1. *The corresponding k-characteristic field is linearly degenerate.*

2. *Locally there exist $p - a(\lambda_k)$ k-Riemann invariants $\psi_j(\mathbf{u})$, $j = 1, \ldots, p - a(\lambda_k)$, whose gradients $\nabla_{\mathbf{u}} \psi_j(\mathbf{u})$ are linearly independent.*

3. *Across the k-characteristic field, these $p - a(\lambda_k)$ Riemann invariants are constant.*

Proof. For statement 1, the original proof is due to Boillat [14]. It is also reproduced in Godlewski and Raviart [38] and Serre [78]. For the proof of statements 2 and 3 we refer to Serre [78]. Note that the proofs are valid also for the case when $\mathbf{A}(\mathbf{u})$ in (2.35) is not the differential of some flux function $\mathbf{f}(\mathbf{u})$. Therefore, the results hold also for the case of non-conservative systems. $\square$

2.4.3 The Riemann problem

Consider the conservation law (2.23). Then the *Riemann problem* for it is the initial-value problem for (2.23) with the piecewise constant initial data

$$\mathbf{u}(x, 0) = \begin{cases} \mathbf{u}_L, & x \leq 0 \\ \mathbf{u}_R, & x > 0. \end{cases} \tag{2.36}$$

This problem plays an important role in the study of hyperbolic conservation laws. Although it has quite simple initial data, the solution to (2.23), (2.36) provides valuable information on the properties of the conservation law (2.23). Besides, it serves as a building block for a class of numerical methods for conservation laws, see Section 3.1.

An essential issue on the Riemann problem (2.23), (2.36) is that its solution is invariant under the self-similar transformation $(x, t) \mapsto (\beta x, \beta t)$, $\beta > 0$. This means that if $\mathbf{u}(x, t)$ is a solution of (2.23), (2.36), then for all $\beta > 0$, the function $\mathbf{u}(\beta x, \beta t)$ is also a solution. Since presumably there is a unique solution to the Riemann problem, it is natural to consider only *self-similar solutions*, i.e. the ones depending only on the ratio x/t.

In Section 2.4.1 we have introduced the discontinuous solutions to a general initial-value problem (2.23), (2.24), the shocks and contact discontinuities. In addition to them, the solution to the Riemann problem (2.23), (2.36) possesses continuous self-similar solutions, the *centered simple waves*. In the special case when the conservation law (2.23) is given by the system of the Euler equations for gas dynamics, the gas is expanded in such a wave, see e.g. Courant and Friedrichs [22]. Therefore, a centered simple wave for a general conservation law (2.23) is referred to as a *rarefaction wave*. Across an *i*-rarefaction wave, the

$p - 1$ i-Riemann invariants are constant, see e.g. Smoller [81]. Remember that across an i-contact the $p - a(\lambda_i)$ i-Riemann invariants are constant, where $a(\lambda_i)$ is the multiplicity of the corresponding eigenvalue λ_i, see Theorem 2.6.

To summarize, the self-similar solutions to the Riemann problem (2.23), (2.36) are composed of shocks, rarefaction waves, and contact discontinuities. It can be shown, that a genuinely nonlinear i-characteristic field results in a solution in form of either a shock wave, or a rarefaction wave, whereas a linearly degenerate i-field forms a contact discontinuity, see e.g. Smoller [81].

Concerning the existence and uniqueness of the solution to the Riemann problem, one has the following results. If the system (2.23) is strictly hyperbolic, then the Riemann problem (2.23), (2.36) has a unique weak self-similar solution, but only for *small* initial data, i.e. if the difference $|\mathbf{u}_L - \mathbf{u}_R|$ is sufficiently small. If the eigenvalues of the Jacobian matrix have constant multiplicity, but the corresponding eigenvectors are still linearly independent, this result also holds, see Godlewski and Raviart [38].

For general (big) initial Riemann data (2.36), the corresponding Riemann problem can have no solution, see Keyfitz and Kranzer [50] for an example. If the system (2.23) is only non-strictly hyperbolic, the solution to the Riemann problem might be non-unique, see e.g. Isaacson and Temple [45] and the references therein.

2.5   Mathematical analysis of the generic model

We start with determining the type of the system of governing equations for the generic model (2.13). Since the *non-differential* source terms on the right-hand side of (2.13) do not influence the type of (2.13), we will consider only the *homogeneneous* system here, without source terms. Assume that each phase is described by the stiffened gas EOS (2.5), i.e.

$$e_k = \frac{p_k + \gamma_k \pi_k}{\rho_k (\gamma_k - 1)}, \qquad k = a, b, \tag{2.37}$$

where $\gamma_k, \pi_k > 0$ are constants, specific for the phase k.

In order to investigate the mathematical structure of (2.13) it is convenient to rewrite it in primitive variables,

$$\frac{\partial \mathbf{v}}{\partial t} + \mathbf{A}(\mathbf{v}) \frac{\partial \mathbf{v}}{\partial x} = 0, \tag{2.38}$$

where

$$\mathbf{v} = (\alpha_a, \rho_a, u_a, p_a, \rho_b, u_b, p_b)^T, \tag{2.39}$$

and the matrix $\mathbf{A} = \mathbf{A}(\mathbf{v})$ is given as

$$\mathbf{A} = \begin{pmatrix} U & 0 & 0 & 0 & 0 & 0 & 0 \\ \frac{\rho_a}{\alpha_a}(u_a - U) & u_a & \rho_a & 0 & 0 & 0 & 0 \\ \frac{p_a - P}{\alpha_a \rho_a} & 0 & u_a & 1/\rho_a & 0 & 0 & 0 \\ \frac{\rho_a c_{\text{int},a}^2}{\alpha_a}(u_a - U) & 0 & \rho_a c_a^2 & u_a & 0 & 0 & 0 \\ -\frac{\rho_b}{\alpha_b}(u_b - U) & 0 & 0 & 0 & u_b & \rho_b & 0 \\ -\frac{p_b - P}{\alpha_b \rho_b} & 0 & 0 & 0 & 0 & u_b & 1/\rho_b \\ -\frac{\rho_b c_{\text{int},b}^2}{\alpha_b}(u_b - U) & 0 & 0 & 0 & 0 & \rho_b c_b^2 & u_b \end{pmatrix}, \qquad (2.40)$$

where

$$c_k^2 = \frac{\frac{p_k}{\rho_k^2} - \left.\frac{\partial e_k}{\partial \rho_k}\right|_{p_k}}{\left.\frac{\partial e_k}{\partial p_k}\right|_{\rho_k}} = \frac{\gamma_k(p_k + \pi_k)}{\rho_k},$$

$$c_{\text{int},k}^2 = \frac{\frac{P}{\rho_k^2} - \left.\frac{\partial e_k}{\partial \rho_k}\right|_{p_k}}{\left.\frac{\partial e_k}{\partial p_k}\right|_{\rho_k}} = \frac{P(\gamma_k - 1) + p_k + \gamma_k \pi_k}{\rho_k}, \quad k = a, b,$$

are the sound speeds for the phase k and for the phase k at the interface, respectively. A straightforward computation gives us the following expressions for the seven eigenvalues

$$\begin{aligned}
\lambda_0 &= U, \\
\lambda_1 &= u_a - c_a, \quad \lambda_2 = u_a, \quad \lambda_3 = u_a + c_a, \\
\lambda_4 &= u_b - c_b, \quad \lambda_5 = u_b, \quad \lambda_6 = u_b + c_b.
\end{aligned} \qquad (2.41)$$

The corresponding right eigenvectors are

$$\mathbf{r}_0 = \begin{bmatrix} \alpha_a \alpha_b \sigma_a \sigma_b \\ -\alpha_b \sigma_b(\rho_a(\sigma_a - c_{\text{int},a}^2) + p_a - P), \\ \alpha_b \sigma_b(u_a - U)(p_a - P - \rho_a c_{\text{int},a}^2)/\rho_a, \\ \alpha_b \sigma_b(\rho_a c_{\text{int},a}^2(u_a - U)^2 - c_a^2(p_a - P)), \\ -\alpha_a \sigma_a(\rho_b(c_{\text{int},b}^2 - \sigma_b) - p_b + P) \\ \alpha_a \sigma_a(u_b - U)(-p_b + P + \rho_b c_{\text{int},b}^2)/\rho_b, \\ \alpha_a \sigma_a(-\rho_b c_{\text{int},b}^2(u_b - U)^2 + c_b^2(p_b - P)) \end{bmatrix}, \qquad (2.42)$$

$$\mathbf{r}_1 = \begin{bmatrix} 0 \\ \rho_a \\ -c_a \\ \rho_a c_a^2 \\ 0 \\ 0 \\ 0 \end{bmatrix}, \mathbf{r}_2 = \begin{bmatrix} 0 \\ 1 \\ 0 \\ 0 \\ 0 \\ 0 \\ 0 \end{bmatrix}, \mathbf{r}_3 = \begin{bmatrix} 0 \\ \rho_a \\ c_a \\ \rho_a c_a^2 \\ 0 \\ 0 \\ 0 \end{bmatrix}, \qquad (2.43)$$

$$\mathbf{r}_4 = \begin{bmatrix} 0 \\ 0 \\ 0 \\ 0 \\ \rho_b \\ -c_b \\ \rho_b c_b^2 \end{bmatrix}, \mathbf{r}_5 = \begin{bmatrix} 0 \\ 0 \\ 0 \\ 0 \\ 1 \\ 0 \\ 0 \end{bmatrix}, \mathbf{r}_6 = \begin{bmatrix} 0 \\ 0 \\ 0 \\ 0 \\ \rho_b \\ c_b \\ \rho_b c_b^2 \end{bmatrix}, \tag{2.44}$$

where

$$\sigma_a = c_a^2 - (u_a - U)^2, \quad \sigma_b = c_b^2 - (u_b - U)^2.$$

Note that the system (2.38), and thus (2.13) is *non-strictly hyperbolic*. Indeed, situations are possible, when some of the eigenvalues of the phase a can coincide with the ones of the phase b. Since the expression for $\lambda_0 = U$ is not determined for the generic model (2.13), the coinciding eigenvalues in general *do not* have constant multiplicity. Moreover, the eigenvectors (2.42)-(2.44) become linearly dependent in the points in the flow, where any one of the conditions

$$\alpha_a = 0, \quad \alpha_b = 0, \quad \sigma_a = 0, \quad \text{or} \quad \sigma_b = 0$$

holds. There, the system (2.13) is not hyperbolic anymore, it is said to be *parabolic degenerate*. Observe that this property holds for *any* choice of the averaged interface velocity U. The conditions $\alpha_k = 0$, $k = a, b$ state that the phase k disappears locally in the domain. This situation is analogous to the occurence of vacuum in the solution of the usual fluid dynamics equations. This problem and the related investigation of low Mach number flows are known to be difficult on its own, see e.g. [30, 67, 68, 74]. In this work, we will not consider this problem and always allow the presence of each phase everywhere in the domain.

Consider the Riemann problem for the system (2.38), i.e. equip it with piecewise-constant initial data

$$\mathbf{v}(x, 0) = \begin{cases} \mathbf{v}_L, & x \leq 0 \\ \mathbf{v}_R, & x > 0. \end{cases} \tag{2.45}$$

For the 1–3 and 4–6 characteristic fields, we can find the corresponding Riemann invariants. Firstly, the volume fraction

$$\alpha_a = \text{const}$$

across these fields. Then, the parameters of the phase b do not change across the waves of the phase a, i.e.

$$\rho_b = \text{const}, \ u_b = \text{const}, \ p_b = \text{const across 1–3 fields}$$

and inversely, i.e.

$$\rho_a = \text{const}, \ u_a = \text{const}, \ p_a = \text{const across 4–6 fields}$$

One can also see that the 1-, 3-, 4-, and 6-characteristic fields are genuinely non-linear, and 2- and 5-fields are linearly degenerate. The corresponding Riemann invariants are

$$\frac{p_a + \pi_a}{\rho_a^{\gamma_a}} = \text{const}, \ \ u_a + \frac{2c_a}{\gamma_a - 1} = \text{const across 1-rarefactions}$$

$$p_a = \text{const}, \ \ u_a = \text{const across 2-contacts}$$

$$\frac{p_a + \pi_a}{\rho_a^{\gamma_a}} = \text{const}, \ \ u_a - \frac{2c_a}{\gamma_a - 1} = \text{const across 3-rarefactions}.$$

Analogously,

$$\frac{p_b + \pi_b}{\rho_b^{\gamma_b}} = \text{const}, \ \ u_b + \frac{2c_b}{\gamma_b - 1} = \text{const across 4-rarefactions}$$

$$p_b = \text{const}, \ \ u_b = \text{const across 5-contacts}$$

$$\frac{p_b + \pi_b}{\rho_b^{\gamma_b}} = \text{const}, \ \ u_b - \frac{2c_b}{\gamma_b - 1} = \text{const across 6-rarefactions}.$$

We see that the Riemann invariants for the phase $k = a, b$ coincide with those for the Euler equations.

An important feature of the system (2.13) is the presence of the so-called *non-conservative terms*. These are the terms

$$\pm P \frac{\partial \alpha_a}{\partial x}, \qquad \pm PU \frac{\partial \alpha_a}{\partial x} \tag{2.46}$$

on the right-hand side of (2.13), and the transport equation for the volume fraction. Due to these terms, the system (2.13) cannot be written in divergence form. Consequently, the notions of weak solution and the Rankine–Hugoniot conditions for conservation laws are in general not applicable for it. Note that the action of the non-conservative terms is reflected in the 0-characteristic field, which corresponds to the eigenvalue $\lambda_0 = U$. Indeed, this eigenvalue results from the evolutionary equation for the volume fraction α_a, cf. (2.13), (2.38)-(2.40). On the other hand, the coupling of the phases is achieved through the variation of α_a, see (2.46). Therefore, the characteristic analysis of this field would give us some insight into the interaction phenomena between the phases. Obviously, this analysis depends on the value which we take for U. We will address this question when discussing the submodels of the generic model (2.13).

Remark 2.7. Note that for the special case of the Riemann problem (2.13), (2.45), the volume fraction α_a changes only across the 0-wave, which is determined by the averaged interface velocity U. Therefore, the action of the non-conservative terms (2.46) is always located and restricted to this wave. On the other hand, the volume fraction α_a is constant across all other waves in the solution of the Riemann problem. Consequently, away from the 0-wave, the non-conservative terms (2.46) vanish, and we are left with the *conservation law* there. But then, we

can use the usual Rankine–Hugoniot conditions there. This fact allows us to speak of shock waves also for the non-conservative system (2.13), but only if considering a Riemann problem for it. Also, we have used the above considerations to define a weak solution to several submodels of the generic model (2.13) in case of a Riemann problem, see Sections 4.6 and 5.3.

2.6   Mathematical analysis of the submodels

2.6.1   Saurel–Abgrall model

For the SA model, the preceeding analysis applies without changes. The 0-characteristic field is given now by

$$\lambda_0 = U = \frac{\alpha_a \rho_a u_a + \alpha_b \rho_b u_b}{\alpha_a \rho_a + \alpha_b \rho_b}. \tag{2.47}$$

However, the characteristic analysis of this field appears to be very extensive and complicated. We were not able to determine the type of this field.

2.6.2   Baer–Nunziato model

For the BN model, the characteristic analysis was done by Embid and Baer [31]. The 0-characteristic field is given now by

$$\lambda_0 = U = u_a,$$

so u_a is the double eigenvalue, $\lambda_0 = \lambda_2$. To investigate this characteristic field, it is convenient to use the variables

$$\tilde{\mathbf{v}} = (\alpha_a, \rho_a, u_a, p_a, \rho_b, u_b, \eta_b)^T,$$

where η_b is the entropy of the phase b.

With the ansatz (2.15), the momentum equation of the phase b in (2.38) reduces to

$$\frac{\partial u_b}{\partial t} + u_b \frac{\partial u_b}{\partial x} + \frac{c_b^2}{\rho_b} \frac{\partial \rho_b}{\partial x} + \frac{1}{\rho_b} \left. \frac{\partial p_b}{\partial \eta_b} \right|_{\rho_b} \frac{\partial \eta_b}{\partial x} = 0.$$

Again using (2.15), we obtain the equation for the internal energy of the phase b,

$$\frac{\partial e_b}{\partial t} + u_b \frac{\partial e_b}{\partial x} + \frac{p_b}{\rho_b} \frac{\partial u_b}{\partial x} + \frac{(u_a - u_b) p_b}{\alpha_a \rho_a} \frac{\partial \alpha_a}{\partial x} = 0. \tag{2.48}$$

From the second law of thermodynamics,

$$\left. \frac{\partial e}{\partial \eta} \right|_{\rho} = T, \quad \left. \frac{\partial e}{\partial \rho} \right|_{\eta} = \frac{p}{\rho^2}. \tag{2.49}$$

Combining (2.48) and (2.49), we get the equation for the entropy of the phase b,

$$\frac{\partial \eta_b}{\partial t} + u_b \frac{\partial \eta_b}{\partial x} = 0. \tag{2.50}$$

Then, the homogeneous system of equations becomes

$$\frac{\partial \tilde{\mathbf{v}}}{\partial t} + \tilde{\mathbf{A}}(\tilde{\mathbf{v}}) \frac{\partial \tilde{\mathbf{v}}}{\partial x} = 0, \tag{2.51}$$

where

$$\tilde{\mathbf{A}} = \begin{pmatrix} u_a & 0 & 0 & 0 & 0 & 0 & 0 \\ 0 & u_a & \rho_a & 0 & 0 & 0 & 0 \\ \frac{p_a - p_b}{\alpha_a \rho_a} & 0 & u_a & 1/\rho_a & 0 & 0 & 0 \\ 0 & 0 & \rho_a c_a^2 & u_a & 0 & 0 & 0 \\ -\frac{\rho_b}{\alpha_b}(u_b - u_a) & 0 & 0 & 0 & u_b & \rho_b & 0 \\ 0 & 0 & 0 & 0 & \frac{c_b^2}{\rho_b} & u_b & \frac{1}{\rho_b}\frac{\partial p_b}{\partial \eta_b}\Big|_{\rho_b} \\ 0 & 0 & 0 & 0 & 0 & 0 & u_b \end{pmatrix}. \tag{2.52}$$

A straightforward calculation gives us the value of the corresponding eigenvectors,

$$\mathbf{r}_0 = \begin{bmatrix} \dfrac{\alpha_b[(u_a - u_b)^2 - c_b^2]}{c_b^2(u_a - u_b)} \\ 0 \\ 0 \\ \dfrac{p_b - p_a}{\alpha_a} \dfrac{\alpha_b[(u_a - u_b)^2 - c_b^2]}{c_b^2(u_a - u_b)} \\ \dfrac{\rho_b(u_a - u_b)}{c_b^2} \\ 1 \\ 0 \end{bmatrix}, \tag{2.53}$$

$$\mathbf{r}_4 = \begin{bmatrix} 0 \\ 0 \\ 0 \\ 0 \\ -\dfrac{\rho_b}{c_b} \\ 1 \\ 0 \end{bmatrix}, \mathbf{r}_5 = \begin{bmatrix} 0 \\ 0 \\ 0 \\ 0 \\ 1 \\ 0 \\ -c_b^2/\left(\frac{\partial p_b}{\partial \eta_b}\Big|_{\rho_b}\right) \end{bmatrix}, \mathbf{r}_6 = \begin{bmatrix} 0 \\ 0 \\ 0 \\ 0 \\ \dfrac{\rho_b}{c_b} \\ 1 \\ 0 \end{bmatrix}, \tag{2.54}$$

and $\mathbf{r}_1$, $\mathbf{r}_2$, and $\mathbf{r}_3$ are the same as in (2.43). As was recognized by Embid and Baer [31], $\mathbf{r}_0$ becomes linearly dependent with $\mathbf{r}_4$ or $\mathbf{r}_6$, when

$$(u_b - u_a)^2 - c_b^2 = 0. \tag{2.55}$$

Also, they established that the 0-characteristic field is linearly degenerate

$$\nabla u_a \cdot \mathbf{r}_0 = 0,$$

and that

$$\psi_1 = u_a$$
$$\psi_2 = \eta_b \tag{2.56}$$

are the two Riemann invariants across it. Further Riemann invariants are

$$\begin{aligned} \psi_3 &= \alpha_b \rho_b (u_a - u_b) \\ \psi_4 &= \alpha_a p_a + \alpha_b p_b + \alpha_b \rho_b (u_a - u_b)^2 \\ \psi_5 &= \frac{(u_a - u_b)^2}{2} + \frac{c_b^2}{\gamma_b - 1}, \end{aligned} \tag{2.57}$$

where $c_b^2 = \frac{\gamma_b(p_b + \pi_b)}{\rho_b}$ is the squared sound speed of the phase b, see Embid and Baer [31] for details. Since the eigenvalue $\lambda_0 = \lambda_2 = u_a$ has constant multiplicity equal to 2, there are only 5 Riemann invariants for the 0-characteristic field, see Theorem 2.6.

Remark 2.8. The original BN model [10] describes the deflagration-to-detonation transition (DDT) in gas-permeable, reactive granular materials. The process begins with ignition of a few grains. The hot gases penetrate into the pores of the solid material and accelerate the flame spread by preheating the grains. This causes considerable compression ahead of the flame front ("compaction of the granular bed"). This complicated process is reflected by inclusion of the third parameter in the EOS for the solid phase, the solid volume fraction,

$$e_a = e_a(\rho_a, \eta_a, \alpha_a).$$

This dependence results in more complicated expression for the eigenvector, corresponding to $\lambda_0 = U$. Apart from this, the characteristic analysis presented above remains unchanged. In particular, the 0-characteristic field remains linearly degenerate, and the Riemann invariants are still given by (2.56)-(2.57). Therefore, in what follows we will always assume for simplicity that the energy of the solid phase does not depend on the volume fraction. Also, we will always use the stiffened gas EOS (2.5) for the thermodynamical description of the both solid and gas phases.

2.6.3   Euler equations in a duct of variable cross-section

As we have shown in Section 2.3, due to the assumptions

$$P = p_b, \quad u_a = U = \mathcal{S} = \mathcal{M} = \mathcal{E} = 0$$

the system of governing equations of the generic model (2.13) reduces to

$$
\begin{aligned}
\frac{\partial A}{\partial t} &= 0 \\
\frac{\partial A\rho}{\partial t} + \frac{\partial A\rho v}{\partial x} &= 0 \\
\frac{\partial A\rho v}{\partial t} + \frac{\partial A(\rho v^2 + p)}{\partial x} &= p\frac{\partial A}{\partial x} \\
\frac{\partial A\rho E}{\partial t} + \frac{\partial Av(\rho E + p)}{\partial x} &= 0.
\end{aligned}
\tag{2.58}
$$

This system corresponds to the well-known Euler equations in a duct of variable cross section $A = A(x)$, see Section 2.3. Here, $A = A(x)$ is the variable cross-section, ρ is the density, v the velocity, p the pressure, $E = e + v^2/2$ the specific total energy. We assume that the gas obeys the stiffened gas EOS (2.5), i.e.

$$
e = \frac{p + \gamma\pi}{\rho(\gamma - 1)},
\tag{2.59}
$$

where $\gamma, \pi > 0$ are the thermodynamic constants. To carry out the characteristic analysis of (2.58), it is convenient to use the primitive variables

$$
\mathbf{v} = (A, \rho, v, p)^T.
\tag{2.60}
$$

Then, the system (2.58) is equivalent to

$$
\mathbf{v}_t + \mathbf{A}(\mathbf{v})\mathbf{v}_x = 0,
\tag{2.61}
$$

where

$$
\mathbf{A} = \begin{bmatrix}
0 & 0 & 0 & 0 \\
\rho v/A & v & \rho & 0 \\
0 & 0 & v & 1/\rho \\
\rho v c^2/A & 0 & \rho c^2 & v
\end{bmatrix},
\tag{2.62}
$$

and $c = \sqrt{\gamma(p + \pi)/\rho}$ is the sound speed. The eigenvalues of $\mathbf{A}$ are

$$
\lambda_0 = 0, \quad \lambda_1 = v - c, \quad \lambda_2 = v, \quad \lambda_3 = v + c,
\tag{2.63}
$$

and the corresponding eigenvectors are

$$
\mathbf{r}_0 = \begin{bmatrix} A(v^2 - c^2)/c^2 \\ -v^2\rho/c^2 \\ v \\ -\rho v^2 \end{bmatrix}, \quad
\mathbf{r}_1 = \begin{bmatrix} 0 \\ -\rho \\ c \\ -\rho c^2 \end{bmatrix}, \quad
\mathbf{r}_2 = \begin{bmatrix} 0 \\ 1 \\ 0 \\ 0 \end{bmatrix}, \quad
\mathbf{r}_3 = \begin{bmatrix} 0 \\ \rho \\ c \\ \rho c^2 \end{bmatrix}.
\tag{2.64}
$$

Note that the situations are possible, when either of λ_1, λ_2, or λ_3 coincides with λ_0. Moreover, when λ_1 or λ_3 coincide with λ_0, the corresponding eigenvectors

become linearly dependent. In this case a parabolic degeneracy occurs. To summarize, the system of governing equations (2.58) is non-strictly hyperbolic away from the points where either $\lambda_0 = \lambda_1$ or $\lambda_0 = \lambda_3$.

We can easily establish that the 1-, 2-, and 3-characteristic fields are exactly the same as for the usual one-dimensional Euler equations. The 1- and 3-characteristic fields are genuinely nonlinear, and the 2-field is linearly degenerate. It is obvious that the 0-characteristic field is also linearly degenerate. Note also that the 0-wave is always *stationary*, i.e. its speed λ_0 is always zero, see (2.63).

It is easy to establish that the Riemann invariants for 1-, 2-, and 3-fields coincide with those of the Euler equations. Also, the cross-section A is constant across them. The Riemann invariants across the 0-contact discontinuity are

$$
\begin{aligned}
A\rho v &= \text{const} \\
\eta &= \text{const} \\
\frac{v^2}{2} + \frac{c^2}{\gamma - 1} &= \text{const},
\end{aligned}
\tag{2.65}
$$

where $\eta = (p + \pi)/\rho^\gamma$ is the isentrope. Note that the relations (2.65) express the conservation of mass, entropy, and Bernoulli's law, respectively, see e.g. Courant and Friedrichs [22].

Chapter 3

Numerical solution of the generic model

Apart from some trivial cases, we must give up hope to get an exact solution to the system of governing equations for the generic model (2.13), provided we have some realistic ansatz for the interface velocity and pressure, cf. Chapter 2. Already for the SA model, which sets these parameters essentially to the mixture values, we were unable to determine the type of the 0-characteristic field, see Section 2.6. Therefore, the numerical solution to the system (2.13) seems to be the only possibility.

There are several difficulties concerning it. Firstly, the system (2.13) is a non-conservative one, i.e. it cannot be written in divergence form. Therefore, the theory of numerical methods developed for conservation laws cannot be used here automatically. On the other hand, the generic model (2.13) has been obtained by averaging of the conservation equations for the phases. Therefore, the most straight-forward approach in constructing the numerical scheme for it would be to take some known method for conservation laws and modify it in order to take into account the non-conservative terms. This is essentially what we will be doing in this chapter.

Secondly, the system (2.13) is quite complicated: The solution to the Riemann problem contains in general seven waves. These can overlap with each other, cf. Section 2.5. Moreover, the system (2.13) can be accomplished with additional equations which account for more detailed physics of interactions, like microinertia and bubble pulsations [37], or detonation phenomena [17]. Therefore, one wishes to construct a numerical method, in which all these additional factors could be integrated easily. This is our second guideline here.

The plan of this chapter is as follows. First, we present some basic ideas from the theory of numerical methods for conservations laws, together with several numerical methods. These will be used as the ingredients of the method for the non-conservative system (2.13). Finally, we will assess the perfomance of the method on some test problems. In doing so, we will use the ansatz of the interface

velocity and pressure due to Saurel and Abgrall [75]. In Chapters 4 and 5 we will test the numerical method on the BN model and the Euler equations in a duct, respectively.

3.1 Numerical methods for conservation laws

Consider the system of hyperbolic conservation laws (2.23), i.e.

$$\mathbf{u}_t + \mathbf{f}(\mathbf{u})_x = 0 \tag{3.1}$$

with the initial data

$$\mathbf{u}(x,0) = \mathbf{u}_0(x). \tag{3.2}$$

Given a uniform grid with time step Δt and spatial mesh size Δx, we define an approximation $\mathbf{u}_j^n \in \mathbb{R}^p$ of $\mathbf{u}(x_j, t^n)$ at the point $x_j = j\Delta x, t^n = n\Delta t$ by the formula

$$\mathbf{u}_j^{n+1} = \mathbf{u}_j^n - \frac{\Delta t}{\Delta x} \left[\mathbf{F}_{j+1/2}^n - \mathbf{F}_{j-1/2}^n \right], \quad j \in \mathbb{Z}, n \geq 0. \tag{3.3}$$

Here the function

$$\mathbf{F}_{j+1/2}^n = \mathbf{F}(\mathbf{u}_{j-k+1}, \ldots, \mathbf{u}_{j+k})$$

is called a *numerical flux function*. The scheme (3.3) is said to be written in the *conservation form*. Provided it is also *consistent*, that is

$$
\begin{aligned}
\mathbf{F}(\mathbf{u}, \mathbf{u}, \ldots, \mathbf{u}) &= \mathbf{f}(\mathbf{u}), &(3.4)\\
|\mathbf{F}(\mathbf{u}_{j-k+1}, \ldots, \mathbf{u}_{j+k}) - \mathbf{f}(\bar{\mathbf{u}})| &\leq K \max_{-k+1 \leq i \leq k} |\mathbf{u}_{j+i} - \bar{\mathbf{u}}|, &(3.5)
\end{aligned}
$$

for all $\mathbf{u}_{j+i}$ sufficiently close to $\bar{\mathbf{u}}$, the Lax–Wendroff theorem holds. It states that in case when the numerical solution converges to a function $\mathbf{u}$ in some strong sense, then $\mathbf{u}$ is a weak solution of (3.1).

In the linear case, the Lax equivalence theorem says that for a consistent method, stability is necessary and sufficient for convergence. Analogously, for the nonlinear problems we need some form of stability to guarantee convergence. For scalar problems, a *total variation diminishing (TVD)* conservative and consistent method ensures convergence of the numerical solution in the L^1 sense. The corresponding definition is as follows. The total variation function of a grid function $v^n = (u_j^n)$ is

$$\mathrm{TV}(v^n) = \sum_{j \in \mathbb{Z}} |u_{j+1}^n - u_j^n|.$$

The method is called TVD, if

$$\mathrm{TV}(v^{n+1}) \leq \mathrm{TV}(v^n) < \infty.$$

If, additionally, the scheme is consistent with a *discrete entropy condition*, then the scheme will converge to a weak solution of (2.23) that satisfies the entropy condition. For the general theory of conservation laws, see e.g. LeVeque [59], Godlewski and Raviart [38], and Kröner [51].

Remark 3.1. Note that the TVD property is a purely scalar notion, which does not hold for systems. However, the common approach is to extend the results for the scalar problems to systems in a relatively straight forward way. This leads in general to satisfactory numerical results.

3.1.1 Godunov's method

The most natural finite difference method to solve the Cauchy problem (3.1), (3.2) is Godunov's method [39]. Let us recall its main features.

Given an approximate solution $(\mathbf{u}_j^n)_{j \in \mathbb{Z}, n \in \mathbb{N}_0}$, we define a piecewise constant function $\tilde{\mathbf{u}}(x, t^n)$,

$$\tilde{\mathbf{u}}(x, t^n) = \mathbf{u}_j^n, \quad x_{j-1/2} \le x < x_{j+1/2}.$$

Using this initial data, we solve the conservation law

$$\tilde{\mathbf{u}}_t + \mathbf{f}(\tilde{\mathbf{u}})_x = 0 \tag{3.6}$$

exactly over the time interval $t^n \le t < t^{n+1}$. Assuming that $\tilde{\mathbf{u}}$ is an exact weak solution, we integrate (3.6) over the rectangle $[x_{j-1/2}, x_{j+1/2}] \times [t^n, t^{n+1}]$ to get

$$\int_{x_{j-1/2}}^{x_{j-1/2}} \tilde{\mathbf{u}}(x, t^{n+1}) dx = \int_{x_{j-1/2}}^{x_{j-1/2}} \tilde{\mathbf{u}}(x, t^n) dx$$
$$+ \int_{t^n}^{t^{n+1}} \mathbf{f}(\tilde{\mathbf{u}}(x_{j-1/2}, t)) dt - \int_{t^n}^{t^{n+1}} \mathbf{f}(\tilde{\mathbf{u}}(x_{j+1/2}, t)) dt.$$

If we set

$$\mathbf{u}_j^{n+1} = \frac{1}{\Delta x} \int_{x_{j-1/2}}^{x_{j-1/2}} \tilde{\mathbf{u}}(x, t^{n+1}) dx,$$

the scheme reads

$$\mathbf{u}_j^{n+1} = \mathbf{u}_j^n - \frac{\Delta t}{\Delta x} \left[\mathbf{F}(\mathbf{u}_j^n, \mathbf{u}_{j+1}^n) - \mathbf{F}(\mathbf{u}_{j-1}^n, \mathbf{u}_j^n) \right],$$

where the numerical flux function is

$$\mathbf{F}(\mathbf{u}_j^n, \mathbf{u}_{j+1}^n) = \frac{1}{\Delta t} \int_{t^n}^{t^{n+1}} \mathbf{f}(\tilde{\mathbf{u}}(x_{j+1/2}, t)) dt. \tag{3.7}$$

The exact solution of the Riemann problem along the line $x = x_{j+1/2}$ is constant, and depends only on the data $\mathbf{u}_j^n$ and $\mathbf{u}_{j+1}^n$. If we denote this value by $\mathbf{u}_{\text{ex}}^*(\mathbf{u}_j^n, \mathbf{u}_{j+1}^n)$, then the flux (3.7) reduces to

$$\mathbf{F}(\mathbf{u}_j^n, \mathbf{u}_{j+1}^n) = \mathbf{f}(\mathbf{u}_{\text{ex}}^*(\mathbf{u}_j^n, \mathbf{u}_{j+1}^n))$$

and the Godunov scheme becomes

$$\mathbf{u}_j^{n+1} = \mathbf{u}_j^n - \frac{\Delta t}{\Delta x} \left[\mathbf{f}(\mathbf{u}_{\text{ex}}^*(\mathbf{u}_j^n, \mathbf{u}_{j+1}^n)) - \mathbf{f}(\mathbf{u}_{\text{ex}}^*(\mathbf{u}_{j-1}^n, \mathbf{u}_j^n)) \right].$$

Note that the scheme is obviously conservative and consistent. One can show that the above derivation remains valid under the CFL condition

$$\left| \frac{\Delta t}{\Delta x} \lambda_i(\mathbf{u}_j^n) \right| \leq 1. \tag{3.8}$$

where λ_i are the eigenvalues of the Jacobian matrix. Concerning the stability of the method, one has the following results. In the scalar case, the Godunov scheme is TVD under the CFL condition

$$\frac{\Delta t}{\Delta x} |\sup_{u \in I_j} f'(u)| \leq 1, \quad I_j = [\min(u_j, u_{j+1}), \max(u_j, u_{j+1})], \quad j \in \mathbb{Z}.$$

which gives a convergent scheme.

For linear systems with $\mathbf{A} = \text{const}$ the Godunov method reduces to the upwind method, which has the stability limit

$$\left| \frac{\Delta t}{\Delta x} \max_i \lambda_i \right| \leq 1,$$

where λ_i are the eigenvalues of the constant matrix $\mathbf{A}$.

In spite of Remark 3.1, we expect the Godunov method to be stable under the condition (3.8). Provided we use entropy-satisfying Riemann solutions, the weak solutions obtained by Godunov's method satisfy the entropy condition.

3.1.2 Roe's method

The Godunov method requires the exact solution of Riemann problems at every cell boundary in each time step. However, the exact solution is often unknown. This is for example the case for the two-phase flow equations or when using a tabulated equation of state. Even if the Riemann problem can be solved, in practice doing so is expensive, and typically requires some iterations. This suggests the use of some approximate Riemann solvers. In this section, we briefly describe one of the most popular numerical schemes for the solution of the conservation law (2.23), which makes use of an approximate Riemann solver. This is the scheme due to Roe [73].

Consider the conservation law (3.1) with the Riemann initial data

$$\mathbf{u}(x, 0) = \begin{cases} \mathbf{u}_L, & x \leq 0 \\ \mathbf{u}_R, & x > 0. \end{cases} \tag{3.9}$$

Carrying out the differentiation in (3.1) and linearizing it, one gets

$$\mathbf{u}_t + \mathbf{A}(\bar{\mathbf{u}}(\mathbf{u}_L, \mathbf{u}_R))\mathbf{u}_x = 0, \tag{3.10}$$

where the *constant* matrix $\mathbf{A}$ is the Jacobian matrix of the flux function $\mathbf{f}$, calculated in some intermediate state $\bar{\mathbf{u}}(\mathbf{u}_L, \mathbf{u}_R)$. For the linear problem (3.10), the solution of the Riemann problem can be found exactly, see e.g. LeVeque [59]. We introduce the characteristic variables

$$\mathbf{s} = \mathbf{R}^{-1}\mathbf{u}, \quad \mathbf{s} = (s_1, \ldots, s_p)^T, \tag{3.11}$$

where $\mathbf{R}$ is the matrix of the right eigenvectors of $\mathbf{A}$. Then the system (3.10) decouples into p scalar advection equations,

$$\frac{\partial s_i}{\partial t} + \lambda_i \frac{\partial s_i}{\partial x} = 0, \quad i = 1, \ldots, p,$$

where λ_i are the eigenvalues of $\mathbf{A}$. The initial data (3.9) in characteristic variables will be

$$\mathbf{s}(x,0) = \begin{cases} \mathbf{s}_L = \mathbf{R}^{-1}\mathbf{u}_L = \begin{pmatrix} s_{L1} \\ \vdots \\ s_{Lp} \end{pmatrix}, & x \leq 0 \\ \mathbf{s}_R = \mathbf{R}^{-1}\mathbf{u}_R = \begin{pmatrix} s_{R1} \\ \vdots \\ s_{Rp} \end{pmatrix}, & x > 0. \end{cases}$$

Thus one has

$$\begin{aligned} \mathbf{u}_R - \mathbf{u}_L &= \mathbf{R}(\mathbf{s}_R - \mathbf{s}_L) = \mathbf{R}\begin{pmatrix} s_{R1} - s_{L1} \\ \vdots \\ s_{Rp} - s_{Lp} \end{pmatrix} \\ &= (s_{R1} - s_{L1})\mathbf{r}_1 + \cdots + (s_{Rp} - s_{Lp})\mathbf{r}_p = \sum_{i=1}^{p} a_i \mathbf{r}_i, \end{aligned}$$

where $a_i = s_{Ri} - s_{Li}$ and $\mathbf{r}_i$ are the right eigenvectors of $\mathbf{A}$. The intermediate state in the solution of Riemann problem is given by

$$\mathbf{u}^* = \mathbf{u}_L + \sum_{\lambda_i < 0} a_i \mathbf{r}_i. \tag{3.12}$$

The numerical flux finction is then

$$\begin{aligned} \mathbf{F}(\mathbf{u}_L, \mathbf{u}_R) &= \mathbf{A}\mathbf{u}^* = \mathbf{A}\mathbf{u}_L + \mathbf{A}\sum_{\lambda_i < 0} a_i \mathbf{r}_i \\ &= \mathbf{f}(\mathbf{u}_L) + \sum_{\lambda_i < 0} \lambda_i a_i \mathbf{r}_i. \end{aligned} \tag{3.13}$$

Then the Roe scheme reads as

$$\mathbf{u}_j^{n+1} = \mathbf{u}_j^n - \frac{\Delta t}{\Delta x} \left[\mathbf{F}(\mathbf{u}_j^n, \mathbf{u}_{j+1}^n) - \mathbf{F}(\mathbf{u}_{j-1}^n, \mathbf{u}_j^n) \right], \tag{3.14}$$

where $\mathbf{F}$ is calculated according to (3.13). For the matrix $\mathbf{A}$, the following conditions given by Roe [73] should hold,

$$\mathbf{A}(\bar{\mathbf{u}}(\mathbf{u}_L, \mathbf{u}_R))(\mathbf{u}_R - \mathbf{u}_L) = \mathbf{f}(\mathbf{u}_R) - \mathbf{f}(\mathbf{u}_L) \tag{3.15}$$

$$\mathbf{A}(\bar{\mathbf{u}}(\mathbf{u}_L, \mathbf{u}_R)) \text{ is diagonalizable with real eigenvalues} \tag{3.16}$$

$$\mathbf{A}(\bar{\mathbf{u}}(\mathbf{u}_L, \mathbf{u}_R)) \to \mathbf{f}'(\tilde{\mathbf{u}}) \text{ smoothly as } \mathbf{u}_L, \mathbf{u}_R \to \tilde{\mathbf{u}}. \tag{3.17}$$

Condition (3.15) guarantees that the scheme (3.14) is consistent with the integral form of the conservation law. Another effect is that, in the special case where $\mathbf{u}_L$ and $\mathbf{u}_R$ are connected by a single shock or contact discontinuity, the approximate Riemann solution agrees with the exact one. Condition (3.16) is required in order that the problem (3.10) is hyperbolic. Condition (3.17) guarantees that the method behaves reasonably on smooth solutions.

Remark 3.2. For many practical situations, the condition (3.15) is difficult, if not impossible, to fulfil. For example, this is the case for the two-phase flow equations or when using tabulated equations of state.

Remark 3.3. Another disadvantage of Roe's linearization is that the resulting approximate Riemann solution consists of only discontinuities, with no rarefaction waves. This can lead to a violation of the entropy condition, see e.g. LeVeque [59]. There are various ways to cure the problem, see e.g. Harten and Hyman [41].

Remark 3.4. It can be shown that the Roe scheme can produce negative pressures and densities in the solution of the Riemann problem. In order to avoid this, some modifications of the scheme have to be made, see Einfeldt *et al.* [30].

3.1.3   VFRoe: an approximate Godunov's method

One way of generalizing Godunov's method is the following. One has to start with the Godunov flux

$$\mathbf{F}(\mathbf{u}_j^n, \mathbf{u}_{j+1}^n) = \mathbf{f}(\mathbf{u}_{\text{ex}}^*(\mathbf{u}_j^n, \mathbf{u}_{j+1}^n)),$$

and replace the exact Riemann solution $\mathbf{u}_{\text{ex}}^*(\mathbf{u}_j^n, \mathbf{u}_{j+1}^n)$ by some approximate solution $\mathbf{u}^*(\mathbf{u}_j^n, \mathbf{u}_{j+1}^n)$. This leads to the approximate Godunov methods

$$\mathbf{u}_j^{n+1} = \mathbf{u}_j^n - \frac{\Delta t}{\Delta x} \left[\mathbf{f}(\mathbf{u}^*(\mathbf{u}_j^n, \mathbf{u}_{j+1}^n)) - \mathbf{f}(\mathbf{u}^*(\mathbf{u}_{j-1}^n, \mathbf{u}_j^n)) \right]. \tag{3.18}$$

Some methods of this kind are described in Toro [89].

In this section we will give a description of one of such methods, which was introduced by Gallouët and Masella in [33]. In what follows, this scheme will be referred to as VFRoe, stands for *Volumes Finis Roe* in French, notion taken from Gallouët and Masella [33].

Again, we start with the conservation law (3.1) and the initial data being (3.9). Provided the condition (3.16) is fulfilled and proceeding exactly as in the previous section, we find the intermediate state in the solution of the Riemann problem (3.1), (3.9) as

$$\mathbf{u}^* = \mathbf{u}_L + \sum_{\lambda_i < 0} a_i \mathbf{r}_i. \tag{3.19}$$

Here λ_i are the eigenvectors of the matrix $\mathbf{A}$, calculated at some intermediate state $\bar{\mathbf{u}}(\mathbf{u}_L, \mathbf{u}_R)$, and $\mathbf{r}_i$ are the corresponding eigenvectors. We use this value of $\mathbf{u}^*$ in the approximate Godunov method (3.18). Then the VFRoe scheme reads as

$$\mathbf{u}_j^{n+1} = \mathbf{u}_j^n - \frac{\Delta t}{\Delta x} \left[\mathbf{f}(\mathbf{u}^*(\mathbf{u}_j^n, \mathbf{u}_{j+1}^n)) - \mathbf{f}(\mathbf{u}^*(\mathbf{u}_{j-1}^n, \mathbf{u}_j^n)) \right]. \tag{3.20}$$

Note that (3.17) is still a necessary condition if we are to recover smoothly the linearized algorithm from the non-linear version. Below we will discuss the properties of the scheme.

Conservation

The scheme (3.20) is obviously written in conservative form for *any* choice of $\bar{\mathbf{u}}$. Thus we do not need the condition (3.15) on the matrix $\mathbf{A}$ in order for the method to be conservative. This is a great advantage of the VFRoe scheme over the Roe scheme, cf. Remark 3.2 above.

Consistency

The consistency condition is given by (3.4)-(3.5). The first condition in the case of the VFRoe scheme reads

$$\mathbf{f}(\mathbf{u}^*) = \mathbf{f}(\mathbf{u}), \quad \mathbf{u}^* = \mathbf{u}^*(\bar{\mathbf{u}}(\mathbf{u}, \mathbf{u})). \tag{3.21}$$

Here $\bar{\mathbf{u}}$ is the state where we calculate the Jacobian matrix $\mathbf{A}$, and the equality must hold for all admissible states $\mathbf{u} \in \mathbb{R}^p$. Note that this condition is satisfied for *any* choice of $\bar{\mathbf{u}}$. Indeed, if we set $\mathbf{u}_L = \mathbf{u}_R = \mathbf{u}$ for all $\mathbf{u}$ in (3.19), then all $a_i = 0$ and one always has

$$\mathbf{u}^* = \mathbf{u}_L = \mathbf{u}_R = \mathbf{u}.$$

The condition (3.5) will be

$$|\mathbf{f}(\mathbf{u}^*(\mathbf{u}_L, \mathbf{u}_R)) - \mathbf{f}(\mathbf{u})| \leq K \max\left(|\mathbf{u}_L - \mathbf{u}|, |\mathbf{u}_R - \mathbf{u}|\right), \tag{3.22}$$

for all admissible states $\mathbf{u}$ and for all $\mathbf{u}_L$, $\mathbf{u}_R$ with $|\mathbf{u}_L - \mathbf{u}|$ and $|\mathbf{u}_R - \mathbf{u}|$ sufficiently small. Assume that

$$\begin{aligned} |\mathbf{u}_L - \mathbf{u}| &\leq \epsilon_1, \\ |\mathbf{u}_R - \mathbf{u}| &\leq \epsilon_2. \end{aligned}$$

Then, using the smoothness of $\mathbf{f}$ and the formula (3.19), one has

$$|\mathbf{f}(\mathbf{u}^*(\mathbf{u}_L, \mathbf{u}_R)) - \mathbf{f}(\mathbf{u})| \leq C\,|\mathbf{u}^*(\mathbf{u}_L, \mathbf{u}_R) - \mathbf{u}| = C|\mathbf{u}_L - \mathbf{u} + \sum_{\lambda_i < 0} a_i \mathbf{r}_i|. \qquad (3.23)$$

Assume that

$$\lambda_1 \leq \lambda_2 \leq \cdots \leq \lambda_k \leq 0 \leq \lambda_{k+1} \leq \cdots \leq \lambda_p.$$

Then we can rewrite the last term in (3.23) using $|\mathbf{r}_i| = 1$ as

$$\begin{aligned} C|\mathbf{u}_L - \mathbf{u} &+ (s_{r1} - s_{l1})\mathbf{r}_1 + \cdots + (s_{rk} - s_{lk})\mathbf{r}_k| \\ &\leq C\{|\mathbf{u}_L - \mathbf{u}| + |(s_{r1} - s_{l1})\mathbf{r}_1| + \cdots + |(s_{rk} - s_{lk})\mathbf{r}_k|\} \\ &= C\{|\mathbf{u}_L - \mathbf{u}| + |s_{r1} - s_{l1}| + \cdots + |s_{rk} - s_{lk}|\}. \end{aligned}$$

Using the Cauchy–Schwartz inequality and (3.11), one has

$$\begin{aligned} |s_{r1} - s_{l1}| + \cdots + |s_{rk} - s_{lk}| &\leq \sqrt{k}\sqrt{(s_{r1} - s_{l1})^2 + \cdots + (s_{rk} - s_{lk})^2} \\ &\leq \sqrt{k}\sqrt{(s_{r1} - s_{l1})^2 + \cdots + (s_{rp} - s_{lp})^2} = \sqrt{k}\,|\mathbf{s}_R - \mathbf{s}_L| = \sqrt{k}|\mathbf{R}^{-1}(\mathbf{u}_R - \mathbf{u}_L)|. \end{aligned}$$

With the above estimations, we obtain that

$$\begin{aligned} |\mathbf{f}(\mathbf{u}^*(\mathbf{u}_L, \mathbf{u}_R)) - \mathbf{f}(\mathbf{u})| &\leq C\{|\mathbf{u}_L - \mathbf{u}| + \sqrt{k}|\mathbf{R}^{-1}||\mathbf{u}_R - \mathbf{u}_L|\} \\ &< C\{\epsilon_1 + \sqrt{k}|\mathbf{R}^{-1}|(\epsilon 1 + \epsilon 2)\} \\ &\leq C(1 + 2\sqrt{k}|\mathbf{R}^{-1}|)\max(\epsilon 1, \epsilon 2). \end{aligned}$$

Here

$$\begin{aligned} |\mathbf{R}^{-1}| &= \sqrt{\text{maximal eigenvalue of } (\mathbf{R}^{-1})^T \mathbf{R}^{-1}} \\ &= \sqrt{\text{maximal eigenvalue of } (\mathbf{R}\mathbf{R}^T)^{-1}}. \end{aligned}$$

With a reasonable choice of $\bar{\mathbf{u}}$ this norm remains bounded as $\mathbf{u}_L, \mathbf{u}_R \to \mathbf{u}$ for all $\mathbf{u}$, so the condition (3.22) is fulfilled. See below for further discussion of the choice of $\bar{\mathbf{u}}$.

Stability

Consider the Riemann problem (3.1), (3.9) in the scalar case,

$$u_t + f(u)_x = 0 \tag{3.24}$$

$$u(x, 0) = \begin{cases} u_L, & x \leq 0 \\ u_R, & x > 0. \end{cases}$$

The linearized equation (3.24) reads

$$u_t + \bar{\lambda} u_x = 0, \quad \bar{\lambda} = f'(\bar{u}(u_L, u_R)). \tag{3.25}$$

For the Riemann problem (3.24), (3.25), the solution u is either a shock or a rarefaction; in both cases

$$u \in I_j = [\min(u_j, u_{j+1}), \max(u_j, u_{j+1})]. \tag{3.26}$$

Then the intermediate state $\bar{u}$ must also lie in this interval.

The condition (3.17) here takes the form

$$\bar{u}(u_L, u_R) \to \tilde{u} \text{ smoothly as } u_L, u_R \to \tilde{u}. \tag{3.27}$$

With the choice (3.26) it is automatically satisfied. In Masella *et al.* [64], it was shown that in scalar case the VFRoe scheme is TVD under some conditions. For the sake of completeness, we briefly review the proof.

In the scalar case, the scheme (3.20) may be written in the incremental form,

$$u_j^{n+1} = u_j^n + C_{j+1/2}^n (u_{j+1}^n - u_j^n) - D_{j-1/2}^n (u_j^n - u_{j-1}^n), \tag{3.28}$$

where

$$C_{j+1/2}^n = \frac{\Delta t}{\Delta x} \frac{f(u_j^n) - h_{j+1/2}}{u_{j+1}^n - u_j^n}, \quad D_{j+1/2}^n = \frac{\Delta t}{\Delta x} \frac{f(u_{j+1}^n) - h_{j+1/2}}{u_{j+1}^n - u_j^n}.$$

Here $h_{j+1/2}$ denotes the VFRoe numerical flux at the interface $j + 1/2$. The Harten's criterion [40] states that in order for the scheme (3.28) be TVD, the following conditions must hold,

$$C_{j+1/2}^n \geq 0, \quad D_{j+1/2}^n \geq 0, \quad C_{j+1/2}^n + D_{j+1/2}^n \leq 1, \quad j \in \mathbb{Z}. \tag{3.29}$$

Following [64], let us introduce

$$\alpha_{j+1/2} = \frac{\bar{\lambda}_{j+1/2}^+}{|\bar{\lambda}_{j+1/2}^+|}, \quad \bar{\lambda}_{j+1/2}^+ = \max(\lambda_{j+1/2}, 0), \quad \bar{\lambda}_{j+1/2} = f'(\bar{u}(u_j, u_{j+1})).$$

Then the VFRoe flux is given as

$$h_{j+1/2} = \alpha_{j+1/2} f(u_j^n) + (1 - \alpha_{j+1/2}) f(u_{j+1}^n).$$

Substituting this expression into the first two inequalities of (3.29), we get

$$\bar{\lambda}_{j+1/2}\frac{f(u_{j+1}^n) - f(u_j^n)}{u_{j+1}^n - u_j^n} \geq 0. \tag{3.30}$$

This inequality expresses the fact that the approximate shock speed $\bar{\lambda}_{j+1/2}$ in the solution of the local Riemann problem must have the same sign as the exact shock speed there.

The last inequality of (3.29) gives

$$\begin{aligned}
\frac{\Delta t}{\Delta x}\frac{\bar{\lambda}_{j+1/2}}{|\bar{\lambda}_{j+1/2}|}\frac{f(u_{j+1}^n) - f(u_j^n)}{u_{j+1}^n - u_j^n} &= \frac{\Delta t}{\Delta x}\left|\frac{f(u_{j+1}^n) - f(u_j^n)}{u_{j+1}^n - u_j^n}\right| = \frac{\Delta t}{\Delta x}|f'(u)| \\
&\leq \frac{\Delta t}{\Delta x}\sup_{u\in I_j}|f'(u)| \leq 1, \quad j \in \mathbb{Z}. \tag{3.31}
\end{aligned}$$

Here $I_j = [\min(u_j, u_{j+1}), \max(u_j, u_{j+1})]$. This condition is the usual CFL condition.

To summarize, the VFRoe scheme in the scalar case is TVD if the conditions (3.26), (3.30) and (3.31) are fulfilled.

A sonic entropy fix

The VFRoe scheme will produce entropy-satisfying numerical solutions, if the approximate solution of the Riemann problem is also entropy-satisfying. The approximate Riemann solution for the VFRoe scheme is obtained as in the Roe method. It is well known that it can be entropy-violating.

One can illustrate the problem in the scalar case. Consider the Burgers equation,

$$u_t + \left(\frac{u^2}{2}\right)_x = 0, \tag{3.32}$$

with the initial data

$$u(x,0) = \begin{cases} -1, & x \leq 0 \\ +1, & x > 0. \end{cases} \tag{3.33}$$

In this case, the entropy satisfying Riemann solution is a sonic rarefaction wave. However, both the Roe and the VFRoe schemes will converge to a stationary shock, located at $x = 0$.

In order to cure the problem, one has to modify the approximate Riemann solution. Note that the only case in which we have to do this is when the *sonic* rarefaction occurs. In all other cases the approximate Riemann solver gives the correct value of the intermediate state of the Riemann problem.

One of the popular ways of fixing the entropy-violating shock problem was proposed by Harten and Hyman [41]. Consider the Riemann problem

$$\mathbf{u}_t + \mathbf{f}(\mathbf{u})_x = 0 \tag{3.34}$$

with the initial data

$$\mathbf{u}(x,0) = \begin{cases} \mathbf{u}_L, & x \le 0 \\ \mathbf{u}_R, & x > 0. \end{cases} \tag{3.35}$$

We can linearize (3.34) to get

$$\mathbf{u}_t + \mathbf{A}(\mathbf{u}_L, \mathbf{u}_R)\mathbf{u}_x = 0, \tag{3.36}$$

where $\mathbf{A}$ is a constant matrix. Proceeding as in Section 3.1.2, we rewrite the system (3.36) as p scalar equations,

$$\frac{\partial v_i}{\partial t} + \lambda_i \frac{\partial v_i}{\partial x} = 0, \qquad i = 1, \dots, p,$$

where v_i are the characteristic variables. Thus, each i-wave in the Riemann problem (3.34), (3.35) is approximated by a jump discontinuity of the size

$$a_i = v_{ir} - v_{il}.$$

As we have seen above, this approximation can result in an entropy violating solution. Suppose that there appears to be a sonic rarefaction in the k-th family for some k. Then we introduce the intermediate state

$$v_k^* = \frac{(\lambda_k - \lambda_{kl})v_{kl} + (\lambda_{kr} - \lambda_k)v_{kr}}{\lambda_{kr} - \lambda_{kl}}, \tag{3.37}$$

where

$$\begin{aligned} \lambda_{kl} &= \lambda_k - \delta_k \\ \lambda_{kr} &= \lambda_k + \delta_k, \end{aligned}$$

and δ_k are still to be determined. Once they are known, the state v_k^* is chosen by the conservation requirement. In scalar case, the following choice of δ gives us an entropy satisfying Riemann solution,

$$\delta = \max[0, \lambda - \lambda(v_L), \lambda(v_R) - \lambda]. \tag{3.38}$$

In the case of systems of conservation laws, (3.38) becomes

$$\delta_k = \max[0, \lambda_k - \lambda_k(\mathbf{u}_{kl}), \lambda_k(\mathbf{u}_{kr}) - \lambda_k], \tag{3.39}$$

where

$$\mathbf{u}_{kl} = \mathbf{u}_L + \sum_{i=1}^{k-1} a_i \mathbf{r}_i, \quad \mathbf{u}_{kr} = \mathbf{u}_{kl} + a_k \mathbf{r}_k.$$

It is illuminating to consider the effect of this entropy fix in terms of numerical viscosity. The numerical flux function for the original Roe scheme is

$$\begin{aligned} \mathbf{F}(\mathbf{u}_L, \mathbf{u}_R) &= \frac{1}{2}\Big[\mathbf{f}(\mathbf{u}_L) + \mathbf{f}(\mathbf{u}_R) - \sum_{k=1}^{p} |\lambda_k| a_k \mathbf{r}_k\Big] \tag{3.40} \\ &= \frac{1}{2}\Big[\mathbf{f}(\mathbf{u}_L) + \mathbf{f}(\mathbf{u}_R) - |\mathbf{A}(\mathbf{u}_L, \mathbf{u}_R)|(\mathbf{u}_R - \mathbf{u}_L)\Big]. \end{aligned}$$

The so-called *viscous form* of the Roe scheme will be

$$\mathbf{u}_j^{n+1} = \mathbf{u}_j^n - \frac{\Delta t}{2\Delta x}\big[\mathbf{f}(\mathbf{u}_{j+1}) - \mathbf{f}(\mathbf{u}_{j-1})\big] + \frac{1}{2}\big[\mathbf{Q}_{j+1/2}^n(\mathbf{u}_{j+1}^n - \mathbf{u}_j^n) - \mathbf{Q}_{j-1/2}^n(\mathbf{u}_j^n - \mathbf{u}_{j-1}^n)\big],$$
(3.41)

where the *numerical viscosity matrix* is

$$\mathbf{Q}_{j+1/2} = \mathbf{Q}(\mathbf{u}_j, \mathbf{u}_{j+1}) = \frac{\Delta t}{\Delta x}|\mathbf{A}(\mathbf{u}_j, \mathbf{u}_{j+1})|.$$

Note that the second brackets on the right of (3.41) mimic a diffusive-like term $\Delta x(\mathbf{Q}\mathbf{u}_x)_x$, see Tadmor [86].

In Harten and Hyman [41], it was shown that the introduction of the intermediate state (3.37) changes the numerical flux of the Roe scheme as follows,

$$\mathbf{F}(\mathbf{u}_L, \mathbf{u}_R) = \frac{1}{2}\big[\mathbf{f}(\mathbf{u}_L) + \mathbf{f}(\mathbf{u}_R) - \sum_{k=1}^p Q_k(\lambda_k)a_k\mathbf{r}_k\big],$$
(3.42)

where

$$Q_k(x) = \begin{cases} |x|, & |x| \geq \delta_k \\ \delta_k, & |x| < \delta_k, \end{cases}$$

and δ_k are given by (3.39). Comparing the expression (3.42) with (3.40) one sees that this corresponds to modifying the λ_k where they are small, i.e. in the neighborhood of sonic points. In terms of viscosity, it amounts to modifying the viscosity matrix $\mathbf{Q}_{j+1/2}$ in (3.41).

The VFRoe scheme is a combination of Godunov's and Roe's methods. For the Godunov method, it is known that it posesses minimal numerical viscosity [85]. Following [64], we add a large amount of viscosity to the VFRoe scheme at sonic points by taking

$$\mathbf{u}^* = \begin{cases} \dfrac{\mathbf{u}_L + \mathbf{u}_R}{2}, & \text{if } \lambda_k(\mathbf{u}_L) < 0 < \lambda_k(\mathbf{u}_R), \\ \mathbf{u}_L + \displaystyle\sum_{\lambda_i<0} a_i\mathbf{r}_i, & \text{otherwise.} \end{cases}$$

The numerical examples of [64] show the perfect resolution of sonic rarefaction waves with such choice of $\mathbf{u}^*$.

Positivity preservation

As was mentioned in Remark 3.4, the Roe scheme may generate nonphysical intermediate states, e.g. negative pressures or densities. Also, the eigenvalues λ_k of the linearized Jacobian matrix can lie outside of the range of the values $(\lambda_k(\mathbf{u}_j), \lambda_k(\mathbf{u}_{j+1}))$, see Einfeldt *et al.* [30] and Vinokur [94].

The VFRoe scheme will also suffer from these drawbacks. In the series of papers [15], [34], [35], [36], [64] Gallouët and coworkers have intensively investigated

the following approach to deal with the problem of positivity non-preservation of the VFRoe scheme. The key idea is that the solution of the Riemann problem should not necessarily be computed in the conservative variables. Indeed, regardless of the choice of state variables one has a conservative and consistent scheme. For the Euler equations, several choices of primitive variables have been considered, e.g. (ρ, u, p), (τ, u, p), (s, u, p), where $\tau = 1/\rho$ is the specific mass and the other notations have their usual meanings. For all cases one can point out conditions, under which the intermediate pressure and density remain positive.

3.2 A numerical method for generic model

The governing equations for the generic model (2.13) consist of the differential part and the non-differential source terms. To account for both parts, we employ the popular operator splitting approach due to Strang [84]. Denote by L_h^t the solution operator over the time t of the homogeneous part of the hyperbolic system (2.13)

$$\frac{\partial \alpha_a}{\partial t} + U\frac{\partial \alpha_a}{\partial x} = 0 \tag{3.43a}$$

$$\frac{\partial \mathbf{u}}{\partial t} + \frac{\partial \mathbf{f}(\mathbf{u}, \alpha_a)}{\partial x} = \mathbf{h}(\mathbf{u}, \alpha_a)\frac{\partial \alpha_a}{\partial x}, \tag{3.43b}$$

where

$$\mathbf{u} = \begin{bmatrix} \alpha_a\rho_a \\ \alpha_a\rho_a u_a \\ \alpha_a\rho_a E_a \\ \alpha_b\rho_b \\ \alpha_b\rho_b u_b \\ \alpha_b\rho_b E_b \end{bmatrix}, \quad \mathbf{f}(\mathbf{u}, \alpha_a) = \begin{bmatrix} \alpha_a\rho_a u_a \\ \alpha_a\rho_a u_a^2 + \alpha_a p_a \\ \alpha_a u_a(\rho_a E_a + p_a) \\ \alpha_b\rho_b u_b \\ \alpha_b\rho_b u_b^2 + \alpha_b p_b \\ \alpha_b u_b(\rho_b E_b + p_b) \end{bmatrix}, \quad \mathbf{h}(\mathbf{u}, \alpha_a) = \begin{bmatrix} 0 \\ P \\ PU \\ 0 \\ -P \\ -PU \end{bmatrix}. \tag{3.44}$$

Also, denote by L_s^t the solution operator over the time t for the system of ordinary differential equations

$$\frac{\partial \hat{\mathbf{u}}}{\partial t} = \mathbf{S}, \qquad \hat{\mathbf{u}} = \begin{pmatrix} \alpha_a \\ \mathbf{u} \end{pmatrix}, \qquad \mathbf{S} = (\mathcal{S}_a, 0, \mathcal{M}, \mathcal{E}, 0, -\mathcal{M}, -\mathcal{E})^T, \tag{3.45}$$

where $\mathbf{u}$ is given by (3.44). Then the Strang splitting approach updates the solution to the system (2.13) at the next time level by alternating between L_h and L_s in the following way,

$$\hat{\mathbf{u}}_j^{n+1} = L_s^{\Delta t/2} L_h^{\Delta t} L_s^{\Delta t/2} \hat{\mathbf{u}}_j^n. \tag{3.46}$$

Below we will give the details on the operators L_h and L_s.

3.2.1 Integration of source terms

It is clear that the non-differential source terms of the system (2.13) normally would have a very complicated form. Indeed, they describe various kinds of phase interactions together with mass, momentum, and energy exchanges which are usually given only heuristically. Moreover, the corresponding terms have different expressions for different kinds of two-phase flows.

However, independently of the particular form of these terms, they all can be more or less easily integrated into the framework of the Strang splitting technique (3.46). Therefore, we do not pursue the problem of finding the exact expressions for the source terms of (2.13). Instead, we consider only some relatively simple terms, which model several important processes of the phase interaction. These are the velocity and pressure relaxation procedures. Since the model (2.13) allows for two different phase velocities and pressures in the same point of the physical domain, there should be some relaxation mechanism, which drives them to equilibrium. In many applications, these non-equilibrium processes occur very rapidly, so that one can consider them as instantaneous. Then, their numerical integration can be performed as described in Saurel and Abgrall [75], Lallemand and Saurel [56]. In this work, we use these procedures unchanged.

Numerically, the interphase source terms tend to effectively increase the amount of numerical viscosity in the method. Indeed, the use of instantaneous velocity and pressure relaxation forces the velocities and the pressures of the phases to be equal at the end of each time step. Imagine we have sharp discontinuities in both phases, moving with different speeds. Then, the action of the relaxation procedures results in smearing of these discontinuities. See Tiselj and Petelin [88], Kapila *et al.* [48] for discussion of the effect of the instantaneous relaxation and its justification.

3.2.2 Hyperbolic operator

Consider again the homogeneous hyperbolic system (3.43). Following the idea of [75], we want to find a discretization of its non-conservative part, i.e. the transport equation for α_a (3.43a) and the term $\mathbf{h}\frac{\partial \alpha_a}{\partial x}$ in (3.43b) in such a way, that the numerical approximation to the system would preserve a contact discontinuity. Imagine we have some Godunov-type discretization of (3.43b), i.e.

$$\mathbf{u}_j^{n+1} = \mathbf{u}_j^n - \frac{\Delta t}{\Delta x}\left[\mathbf{f}(\mathbf{u}^*(\mathbf{u}_j^n,\mathbf{u}_{j+1}^n)) - \mathbf{f}(\mathbf{u}^*(\mathbf{u}_{j-1}^n,\mathbf{u}_j^n))\right] + \Delta t\,\mathbf{h}_j\Delta_j, \qquad (3.47)$$

where Δ_j is some discrete form of $\frac{\partial \alpha_a}{\partial x}$, which is still to be determined, and $\mathbf{u}^*(\mathbf{u}_j^n,\mathbf{u}_{j+1}^n)$ the value of $\mathbf{u}$ along the line $x = x_{j+1/2}$ for the Riemann problem with the states $\mathbf{u}_j^n, \mathbf{u}_{j+1}^n$, see Fig. 3.1. Rewriting the scheme (3.47) componentwise, we get
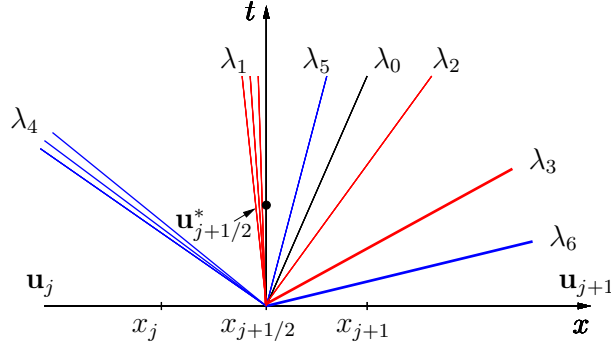
Fig. 3.1. A typical Riemann problem, λ_i are given by (2.41).

$$
\begin{aligned}
(\alpha\rho)_j^{n+1} &= (\alpha\rho)_j^n - \frac{\Delta t}{\Delta x}\left[(\alpha\rho u)_{j+1/2}^* - (\alpha\rho u)_{j-1/2}^*\right] \\
(\alpha\rho u)_j^{n+1} &= (\alpha\rho u)_j^n - \frac{\Delta t}{\Delta x}\left[(\alpha\rho u^2 + \alpha p)_{j+1/2}^* - (\alpha\rho u^2 + \alpha p)_{j-1/2}^*\right] \\
&\quad + \Delta t\, P_j^n \Delta_j \\
(\alpha\rho E)_j^{n+1} &= (\alpha\rho E)_j^n - \frac{\Delta t}{\Delta x}\left[(\alpha\rho u E + \alpha p u)_{j+1/2}^* - (\alpha\rho u E + \alpha p u)_{j-1/2}^*\right] \\
&\quad + \Delta t\, P_j^n U_j^n \Delta_j,
\end{aligned}
\tag{3.48}
$$

where we have omitted the subscript a or b for brevity.

Assume for the moment that the state $\mathbf{u}_{j+1/2}^*$ has been determined. Then discretizations for Δ_j and for the transport equation of α_a (3.43a) are obtained as follows. According to a principle due to Abgrall [1], a flow, uniform in pressure and velocity must remain uniform in the same variables during its time evolution, i.e. a contact dicontinuity is preserved. In other words, if we had constant pressure and velocity everywhere in a flow at the time level t^n, then we will get the same pressure and velocity at the time t^{n+1}. Substituting constant pressures and velocities in the numerical scheme (3.48) we get

$$
\begin{aligned}
u_j^n = u_j^{n+1} &= u_{j\pm1/2}^* = U_j = u = \text{const}, \\
p_j^n = p_j^{n+1} &= p_{j\pm1/2}^* = P_j = p = \text{const}.
\end{aligned}
\tag{3.49}
$$

The first two equations of (3.48) will be

$$
(\alpha\rho)_j^{n+1} = (\alpha\rho)_j^n - u\frac{\Delta t}{\Delta x}\left[(\alpha\rho)_{j+1/2}^* - (\alpha\rho)_{j-1/2}^*\right],
\tag{3.50}
$$

$$
\begin{aligned}
(\alpha\rho)_j^{n+1}u &= (\alpha\rho)_j^n u - \frac{\Delta t}{\Delta x}\big[(\alpha\rho)_{j+1/2}^* u^2 + \alpha_{j+1/2}^* p \\
&\quad - (\alpha\rho)_{j-1/2}^* u^2 - \alpha_{j-1/2}^* p\big] + \Delta t\, p\Delta_j.
\end{aligned}
\tag{3.51}
$$

Multiplying (3.50) by u and substracting the result from (3.51), we get a discretization for Δ_j,

$$\Delta_j = \frac{1}{\Delta x}(\alpha^*_{j+1/2} - \alpha^*_{j-1/2}). \tag{3.52}$$

Using the definition of E and (3.52) in the last equation of (3.48), and combining it with (3.50), we get for internal energy,

$$(\alpha \rho e)^{n+1}_j = (\alpha \rho e)^n_j - \frac{\Delta t}{\Delta x} \left[(\alpha \rho e)^*_{j+1/2} u - (\alpha \rho e)^*_{j-1/2} u \right].$$

Now using the equation of state (2.37) and the uniformity of pressure,

$$\rho e = \frac{p + \gamma \pi}{\gamma - 1} = \text{const},$$

one gets

$$\alpha^{n+1}_j = \alpha^n_j - u \frac{\Delta t}{\Delta x}(\alpha^*_{j+1/2} - \alpha^*_{j-1/2}). \tag{3.53}$$

Note that we have obtained this equation assuming that the velocities and pressures are uniform, see (3.49). If we substitute U_j instead of u in (3.53), we can use it as a discretization of the transport equation (3.43a).

To summarize, the Godunov-type scheme for the system (3.43) reads

$$\begin{aligned} \alpha^{n+1}_j &= \alpha^n_j - U^n_j \frac{\Delta t}{\Delta x}(\alpha^*_{j+1/2} - \alpha^*_{j-1/2}) \\ \mathbf{u}^{n+1}_j &= \mathbf{u}^n_j - \frac{\Delta t}{\Delta x} \left[\mathbf{f}(\mathbf{u}^*(\mathbf{u}^n_j, \mathbf{u}^n_{j+1})) - \mathbf{f}(\mathbf{u}^*(\mathbf{u}^n_{j-1}, \mathbf{u}^n_j)) \right] + \Delta t \, \mathbf{h}_j \Delta_j, \end{aligned} \tag{3.54}$$

where $\Delta_j = \frac{1}{\Delta x}(\alpha^*_{j+1/2} - \alpha^*_{j-1/2})$. In the following subsection we will specify $\mathbf{u}^*_{j+1/2}$, the intermediate value of the solution of the Riemann problem.

3.2.3   Approximate solution to the Riemann problem

As we have discussed at the beginning of this chapter, finding the exact solution to the Riemann problem for the system (2.13) is complicated. Even if we would find it, it would be too complicated to use it at each cell boundary, as it needed for the scheme (3.54). Therefore, we have to look for some approximate Riemann solver. Here, we adopt the approach due to Gallouët and Masella [33], which we have already considered in case of conservation laws, see Section 3.1.3.

Let us rewrite the homogeneous hyperbolic system (3.43) in primitive variables,

$$\frac{\partial \mathbf{v}}{\partial t} + \mathbf{A}(\mathbf{v})\frac{\partial \mathbf{v}}{\partial x} = 0, \tag{3.55}$$

where $\mathbf{v}$, $\mathbf{A}(\mathbf{v})$ are given by (2.39), (2.40). Consider the Riemann problem for (3.55) at each cell boundary $j + 1/2$, i.e. with the following initial data

$$\mathbf{v}(x,0) = \begin{cases} \mathbf{v}_j, & x \leq x_{j+1/2} \\ \mathbf{v}_{j+1}, & x > x_{j+1/2}. \end{cases} \tag{3.56}$$

Following [33], we calculate the Jacobian matrix $\mathbf{A}(\bar{\mathbf{v}})$ in the average state

$$\bar{\mathbf{v}}_{j+1/2} = \frac{\mathbf{v}_j + \mathbf{v}_{j+1}}{2}.$$

The intermediate state in the solution of the Riemann problem (3.55), (3.56) is

$$\mathbf{v}^*_{j+1/2} = \mathbf{v}_j + \sum_{\lambda_i < 0} a_i \mathbf{r}_i,$$

where the eigenvalues λ_i and the eigenvectors $\mathbf{r}_i$ of the matrix $\mathbf{A}(\bar{\mathbf{v}}_{j+1/2})$ are given by (2.41), (2.42)-(2.44), and a_i are the coefficients of eigenvector decomposition of $\mathbf{v}_{j+1} - \mathbf{v}_j$,

$$\mathbf{v}_{j+1} - \mathbf{v}_j = \sum_{i=0}^{6} a_i \mathbf{r}_i.$$

With the choice of the primitive variables (2.39), they are given by the following expressions,

$$
\begin{aligned}
a_0 &= \Delta_1/r_{01}, \\
a_3 &= \frac{\Delta_3 \rho_a c_a + \Delta_4 - a_0(r_{03}\rho_a c_a + r_{04})}{2\rho_a c_a^2}, \\
a_1 &= \frac{-\Delta_3 \rho_a c_a + \Delta_4 + a_0(r_{03}\rho_a c_a - r_{04})}{2\rho_a c_a^2}, \\
a_2 &= \Delta_2 - a_0 r_{02} - \rho_a(a_1 + a_3), \\
a_6 &= \frac{\Delta_6 \rho_b c_b + \Delta_7 - a_0(r_{06}\rho_b c_b + r_{07})}{2\rho_b c_b^2}, \\
a_4 &= \frac{-\Delta_6 \rho_b c_b + \Delta_7 + a_0(r_{06}\rho_b c_b - r_{07})}{2\rho_b c_b^2}, \\
a_5 &= \Delta_5 - a_0 r_{05} - \rho_b(a_4 + a_6),
\end{aligned}
$$

where r_{0k} are the components of $\mathbf{r}_0$, Δ_k is the k-th component of $\mathbf{v}_{j+1} - \mathbf{v}_j$.

Recalculating $\mathbf{v}^*_{j+1/2}$ into the conservative vector $\mathbf{u}^*_{j+1/2}$, we fully determine the Godunov-type scheme (3.54) for the homogeneous system (3.43).

3.2.4 Extension to the second order

We use the MUSCL piecewise linear data reconstruction to achieve second order in space. For second order in time, we employ a predictor-corrector scheme. The solution procedure can be summarized as follows.

Extrapolation. Given piecewise constant values $\mathbf{v}_j^n$, we obtain the linearly extrapolated values

$$\mathbf{v}_{j-1/2}^+ = \mathbf{v}_j^n - \frac{1}{2}\bar{\sigma}_j, \qquad \mathbf{v}_{j+1/2}^- = \mathbf{v}_j^n + \frac{1}{2}\bar{\sigma}_j.$$

The essential point is that this step is performed in primitive variables

$$\mathbf{v} = (\alpha_a, \rho_a, u_a, p_a, \rho_b, u_b, p_b)^T,$$

cf. (2.39); this ensures preservation of uniformity of pressure and velocity. We limit the slopes $\bar{\sigma}_j$ according to the usual TVD constraints. We take $\bar{\sigma}_j$ in the the following form,

$$\bar{\sigma}_j = \left\{ \begin{array}{ll} \max[0, \min(\beta\Delta_{j-1/2}, \Delta_{j+1/2}), \min(\Delta_{j-1/2}, \beta\Delta_{j+1/2})], & \Delta_{j+1/2} > 0, \\ \min[0, \max(\beta\Delta_{j-1/2}, \Delta_{j+1/2}), \max(\Delta_{j-1/2}, \beta\Delta_{j+1/2})], & \Delta_{j+1/2} < 0, \end{array} \right.$$

where

$$\Delta_{j-1/2} = \mathbf{v}_j^n - \mathbf{v}_{j-1}^n, \qquad \Delta_{j+1/2} = \mathbf{v}_{j+1}^n - \mathbf{v}_j^n.$$

In particular, $\beta = 1$ corresponds to the minmod limiter, $\beta = 2$ to the superbee limiter.

Predictor. We evolve the values of $\mathbf{v}_{j\mp1/2}^\pm$ according to

$$\begin{aligned} \bar{\mathbf{v}}_{j-1/2}^+ &= \mathbf{v}_{j-1/2}^+ - \frac{\Delta t}{2\Delta x}\mathbf{A}(\mathbf{v}_j)(\mathbf{v}_{j+1/2}^- - \mathbf{v}_{j-1/2}^+) \\ \bar{\mathbf{v}}_{j+1/2}^- &= \mathbf{v}_{j+1/2}^- - \frac{\Delta t}{2\Delta x}\mathbf{A}(\mathbf{v}_j)(\mathbf{v}_{j+1/2}^- - \mathbf{v}_{j-1/2}^+) \end{aligned}$$

where the matrix $\mathbf{A}(\mathbf{v})$ is given by (2.40).

Next, we rewrite the vectors $\bar{\mathbf{v}}_{j\pm1/2}^\pm$ in conservative variables, solve the Riemann problems with piecewise constant data $(\bar{\mathbf{u}}_{j+1/2}^-, \bar{\mathbf{u}}_{j+1/2}^+)$ and get the intermediate states $\mathbf{u}_{j+1/2}^*$.

Corrector. We update the solution on the next time level according to

$$\begin{aligned} \alpha_j^{n+1} &= \alpha_j^n - U_j^n\frac{\Delta t}{\Delta x}(\bar{\alpha}_{j+1/2}^* - \bar{\alpha}_{j-1/2}^*) \\ \mathbf{u}_j^{n+1} &= \mathbf{u}_j^n - \frac{\Delta t}{\Delta x}\left[\mathbf{f}(\mathbf{u}^*(\bar{\mathbf{u}}_{j+1/2}^-, \bar{\mathbf{u}}_{j+1/2}^+)) - \mathbf{f}(\mathbf{u}^*(\bar{\mathbf{u}}_{j-1/2}^-, \bar{\mathbf{u}}_{j-1/2}^+))\right] \\ &\quad + \Delta t\,\mathbf{h}_j\Delta_j, \end{aligned}$$

where $\Delta_j = \frac{1}{\Delta x}(\bar{\alpha}_{j+1/2}^* - \bar{\alpha}_{j-1/2}^*)$.

3.3   Numerical results

To assess the perfomance of the new scheme we have used it for all submodels of Section 2.3. Here, we present the results for the SA model [75], the results for the BN model and for the Euler equations in a duct see in Chapters 4 and 5, respectively. Everywhere in this section, we have used the SA ansatz for the interface velocity and pressure (2.14)

$$U = \frac{\alpha_a \rho_a u_a + \alpha_b \rho_b u_b}{\alpha_a \rho_a + \alpha_b \rho_b}, \qquad P = \alpha_a p_a + \alpha_b p_b. \tag{3.57}$$

For testing of the new scheme we have chosen most of the test problems of Saurel and Abgrall [75]. Each problem was solved with the new scheme and with the original method of [75]. In what follows, the new scheme will be referred to as VFRoe, and the original method of [75] to as HLL due to the Harten-Lax-van Leer numerical flux function used there. The calculations were made with the second order accurate scheme using a CFL number of 0.9. The numerical results were then compared with the exact solution for the first two problems and with the experimental data for the third problem.

3.3.1   Water-air shock tube

We consider the shock tube filled with liquid water (phase b) under high pressure at the left, and with the gas (phase a) at the right. Each fluid is governed by the stiffened gas EOS

$$p_k = (\gamma_k - 1)\rho_k e_k - \gamma_k \pi_k, \quad k = a, b,$$

with the following parameters

	Liquid	Gas
	$\gamma_b = 4.4$	$\gamma_a = 1.4$
	$\pi_b = 6 \cdot 10^8$	$\pi_a = 0.$

The initial conditions for the system (2.13) are

Left:	$x \leq 0.7$	Right:	$x > 0.7$	
	$\rho_b = 1000$ kg/m^3		$\rho_a = 50$ kg/m^3	
	$p_b = 10^9$ Pa		$p_a = 10^6$ Pa	(3.58)
	$u_b = 0$ m/s		$u_a = 0$ m/s	
	$\alpha_b = 1$		$\alpha_a = 1.$	

Note that at the both sides of the interface the system (2.13) reduces to the Euler equations for liquid and gas. The solution of the Riemann problem (2.13), (3.58) is schematically depicted in Fig. 3.2. Using that $p_a^* = p_b^*$, $u_a^* = u_b^*$, we can get the exact solution to the Riemann problem.
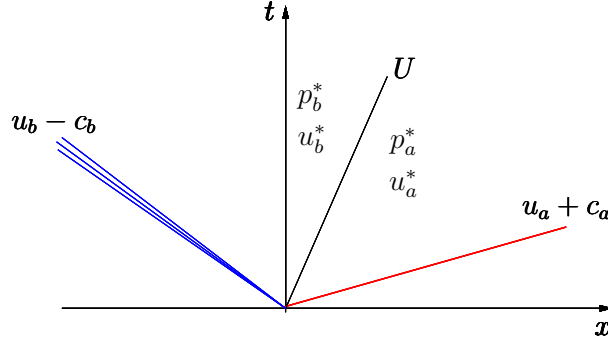
Fig. 3.2. The Riemann problem (2.13)-(3.58). The interface $x/t = U$ separates the phases, liquid at the left and gas at the right.

To solve it numerically, we allow the presence of a negligibly small amount of gas, e.g. $\alpha_a = 10^{-8}$, at the left of the shock tube, and a small amount of water at the right. Thus the initial data will be as follows,

$$
\begin{array}{llll}
\text{Left:} & x \leq 0.7 & \text{Right:} & x > 0.7 \\
& \rho_a = 50 \text{ kg/m}^3 & & \rho_a = 50 \text{ kg/m}^3 \\
& \rho_b = 1000 \text{ kg/m}^3 & & \rho_b = 1000 \text{ kg/m}^3 \\
& p_a = p_b = 10^9 \text{ Pa} & & p_a = p_b = 10^6 \text{ Pa} \\
& u_a = u_b = 0 \text{ m/s} & & u_a = u_b = 0 \text{ m/s} \\
& \alpha_a = 10^{-8} & & \alpha_b = 10^{-8}.
\end{array}
\tag{3.59}
$$

For this problem, we use both the pressure and velocity relaxation procedures [56, 75]. We consider the exact solution of (2.13), (3.58) to be a reference solution for the numerical solution of (2.13), (3.59), having in mind that we have the exact solution for the liquid at the left, and for the gas at the right.

The comparison of the numerical results for the VFRoe and HLL solvers with the exact solution at time $t = 2.2\text{e-}4$ is presented in Fig. 3.3-3.5. As expected, the VFRoe solver gives a much sharper resolution of discontinuities compared to HLL. The numerical results, obtained with the VFRoe scheme over 100 mesh cells are comparable to the results of HLL over 300 mesh cells. The calculations with 1000 mesh cells show that the shock speeds are also correctly computed.

In Fig. 3.3, some peaks are visible in the gas parameters at the left of the interface, and in the liquid parameters to the right of it. We have observed this behavior of the solution with the both HLL and VFRoe schemes. As mentioned before, it is not possible to fully compare these numerical results for initial data (3.59) with the reference solution to the system (2.13) with initial data (3.58).

In Fig. 3.4-3.5 the distributions of the mixture density,

$$
\rho_{\text{mix}} = \alpha_a \rho_a + \alpha_b \rho_b,
$$
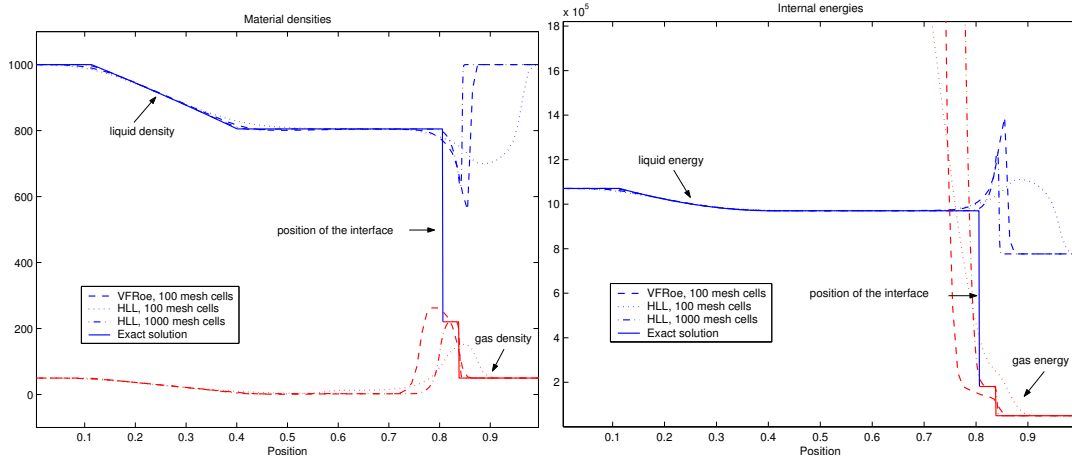
Fig. 3.3. Water-air shock tube, material densities and energies of the phases.
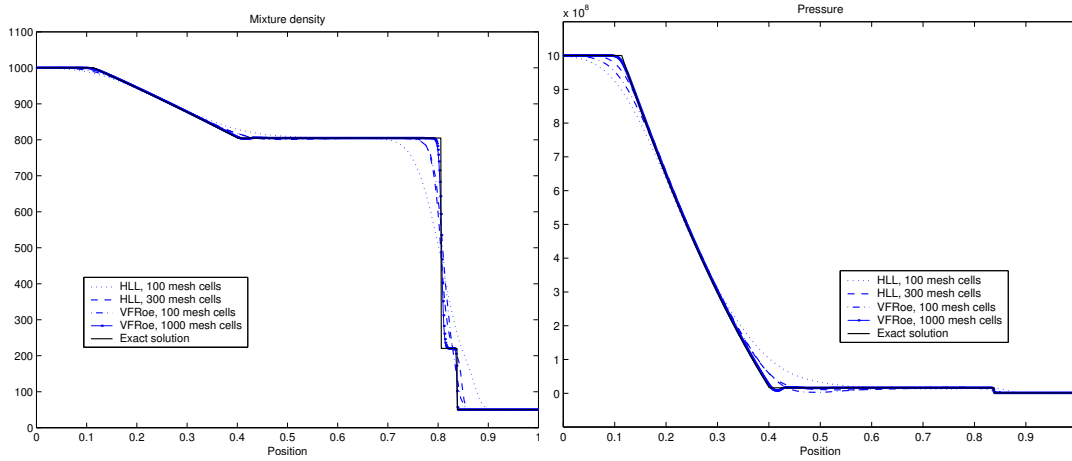
Fig. 3.4. Water-air shock tube, mixture density and pressure.

the relaxed pressures and velocities

$$p = p_a = p_b$$

$$u = u_a = u_b,$$

and gas volume fraction α_a are presented. The reference solution for the gas volume fraction is obtained as follows. Knowing the interface velocity U from the solution of the Riemann problem (2.13) with initial data (3.58), we find the displacement of the interface ΔS over the time Δt as

$$\Delta S = U \, \Delta t.$$
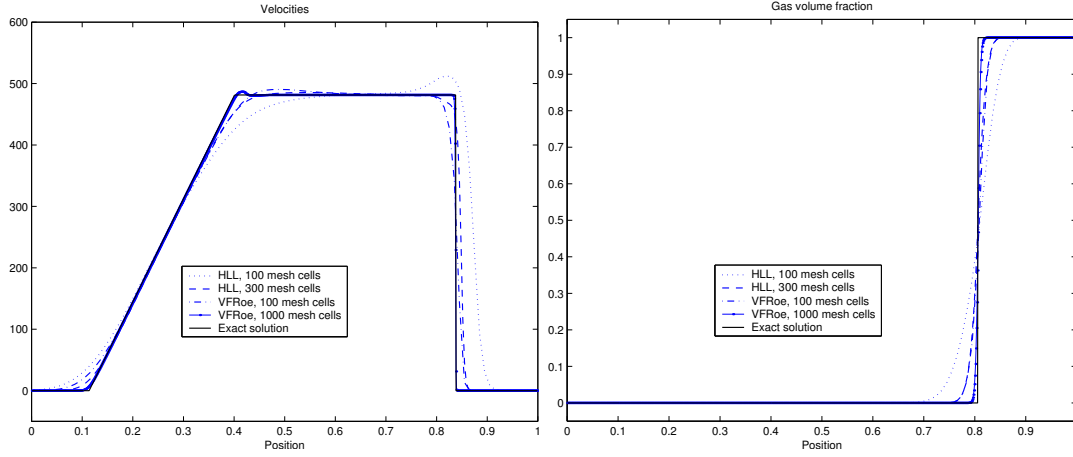
Fig. 3.5. Water-air shock tube, velocities and gas volume fraction.

In some extreme situations with very large ratios of initial pressures and densities, the VFRoe solver fails to preserve positivity of density of pressure in the intermediate state of the Riemann problem. The problem of positivity preservation of the VFRoe solver is an interesting question and will be the subject of future research.

3.3.2   Water faucet problem

This test, which is due to Ransom [71], consists of a vertical tube 12 m in length, which contains a liquid (water) column, surrounded by gas (air). At the top, the volume fractions and the liquid velocity are given, and the gas velocity is zero. The bottom is open to atmospheric conditions. Under the action of gravity, a narrowing of the liquid jet takes place. Several stages of the process are depicted in Fig. 3.6.

The initial conditions are as follows,

$$
\begin{array}{ll}
\text{Liquid} & \text{Gas} \\
\rho_b = 1000 \text{ kg/m}^3 & \rho_a = 1 \text{ kg/m}^3 \\
p_b = 10^5 \text{ Pa} & p_a = 10^5 \text{ Pa} \\
u_b = 10 \text{ m/s} & u_a = 0 \text{ m/s} \\
\alpha_b = 0.8 & \alpha_a = 0.2.
\end{array}
\tag{3.60}
$$

The boundary conditions are

$$
\begin{array}{lll}
& \text{Liquid} & \text{Gas} \\
\text{Top(inflow)} & u_b = 10 \text{ m/s} & u_a = 0 \text{ m/s} \\
& \alpha_b = 0.8 & \alpha_a = 0.2 \\
\text{Bottom(outflow)} & p_b = 10^5 \text{ Pa} & p_a = 10^5 \text{ Pa} \\
& \alpha_b, \alpha_a \text{ are extrapolated,}
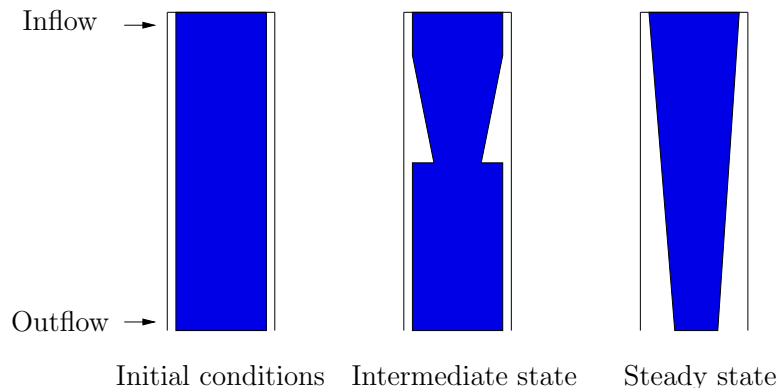\end{array}
\tag{3.61}
$$

Fig. 3.6. Water faucet problem.

other flow variables are found by the solution of the boundary Riemann problem for the phases at the top and at the bottom of the tube.

Under the assumption that the liquid is incompressible and the pressure variation in gas is zero, one can get the exact solution for the evolution of the gas volume fraction,

$$
\alpha_a(x,t) = \begin{cases} 1 - \frac{(1-\alpha_a^0)u_b^0}{\sqrt{2gx+(u_b^0)^2}}, & x \le u_b^0 t + \frac{gt^2}{2}, \\ 0.2, & \text{otherwise.} \end{cases}
$$

where α_a^0 is the initial gas volume fraction, u_b^0 the initial liquid velocity, g the gravity acceleration, see e.g. Coquel *et al.* [19]. For the numerical solution of the problem, the parameters of the stiffened gas EOS were taken as follows,

Liquid	Gas
$\gamma_b = 4.4$	$\gamma_a = 1.4$
$\pi_b = 6 \cdot 10^6$	$\pi_a = 0.$

For this problem, only the pressure relaxation, not the velocity relaxation was used, because the phases have two distinct velocities. The comparison of the numerical results with the exact solution is presented in Fig. 3.7.

Again, the VFRoe solver gives better results compared to that of HLL solver. The resolution of the discontinuity in gas volume fraction is not perfect, which is due to the following reasons. The sound speed in the liquid is much higher than that of the gas, so one has to choose very small time steps in order to satisfy the CFL condition, which leads to numerical inaccuracies. Further, the gas pressure is not always constant along the tube, which causes a gas flow in the negative direction and thus smearing of the interface.
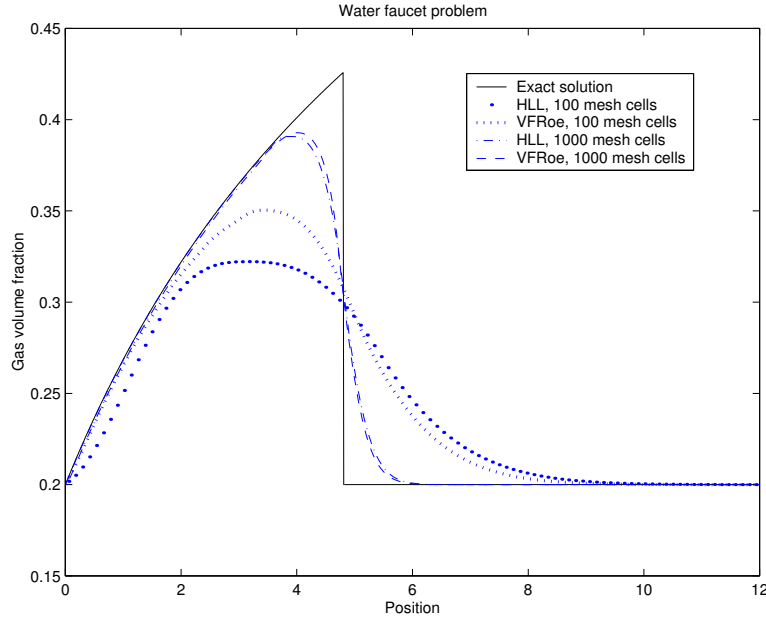
Fig. 3.7. Water faucet problem: gas volume fraction at $t = 0.4$.

3.3.3 Mixture Hugoniot test problem

Description

Consider a two-phase mixture, where each component k is governed by the stiffened gas EOS,

$$p_k = (\gamma_k - 1)\rho_k e_k - \gamma_k \pi_k, \quad k = a, b.$$

In this test, we are interested in mixtures of solid materials, which can be considered as compressible under high pressures. One can determine the constants γ_k, π_k for some materials from Marsh [63]. The corresponding values are summarized in Table 3.1.

	γ	π, 10^9 Pa
Copper	4.22	32.32
Zinc	4.17	15.71
Epoxy	2.94	3.21
Spinel	1.62	141.45

Table 3.1. Thermodynamic constants for selected materials.

Consider a shock wave propagating in two-phase mixtures of copper/zinc (brass) and epoxy/spinel. Using the constants from Table 3.1, we can calculate the shock speed in the mixtures of solids with the two-phase flow model and the numerical method described previously. This shock speed can also be

	Γ	Π, 10^9 Pa
Brass (copper/zinc)	4.20	27.49
Epoxy/Spinel	2.04	77.85

Table 3.2. Thermodynamic constants for selected mixtures.

estimated from the Rankine-Hugoniot conditions of the mixture Euler equations closed by an appropriate equation of state. Such type of mixture equation of state is described in Massoni *et al.* [65]. Both numerical results are compared with the experimental data of Marsh [63].

Two-phase flow model

There are no classical Rankine-Hugoniot conditions for the system (2.13), so we cannot find the shock speed analytically. The approach we use here is straightforward. We calculate the shock speed as the ratio of the biggest (and the only one, in case of a single shock wave) pressure gradient displacement over the time interval.

Euler equations coupled with the mixture EOS

For the Euler equations, we can find the shock speed analytically from the Rankine-Hugoniot jump relations. To close the system, we use the mixture EOS due to Massoni *et al.* [65]. It is based on the conservation of the energy and mass of the mixture, and on the equality of pressures between phases. It reads

$$P = (\Gamma - 1)\rho e - \Gamma\Pi,$$

where ρ is the mixture density, e the mixture internal energy,

$$\Gamma = 1 + \frac{1}{\frac{\alpha_a}{\gamma_a - 1} + \frac{\alpha_b}{\gamma_b - 1}}, \quad \Pi = \frac{\Gamma - 1}{\Gamma}\left(\alpha_a \frac{\gamma_a \pi_a}{\gamma_a - 1} + \alpha_b \frac{\gamma_b \pi_b}{\gamma_b - 1}\right),$$

and α_k, γ_k, π_k are the volume fractions and the thermodynamic constants for the phase $k = a, b$. The constants Γ, Π for the mixtures copper/zinc and epoxy/spinel are given in Table 3.2.
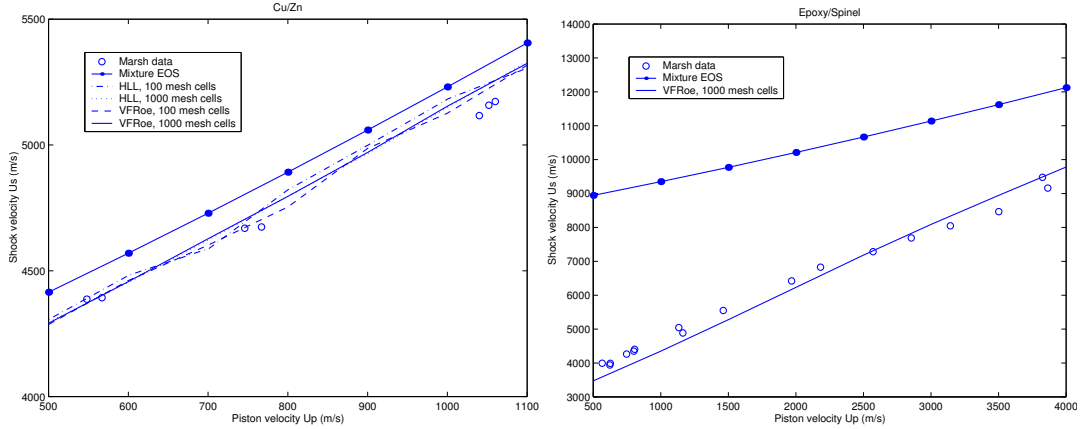
Fig. 3.8. Mixture Hugoniot problem.

Numerical results

Consider the two sets of initial data for the copper/zinc mixture (brass),

Copper	Zinc
$\rho_a = 8924$ kg/m^3	$\rho_b = 7139$ kg/m^3
$p_a = 10^5$ Pa	$p_b = 10^5$ Pa
$u_a = 0$ m/s	$u_b = 0$ m/s
$\alpha_a = 0.71$	$\alpha_b = 1 - \alpha_a,$

and the epoxy/spinel mixture,

Epoxy	Spinel
$\rho_a = 1185$ kg/m^3	$\rho_b = 3622$ kg/m^3
$p_a = 10^5$ Pa	$p_b = 10^5$ Pa
$u_a = 0$ m/s	$u_b = 0$ m/s
$\alpha_a = 0.595$	$\alpha_b = 1 - \alpha_a.$

We use a piston boundary condition on the left side to initiate the shock wave. The comparison of the calculated shock speed U_s as a function of piston velocity U_p with the experimental data of Marsh [63] is presented in Fig. 3.8.

The two-phase flow model gives a very good prediction of the shock speed even on 100 mesh cells compared to the Euler equations for the mixture. Note that the two-phase model does not need any empirically determined parameter. Only the pure material equations of state are used, in conjunction with the hyperbolic solver and relaxation procedures. The results of the VFRoe and HLL solvers do not differ qualitatively on 100 mesh cells. They both show some slight deviations from the experimental results. This is due to the non-accurate way of determining the shock speed for the two-phase flow model. Nevertheless, the results with 1000 cells show an excellent agreement with the experimental data.

Chapter 4

Analysis of the Baer-Nunziato model of two-phase flows

In order to carry out the mathematical analysis of the generic model (2.13) introduced in Chapter 2, one has to use some relatively simple ansatz for the interface velocity and pressure. It appears that the ansatz of Saurel and Abgrall, which leads to the SA model [75], is too complicated for this goal, see Section 2.6. On the other hand, however, it gives good results for a variety of two-phase flows, see Section 3.3.

In choosing more simple expressions for the interface velocity and pressure, the next model is the BN model for the deflagration-to-detonation transition (DDT) in gas-permeable, reactive granular materials, see Section 2.3. The characteristic analysis of this model was carried out by Embid and Baer [31] and is briefly presented in Section 2.6. In this chapter, we will be mostly concerned with the Riemann problem for this model. We have two main reasons for being interested in it.

Firstly, the solution of the Riemann problem provides a building block for a large variety of Godunov-type schemes, cf. the schemes discussed in Chapter 3. Understanding the structure of the Riemann problem would give us information for constructing efficient numerical schemes. Also, as we will shortly see, the solution to the Riemann problem is interesting on its own: The non-strict hyperbolicity of the governing equations results in a complicated wave structure of the Riemann problem, see Section 4.5; across one wave, the solution is not unique, see Section 4.3; some instabilities may arise in the solution when the system becomes parabolic degenerate, see Section 4.5.2.

Secondly, note that all numerical examples of Section 3.3 involve difficulties in the mathematical modelling of the physics. In the problem formulations, we have to deal simultaneously with several points: Controversial equation of state for the phases (e.g. water, solid mixtures), relaxation phenomena, modelling of an essentially two-dimensional problem by a one-dimensional one (water faucet). In addition to these shortcomings, there are just too few test cases available in

the literature, see e.g. Ransom [71]. All these factors make it difficult to compare different numerical methods for the non-conservative two-phase models. Here, we present a procedure for the construction of exact solutions to the Riemann problem for the BN model. In particular, we can construct certain exact solutions to Riemann problems which are specific to non-strictly hyperbolic systems, e.g. with coinciding wave speeds. Our experience shows that these situations are especially difficult to handle properly with a numerical method, cf. Section 4.7. Our idea in providing a number of such specific examples is that interested researchers may try their numerical methods on the BN model, and compare their numerical results with the exact solution. The same can be done for the Euler equations in a duct of variable cross-section, see Chapter 5.

At last, as we have mentioned in Chapter 2, one cannot directly use the definition of a weak solution for conservation laws in the case of the generic model of two-phase flows. Due to the presence of non-conservative terms in the system of governing equations, one cannot write it in divergence form. However, it appears that for solutions to the Riemann problem for the BN model, the system of governing equations is locally equivalent to some conservative system. This allows us to define a weak solution to the Riemann problem for the BN model, see Section 4.6.

4.1   Exact solution to the Riemann problem

Consider the homogeneous part of the system of governing equations for the BN model, i.e. the system (2.13) with the ansatz (2.15) and consider the Riemann problem for it,

$$\frac{\partial \mathbf{u}}{\partial t} + \frac{\partial \mathbf{f}(\mathbf{u})}{\partial x} = \mathbf{h}(\mathbf{u})\frac{\partial \alpha_a}{\partial x}, \tag{4.1}$$

with

$$\mathbf{u} = \begin{bmatrix} \alpha_a \\ \alpha_a\rho_a \\ \alpha_a\rho_a u_a \\ \alpha_a\rho_a E_a \\ \alpha_b\rho_b \\ \alpha_b\rho_b u_b \\ \alpha_b\rho_b E_b \end{bmatrix}, \quad \mathbf{f}(\mathbf{u}) = \begin{bmatrix} 0 \\ \alpha_a\rho_a u_a \\ \alpha_a\rho_a u_a^2 + \alpha_a p_a \\ \alpha_a u_a(\rho_a E_a + p_a) \\ \alpha_b\rho_b u_b \\ \alpha_b\rho_b u_b^2 + \alpha_b p_b \\ \alpha_b u_b(\rho_b E_b + p_b) \end{bmatrix}, \quad \mathbf{h}(\mathbf{u}) = \begin{bmatrix} -u_a \\ 0 \\ p_b \\ p_b u_a \\ 0 \\ -p_b \\ -p_b u_a \end{bmatrix}. \tag{4.2}$$

and the initial data

$$\mathbf{u}(x,0) = \begin{cases} \mathbf{u}_L, & x \leq 0 \\ \mathbf{u}_R, & x > 0. \end{cases} \tag{4.3}$$

Since there are six distinct waves in the solution to this Riemann problem, cf. Section 2.6, there are at most seven states there. The usual "direct" solution of the Riemann problem is found as follows: Given the end states $\mathbf{u}_L, \mathbf{u}_R$, one
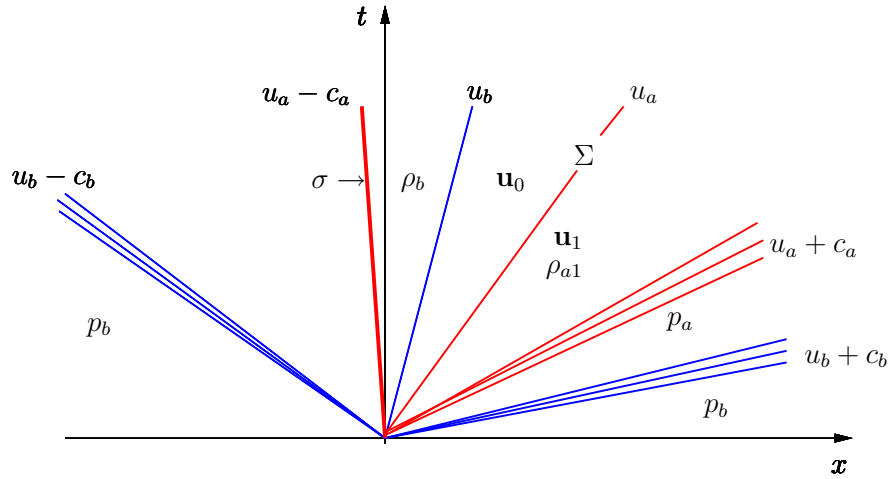
Fig. 4.1. "Inverse" solution of the Riemann problem.

has to find the at most five intermediate states. However, it is problematic to find them for the two-phase model, since the structure of the Riemann problem is quite complicated: For each phase, one has four possible configurations (rarefaction/shock, shock/rarefaction, rarefaction/rarefaction, shock/shock), and the waves can overlap with each other.

Our interest in the exact solution to a Riemann problem is to get a benchmark for testing of numerical schemes. Therefore, instead of solving the "direct" Riemann problem, we can look at what we call the "inverse" Riemann problem: Given some intermediate state $\mathbf{u}_0$ and the configuration of the Riemann problem, one determines end states $\mathbf{u}_L, \mathbf{u}_R$, which can be connected to $\mathbf{u}_0$ by admissible waves.

Let us concretize the procedure of the "inverse" solution, see Fig. 4.1. We choose the intermediate state $\mathbf{u}_0$ at the left to the solid contact Σ, and fix the volume fractions to the left and to the right of Σ. Given also the configuration, which means that we prescribe, which waves should be at the left of Σ, and which to the right. Depending on the wave, we determine the position of the wave by specifying the following quantities

- Shock: given shock speed, family

- Rarefaction: given pressure behind, family

- Contact: given density behind

For now, we make the assumption that the solid contact Σ with speed u_a does not coincide with any other wave. Therefore, we can use the usual Rankine–Hugoniot conditions across the admissible shocks, see Remark 2.7. Then, using

the configuration data, for each wave we can find the state behind it. The case of coinciding wave speeds is discussed in detail in Section 4.5.

It appears that across the solid contact Σ the solution is not trivial. In the following we denote the state to the left of the solid contact Σ by the subscript 0 and the right state by 1. The Riemann invariants for the solid phase (2.56), (2.57) are

$$u_{a0} = u_{a1} = u_a \tag{4.4a}$$

$$\eta_{b0} = \eta_{b1} = \eta_b \tag{4.4b}$$

$$\alpha_{b0}\rho_{b0}(u_{b0} - u_a) = \alpha_{b1}\rho_{b1}(u_{b1} - u_a) = M \tag{4.4c}$$

$$\alpha_{a0}p_{a0} + \alpha_{b0}p_{b0} + \alpha_{b0}\rho_{b0}(u_{b0} - u_a)^2 = \alpha_{a1}p_{a1} + \alpha_{b1}p_{b1} + \alpha_{b1}\rho_{b1}(u_{b1} - u_a)^2 = P \tag{4.4d}$$

$$\frac{(u_{b0} - u_a)^2}{2} + \frac{c_{b0}^2}{\gamma_b - 1} = \frac{(u_{b1} - u_a)^2}{2} + \frac{c_{b1}^2}{\gamma_b - 1} = E. \tag{4.4e}$$

Here

$$\eta_b = \frac{p_b + \pi_b}{\rho_b^{\gamma_b}}, \qquad c_b^2 = \frac{\gamma_b(p_b + \pi_b)}{\rho_b}$$

are respectively the isentrope and the squared sound speed of the gas phase. Note that the solid density ρ_a does not appear in (4.4), it acts as a free parameter. Note also, that the system (4.4) is an *underdetermined* system for the parameters to the left and to the right of the solid contact. Indeed, we have 14 unknowns

$$\alpha_{ai}, \rho_{ai}, u_{ai}, p_{ai}, \rho_{bi}, u_{bi}, p_{bi}, \qquad i = 0, 1,$$

but only 5 equations. Therefore, one has to arbitrarily fix 9 unknowns. We choose to fix the following variables

$$\alpha_{a0}, \rho_{a0}, u_{a0}, p_{a0}, \rho_{b0}, u_{b0}, p_{b0}, \alpha_{a1}, \rho_{a1}.$$

Then, the number of the equations in (4.4) and the number of unknowns coincide and one might hope to get a solution.

Note that the system (4.4) is reminiscent of the mass, momentum, and energy balance across a discontinuity, propagating with the speed u_a, for the Euler equations for the gas phase. Consider the case

$$\alpha_{b0} = \alpha_{b1},$$

and that the other parameters keep their values. Remember that this corresponds to the decoupled Euler equations for the gas and solid phases, see the system (4.1). So, the gas flow does not see the solid phase, and obviously the gas parameters do not change across u_a. Thus, there always exists the trivial solution

$$
\begin{aligned}
\rho_{b0} &= \rho_{b1} \\
u_{b0} &= u_{b1} \\
p_{b0} &= p_{b1}.
\end{aligned}
\tag{4.5}
$$

Note that this is the unique *admissible* solution of (4.4). In what follows, we will refer to this case as the "Euler case", and the case

$$\alpha_{b0} \neq \alpha_{b1}$$

as the "multiphase case". In what follows, we will often fix the phase variables $\rho_k, u_k, p_k, k = a, b$, and consider the Euler case $\alpha_{b0} = \alpha_{b1}$ or the multiphase case $\alpha_{b0} \neq \alpha_{b1}$. If we let

$$\frac{\alpha_{b0}}{\alpha_{b1}} \to 1,$$

then the multiphase case will turn into the Euler case asymptotically.

Combining the equations of (4.4), we get the following nonlinear equation for the gas density to the right of u_a

$$F(\rho_{b1}) = \frac{1}{2} \left(\frac{M}{\alpha_{b1}\rho_{b1}} \right)^2 + \frac{\gamma_b \eta_b \rho_{b1}^{\gamma_b - 1}}{\gamma_b - 1} - E = 0. \tag{4.6}$$

The derivative of $F(\rho)$ is

$$F'(\rho) = -\frac{M^2}{\alpha_{b1}^2 \rho^3} + \gamma_b \eta_b \rho^{\gamma_b - 2}. \tag{4.7}$$

At the point ρ_*, the function $F(\rho)$ reaches its minimum

$$\rho_* = \left(\frac{M^2}{\alpha_{b1}^2 \gamma_b \eta_b} \right)^{\frac{1}{\gamma_b + 1}}. \tag{4.8}$$

Indeed, for all $\rho < \rho_*$ we have

$$\rho^{\gamma_b + 1} < \rho_*^{\gamma_b + 1} = \frac{M^2}{\alpha_{b1}^2 \gamma_b \eta_b},$$

giving

$$\gamma_b \eta_b \rho^{\gamma_b - 2} < \frac{M^2}{\alpha_{b1}^2 \rho^3}.$$

Consequently,

$$F'(\rho) < 0$$

for all $\rho < \rho_*$. Analogously,

$$F'(\rho) > 0$$

for all $\rho > \rho_*$. Note also that $F(\rho) \to +\infty$ as $\rho \to +0$ or $\rho \to +\infty$.

Depending on the sign of $F(\rho_*)$, the equation (4.6) can have no, one, or two roots. We will investigate each case separately.

4.1.1   No roots

Consider the Riemann invariants for the solid phase (4.4). We will fix the left state 0, and look for a root of the equation (4.6) while the varying right gas volume fraction α_{b1}.

     We can rewrite (4.4c) as

$$\rho_{b0}(u_{b0} - u_a) = \frac{\alpha_{b1}}{\alpha_{b0}}\rho_{b1}(u_{b1} - u_a) = \frac{M}{\alpha_{b0}} = M_E,$$

where the subscript E stands for Euler. Indeed, M_E is equal to the mass flow for the Euler case $\alpha_{b0} = \alpha_{b1}$. With a *constant* α_{b0}, we have the constant M_E on the right hand side.

     Let us rewrite the equation (4.6) as follows,

$$F(\rho_{b1}) = \frac{1}{2}M_E^2\left(\frac{\alpha_{b0}}{\alpha_{b1}}\right)^2\frac{1}{\rho_{b1}^2} + \frac{\gamma_b\eta_b\rho_{b1}^{\gamma_b-1}}{\gamma_b - 1} - E = 0. \tag{4.9}$$

For the Euler case

$$\frac{\alpha_{b0}}{\alpha_{b1}} = 1$$

and (4.9) always has at least one trivial solution (4.5). For variable $\alpha_{b1} \in]0,1[$ (multiphase case), we have

$$\frac{\alpha_{b0}}{\alpha_{b1}} \in]\alpha_{b0}, \infty[.$$

It is obvious that if for some positive A, A big enough,

$$\frac{\alpha_{b0}}{\alpha_{b1}} > A, \tag{4.10}$$

then (4.9) has no roots, since $E, \eta_b, \rho_b > 0$ and $\gamma_b > 1$. Thus for all $\alpha_{b1}, \alpha_{b1} < \alpha_{b0}/A$, the equation (4.9) has no roots. Decreasing α_{b1} (or increasing $\alpha_{a1}, \alpha_{a1} = 1 - \alpha_{b1}$), one necessarily gets no solution for some value of α_{b1}.

4.1.2   One or two roots

Consider again the equations

$$F(\rho_{b1}) = \frac{1}{2}\left(\frac{M}{\alpha_{b1}\rho_{b1}}\right)^2 + \frac{\gamma_b\eta_b\rho_{b1}^{\gamma_b-1}}{\gamma_b - 1} - E = 0 \tag{4.11}$$

$$F'(\rho) = -\frac{M^2}{\alpha_{b1}^2\rho^3} + \gamma_b\eta_b\rho^{\gamma_b-2}. \tag{4.12}$$

Suppose first that (4.11) has two roots. Denote them $\tilde{\rho}_{b1}, \tilde{\tilde{\rho}}_{b1}$ and assume that

$$\tilde{\rho}_{b1} < \tilde{\tilde{\rho}}_{b1}.$$

Then

$$F'(\tilde{\rho}_{b1}) < 0, \qquad F'(\tilde{\tilde{\rho}}_{b1}) > 0.$$

Using (4.4c)

$$\frac{M^2}{\alpha_{b1}^2} = (u_{b1} - u_a)^2 \rho_{b1}^2$$

we can rewrite (4.12) as

$$-(u_{b1} - u_a)^2 + c_{b1}^2 = F'(\rho_{b1})\rho_{b1}, \tag{4.13}$$

where $c_{b1}^2 = \gamma_b(p_{b1} + \pi_b)/\rho_{b1}$ is the squared gas sound speed. We see that the volume fraction α_b does not appear in this equation. This means that it should hold for *any* values of α_{b0}, α_{b1} on both sides of Σ. In particular, for the Euler case $\alpha_{b0} = \alpha_{b1}$, the admissible solution is (4.5), i.e.

$$\begin{aligned} \rho_{b0} &= \rho_{b1} \\ u_{b0} &= u_{b1} \\ p_{b0} &= p_{b1}. \end{aligned}$$

Thus, we have the two roots $\tilde{\rho}_{b1}$, $\tilde{\tilde{\rho}}_{b1}$ of (4.11) as candidates for ρ_{b1}. We choose the one for which

$$\operatorname{sign}(-(u_{b0} - u_a)^2 + c_{b0}^2) = \operatorname{sign}(-(u_{b1} - u_a)^2 + c_{b1}^2) \tag{4.14}$$

since all these quantities are identical on the left and right side. By (4.13), it is equivalent to the condition

$$\operatorname{sign}(F'(\rho_{b0})) = \operatorname{sign}(F'(\rho_{b1})). \tag{4.15}$$

For the multiphase case $\alpha_{b0} \neq \alpha_{b1}$, we also choose by a continuity argument the root of (4.11), which satisfies the condition (4.15). It corresponds to the admissible root for the Euler case, when α_{b1} is equal to α_{b0}.

Physically, this choice has the following meaning. Consider the Euler case $\alpha_{b0} = \alpha_{b1}$, and let the admissible Euler root be $\tilde{\rho}_{b1}$. Then, it satisfies the criterion (4.15). Now let us deviate the ratio α_{b0}/α_{b1} from 1 slightly, i.e.,

$$\frac{\alpha_{b0}}{\alpha_{b1}} := 1 + \epsilon, \quad \epsilon \text{ small}.$$

Then, for this *multiphase* case the admissible root is also $\tilde{\rho}_{b1}$, it cannot suddenly become $\tilde{\tilde{\rho}}_{b1}$. We summarize these ideas by formulating the following definition.

Definition 4.1. *The **physically admissible state** behind the solid contact is determined by the root of (4.6), which satisfies the condition (4.15).*

The case of the single root of (4.11) corresponds to the degenerate situation, when the gas velocity relative to u_a is *sonic* to the right of Σ, i.e.,

$$|u_{b1} - u_a| = c_{b1}.$$

Note that this is exactly the condition (2.55), under which the system of the governing equations (4.1) becomes parabolic degenerate, see Section 2.6. We will give an interpretation of this case in Section 4.5.2 below.

Remark 4.2. Since the Euler equations in a duct (2.19) can be formally obtained from the BN model (4.1) using assumptions (2.16), see Section 2.3.3, we can extend Definition 4.1 also for the system (2.19). The solid contact Σ in the BN model (4.1) becomes the stationary contact in (2.19), and the correspondence (2.20) holds. Then, the physically admissible state behind the stationary contact in the Riemann problem for the system (2.19) is given by the condition

$$\mathrm{sign}(-v_0^2 + c_0^2) = \mathrm{sign}(-v_1^2 + c_1^2).$$

4.1.3   The software package CONSTRUCT

The procedure of the inverse solution to Riemann problems for the BN model (4.1)-(4.3) has been implemented for this thesis in the package CONSTRUCT [5]. It is a set of MATLAB routines and is freely available, see [5].

The package allows to build exact solutions to Riemann problems interactively. The process starts by setting up the state to the left of the solid contact Σ, and the solid volume fraction as well as the density to the right of it. From this data, CONSTRUCT tries to find an admissible state to the right of the solid contact. There are at most two solutions, see Section 4.1, and the non-admissible state is ruled out using Definition 4.1. At this stage, the solution to the Riemann problem appears, which now consists only of the solid contact. One can add other waves, edit or delete them and see the changed solution. The resulting solution can be printed or saved as a data file.

CONSTRUCT is a useful tool in investigating the properties of Riemann problems for the BN model (4.1), and for the Euler equations in a duct of variable cross section (2.19). For the latter case, one needs to set the solid velocity to zero and consider only gas waves in the solution to Riemann problems.

In Section 4.7 and Chapter 5 we CONSTRUCT several test cases for both models. These tests are used to assess the perfomance of the VFRoe method, presented in Section 3.2, and the Godunov-type method of Section 5.7. We hope that interested researchers will find the package helpful for testing of numerical schemes for non-conservative systems. Also, it might be useful for the investigation of properties of Riemann solutions for systems like (4.1) and (2.19).

4.2 Evolutionary discontinuities

The results of Section 4.1 show that the solution across the solid contact is not unique. That is, for a fixed state on one side of it, one can find at most two states on the other side of it. Then, one of these states is considered to be non-admissible according to Definition 4.1. Note that the condition behind it is actually more intuitive than physical. Also, it is restricted only to the Riemann problem for the BN model.

However, a non-unique solution across a discontinuity is not something reserved for a particular system. As we have seen in Section 2.4.1, for a *general* conservation law, a weak solution is not unique. In that case, one employs different kinds of *entropy conditions*, in order to rule out the non-physical solutions. The classical condition here is the Lax entropy condition (2.32).

A naive use of an entropy condition would be to look at the entropy across the solid contact and to draw conclusions on its basis. Observe that this would not work: Entropy is constant across the solid contact, see (4.4b). We also cannot use the entropy inequality (2.29) from the theory of conservation laws, since our system (4.1) is non-conservative.

It seems now that it is impossible to integrate the admissibility criterion for the solid contact, given by the Definition 4.1, into the framework of the admissible entropy solutions of conservation laws. Therefore, we will strive to find a more general admissibility criterion, which will embody both the case of the solid contact, and the discontinuities of conservation laws. This will be the ultimate purpose of this section.

In searching for such general admissibility criterion, one inevitably goes back to the *physical foundations* behind the admissibility conditions. One of such foundations is the second law of thermodynamics, which leads to the entropy condition for conservation laws, see Section 2.4.1.

Another principle is based on the following simple idea: At each point of a physical flow, the number of unknown variables should be equal to the number of relations for determining them. At the points where the flow is *smooth*, this is obviously satisfied for any closed system. However, this condition is *not* automatically valid for discontinuities. In fact, it poses several restrictions on them.

Consider a physical flow, which is governed by the system of hyperbolic conservation laws

$$\mathbf{u}_t + \mathbf{f}(\mathbf{u})_x = 0, \tag{4.16}$$

where $\mathbf{u} \in \mathbb{R}^p$ and $\mathbf{f}(\mathbf{u}) : \mathbb{R}^p \to \mathbb{R}^p$ is a smooth function. Denote the eigenvalues of the Jacobian matrix $\mathbf{A}(\mathbf{u}) := \mathbf{f}'(\mathbf{u})$ by λ_i, $i = 1, \ldots, p$. We do not assume that the system (4.16) is strictly hyperbolic, so some of these eigenvalues may coincide. For simplicity, we consider here only the one-dimensional case. However, the considerations presented below can be generalized to the three-dimensional case
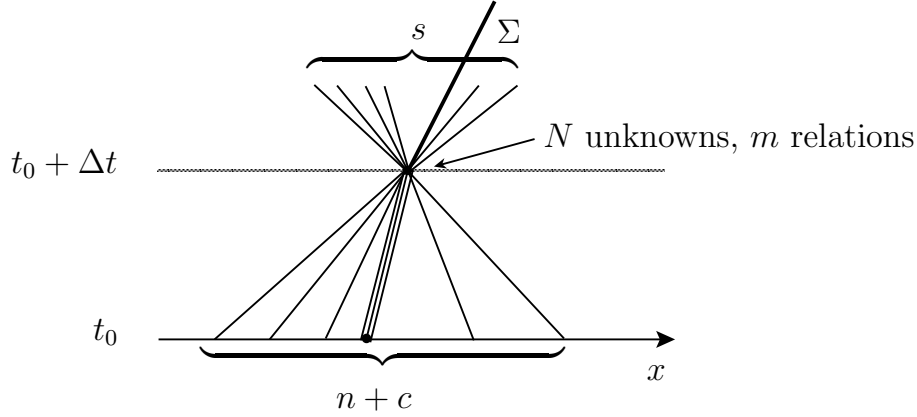
Fig. 4.2. There are n characteristics, incoming into a discontinuity Σ at time $t_0 + \Delta t$, c characteristics, coinciding with Σ, and s characteristics, outgoing from it. Across Σ, m relations are given. The total number of unknowns at Σ is N.

as well.

Assume that at the initial time t_0, there is a discontinuity Σ in the flow, which propagates with the speed $\sigma = \sigma(\mathbf{u})$, see Fig. 4.2. Then, in order for Σ to be determined for subsequent times $t_0 + \Delta t$, all N unknown variables on the both sides of the discontinuity should be specified. Since one has p unknown variables on each side of Σ, plus the speed σ of Σ, it follows that

$$N = 2p + 1.$$

There are two kinds of relations for determining of these N unknowns. Firstly, there are relations across the discontinuity Σ at the time $t_0 + \Delta t$, e.g. Rankine–Hugoniot conditions. Denote their number by m.

Secondly, there are certain relations along the characteristics, which go into Σ at the time $t_0 + \Delta t$. To make them precise, let us carry out the differentiation in (4.16) and linearize the resulting system on both sides of Σ at time t_0, i.e., assume $\mathbf{u} = \mathbf{u}_0 + \tilde{\mathbf{u}}$ on the left, and $\mathbf{u} = \mathbf{u}_1 + \tilde{\tilde{\mathbf{u}}}$ on the right. Then, small perturbations $\tilde{\mathbf{u}}$ and $\tilde{\tilde{\mathbf{u}}}$ must satisfy the linear systems

$$\frac{\partial \tilde{\mathbf{u}}}{\partial t} + \mathbf{A}(\mathbf{u}_0)\frac{\partial \tilde{\mathbf{u}}}{\partial x} = 0, \qquad \frac{\partial \tilde{\tilde{\mathbf{u}}}}{\partial t} + \mathbf{A}(\mathbf{u}_1)\frac{\partial \tilde{\tilde{\mathbf{u}}}}{\partial x} = 0 \tag{4.17}$$

to second order of accuracy. Assume that the systems (4.17) are diagonalisable, i.e. that we can introduce the characteristic variables $\mathbf{w} = \mathbf{R}^{-1}\mathbf{u}$. Here $\mathbf{R}$ is the matrix of right eigenvectors of $\mathbf{A}$. Then, by changing to characteristic variables on the both sides of Σ, the two systems (4.17) split into $2p$ scalar equations

$$\frac{\partial \tilde{w}_i}{\partial t} + \lambda_i(\mathbf{u}_0)\frac{\partial \tilde{w}_i}{\partial x} = 0, \qquad \frac{\partial \tilde{\tilde{w}}_i}{\partial t} + \lambda_i(\mathbf{u}_1)\frac{\partial \tilde{\tilde{w}}_i}{\partial x} = 0, \tag{4.18}$$

where $i = 1, \ldots, p$ and λ_i are the eigenvalues of **A** at the states $\mathbf{u}_0$ and $\mathbf{u}_1$. Thus, small disturbances propagate with the characteristic speeds λ_i. We can subdivide these characteristics into

 (i) incoming: $\lambda_i(\mathbf{u}_0) > \sigma$ or $\lambda_i(\mathbf{u}_1) < \sigma$

 (ii) coinciding: $\lambda_i(\mathbf{u}_0) = \sigma$ or $\lambda_i(\mathbf{u}_1) = \sigma$

 (iii) outgoing: $\lambda_i(\mathbf{u}_0) < \sigma$ or $\lambda_i(\mathbf{u}_1) > \sigma$.

Denote the number of characteristics, incoming towards Σ by n, coinciding with Σ by c, and outgoing by s. The relations (4.18) along the incoming and coinciding characteristics are fully determined from the initial data, i.e. from the "past". Therefore, they provide additional relations to determine the N unknowns on the discontinuity Σ at time $t_0 + \Delta t$.

Consequently, in order for Σ to be determined, the following equality must hold

$$N = n + c + m.$$

Then, and only then, the discontinuity Σ is well determined in the flow, i.e. it *evolves* in time. We summarize the above considerations in the following definition.

Definition 4.3 (Evolutionarity criterion). *Consider a discontinuity Σ in a physical flow, which is governed by the hyperbolic system* (4.16). *Denote the number of characteristics, incoming to Σ by n, coinciding with Σ by c, and outgoing from Σ by s. Further, denote the number of unknown variables on the both sides of Σ together with the speed σ by $N = 2p + 1$ and the number of relations across Σ by m. Then Σ is called **evolutionary**, if*

$$N = n + c + m.$$

The notion of *evolutionarity* is not new: In different contexts, it appears in several classical books on gas dynamics and theory of conservation laws. Landau and Lifshitz [55, §88] introduce an evolutionarity condition for shock waves while studying their stability. Smoller [81, Chapter 15, §C] calls a system of differential equations evolutionary if the initial-value problem is well posed. Actually he uses the notion of evolutionary discontinuity when deriving the Lax shock conditions (2.32). We note that Lax in his paper [57] also uses the evolutionarity property without calling it so. More recently, Dafermos [25, Section 9.2] uses the notion of evolutionarity in slightly different sense: For him, it characterizes time irreversibility of the solution. However, to our knowledge the notion of evolutionarity has been systematically used only by Cherny [16] and in particular by Kulikovskii *et al.* [52], who discuss it in very different physical frameworks.

For an evolutionary discontinuity Σ, we can easily derive a condition on the number of outgoing characteristics from it. Namely, the following theorem holds.

Theorem 4.4. *For a discontinuity Σ in the solution of the system* (4.16), *denote the number of the outgoing characteristics by s, and the number of relations across Σ by m. Then Σ is evolutionary, iff*

$$s + 1 = m.$$

Proof. Since the order of the system (4.16) is p, there are p characteristics on the either side of Σ. So the total number of characteristics is $2p$. Then with the notations of Definition 4.3 one has $n + c + s = 2p$. Using this in Definition 4.3, we get the desired result. $\square$

For an evolutionary discontinuity Σ, all unknowns on both sides of it are determined for all $t > 0$, see Definition 4.3. Therefore, we can consider Σ as a *free boundary* in the flow, and formulate initial boundary value problems (IBVP) for the systems (4.17) (or, equivalently (4.18)) on the both sides of Σ. Let us put the eigenvalues $\lambda_1, \ldots, \lambda_p$ in increasing order, i.e. introduce the indices $i_1, \ldots, i_p$ such that for all $\mathbf{u} \in \mathbb{R}^p$,

$$\lambda_{i_1}(\mathbf{u}) \leq \lambda_{i_2}(\mathbf{u}) \leq \cdots \leq \lambda_{i_p}(\mathbf{u}).$$

Since the system (4.16) is only *non-strictly* hyperbolic, the nature of each λ_{i_k} for fixed k can be different for different $\mathbf{u} \in \mathbb{R}^p$. For the case of strictly hyperbolic system (4.16), one has $i_k \equiv k$. Denote the number of outgoing characteristics to the left of the discontinuity Σ by s_0, and to the right of it by s_1. Then

$$\lambda_{i_1}(\mathbf{u}_0) \leq \cdots \leq \lambda_{i_{s_0}}(\mathbf{u}_0) < \sigma \leq \lambda_{i_{s_0+1}}(\mathbf{u}_0) \leq \cdots \leq \lambda_{i_p}(\mathbf{u}_0) \qquad (4.19)$$

$$\lambda_{i_1}(\mathbf{u}_1) \leq \cdots \leq \lambda_{i_{p-s_1}}(\mathbf{u}_1) \leq \sigma < \lambda_{i_{p-s_1+1}}(\mathbf{u}_1) \leq \cdots \leq \lambda_{i_p}(\mathbf{u}_1), \qquad (4.20)$$

where $\sigma = \sigma(\mathbf{u})$ is the speed of Σ. Note that these inequalities remind of the Lax shock conditions (2.32). We will discuss the relationships between them in Section 4.2.1 below.

Since Σ is evolutionary, precisely s_0 parameters are given at the left of Σ, and s_1 at the right of it. We can interpret these *known* parameters as the boundary conditions for the following *linear* IBVPs at the left and at the right of Σ, respectively:

$$\frac{\partial \tilde{\mathsf{w}}_{i_k}}{\partial t} + \lambda_{i_k}(\mathbf{u}_0) \frac{\partial \tilde{\mathsf{w}}_{i_k}}{\partial x} = 0, \quad \tilde{\mathsf{w}}_{i_1}, \ldots, \tilde{\mathsf{w}}_{i_{s_0}} \text{ are prescribed on } \Sigma \atop \tilde{\mathsf{w}}_{i_{s_0+1}}, \ldots, \tilde{\mathsf{w}}_{i_p} \text{ are prescribed at } t = 0 \qquad (4.21)$$

$$\frac{\partial \tilde{\tilde{\mathsf{w}}}_{i_k}}{\partial t} + \lambda_{i_k}(\mathbf{u}_1) \frac{\partial \tilde{\tilde{\mathsf{w}}}_{i_k}}{\partial x} = 0, \quad \tilde{\tilde{\mathsf{w}}}_{i_1}, \ldots, \tilde{\tilde{\mathsf{w}}}_{i_{p-s_1}} \text{ are prescribed at } t = 0 \atop \tilde{\tilde{\mathsf{w}}}_{i_{p-s_1+1}}, \ldots, \tilde{\tilde{\mathsf{w}}}_{i_p} \text{ are prescribed on } \Sigma. \qquad (4.22)$$
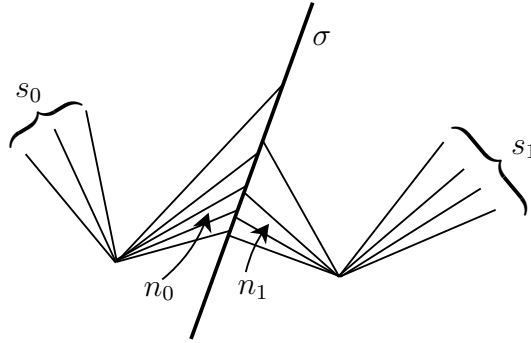
Fig. 4.3. At the left of a shock with speed σ, n_0 characteristics impinge on it, and s_0 leave it. At the right, n_1 characteristics impinge on the shock, and s_1 leave it.

The IBVPs (4.21) and (4.22) imply that $\tilde{\mathbf{w}}_{i_k}$ and $\tilde{\tilde{\mathbf{w}}}_{i_k}$ are constant along the characteristics $\lambda_{i_k}(\mathbf{u}_0)$ and $\lambda_{i_k}(\mathbf{u}_1)$ respectively, and the initial values for $\tilde{\mathbf{w}}_{i_k}$ and $\tilde{\tilde{\mathbf{w}}}_{i_k}$ are given. Obviously, the IBVPs (4.21) and (4.22) are well-posed and have unique solutions. Thus, we have the following theorem.

Theorem 4.5. *For an evolutionary discontinuity Σ, the linear IBVPs (4.21) and (4.22) are well-posed and have unique solutions.*

Next, we check if the classical discontinuous solutions of the system of conservation laws (4.16), namely the Lax shock and the contact discontinuity, are evolutionary.

4.2.1 Lax shock

By definition of the Lax k-shock (2.32),

$$\lambda_k(\mathbf{u}_0) > \sigma > \lambda_k(\mathbf{u}_1), \tag{4.23}$$

where $\sigma = \sigma(\mathbf{u})$ is the shock speed and $\mathbf{u}_{0,1}$ are the states to the left on the right of the shock, respectively. The meaning of (4.23) is that the information, carried by the k-characteristic from the past, is lost in the shock thus determining its speed.

The condition (4.23) implies that there are no characteristics which coincide with the shock, i.e. $c = 0$. Denote the number of characteristics, impinging on the shock from the left by n_0, and from the right by n_1. Also, denote the number of the outgoing characteristics from the left and from the right by s_0 and s_1 respectively, see Fig. 4.3. Obviously the total number of incoming characteristics is then $n = n_0 + n_1$, and the total number of outgoing characteristics is $s = s_0 + s_1$.

At the shock, there are $N = 2p + 1$ unknowns, and across it one has $m = p$ Rankine–Hugoniot conditions. Using $n_0 = p - s_0$ in the the evolutionarity criterion of Definition 4.3, one gets

$$s_0 = n_1 - 1. \tag{4.24}$$

Analogously, using $n_1 = p - s_1$ in Definition 4.3, we obtain

$$s_1 = n_0 - 1. \tag{4.25}$$

The equation (4.24) states that among all characteristics which impinge on the shock from the left, precisely one characteristic does not pass through the shock, but lost in it. According to (4.25), there is also precisely one characteristic to the right of the shock, which does not pass it. By the Lax shock condition (4.23), this is the characteristic of the same k-th family.

Let us show that in the case of a general *non-strictly* hyperbolic conservation law (4.16), the Lax condition (4.23) is *not* equivalent to the evoluionarity criterion, given by Definition 4.3. Indeed, using $s = s_0 + s_1$ and $m = p$ in Theorem 4.4, we obtain

$$s_0 + 1 = p - s_1.$$

Denote this number by $k := s_0 + 1 = p - s_1$. Now substituting this into the inequalities (4.19), (4.20) results in

$$\lambda_{i_1}(\mathbf{u}_1) \leq \cdots \leq \lambda_{i_k}(\mathbf{u}_1) \leq \sigma \leq \lambda_{i_k}(\mathbf{u}_0) \leq \cdots \leq \lambda_{i_p}(\mathbf{u}_0). \tag{4.26}$$

Note that for a general non-strictly hyperbolic system (4.16) the characteristic family, corresponding to the eigenvalue $\lambda_{i_k}(\mathbf{u}_1)$ will be possibly *not* the same as the family, corresponding to the eigenvalue $\lambda_{i_k}(\mathbf{u}_0)$. However, it will be the same for a *strictly* hyperbolic system (4.16), since $i_k \equiv k$ for such systems. Then, the condition (4.26) recovers the Lax shock condition (4.23) when both parts of (4.26) hold as strict inequalities. In case of equalities in (4.26) we obtain the condition for a contact discontinuity.

Another consequence of (4.26) is that for a general non-strictly hyperbolic system (4.16) we cannot speak of a k-shock, i.e. a shock belonging to the k-characteristic field. Indeed, according to (4.26), a shock propagating with the speed σ is associated only with the *index k* of the i_k-characteristic field. For the case of a strictly hyperbolic system $i_k \equiv k$, we recover the usual notion of a k-shock.

4.2.2   Contact discontinuity

Consider the system of hyperbolic conservation laws (4.16), and assume that one of its characteristic fields, say the k-field, is linearly degenerate. Assume that the multiplicity $a(\lambda_k)$ is constant. Note that if $a(\lambda_k) \geq 2$, then the k-field will
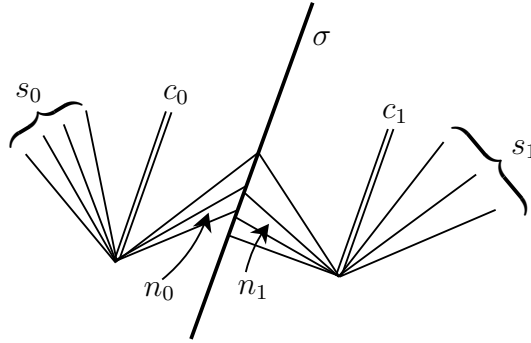
Fig. 4.4. At the left of a k-contact with speed $\sigma = \lambda_k$, n_0 character-
istics impinge on it, c_0 coincide with it, and s_0 leave it. At the right,
n_1 characteristics impinge on the shock, c_1 coincide with it, and s_1
leave it.

be automatically linearly degenerate, and $p - a(\lambda_k)$ Riemann invariants will be
constant across it, see Theorem 2.6. In the solution to the conservation law (4.16),
the k-field will correspond to the k-contact discontinuity.

Denote by n_0 and n_1 the number of characteristics, impinging on the k-contact
from the left and from the right, and by s_0 and s_1 the number of characteristics,
leaving it from the left and from the right, respectively. Further, observe that the
number of the characteristics, coinciding with the k-contact, will be the same on
the both sides of it. Indeed, for each $\lambda_j = \lambda_k$, λ_j will be the Riemann invariant
across the j-field. Therefore, there are $c_0 = c_1 = a(\lambda_k)$ characteristics, coinciding
with λ_k from the either side, see Fig. 4.4.

Next, we determine the number of conditions, which hold across the k-contact
described above. A part of these conditions are provided by the constancy of
$p - a(\lambda_k)$ Riemann invariants across it. In addition, the speed of the k-contact is

$$\sigma \equiv \lambda_k,$$

so there are $m = p - a(\lambda_k) + 1$ conditions across the k-contact. Using $N = 2p + 1$
in the evolutionarity criterion, given by Definition 4.3, we get

$$p = n_0 + n_1 + a(\lambda_k). \tag{4.27}$$

Since $s_0 = p - n_0 - c_0$, we can rewrite (4.27) as

$$s_0 = n_1. \tag{4.28}$$

Analogously, since $s_1 = p - n_1 - c_1$, we get

$$s_1 = n_0. \tag{4.29}$$

Therefore, a k-contact discontinuity is evolutionary, iff the conditions (4.28) and (4.29) are satisfied. These conditions state that in contrast to an evolutionary shock, the characteristics do not disappear in evolutionary contacts. In other words, the number of the characteristics, entering the evolutionary contact from one side, is the same as the number of the characteristics leaving it from the other side. However, in case of a general *non-strictly* hyperbolic system (4.16), it does not imply that each particular characteristic, which enters the evolutionary contact from one side, will leave it from the other side. Indeed, there are n_0 characteristics, impinging on the evolutionary contact from the left. Denote them by

$$\sigma < \lambda_{i_{p-n_0+1}}(\mathbf{u}_0) \leq \cdots \leq \lambda_{i_p}(\mathbf{u}_0).$$

According to (4.29), there are $s_1 = n_0$ characteristics leaving this contact from the right, so

$$\sigma < \lambda_{i_{p-n_0+1}}(\mathbf{u}_1) \leq \cdots \leq \lambda_{i_p}(\mathbf{u}_1).$$

But since the system (4.16) is only non-strictly hyperbolic, some of the characteristics $\lambda_{i_j}(\mathbf{u}_0)$ may belong to a different family than $\lambda_{i_j}(\mathbf{u}_1)$ for $j = p-n_0+1, \ldots, p$. One needs additional constraints on the characteristics to ensure that the characteristics of each particular type will pass the evolutionary contact.

It is a trivial matter to show that in case of a strictly hyperbolic system (4.16) every contact discontinuity is evolutionary. In this case the evolutionarity conditions (4.28) and (4.29) are equivalent to

$$\text{sign}\,(\lambda_i(\mathbf{u}_0) - \lambda_k) = \text{sign}\,(\lambda_i(\mathbf{u}_1) - \lambda_k), \quad i = 1, \ldots, p, \quad i \neq k. \tag{4.30}$$

This equality states that for a strictly hyperbolic system (4.16), a k-contact is evolutionary iff *each i-characteristic with $i \neq k$* passes through the k-contact.

Note that the notions of a linearly degenerate field and a Riemann invariant are valid also for the case of a general quasilinear hyperbolic system, even if it cannot be written in form of a conservation law (4.16). The difficulty there is that we cannot define a discontinuous weak solution to it analogously to the case of conservation laws, see Section 2.4.1. Instead, Dal Maso, LeFloch, and Murat [26] proposed a definition of a weak solution based on the theory of non-conservative products. Also, in Section 4.6 we propose a definition of a weak solution to the Riemann problem for the BN model of two-phase flows. With this definition, we can use the evolutionary criterion introduced above for the Riemann problem to the BN model as well. This is what we will be doing in the following section.

4.3   Evolutionarity of the solid contact

Consider the solution of the Riemann problem (4.1), (4.3) for the BN model and denote the states to the left and right of the solid contact Σ, propagating with the

speed u_a, by $\mathbf{u}_0$ and $\mathbf{u}_1$ respectively. Let us investigate, under which conditions the solid contact will be an evolutionary discontinuity.

Consider the primitive variable formulation of the system (4.1),

$$\frac{\partial \mathbf{v}}{\partial t} + \mathbf{A}(\mathbf{v})\frac{\partial \mathbf{v}}{\partial x} = 0, \tag{4.31}$$

with

$$\mathbf{A} = \begin{bmatrix} u_a & 0 & 0 & 0 & 0 & 0 & 0 \\ 0 & u_a & \rho_a & 0 & 0 & 0 & 0 \\ \frac{p_a - p_b}{\alpha_a \rho_a} & 0 & u_a & 1/\rho_a & 0 & 0 & 0 \\ 0 & 0 & \rho_a c_a^2 & u_a & 0 & 0 & 0 \\ -\frac{\rho_b}{\alpha_b}(u_b - u_a) & 0 & 0 & 0 & u_b & \rho_b & 0 \\ 0 & 0 & 0 & 0 & 0 & u_b & 1/\rho_b \\ -\frac{\rho_b c_b^2}{\alpha_b}(u_b - u_a) & 0 & 0 & 0 & 0 & \rho_b c_b^2 & u_b \end{bmatrix}, \quad \mathbf{v} = \begin{bmatrix} \alpha_a \\ \rho_a \\ u_a \\ p_a \\ \rho_b \\ u_b \\ p_b \end{bmatrix}. \tag{4.32}$$

Analogously how it was done in Section 4.2, we linearize this system on both sides of Σ, and change to characteristic variables there. Note that the transformation to the characteristic variables exists as long as $(u_b - u_a)^2 - c_b^2 \neq 0$. For now, we will be dealing only with this case. The case when $(u_b - u_a)^2 - c_b^2 = 0$ is considered in Section 4.5.2.

Denote the number of characteristics, impinging on the solid contact Σ from the both sides by n, coinciding with Σ by c, and leaving it by s. Since the order of the system is $p = 7$, there will be $N = 2p + 1 = 15$ unknowns at Σ. Note that the solid contact corresponds to the eigenvalue $\lambda_0 = \lambda_2 = u_a$, so that the multiplicity of the corresponding eigenvalue is 2. For now, we assume that this multiplicity is always *constant*, i.e. there are no other characteristics which coincide with Σ. The case of coinciding characteristics will be considered in Section 4.5. By Theorem 2.6, the $p - 2 = 5$ Riemann invariants are constant across the solid contact. Since the speed of Σ is $u_a = \lambda_0 = \lambda_2$, there are $m = 5 + 1 = 6$ conditions across it. Also, there are $c = 2 + 2 = 4$ characteristics, coinciding with Σ from the both sides.

According to Definition 4.3, the solid contact to be evolutionary if

$$N = n + c + m.$$

Using the values for N, c, and m found above, we obtain

$$15 = n + 4 + 6, \text{ so } n = 5. \tag{4.33}$$

At this stage, it is advantageous to separate the incoming characteristics according to the phases a and b. Denote the number of the incoming characteristics for the solid phase by n_a and for the gas phase by n_b, so that $n = n_a + n_b$. Remember that the characteristics of each phase are *ordered*. Indeed, for the phase a

$$\lambda_1 = u_a - c_a < \lambda_2 = u_a < \lambda_3 = u_a + c_a. \tag{4.34}$$

Analogously for the phase b,

$$\lambda_4 = u_b - c_b < \lambda_5 = u_b < \lambda_6 = u_b + c_b. \tag{4.35}$$

Since the characteristics with the speed $\lambda_0 = \lambda_2 = u_a$ coincide with the solid contact Σ, the characteristic with the speed $\lambda_3(\mathbf{u}_0) = u_{a0} + c_{a0}$ will always impinge on Σ from the left, and the one with $\lambda_1(\mathbf{u}_1) = u_{a1} - c_{a1}$ from the right. Therefore, we have

$$n_a = 2.$$

Using this in (4.33), we obtain

$$n_b = 3. \tag{4.36}$$

Therefore, the solid contact Σ is evolutionary iff there are precisely three gas characteristics, which impinge on it from the both sides. Note that we do not know at this point, what happens with a particular family of gas characteristics as it crosses Σ. However, the gas characteristics are always ordered by increasing, see (4.35). Then, the following results follows easily.

Theorem 4.6. *Consider the Riemann problem* (4.1), (4.3) *for the BN model and assume that there are no gas characteristics, which coincide with the solid contact Σ, propagating with the velocity u_a. Then Σ is evolutionary iff all gas characteristics pass through it, i.e.*

$$\operatorname{sign}\left(\lambda_k(\mathbf{u}_0) - u_a\right) = \operatorname{sign}\left(\lambda_k(\mathbf{u}_1) - u_a\right), \quad k = 4, 5, 6.$$

The condition that the gas characteristics do not coincide with Σ is equivalent to our assumption that the multiplicity of the eigenvalue $\lambda_0 = \lambda_2 = u_a$ is constant and equal to 2. The situations when it is not the case will be addressed in Section 4.5.

Proof. We prove the theorem by considering all possible cases. For example, let $\lambda_4 = u_{b0} - c_{b0} > u_a$. Then also

$$\lambda_6 = u_{b0} + c_{b0} > \lambda_5 = u_{b0} > u_a,$$

so that there are three gas characteristics, impinging on the solid contact Σ from the left. By (4.36), there are no incoming gas characteristics from the right, so they are all outgoing. But then their speeds are greater than u_a, i.e.

$$\lambda_k(\mathbf{u}_1) > u_a, \quad k = 4, 5, 6.$$

The gas characteristics around the solid contact for this case are depicted in Fig. 4.5 (A). The other cases are done analogously, see Fig. 4.5 for the corresponding wave configurations. $\qquad\square$
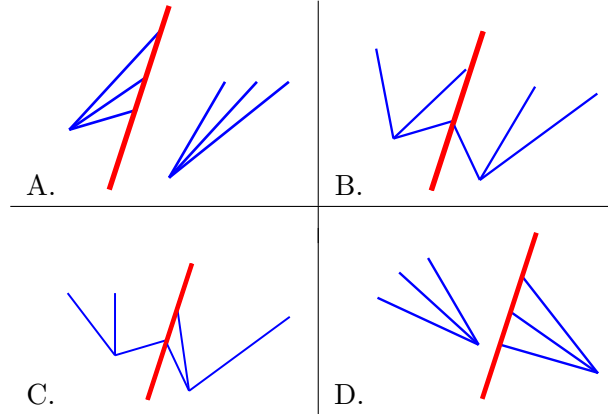
Fig. 4.5. Four possible positions of the gas characteristics around an evolutionary solid contact.

Finally, we wish to show that the physically admissible state behind the solid contact in the sense of Definition 4.1, implies that the solid contact will be an evolutionary discontinuity. Namely, the following theorem holds.

Theorem 4.7. *Consider the Riemann problem* (4.1), (4.3) *for the BN model and assume that there are no gas characteristics, which coincide with the solid contact* Σ, *propagating with the velocity* u_a. *Then* Σ *is evolutionary iff the state behind* Σ *is physically admissible in the sense of Definition 4.1, i.e.*

$$\operatorname{sign}\left(-(u_{b0} - u_a)^2 + c_{b0}^2\right) = \operatorname{sign}\left(-(u_{b1} - u_a)^2 + c_{b1}^2\right). \tag{4.37}$$

Proof. From the constancy of the third Riemann invariant across the solid contact, i.e. from (4.4c), it follows that

$$u_{b0} < u_a \Longleftrightarrow u_{b1} < u_a.$$

Analogously,

$$u_{b0} > u_a \Longleftrightarrow u_{b1} > u_a.$$

We prove the statement of the theorem by considering the different cases in the equation (4.37).

	$u_{b0} > u_a$	$u_{b1} > u_a$
A.	$-(u_{b0} - u_a)^2 + c_{b0}^2 < 0$	$-(u_{b1} - u_a)^2 + c_{b1}^2 < 0$
	$\Leftrightarrow |u_{b0} - u_a| > c_{b0}$	$\Leftrightarrow |u_{b1} - u_a| > c_{b1}$
	$\Leftrightarrow u_{b0} - c_{b0} > u_a$	$\Leftrightarrow u_{b1} - c_{b1} > u_a$
B.	$-(u_{b0} - u_a)^2 + c_{b0}^2 > 0$	$-(u_{b1} - u_a)^2 + c_{b1}^2 > 0$
	$\Leftrightarrow |u_{b0} - u_a| < c_{b0}$	$\Leftrightarrow |u_{b1} - u_a| < c_{b1}$
	$\Leftrightarrow u_{b0} - c_{b0} < u_a$	$\Leftrightarrow u_{b1} - c_{b1} < u_a$

	$u_{b0} < u_a$	$u_{b1} < u_a$
C.	$-(u_{b0} - u_a)^2 + c_{b0}^2 > 0$	$-(u_{b1} - u_a)^2 + c_{b1}^2 > 0$
	$\Leftrightarrow |u_{b0} - u_a| < c_{b0}$	$\Leftrightarrow |u_{b1} - u_a| < c_{b1}$
	$\Leftrightarrow u_{b0} + c_{b0} > u_a$	$\Leftrightarrow u_{b1} + c_{b1} > u_a$
D.	$-(u_{b0} - u_a)^2 + c_{b0}^2 < 0$	$-(u_{b1} - u_a)^2 + c_{b1}^2 < 0$
	$\Leftrightarrow |u_{b0} - u_a| > c_{b0}$	$\Leftrightarrow |u_{b1} - u_a| > c_{b1}$
	$\Leftrightarrow u_{b0} + c_{b0} < u_a$	$\Leftrightarrow u_{b1} + c_{b1} < u_a$

The mutual positions of the gas characteristics around the solid contact are shown in Fig. 4.5. □

Remark 4.8. In the formulation of the "inverse" problem in Section 4.1, the unknowns on the solid contact are

$$\underbrace{\rho_{a0}, u_{a0}, p_{a0}, \rho_{a1}, \alpha_{a0}, \alpha_{a1}}_{\substack{\text{from 6 incoming or coinciding} \\ \text{solid characteristics}}}, \quad \underbrace{\rho_{b0}, u_{b0}, p_{b0}}_{\substack{\text{from 3 incoming} \\ \text{gas characteristics}}}, \quad \underbrace{u_{a1}, p_{a1}}_{\substack{\text{for 2 outcoming} \\ \text{solid characteristics}}}, \quad \underbrace{\rho_{b1}, u_{b1}, p_{b1}}_{\substack{\text{for 3 outcoming} \\ \text{gas characteristics}}},$$

i.e., there are 6 solid variables, which are assumed to be known from the solid-related impinging characteristics, and 3 gas variables from the gas characteristics. The remaining 5 unknowns are found from the solution of the 5 equations (4.4) as described in Section 4.1.

Using Theorem 4.7, we can introduce the following definitions.

Definition 4.9. *The side of the solid contact through which the gas enters is called the **front side**, while the other side is called the **back side**.*

Remark 4.10. Note that the Definition 4.9 makes sense: For the admissible solid contact, the gas may enter the solid contact only from one side. To see this, consider the different cases in the proof of Theorem 4.7.

4.4   Gas dynamics analogy

As we have shown in Section 2.3, the Euler equations in a duct of variable cross-section can be formally obtained from the BN model (4.1) under the assumptions (2.16). In Chapter 5, we present an extensive analysis of this system. Here, we wish to track another analogy between the BN model and the Euler equations in a duct. Namely, we notice that the relations (4.4), which express the constancy of the Riemann invariants across the solid contact, remind the integral relations in a converging-diverging nozzle for the stationary, isentropic Euler equations in a duct of variable cross-section

$$
\begin{aligned}
A\rho v &= \text{const} \\
\eta &= \text{const} \\
\frac{v^2}{2} + \frac{c^2}{\gamma - 1} &= \text{const},
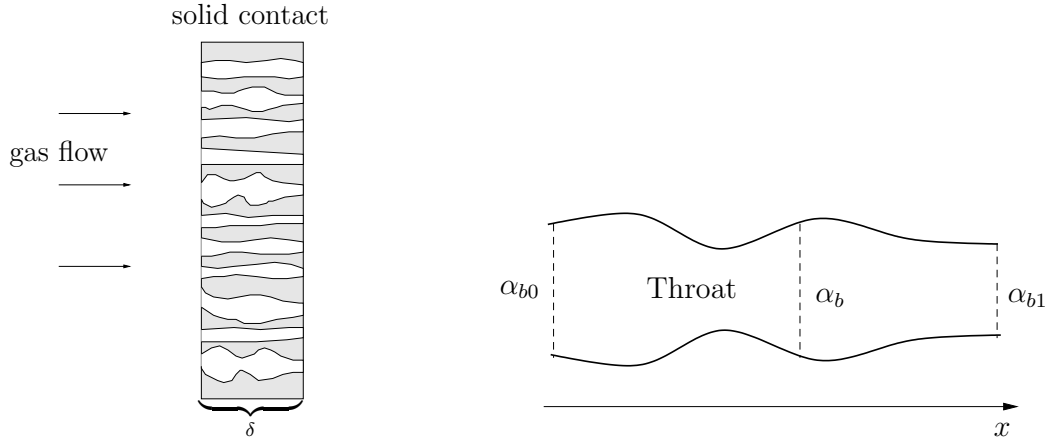\end{aligned}
\tag{4.38}
$$

Fig. 4.6. Left: Gas flow through the solid contact. Right: a pore of the variable cross-section.

see e.g. Courant and Friedrichs [22]. Here η is the isentrope and c is the sound speed. This similarity gives us reason to consider the solid contact as a *porous film* of infinitesimal thickness δ, $\delta \to 0$, see Fig. 4.6. Each pore represents a duct of variable cross section. The solid phase forms the walls of the duct. The values of α_b at the both sides of this porous film are given and equal to α_{b0} and α_{b1}, respectively. Within the duct, the gas volume fraction α_b changes from α_{b0} to α_{b1} and represents the change of the area of cross-section. The gas flow in the duct is governed by the relations (4.4). Using the similarity between (4.4) and (4.38), we can repeat the classical analysis of [22] to obtain the equality

$$\frac{d\alpha_b}{\alpha_b} = \left(\frac{v^2}{c_b^2} - 1\right) \frac{dv}{v}, \tag{4.39}$$

where now $v = u_b - u_a$ is the gas velocity relative to the velocity of the solid contact, and c_b is the gas sound speed. It is analogous to the well-known relation for the steady, isentropic Euler equations in a duct of variable cross-section, see [22].

We can easily establish several properties of this pore flow. Firstly, we know that the flow is isentropic, see (4.4b). Therefore, *no shocks are allowed in the flow.* For simplicity, let the relative velocity v be positive, $v > 0$. The case of negative v can be considered analogously. Then, from (4.39) we can state that *for increasing α_b the relative speed v increases when $v^2 > c_b^2$ and decreases when $v^2 < c_b^2$.* Using (4.4), we conclude that *in the direction of increasing α_b the gas flow is expanded when it is supersonic, and compressed when it is subsonic.* Finally, the *gas flow relative to the solid contact is supersonic(subsonic) at one side of the solid contact, iff it is also supersonic(subsonic) at the other side of it.* To see this, consider the different cases in the proof of Theorem 4.7. It

is convenient to represent these results in the following table, where ↑ denotes increase, and ↓ decrease:

Supersonic	$\alpha_b \uparrow$	$v \uparrow$	$\rho_b \downarrow$	$c_b \downarrow$
	$\alpha_b \downarrow$	$v \downarrow$	$\rho_b \uparrow$	$c_b \uparrow$
Subsonic	$\alpha_b \uparrow$	$v \downarrow$	$\rho_b \uparrow$	$c_b \uparrow$
	$\alpha_b \downarrow$	$v \uparrow$	$\rho_b \downarrow$	$c_b \downarrow$

Note that the duct can have several throats, see Fig. 4.6. By the classical theory of the Laval nozzle, see e.g. [22], the gas flow can change its character from subsonic to supersonic and vice versa only at the throat. From the property established above, we conclude that this change can occur only an *even* number of times.

Consider again the homogeneous system of the governing equations for the BN model (4.1). The action of the non-conservative terms $\mathbf{h}(\mathbf{u})\frac{\partial \alpha_a}{\partial x}$ there is reflected in the characteristic field, corresponding to the eigenvalue u_a, cf. Section 2.5, i.e. in the properties of the solid contact. Thus, the above analysis allows us to make several conclusions on the role of the the non-conservative terms in the system (4.1). Namely, we have rigorously shown that the gas volume fraction measures the *porosity* of the solid phase. Then, *the change in porosity acts as a nozzle which can either accelerate or decelerate the gas flow*. Note that this was previously stated by Embid and Baer [31], Bdzil *et al.* [12] from physical considerations.

4.5   Coinciding waves

As we mentioned previously, the characteristic speeds for the Riemann problem (4.1)-(4.3) can coincide with each other. Namely, each of the gas eigenvalues

$$u_b - c_b, \quad u_b, \quad u_b + c_b$$

can coincide with either of the solid eigenvalues

$$u_a - c_a, \quad u_a, \quad u_a + c_a.$$

However, the solid parameters do not change across the gas waves, and the gas parameters can change only across the solid contact (and of course across the gas waves), see Section 2.5. Therefore, the potentially interesting cases arise only when the solid contact, propagating with speed u_a, coincides with either $u_b \pm c_b$ or u_b. Since the characteristic fields $u_b \pm c_b$ can be either rarefactions or shock waves, and u_b is the contact discontinuity, we will consider these three cases separately.

4.5.1 Coinciding contacts

Let us fix α_{b0}, ρ_{b0}, p_{b0} to the left of the solid contact Σ as well as α_{b1} to the right of it. Further let the gas velocity approach u_a from the left, i.e.,

$$u_{b0} + \epsilon = u_a, \qquad \epsilon \to +0. \tag{4.40}$$

Under these conditions, we are interested in the change of the state to the right of the solid contact.

Consider the system of Riemann invariants (4.4) across the solid contact Σ. With $\eta_b = \frac{p_b + \pi_b}{\rho_b^{\gamma_b}} = \text{const}$, we can rewrite (4.4c) as

$$\alpha_{b0}(p_{b0} + \pi_b)^{1/\gamma_b}(u_{b0} - u_a) = \alpha_{b1}(p_{b1} + \pi_b)^{1/\gamma_b}(u_{b1} - u_a). \tag{4.41}$$

Using $c_b^2 = \frac{\gamma_b(p_b + \pi_b)}{\rho_b}$ in (4.4e), we get

$$\frac{(u_{b0} - u_a)^2}{2} + \frac{\gamma_b \eta_b^{1/\gamma_b}(p_{b0} + \pi_b)^{1-1/\gamma_b}}{\gamma_b - 1} = \frac{(u_{b1} - u_a)^2}{2} + \frac{\gamma_b \eta_b^{1/\gamma_b}(p_{b1} + \pi_b)^{1-1/\gamma_b}}{\gamma_b - 1}. \tag{4.42}$$

Let us show that p_{b1} remains bounded, i.e. $p_{b1} \not\to \infty$. Indeed, assume that it is not true. Then p_{b1} must exceed p_{b0}, $p_{b1} > p_{b0}$. However, since the left-hand side of (4.42) is bounded, the following estimate

$$\frac{(u_{b1} - u_a)^2}{2} + \frac{\gamma_b \eta_b^{1/\gamma_b}(p_{b1} + \pi_b)^{1-1/\gamma_b}}{\gamma_b - 1} > \frac{\gamma_b \eta_b^{1/\gamma_b}(p_{b1} + \pi_b)^{1-1/\gamma_b}}{\gamma_b - 1}$$

implies that $p_{b1} < \text{const}$, since γ_b, η_b, π_b are constants. Using this in (4.41), we get $u_{b1} \to u_a$. But then according to (4.42) is $p_{b1} \to p_{b0}$. Finally using again that the entropy $\eta_b = \frac{p_b + \pi_b}{\rho_b^{\gamma_b}} = \text{const}$ across the solid contact, we get also $\rho_{b1} \to \rho_{b0}$.

For the case of coinciding contacts, i.e. $u_{b0} = u_a$, we can easily find the solution of the system (4.4). Indeed, from (4.4c) it follows that $u_{b1} = u_a$. Then (4.4b) and (4.4e) imply that $\rho_{b0} = \rho_{b1}$ and $p_{b0} = p_{b1}$.

Thus, we have proved the following theorem.

Theorem 4.11. *Let us fix α_{b0}, ρ_{b0}, p_{b0} to the left of the solid contact Σ as well as α_{b1} to the right of it. Then, as the gas velocity u_{b0} approaches u_a, the gas variables to the right of Σ approach the ones to the left,*

$$\rho_{b1} \to \rho_{b0}, \quad u_{b1} \to u_a, \quad p_{b1} \to p_{b0}.$$

For the case $u_{b0} = u_a$,

$$\rho_{b1} = \rho_{b0}, \quad u_{b1} = u_a, \quad p_{b1} = p_{b0}.$$

Remark 4.12. Since the system of Riemann invariants (4.4) is symmetric with respect to subscripts 0 and 1, we can reverse the statement of Theorem 4.11. Namely, for fixed α_{b1}, ρ_{b1}, p_{b1} to the right of the solid contact Σ as well as α_{b0} to the left of it, and for $u_{b1} + \epsilon = u_a$, $\epsilon \to -0$, the gas variables to the left of the solid contact

$$\rho_{b0} \to \rho_{b1}, \quad u_{b0} \to u_a, \quad p_{b0} \to p_{b1}.$$

4.5.2   Sonic state attached to the solid contact

Let us consider the critical case when

$$(u_b - u_a)^2 \to c_b^2 \tag{4.43}$$

from either side of the solid contact Σ. At the limit, i.e. when $(u_b - u_a)^2 = c_b^2$, the system of governing equations (4.1) becomes *parabolic degenerate*, it is not hyperbolic anymore. Since the notion of an evolutionary discontinuity is defined only for a hyperbolic system, see Section 4.2, it is not applicable here.

Using the gas dynamics analogy of preceeding section, it is easy to establish the physical meaning for this phenomena. Remember that the difference of $\alpha_{b0} - \alpha_{b1}$ determines a pore in the solid contact, which is a converging or diverging nozzle, see Fig. 4.6. The flow in this pore is governed by the equation (4.39). Assume for simplicity that the gas relative speed is positive, $v = u_b - u_a > 0$, so the gas flow from the left to the right. If the condition (4.43) holds at the cross-section α_{b0}, i.e. at the state $\mathbf{u}_0$ to the left of Σ, then the relative gas flow is almost sonic there,

$$\mathrm{M}_0 = \frac{u_{b0} - u_a}{c_{b0}} = 1 + \epsilon, \qquad \epsilon \to \pm 0,$$

where M_0 is the signed relative Mach number at the state $\mathbf{u}_0$. Depending on the sign of ϵ and on the difference $\alpha_{b1} - \alpha_{b0}$, the gas flow in the pore either accelerates and expands, or decelerates and compresses, leading to very different states $\mathbf{u}_1$ to the right of Σ. Thus, such a sonic configuration is not stable.

We can also give an interpretation to the case in which the equation (4.11) has no roots. As it was mentioned in Section 4.1, it happens when α_{b1} becomes sufficiently small, cf. (4.10). According to the results of Section 4.4, the change of the gas parameters to the right of the solid contact is determined by whether the relative gas speed $u_b - u_a$ is subsonic or supersonic. When it is subsonic, then the gas flow accelerates and expands, so that the sound speed decreases and the relative Mach number $\mathrm{M} = |u_{b1} - u_a|/c_{b1}$ increases. As soon as the gas volume fraction falls below its critical value, where $\mathrm{M} = 1$, a shock intervenes and isentropic flow does not exist anymore. On the other hand, when the relative gas flow is supersonic, the relative Mach number decreases. Again, for the gas volume fraction below its critical value, an isentropic flow does not exist. Geometrically, we can illustrate the possible scenarios by considering the different cases in the proof of Theorem 4.7, see Fig. 4.7.

It is an easy matter to check that the solid contact can lie *inside* of the gas rarefaction only in the trivial case when $\mathbf{u}_0 = \mathbf{u}_1$, where $\mathbf{u}$ is given by (4.2). Then in particular $\alpha_{b0} = \alpha_{b1}$, so that the phases are decoupled. For simplicity, consider the gas 4-rarefaction (the case of 6-rarefaction can be done analogously). In the rarefaction wave, $u_b - c_b$ varies monotonically across the wave, so that the
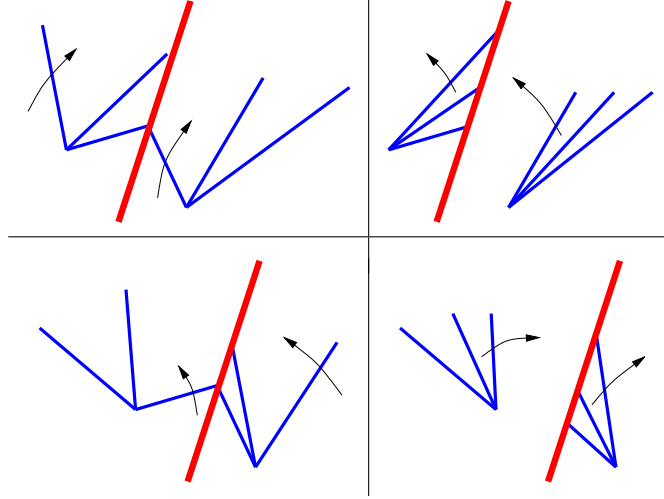
Fig. 4.7. Gas characteristics around the solid contact. As the characteristic $u_{b0} \pm c_{b0}$ moves in the arrow direction, the corresponding $u_{b1} \pm c_{b1}$ becomes equal to u_a (one root). Further change in $u_{b0} \pm c_{b0}$ leads to no roots in (4.11).

following equality should hold true,

$$u_{b0} - c_{b0} = u_a = u_{b1} - c_{b1}.$$

But using this in (4.4) implies

$$\mathbf{u}_0 = \mathbf{u}_1.$$

4.5.3   Shock vs. solid contact

Finally, let us describe the behaviour of the solution, when the (admissible) gas shock wave approaches the solid contact. For simplicity, we consider the shock at the left of the solid contact, i.e., $\sigma \to u_a$, $\sigma < u_a$, see Fig. 4.8.

Across the shock, the Rankine–Hugoniot conditions hold, and across the solid contact — the relations (4.4). Combining them, we get

$$\rho_b(u_b - \sigma) = \rho_{b0}(u_{b0} - \sigma) \to \rho_{b1}\frac{\alpha_{b1}}{\alpha_{b0}}(u_{b1} - u_{b0}) = \frac{M}{\alpha_{b0}} =: M_1 \tag{4.44a}$$

$$\rho_b(u_b - \sigma)^2 + p_b = \rho_{b0}(u_{b0} - \sigma)^2 + p_{b0} \to \frac{1}{\alpha_{a1}}(P - \alpha_{a0}p_{a0}) =: P_1 \tag{4.44b}$$

$$\frac{(u_b - \sigma)^2}{2} + \frac{c_b^2}{\gamma_b - 1} = \frac{(u_{b0} - \sigma)^2}{2} + \frac{c_{b0}^2}{\gamma_b - 1} \to \frac{(u_{b1} - u_a)^2}{2} + \frac{c_{b1}^2}{\gamma_b - 1} = E \tag{4.44c}$$

as $\sigma \to u_a$. Multiply (4.44c) by $2\rho_b$, and substract the result from (4.44b). Then

$$p_b\frac{\gamma_b + 1}{1 - \gamma_b} - \frac{2\gamma_b\pi_b}{\gamma_b - 1} \to P_1 - 2\rho_b E. \tag{4.45}$$
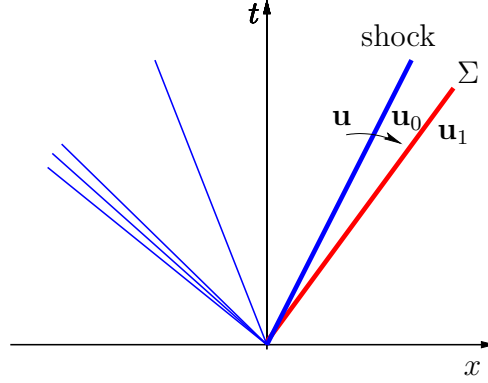
Fig. 4.8. Gas shock approaches the solid contact Σ from the left.

From (4.44a) and (4.44b)

$$p_b \to P_1 - \frac{M_1^2}{\rho_b}.$$

Substituting this into (4.45), we get the following relation for ρ_b,

$$(P_1 - \frac{M_1^2}{\rho_b})\frac{\gamma_b + 1}{1 - \gamma_b} - \frac{2\gamma_b \pi_b}{\gamma_b - 1} \to P_1 - 2\rho_b E.$$

In the limit it reveals the quadratic equation for ρ_b,

$$(P_1 - \frac{M_1^2}{\rho_b})\frac{\gamma_b + 1}{1 - \gamma_b} - \frac{2\gamma_b \pi_b}{\gamma_b - 1} = P_1 - 2\rho_b E,$$

with $\rho_b \neq 0$. This equation has two roots. One of them is always ρ_{b0}, and corresponds to the state $\mathbf{u} \equiv \mathbf{u}_0$. The other is necessarily admissible, since we consider the admissible shock wave. Using this root, we can find the state behind the shock

$$
\begin{aligned}
u_b &= \frac{M_1^2}{\rho_b} + \sigma \\
p_b &= P_1 - \frac{M_1^2}{\rho_b}.
\end{aligned}
\tag{4.46}
$$

Thus, we see that the state behind the shock approaches some finite state which is given by (4.46), as the shock approaches the solid contact.

4.6   Weak solution to the Riemann problem

As we have mentioned before, one cannot define a weak solution to the system (4.1) in the usual manner, as it is done for systems of conservation laws.

The reason is that the system (4.1) cannot be written in divergence form. For the Riemann problem (4.1)-(4.3), however, this difficulty appears only along one line, namely the solid contact, where the volume fraction α_a is discontinuous. In the rest of domain, the volume fraction is constant and equal to its left or right value,

$$\alpha(x,t) = \begin{cases} \alpha_{aL}, & \text{if } (x,t) \text{ lies to the left of solid contact} \\ \alpha_{aR}, & \text{if } (x,t) \text{ lies to the right of it.} \end{cases}$$

Therefore, everywhere away from the solid contact the system (4.1) reduces to the system of *conservation laws*

$$\mathbf{u}_t + \mathbf{f}(\mathbf{u})_x = 0, \tag{4.47}$$

where

$$\mathbf{u} = \begin{bmatrix} \rho_a \\ \rho_a u_a \\ \rho_a E_a \\ \rho_b \\ \rho_b u_b \\ \rho_b E_b \end{bmatrix}, \quad \mathbf{f}(\mathbf{u}) = \begin{bmatrix} \rho_a u_a \\ \rho_a u_a^2 + p_a \\ u_a(\rho_a E_a + p_a) \\ \rho_b u_b \\ \rho_b u_b^2 + p_b \\ u_b(\rho_b E_b + p_b) \end{bmatrix}. \tag{4.48}$$

Note that this system is just the two sets of uncoupled Euler equations for the phase a and b. For the system (4.47), we can define a weak solution in the usual manner, see Definition 4.14 below.

On the other hand, across the solid contact, the relations (4.4) hold. Our main idea is to find a *conservative* system of equations, which gives the relations (4.4) across the solid contact. In other words, we reverse the usual process of obtaining the Rankine–Hugoniot conditions for the system of conservation laws. There, one starts with a system of equations and gets the relations across a discontinuity. Here, we start from the relations across the discontinuity and wish to find the system of equations.

Let us rewrite the relations (4.4) in the form, which is reminiscent of the Rankine–Hugoniot conditions $\sigma[\mathbf{u}] = [\mathbf{f}]$. The mass balance (4.4c) is

$$u_a(\alpha_{b1}\rho_{b1} - \alpha_{b0}\rho_{b0}) = \alpha_{b1}\rho_{b1}u_{b1} - \alpha_{b0}\rho_{b0}u_{b0}. \tag{4.49}$$

The momentum equation (4.4d) can be rewritten as

$$P_0 + Mu_{b0} = P_1 + Mu_{b1}, \tag{4.50}$$

where $P_i = \alpha_{ai}p_{ai} + \alpha_{bi}p_{bi}$, $i = 0, 1$. This is equivalent to

$$u_a(\alpha_{b1}\rho_{b1}u_{b1} - \alpha_{b0}\rho_{b0}u_{b0}) = (P_1 + \alpha_{b1}\rho_{b1}u_{b1}^2) - (P_0 + \alpha_{b0}\rho_{b0}u_{b0}^2). \tag{4.51}$$

Multiply the energy equation (4.4e) by M, and add it to (4.50), multiplied by u_a. The result can be rewritten as

$$u_a\left[(\alpha_{b1}\rho_{b1}E_{b1} - \alpha_{a1}p_{a1}) - (\alpha_{b0}\rho_{b0}E_{b0} - \alpha_{a0}p_{a0})\right] =$$
$$\alpha_{b1}u_{b1}(\rho_{b1}E_{b1} + p_{b1}) - \alpha_{b0}u_{b0}(\rho_{b0}E_{b0} + p_{b0}). \tag{4.52}$$

Finally, near the solid contact

$$
\begin{aligned}
u_a &= \text{const} \\
\eta_b &= \text{const.}
\end{aligned}
\tag{4.53}
$$

The relations (4.49), (4.49), and (4.52) may be written in the vector form

$$
u_a \left(\tilde{\mathbf{U}}_1 - \tilde{\mathbf{U}}_0 \right) = \tilde{\mathbf{F}}_1 - \tilde{\mathbf{F}}_0,
\tag{4.54}
$$

where

$$
\tilde{\mathbf{U}} =
\begin{bmatrix}
\alpha_b \rho_b \\
\alpha_b \rho_b u_b \\
\alpha_b \rho_b E_b - \alpha_a p_a
\end{bmatrix}, \quad
\tilde{\mathbf{F}} =
\begin{bmatrix}
\alpha_b \rho_b u_b \\
\alpha_b \rho_b u_b^2 + P_i \\
\alpha_b u_b (\rho_b E_b + p_b)
\end{bmatrix},
$$

$P_i = \alpha_{ai} p_{ai} + \alpha_{bi} p_{bi}$, $i = 0, 1$. The equations (4.54) can be interpreted as the Rankine–Hugoniot relations across the solid contact for the system

$$
\frac{\partial \tilde{\mathbf{U}}(\mathbf{u}; \alpha_a)}{\partial t} + \frac{\partial \tilde{\mathbf{F}}(\mathbf{u}; \alpha_a)}{\partial x} = 0.
\tag{4.55}
$$

Note that (4.55) is the *underdetermined* system for finding all seven unknowns α_a, ρ_k, u_k, p_k for $k = a, b$. This is not surprising since we have started with the relations (4.4), which also do not give the values of all unknowns on the both sides of the solid contact. In addition to them, we have to prescribe the values of some parameters, see Section 4.1.

Let us show that for the Riemann problem (4.1) with the Riemann initial data of the form (4.3), the original system (4.1) reduces to a *conservative* system, such that

- A part of this system is equivalent to the system (4.55) and

- The Rankine–Hugoniot conditions for this system across the solid contact are equivalent to the relations (4.4)

$$\tag{4.56}$$

near the solid contact. We will investigate, to which system the original system (4.1) reduces under the conditions (4.53). Using $u_a = \text{const}$ in (4.1), we get

$$\frac{\partial \alpha_a}{\partial t} + \frac{\partial u_a \alpha_a}{\partial x} = 0 \tag{4.57a}$$

$$\frac{\partial \alpha_a \rho_a}{\partial t} + \frac{\partial \alpha_a \rho_a u_a}{\partial x} = 0 \tag{4.57b}$$

$$(p_a - p_b)\frac{\partial \alpha_a}{\partial x} + \alpha_a \frac{\partial p_a}{\partial x} = 0 \tag{4.57c}$$

$$\frac{\partial p_a}{\partial t} + \frac{\partial u_a p_a}{\partial x} = 0 \tag{4.57d}$$

$$\frac{\partial \alpha_b \rho_b}{\partial t} + \frac{\partial \alpha_b \rho_b u_b}{\partial x} = 0 \tag{4.57e}$$

$$\frac{\partial \alpha_b \rho_b u_b}{\partial t} + \frac{\partial (\alpha_b \rho_b u_b^2 + \alpha_b p_b)}{\partial x} = -p_b \frac{\partial \alpha_a}{\partial x} \tag{4.57f}$$

$$\frac{\partial \alpha_b \rho_b E_b}{\partial t} + \frac{\partial \alpha_b u_b (\rho_b E_b + p_b)}{\partial x} = -p_b u_a \frac{\partial \alpha_a}{\partial x}. \tag{4.57g}$$

Using (4.57c), (4.57d) in (4.57f) and (4.57g), we obtain

$$\frac{\partial \alpha_b \rho_b u_b}{\partial t} + \frac{\partial (\alpha_b \rho_b u_b^2 + \alpha_a p_a + \alpha_b p_b)}{\partial x} = 0 \tag{4.58}$$

$$\frac{\partial (\alpha_b \rho_b E_b - \alpha_a p_a)}{\partial t} + \frac{\partial \alpha_b u_b (\rho_b E_b + p_b)}{\partial x} = 0. \tag{4.59}$$

Also, the equation (4.57g) is equivalent to

$$\frac{\partial \eta_b}{\partial t} + u_b \frac{\partial \eta_b}{\partial x} = 0. \tag{4.60}$$

It is an easy matter to check that the system

$$\frac{\partial \alpha_a}{\partial t} + \frac{\partial u_a \alpha_a}{\partial x} = 0 \tag{4.61a}$$

$$\frac{\partial \alpha_a \rho_a}{\partial t} + \frac{\partial \alpha_a \rho_a u_a}{\partial x} = 0 \tag{4.61b}$$

$$\frac{\partial p_a}{\partial t} + \frac{\partial u_a p_a}{\partial x} = 0 \tag{4.61c}$$

$$\frac{\partial \alpha_b \rho_b}{\partial t} + \frac{\partial \alpha_b \rho_b u_b}{\partial x} = 0 \tag{4.61d}$$

$$\frac{\partial \alpha_b \rho_b u_b}{\partial t} + \frac{\partial (\alpha_b \rho_b u_b^2 + \alpha_a p_a + \alpha_b p_b)}{\partial x} = 0 \tag{4.61e}$$

$$\frac{\partial (\alpha_b \rho_b E_b - \alpha_a p_a)}{\partial t} + \frac{\partial \alpha_b u_b (\rho_b E_b + p_b)}{\partial x} = 0 \tag{4.61f}$$

$$\frac{\partial \eta_b}{\partial t} + u_b \frac{\partial \eta_b}{\partial x} = 0 \tag{4.61g}$$

is equivalent to the system (4.57) when $u_a = $ const. Posing also the second condition of (4.53), $\eta_b = $ const, the equations (4.57g) and (4.61g) are eliminated. Thus, the original system (4.1) is equivalent to the system

$$\frac{\partial \mathbf{U}}{\partial t} + \frac{\partial \mathbf{F}(\mathbf{U}, u_a)}{\partial x} = 0. \tag{4.62}$$

under the conditions (4.53) with

$$\mathbf{U} = \begin{bmatrix} \alpha_a \\ \alpha_a \rho_a \\ p_a \\ \alpha_b \rho_b \\ \alpha_b \rho_b u_b \\ \alpha_b \rho_b E_b - \alpha_a p_a \end{bmatrix}, \quad \mathbf{F}(\mathbf{U}, u_a) = \begin{bmatrix} \alpha_a u_a \\ \alpha_a \rho_a u_a \\ p_a u_a \\ \alpha_b \rho_b u_b \\ \alpha_b \rho_b u_b^2 + \alpha_a p_a + \alpha_b p_b \\ \alpha_b u_b (\rho_b E_b + p_b) \end{bmatrix}. \tag{4.63}$$

We see that both conditions (4.56) are fulfilled. Indeed, the system (4.55) just consists of the last three equations of (4.62). Across the solid contact, which is a discontinuity propagating with speed u_a, the Rankine–Hugoniot conditions coincide with (4.4).

Next, let us define a weak solution to the Riemann problem for a conservation law

$$\mathbf{u}_t + \mathbf{f}(\mathbf{u})_x = 0, \qquad \mathbf{u}(x, 0) = \begin{cases} \mathbf{u}_L, & x \le 0 \\ \mathbf{u}_R, & x > 0. \end{cases} \tag{4.64}$$

As usual, we consider the self-similar solutions, i.e.,

$$\mathbf{u}(x, t) = \mathbf{v}(\xi), \qquad \xi = \frac{x}{t}.$$

Then, the Riemann problem (4.64) is equivalent to

$$-\mathbf{v}_\xi \, \xi + \mathbf{f}(\mathbf{v})_\xi = 0, \quad \mathbf{v}(-\infty) = \mathbf{v}_L, \quad \mathbf{v}(\infty) = \mathbf{v}_R. \tag{4.65}$$

Let us suppose for the moment, that $\mathbf{v}$ is a classical solution of (4.65). Denote by $S(\xi_0, \xi_1)$ the sector, bounded by the rays ξ_0 and ξ_1. Also, let $C_0^1(]\xi_0, \xi_1[)$ be the class of all test functions ϕ which vanish outside of the open interval $]\xi_0, \xi_1[$, see Fig. 4.9. We multiply (4.65) by ϕ and integrate over all ξ,

$$\int_{-\infty}^{\infty} (-\mathbf{v}_\xi \, \xi + \mathbf{f}(\mathbf{v})_\xi) \phi(\xi) \, d\xi = \int_{\xi_0}^{\xi_1} (-\mathbf{v}_\xi \, \xi + \mathbf{f}(\mathbf{v})_\xi) \phi(\xi) \, d\xi.$$

Integrating by parts gives

$$\begin{aligned} \int_{\xi_0}^{\xi_1} (-\mathbf{v}_\xi \, \xi + \mathbf{f}(\mathbf{v})_\xi) \phi \, d\xi &= (-\xi \phi \mathbf{v} + \phi \mathbf{f}(\mathbf{v}))\Big|_{\xi_0}^{\xi_1} + \int_{\xi_0}^{\xi_1} (\mathbf{v}(\phi \, \xi)_\xi - \mathbf{f}(\mathbf{v}) \phi_\xi) \, d\xi \\ &= \int_{\xi_0}^{\xi_1} (\mathbf{v}(\phi \, \xi)_\xi - \mathbf{f}(\mathbf{v}) \phi_\xi) \, d\xi = 0. \end{aligned} \tag{4.66}$$
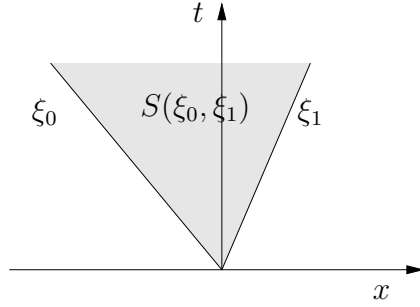
Fig. 4.9. A test function $\phi \equiv 0$ outside of $S(\xi_0, \xi_1)$ and on the rays ξ_0, ξ_1.

Thus, if $\mathbf{v}$ is a classical solution of (4.65), then (4.66) holds for all $\phi \in C_0^1(]\xi_0, \xi_1[)$. However, $\mathbf{v}$ does not need to be differentiable anymore. This gives rise to the following definition.

Definition 4.13. *A bounded measurable function $\mathbf{v} = \mathbf{v}(\xi)$ is called a weak solution to the Riemann problem (4.65) if $\mathbf{v}$ satisfies (4.66) for all $\phi \in C_0^1(]\xi_0, \xi_1[)$.*

Let us check, if we can get the Rankine–Hugoniot conditions across a discontinuity from this definition for these special self-similar solutions. Consider a discontinuity s and a sector $S(s_0, s_1)$ such that $s \in S(s_0, s_1)$ and s is the only discontinuity there. Let $\phi \in C_0^1(]s_0, s_1[)$ be some test function. The weak solution of (4.65) in $S(s_0, s_1)$ is defined by

$$\int_{s_0}^{s_1} (\mathbf{v}(\phi\,\xi)_\xi - \mathbf{f}(\mathbf{v})\phi_\xi)\,d\xi = 0.$$

Splitting the integral and integrating by parts,

$$\int_{s_0}^{s_1} (\mathbf{v}(\phi\,\xi)_\xi - \mathbf{f}(\mathbf{v})\phi_\xi)\,d\xi$$

$$= \int_{s_0}^{s} (\mathbf{v}(\phi\,\xi)_\xi - \mathbf{f}(\mathbf{v})\phi_\xi)\,d\xi + \int_{s}^{s_1} (\mathbf{v}(\phi\,\xi)_\xi - \mathbf{f}(\mathbf{v})\phi_\xi)\,d\xi$$

$$= (-\xi\phi\mathbf{v} + \phi\mathbf{f}(\mathbf{v}))\Big|_{\mathbf{s}_0}^{s} + \int_{s_0}^{s} (-\mathbf{v}_\xi\,\xi + \mathbf{f}(\mathbf{v})_\xi)\phi\,d\xi$$

$$+ (-\xi\phi\mathbf{v} + \phi\mathbf{f}(\mathbf{v}))\Big|_{s}^{s_1} + \int_{s}^{s_1} (-\mathbf{v}_\xi\,\xi + \mathbf{f}(\mathbf{v})_\xi)\phi\,d\xi$$

$$= \phi(s)s(\mathbf{v}_l - \mathbf{v}_r) + \phi(s)(\mathbf{f}(\mathbf{v}_r) - \mathbf{f}(\mathbf{v}_l)) = 0, \qquad (4.67)$$

where $\mathbf{v}_l = \mathbf{v}(s - 0)$ and $\mathbf{v}_r = \mathbf{v}(s + 0)$. Dividing (4.67) by $\phi(s) \neq 0$, we obtain the usual Rankine–Hugoniot relations across s.

Now, using Definition 4.13, we can define a weak solution to the Riemann problem for the *non-conservative* system (4.1). We will utilize the fact established above that everywhere locally this non-conservative system is equivalent to the conservative one, either (4.47) or (4.62).

Definition 4.14. *Consider a sector $S(\xi_0, \xi_1)$, such that the solid contact lies in it, and assume that the solid contact is the only surface of discontiuity in $S(\xi_0, \xi_1)$. Then, a function $\mathbf{v} = \mathbf{v}(\xi) \in L^\infty_{loc}(\mathbb{R})$ is called a weak solution of the Riemann problem (4.1)-(4.3), if for any small $\epsilon > 0$*

1. *To the left of $S(\xi_0, \xi_1)$, i.e., $\xi \in [-\infty, \xi_0]$, $\mathbf{v} = \mathbf{v}(\xi)$ is a weak solution of (4.47),*

$$\int_{-\infty}^{\xi_0} (\mathbf{v}(\phi\,\xi)_\xi - \mathbf{f}(\mathbf{v})\phi_\xi)\,d\xi = 0, \qquad \phi \in C_0^1(]-\infty, \xi_0 + \epsilon[),$$

   $\mathbf{v}(\xi) = \mathbf{u}(x,t)$, $\mathbf{f}(\mathbf{v}) = \mathbf{f}(\mathbf{u})$, and $\mathbf{u}$, $\mathbf{f}(\mathbf{u})$ are given by (4.48).

2. *To the right of $S(\xi_0, \xi_1)$, i.e., $\xi \in [\xi_1, \infty]$, $\mathbf{v} = \mathbf{v}(\xi)$ is a weak solution of (4.47),*

$$\int_{\xi_1}^{\infty} (\mathbf{v}(\phi\,\xi)_\xi - \mathbf{f}(\mathbf{v})\phi_\xi)\,d\xi = 0, \qquad \phi \in C_0^1(]\xi_1 - \epsilon, \infty[),$$

   $\mathbf{v}(\xi) = \mathbf{u}(x,t)$, $\mathbf{f}(\mathbf{v}) = \mathbf{f}(\mathbf{u})$, and $\mathbf{u}$, $\mathbf{f}(\mathbf{u})$ are given by (4.48).

3. *Inside of $S(\xi_0, \xi_1)$, i.e., $\xi \in [\xi_0, \xi_1]$, $\mathbf{v} = \mathbf{v}(\xi)$ is a weak solution of (4.62),*

$$\int_{\xi_0}^{\xi_1} (\mathbf{v}(\phi\,\xi)_\xi - \mathbf{f}(\mathbf{v}, u_a)\phi_\xi)\,d\xi = 0, \qquad \phi \in C_0^1(]\xi_0 - \epsilon, \xi_1 + \epsilon[),$$

   $\mathbf{v}(\xi) = \mathbf{U}(x,t)$, $\mathbf{f}(\mathbf{v}, u_a) = \mathbf{F}(\mathbf{U}, u_a)$, and $\mathbf{U}$, $\mathbf{F}(\mathbf{U}, u_a)$ are given by (4.63).

Remark 4.15. Note that in the sector $S(\xi_0 - \epsilon, \xi_0 + \epsilon)$, the definitions 1 and 3 coincide, and in the sector $S(\xi_1 - \epsilon, \xi_1 + \epsilon)$, the definitions 2 and 3 coincide.

Remark 4.16. In [26], Dal Maso, LeFloch, and Murat introduce a notion of the non-conservative product and give a definition of a weak solution to a general non-conservative system on its basis. In particular, this applies also to the system (4.1). In contrast to the definition of [26], we have used some physical observations in Definition 4.14, which are valid only for systems of a certain structure like (4.1). In particular, we will use the same approach in defining a weak solution to the Riemann problem for the Euler equations in a duct of variable cross-section (2.19), see Section 5.3 below. There are several reasons why such definitions might be helpful. Firstly, they may give an idea for constructing of approximate Riemann solvers for the non-conservative systes like (4.1). Secondly, we establish in Section 5.4 below, that the solution to the Riemann problem for the Euler equations in a duct (2.19) is *not unique*. Then, the physical considerations behind the definition of a weak solution can help in determining of an admissibility selection criterion.

4.7   Test cases

As we have seen in Chapter 2, the generic system of two-phase flow equations (2.13) consists of the two sets of the Euler equations for both phases, coupled with the non-conservative terms and the source terms. Therefore, a "good" numerical scheme for the equations (2.13) should be necessarily "good" for the Euler equations. The notion "good" denotes well-known properties, like convergence to the entropy solution, reasonable accuracy, robustness etc. For the Euler equations, one has a number of test cases, intended to check these properties for each particular scheme. An excellent reference is Toro [89].

However, for the two-phase problems, there exists only a small number of test cases, and usually they incorporate several physical effects, specific material properties, and external forces, see e.g. Ransom [71]. All these make it difficult to compare the numerical methods for two-phase flows.

Here, we propose a number of test cases for the homogeneous BN model, using the exact solution to the Riemann problem, which was obtained in Section 4.1. The tests are aimed at the investigation of some specific two-phase phenomena, which do not have a counterpart in one-phase flows. In particular, a number of tests are designed to assess the behaviour of numerical methods for the Riemann problem with almost coinciding wave speeds. The exact solutions were found by running our package CONSTRUCT [5], which is an implementation of the algorithm of Section 4.1. In Section 2.3 we have shown that the system of equations for the BN model (4.1) reduces to the system of the Euler equations in a duct of variable cross section (2.19) under the assumptions (2.16). Thus, under these conditions and if we consider only gas waves in the solution of the Riemann problem, we can use CONSTRUCT for the system (2.19) too, see Chapter 5.

In Chapter 3, we have proposed a numerical method for compressible multi-phase flows, which will always be referred to as VFRoe. In Chapter 5, we compare the numerical results of VFRoe with the exact solutions to the Riemann problems for the Euler equations in a duct of variable cross section. Here we consider the BN model of two-phase flows. To see clearly the effects of the VFRoe discretization, we present here numerical results of first order accuracy. The extension to the second order is described in Section 3.2.4. We have always used 300 mesh cells and CFL = 0.9 in the calculations presented below. For some of the test cases, calculations on finer meshes with 500 and 1000 mesh cells were carried out, but the results are not reproduced here. We mention some of them in the discussion. For simplicity, we have used the ideal gas EOS, i.e., $\gamma_k = 1.4, \pi_k = 0$ in the stiffened gas EOS (2.5) for the phase $k = a, b$. The initial position of the discontinuity is always 0.5.

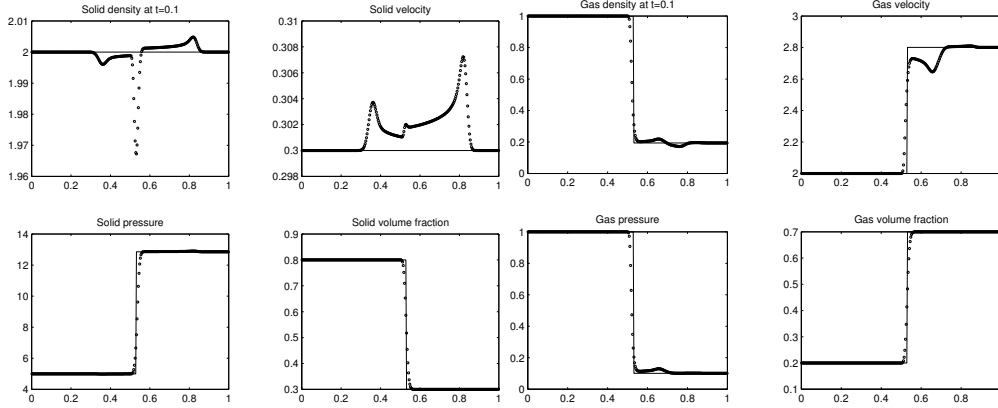**Test 1: Single solid contact**   Consider the following Riemann problem for the BN model

Fig. 4.10. The comparison of the VFRoe numerical results (dots) with the exact solution (line) for Test 1.

Phase k	α_{kL}	ρ_{kL}	u_{kL}	p_{kL}	a_{kR}	ρ_{kR}	u_{kR}	p_{kR}
a	0.8	2	0.3	5	0.3	2	0.3	12.8567
b	0.2	1	2	1	0.7	0.1941	2.8011	0.10

Its solution consists of the single solid contact, propagating with the velocity 0.3. The numerical results are presented in Fig. 4.10. In this test, the jump of the volume fraction $\alpha_{aR} - \alpha_{aL} = 0.5$.

Test 2: Coinciding shocks and rarefactions A particular issue on the Riemann problem for the equations (4.1) is that several waves can coincide with each other. However, the gas parameters do not change across the solid waves (except for the solid contact) and vice versa, see Section 2.5. Thus, the numerical solution across these waves should be independent of the presence of the waves of the other phase. If we take the initial data as follows

Phase k	α_{kL}	ρ_{kL}	u_{kL}	p_{kL}	a_{kR}	ρ_{kR}	u_{kR}	p_{kR}
a	0.1	0.2068	1.4166	0.0416	0.2	2.2263	0.9366	6.0
b	0.9	0.5806	1.5833	1.375	0.8	0.4890	-0.70138	0.986

then the Riemann solution consists of two coinciding shock waves for the gas and solid, as well as a gas shock inside of the solid rarefaction. The structure of the Riemann problem and the numerical results for this test are presented in Fig. 4.11.

Test 3: Coinciding contacts When the solid and gas contacts approach each other, both u_a and p_b are almost constant there, see Section 4.5. Therefore, the non-conservative terms (2.46)

$$p_b \frac{\partial \alpha_a}{\partial x} \approx \frac{\partial p_b \alpha_a}{\partial x}, \qquad p_b u_a \frac{\partial \alpha_a}{\partial x} \approx \frac{\partial p_b u_a \alpha_a}{\partial x}$$
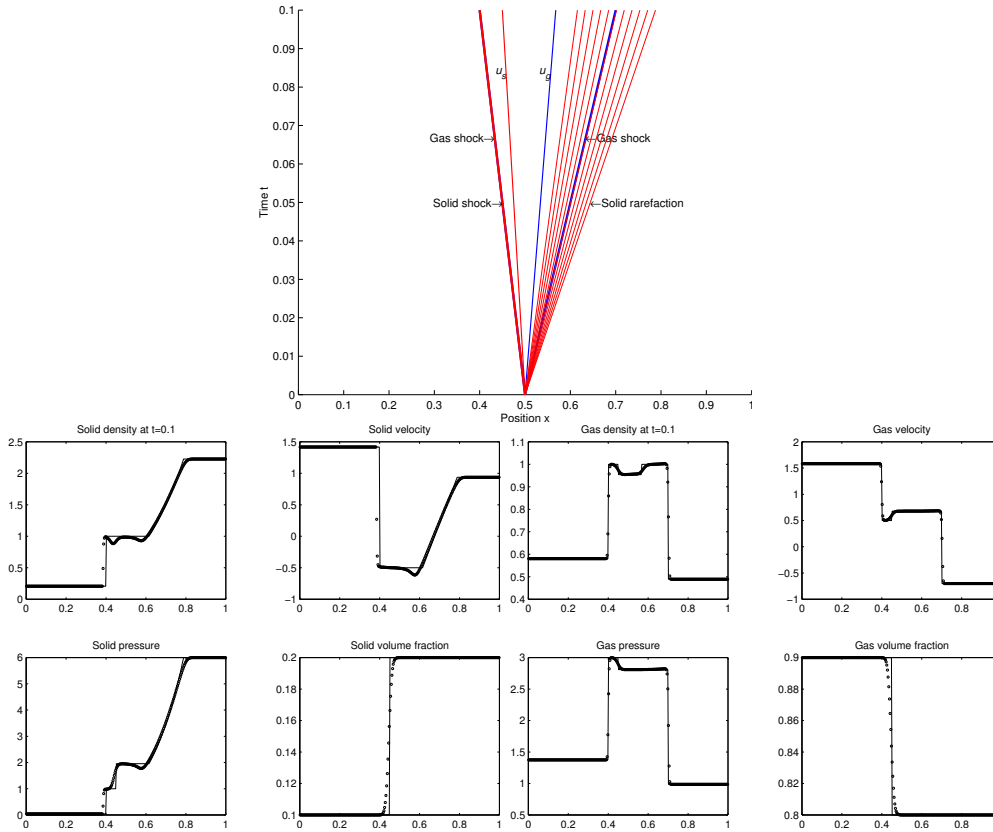
Fig. 4.11. The comparison of the VFRoe numerical results (dots) with the exact solution (line) for Test 2.

near the solid contact. Thus, this test should not pose serious difficulties. This configuration occurs if we take the following initial data

Phase k	α_{kL}	ρ_{kL}	u_{kL}	p_{kL}	a_{kR}	ρ_{kR}	u_{kR}	p_{kR}
a	0.1	0.9123	1.6305	1.5666	0.9	0.8592	-0.0129	1.1675
b	0.9	2.6718	-0.050	1.5	0.1	1.3359	0.5438	1.5

The structure of the Riemann problem and the numerical results for this test are presented in Fig. 4.12.

Test 4: Gas shock approaches solid contact   At the limit, i.e. when the gas shock coincides with the solid contact, the jump conditions across this "double discontinuity" are given in Section 4.5. To achieve such a configuration, one may take the following initial data

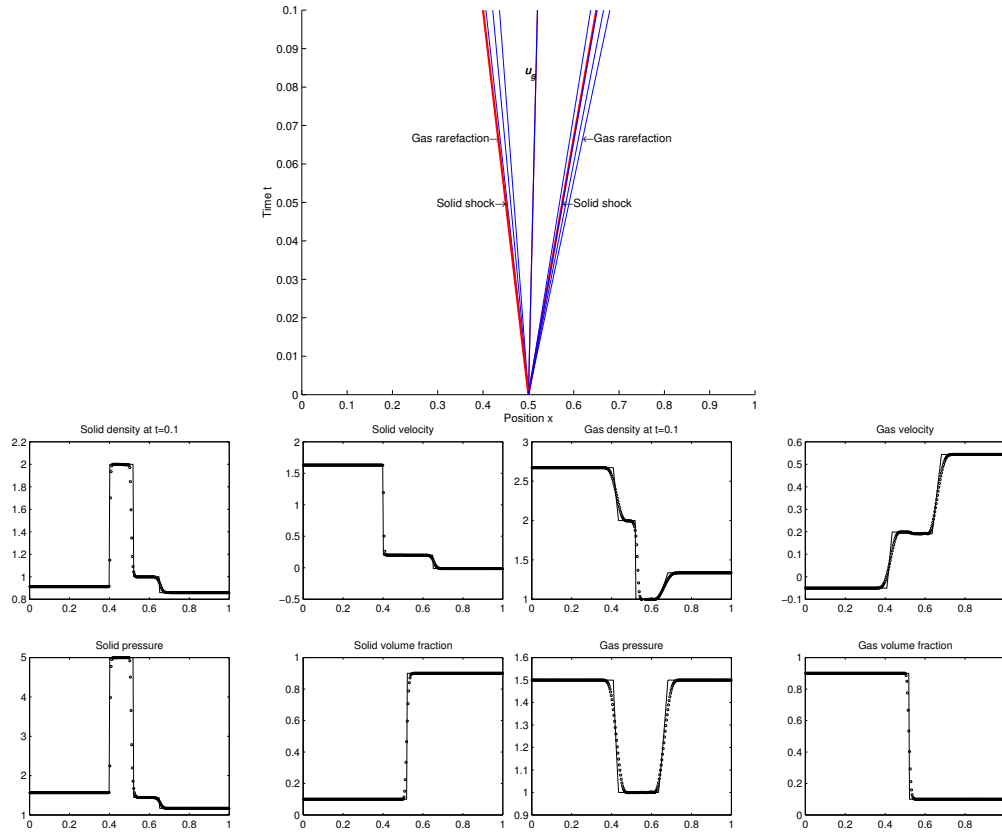| Phase k	α_{kL}	ρ_{kL}	u_{kL}	p_{kL}	a_{kR}	ρ_{kR}	u_{kR}	p_{kR}
a	0.5	2.1917	-0.995	3.0	0.1	0.6333	-1.1421	2.5011
b	0.5	6.3311	-0.789	1	0.9	0.4141	-0.6741	0.0291

Fig. 4.12. The comparison of the VFRoe numerical results (dots) with the exact solution (line) for Test 3.

The structure of the Riemann problem and the numerical results for this case are presented in Fig. 4.13.

Test 5: Gas rarefaction attached to the solid contact   Consider the following Riemann problem

Phase k	α_{kL}	ρ_{kL}	u_{kL}	p_{kL}	a_{kR}	ρ_{kR}	u_{kR}	p_{kR}
a	0.5	2	-1	2	0.1	1	-1	8.3994
b	0.5	0.2702	-3.4016	0.1	0.9	0.4666	-2.6667	0.2148

The exact solution to this test consists of a gas rarefaction, approaching the solid contact from the left. In the limit, a parabolic degeneracy occurs, see Section 4.5.2. The structure of the Riemann problem and the numerical results are shown in Fig. 4.14.

Discussion of the numerical results

The results presented have a very different quality for the various configurations. It is obvious that for big jumps in volume fraction the VFRoe method gives
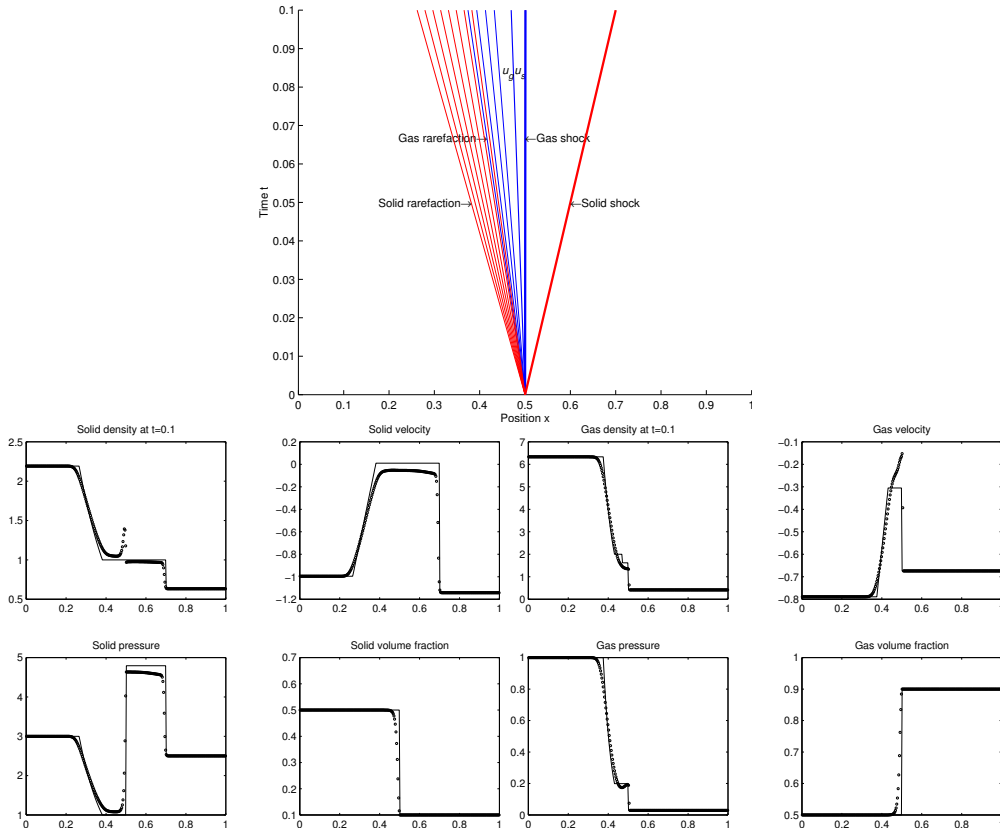
Fig. 4.13. The comparison of the VFRoe numerical results (dots) with the exact solution (line) for Test 4.

inadequate results, see e.g. Test 1 in Fig. 4.10. The numerical solution exhibits oscillations near the solid contact, which do not disappear as the mesh is refined. On finer meshes, one just has sharper peaks in the solid density and velocity. In the course of time, these oscillations are transported downstream, see Fig. 4.10. The results for Test 2 in Fig. 4.11 show that the waves of different phases affect each other, which should not be the case. Observe the undershoots in the solid density and velocity in Fig. 4.11. As expected, we obtain good numerical solution for Test 3 in Fig. 4.12. The discontinuities are extensively smeared, which is typical for the first order method. The second order method scheme resolves the discontinuities much better. The method behaves very unsatisfactorily in Test 4, where the gas shock approaches the solid contact. The numerical solution deviates strongly from the exact one, see Fig. 4.13. We note that poor numerical resolution of the solid velocity and pressure there is not due to the first order method used. Indeed, the numerical solution actually underestimates the values for the solid velocity and pressure in Fig. 4.13, which cannot be explained just by first order smearing, see the results for e.g. Test 3 in Fig. 4.12. The results for
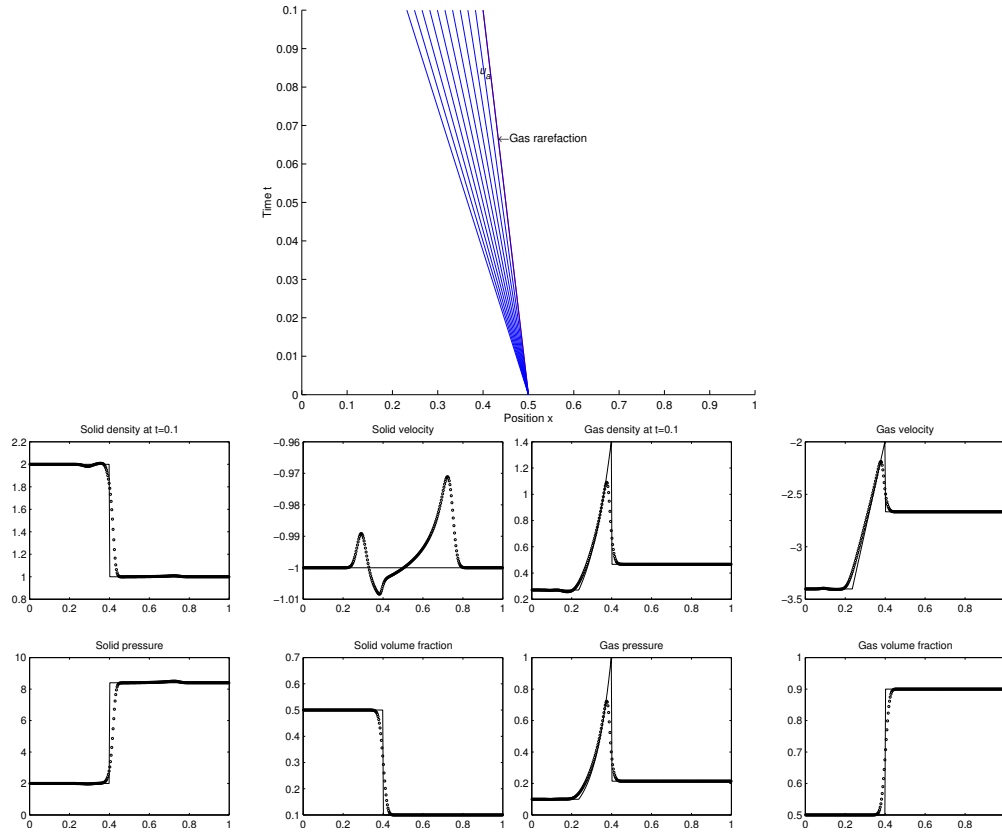
Fig. 4.14. The comparison of the VFRoe numerical results (dots) with the exact solution (line) for Test 5.

Test 5 are quite satisfactory, except for the solid velocity, which exhibits strong oscillations, see Fig. 4.14.

The reason such behaviour of the VFRoe scheme lies in the chosen discretization of the non-conservative terms (2.46). It is is obtained via the assumption of constant velocity and pressure, see Section 3.2. For all tests presented above this assumption is of course violated. Depending on the particular problem, the numerical results differ more or less from the exact solution.

We note that although VFRoe gives poor results for some patalogical cases described above, it behaves quite reasonadly for a large variety of test problems, see the results of Section 4.7. Also, we have used VFRoe for the solution of several Riemann problems to Euler equations in a duct, see Chapter 5. The test problems considered there do not contain coinciding waves, and therefore the numerical approximation is quite satisfactory.

Chapter 5

Analysis of the compressible duct flow

Since the Euler equations in a duct of variable cross-section can be viewed as a particular case of the BN model, see Chapter 4, the analysis presented there can be repeated here almost without changes. In particular, we can define a weak solution to the corresponding Riemann problem and build exact solutions to it with CONSTRUCT [5].

It appears that the solution to the Riemann problem is not unique. Therefore, it must also the case for the BN model. The non-uniqueness of the Riemann solution is closely related to the non-strict hyperbolicity of the governing equations. It leads to the situations, that for certain Riemann initial data, several *configurations* (i.e., mutual positions of the waves) of the Riemann solution are possible, and each of these configurations provides its own solution. Each discontinuity in these non-unique solutions locally satisfies the entropy conditions of Section 2.4, so these conditions are not sufficient to rule out physically irrelevant solutions. To this end, we employ the following idea. Remember that the quasi-one-dimensional Euler equations in a duct are obtained by averaging of the usual multi-dimensional Euler equations over a duct, see e.g. Zucrow and Hoffman [97]. Thus, a multi-dimensional calculation of the Euler equations in a duct can help us in determining which solution is not physically realizable. Here, we provide only 2D calculations. According to them, the 1D solutions picked out by these 2D computations satisfy a kind of an *entropy rate admissibility criterion*, proposed by Dafermos [24] in the context of conservation laws. Of course, the experimental data as well as further theoretical investigations would give a more solid basis for this kind of criterion.

The plan of this Chapter is as follows. In Section 5.1 we consider a "naive" procedure for finding of a solution to the Euler equations in a duct, which is based on adopting some approximate Rankine–Hugoniot conditions for the system of governing equations. Although in some cases this approach may give correct solutions, one inevitably introduces some assumptions, which may lead to different

results. In Section 5.3 we define a weak solution to the Riemann problem, which is analogous to the case of the BN model, see Chapter 4. Section 5.4 is devoted to the study of the non-uniqueness of the Riemann solution. We analyse different configurations in the solution, and prove several uniqueness criteria. Further, in Section 5.5 we provide 2D calculations of test problems and propose a criterion for picking up the unique physically relevant solution. In Section 5.6 we discuss the procedure of finding the exact solution to the Riemann problem. It reduces to the solution of the nonlinear algebraic system, which can be solved e.g. with Newton's method. Finally, in Section 5.7 we propose a Godunov-type method for the numerical solution of the Euler equations in a duct, based on the exact Riemann solver of Section 5.6. In the construction of the scheme we use the fact that the non-conservative term plays a role only across a *stationary* discontinuity in the solution to the local Riemann problems at cell interfaces. Therefore, inside a computational cell, we are left with the conservation law. Integrating it over the cell, we get the updated cell averages at the next time step. It is worth mentioning that we obtain a *conservative* method for the *non-conservative* system.

5.1   Naive solution to the Riemann problem

Consider the Riemann problem for the system of Euler equations in the duct of variable cross section $A = A(x)$. It has the form

$$\frac{\partial \mathbf{u}}{\partial t} + \frac{\partial \mathbf{f}(\mathbf{u})}{\partial x} \;=\; \mathbf{h}(\mathbf{u})\frac{\partial A}{\partial x}, \tag{5.1}$$

$$\mathbf{u}(x,0) \;=\; \begin{cases} \mathbf{u}_L, & x \le x_0 \\ \mathbf{u}_R, & x > x_0, \end{cases} \tag{5.2}$$

where

$$\mathbf{u} = \begin{bmatrix} A \\ A\rho \\ A\rho v \\ A\rho E \end{bmatrix}, \qquad \mathbf{f}(\mathbf{u}) = \begin{bmatrix} 0 \\ A\rho v \\ A(\rho v^2 + p) \\ Av(\rho E + p) \end{bmatrix}, \qquad \mathbf{h}(\mathbf{u}) = \begin{bmatrix} 0 \\ 0 \\ p \\ 0 \end{bmatrix}. \tag{5.3}$$

We use the stiffened gas EOS (2.5) to close the system. The Riemann problem (5.1), (5.2) can be viewed as the decay of the initial discontinuity in the tube with a sudden change in the cross-section, see Fig. 5.1. Note that the equations (5.1) cannot be written in divergence form, exactly as the governing equations for the two-phase flow (2.13).

Experimental results show that in some short time, the flow near the jump in cross-section becomes stationary, see Dulov [29]. The naive approach in finding relations across this jump would be to employ some approximate Rankine–
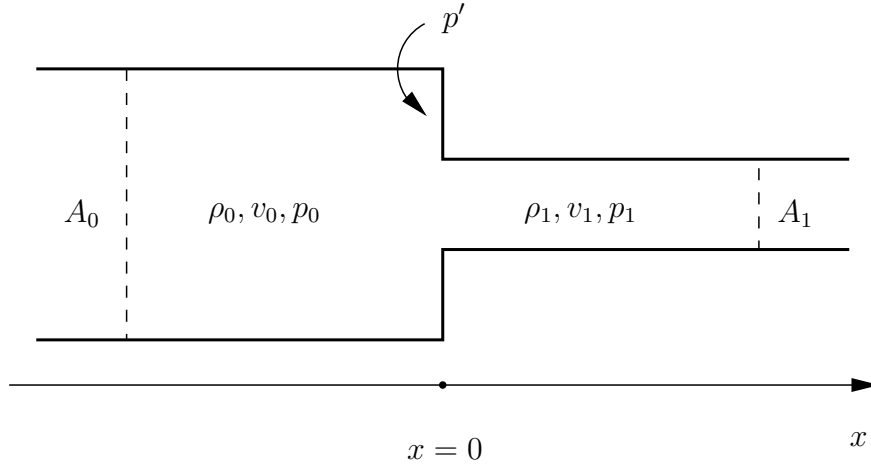
Fig. 5.1. The Riemann problem for the Euler equations in a duct with the sudden change in the cross-section at $x = 0$.

Hugoniot conditions for the system (5.1)

$$\begin{aligned}
[A\rho u] &= 0 \\
[A(\rho v^2 + p)] &= [A]\,p' \\
[Av(\rho E + p)] &= 0,
\end{aligned}$$

where the jumps are denoted by $[\cdot] = (\cdot)_1 - (\cdot)_0$, and p' is the pressure at the ledge, see Fig. 5.1. However, one has to use some additional considerations to determine p'. In [29, 96], the authors make different assumptions to this end. This freedom in the choice for p' can lead to different wave patterns in the solution to the Riemann problem (5.1), (5.2). In particular, the analysis of [29] does not cover some possible configurations of this Riemann problem.

5.2 Admissibility criterion for the stationary contact

The system (5.1) is an important particular case of a so-called nonlinear *resonant* non-strictly hyperbolic system of the form

$$\begin{aligned}
A_t &= 0 \\
\mathbf{u}_t + \mathbf{f}(\mathbf{u})_x &= \mathbf{h}(A, \mathbf{u})A_x,
\end{aligned} \tag{5.4}$$

where $\mathbf{u} \in \mathbb{R}^p$, $\mathbf{f} : \mathbb{R}^p \to \mathbb{R}^p$, and $\mathbf{h} : \mathbb{R}^{p+1} \to \mathbb{R}^p$. Indeed, for the choice

$$\mathbf{u} = \begin{bmatrix} \rho \\ \rho v \\ \rho E \end{bmatrix}, \quad \mathbf{f}(\mathbf{u}) = \begin{bmatrix} \rho v \\ \rho v^2 + p \\ v(\rho E + p) \end{bmatrix}, \quad \mathbf{h}(A, \mathbf{u}) = \begin{bmatrix} -\rho v/A \\ -\rho v^2/A \\ -v(\rho E + p)/A \end{bmatrix} \tag{5.5}$$

we recover the system (5.1). Systems of the type (5.4) were studied by Liu [61, 62], Isaacson and Temple [44, 45]. For each fixed A, the system (5.4) is assumed to be strictly hyperbolic, and each characteristic field is either genuinely nonlinear, or linearly degenerate. A nonlinear resonance occurs when two characteristic speeds coincide with each other. Therefore, the usual approach is to consider solutions in a neighborhood of this resonance state.

Let us rewrite the system (5.4) as

$$\mathbf{V}_t + \mathbf{B}(\mathbf{V})\,\mathbf{V}_x = 0, \qquad \mathbf{V} = \begin{pmatrix} A \\ \mathbf{u} \end{pmatrix}, \quad \mathbf{B}(\mathbf{V}) = \begin{pmatrix} 0 & 0 \\ \mathbf{f}_A - \mathbf{h} & \mathbf{f_u} \end{pmatrix}, \qquad (5.6)$$

and consider the Riemann problem for it, i.e.

$$\mathbf{V}(x,0) = \begin{cases} \mathbf{V}_L, & x \le 0 \\ \mathbf{V}_R, & x > 0. \end{cases} \qquad (5.7)$$

The matrix $\mathbf{B}(\mathbf{V})$ has $p+1$ eigenvalues $\lambda_0 = 0, \lambda_1, \ldots, \lambda_p$ and $p+1$ corresponding right eigenvectors $\mathbf{R}_0, \mathbf{R}_1, \ldots, \mathbf{R}_p$. Here we do not assume that they are linearly independent. We will search for the eigenvector $\mathbf{R}_0$ in the form $\mathbf{R}_0 = \begin{pmatrix} b_0 \\ \mathbf{r}_0 \end{pmatrix}$. A straightforward calculation gives the values of $\mathbf{R}_i = \begin{pmatrix} 0 \\ \mathbf{r}_i \end{pmatrix}$, $i = 1, \ldots, p$. Here λ_i and $\mathbf{r}_i$ are respectively the eigenvalues and eigenvectors of the matrix $\mathbf{f_u}$ for $i = 1, \ldots, p$. Also, let us introduce the left eigenvectors (row vectors) $\mathbf{l}_i$. Since all eigenvalues of $\mathbf{f}_u$ are distinct, the right eigenvectors $\mathbf{r}_i$ are linearly independent. Then, we can always normalize the row vectors $\mathbf{l}_i$ in such a way that

$$\mathbf{l}_i \mathbf{r}_j = \delta_{ij},$$

where δ_{ij} is the Kronecker delta symbol.

Observe that the 0-characteristic field, corresponding to the eigenvalue $\lambda_0 = 0$, is linearly degenerate, $\nabla_{\mathbf{V}} \lambda_0 \cdot \mathbf{R}_0 = 0$. Therefore, the 0-wave will be the *stationary* 0-contact. Let us write down the evolutionarity criterion for this wave. By the analysis of Section 4.2.2, the 0-contact will be evolutionary iff

$$\text{sign}\,(\lambda_i(\mathbf{V}_0)) = \text{sign}\,(\lambda_i(\mathbf{V}_1)), \quad i = 1, \ldots, p. \qquad (5.8)$$

For the resonant systems of the type (5.4), Isaacson and Temple [44] observed that the solution across this stationary 0-contact is not unique. To deal with it, they proposed an admissibility criterion in order to pick out the relevant wave. In what follows, we will discuss this criterion and show that it is equivalent to the evolutionarity condition (5.8).

Following Isaacson and Temple [44], consider the solution to the Riemann problem (5.6), (5.7) in a neighborhood of a state $\mathbf{V}_* = \begin{pmatrix} A_* \\ \mathbf{u}_* \end{pmatrix}$ at which

$$\lambda_1 < \cdots < \lambda_k = \lambda_0 < \cdots < \lambda_p.$$

Note that as long as $\lambda_k \neq \lambda_0 = 0$ for any k, the matrix $\mathbf{B}(\mathbf{V})$ has rank p and thus p linearly independent eigenvectors, i.e. $\mathbf{R}_1, \ldots, \mathbf{R}_p$. Therefore, we can express $\mathbf{r}_0$ as a linear combination of the vectors $\mathbf{r}_k$, $k = 1, \ldots, p$,

$$\mathbf{r}_0 = \sum_{i=1}^{p} a_i \mathbf{r}_i. \tag{5.9}$$

By definition of $\mathbf{R}_0$ we have $\mathbf{B}(\mathbf{V})\mathbf{R}_0 = 0$, i.e.

$$(\mathbf{f}_A - \mathbf{h})b_0 + \mathbf{f_u}\,\mathbf{r}_0 = 0. \tag{5.10}$$

We substitute (5.9) into (5.10), and multiply (5.10) by each left eigenvector (row vector) $\mathbf{l}_i$ of the matrix $\mathbf{f_u}$. Then

$$\mathbf{l}_i(\mathbf{f}_A - \mathbf{h})b_0 + \lambda_i a_i = 0, \qquad i = 1, \ldots, p$$

and therefore $a_i = -\mathbf{l}_i(\mathbf{f}_A - \mathbf{h})b_0/\lambda_i$, $i = 1, \ldots, p$. Using this in (5.9), we get

$$\mathbf{R}_0 = \left(\begin{array}{c} b_0 \\ -\sum_{i=1}^{p} \dfrac{\mathbf{l}_i(\mathbf{f}_A - \mathbf{h})b_0}{\lambda_i} \mathbf{r}_i \end{array} \right). \tag{5.11}$$

The 0-characteristic field is linearly degenerate, i.e. $\nabla_{\mathbf{V}} \lambda_0 \cdot \mathbf{R}_0 = 0$, since $\lambda_0(\mathbf{V}) = 0$. Then, there exists a one-parameter family of states $\epsilon \mapsto \mathbf{V}(\epsilon)$, connected with the state $\mathbf{V}(0)$ by a 0-wave, see e.g. Smoller [81]. Here $\mathbf{V}(\epsilon)$ is the integral curve of the equation

$$\frac{d\mathbf{V}(\epsilon)}{d\epsilon} = \mathbf{R}_0(\mathbf{V}(\epsilon)) \tag{5.12}$$

with the prescribed initial data $\mathbf{V}(0)$. The solution to (5.12) exists at least locally, i.e., for ϵ close to 0, and it determines the *0-wave curve*, passing through the state $\mathbf{V}(0)$. Note that the tangent vector to the 0-wave curve is given by $\mathbf{R}_0$.

Under the assumptions that

$$\lambda_k(A_*, \mathbf{u}_*) = 0 \tag{5.13a}$$
$$\nabla_{\mathbf{V}} \lambda_k(A_*, \mathbf{u}_*) \cdot \mathbf{R}_k(A_*, \mathbf{u}_*) \neq 0 \tag{5.13b}$$

the equation $\lambda_k(A, \mathbf{u}) = 0$ determines locally a smooth p-dimensional surface

$$\mathcal{T} = \{(A, \mathbf{u}) \in \mathbb{R}^{p+1} \mid \lambda_k(A, \mathbf{u}) = 0\} \tag{5.14}$$

that passes through $\mathbf{V}_* = \binom{A_*}{\mathbf{u}_*}$. The smoothness follows from the implicit function theorem, since the partial derivatives of $\lambda_k(A, \mathbf{u})$ do not vanish simultaneously at $\mathbf{V}_*$, see (5.13b). Note that the condition (5.13b) is equivalent to

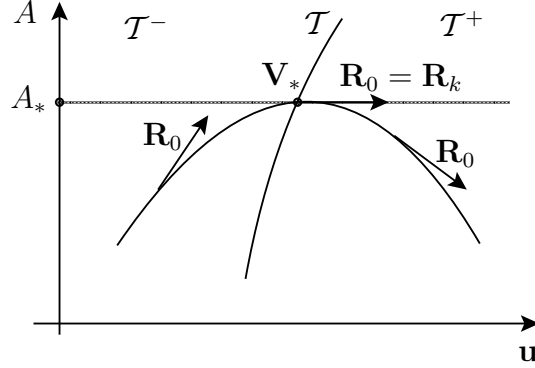$$\nabla_{\mathbf{u}} \lambda_k(A_*, \mathbf{u}_*) \cdot \mathbf{r}_k(A_*, \mathbf{u}_*) \neq 0, \tag{5.15}$$

Fig. 5.2. Integral curve of $\mathbf{R}_0$ crosses $\mathcal{T}$ at $\mathbf{V}_*$, and remains on one side of $A = A_*$.

since $\mathbf{R}_k = \begin{pmatrix} 0 \\ \mathbf{r}_k \end{pmatrix}$. This is nothing else but the definition of *genuine nonlinearity* of the k-characteristic field. Also, the assumption (5.13b) guarantees that the integral curves of $\mathbf{R}_k$ cut the surface $\mathcal{T}$ transversally. Following Isaacson and Temple [44], we will call it the *transition surface*.

As the state $\mathbf{V}$ on the integral curve of $\mathbf{R}_0$, i.e. on the solution to (5.12), approaches $\mathcal{T}$ one has $\lambda_k \to \lambda_0 = 0$. To avoid a singularity in (5.11), we can locally choose $b_0 := -\lambda_k$ there. Normalizing $\mathbf{R}_0$, we get

$$\mathbf{R}_0 = c \begin{pmatrix} -\lambda_k \\ \displaystyle\sum_{i=1}^{p} \frac{\lambda_k}{\lambda_i} \big(\mathbf{l}_i(\mathbf{f}_A - \mathbf{h})\big)\mathbf{r}_i \end{pmatrix}, \quad \frac{1}{c^2} = \lambda_k^2 + \sum_{i=1}^{p} \left(\frac{\lambda_k}{\lambda_i}\mathbf{l}_i(\mathbf{f}_A - \mathbf{h}) \right)^2. \quad (5.16)$$

Since all λ_i are bounded away from zero for $i = 1, \ldots, p,\ i \neq k$,

$$\mathbf{R}_0 \to \frac{1}{\mathbf{l}_k(\mathbf{f}_A - \mathbf{h})} \begin{pmatrix} 0 \\ \big(\mathbf{l}_k(\mathbf{f}_A - \mathbf{h})\big)\mathbf{r}_k \end{pmatrix} = \mathbf{R}_k, \quad \lambda_k \to \lambda_0 = 0. \quad (5.17)$$

Here, following Isaacson and Temple [44, 45], we assume that

$$\mathbf{l}_k(\mathbf{f}_A - \mathbf{h})\big|_{\mathbf{V}_*} \neq 0. \quad (5.18)$$

It is easy to show that the 0-wave curves, given by (5.12), lie on one side of the hyperplane $A = A_*$. Indeed, the transition surface $\mathcal{T}$, given by (5.14), separates two half-spaces $\mathcal{T}^\pm$ locally near $\mathbf{V}_*$. We distinguish them by the orientation of the normal $\nabla_{\mathbf{V}}\lambda_k$, i.e. $\nabla_{\mathbf{V}}\lambda_k$ points from $\mathcal{T}^-$ to $\mathcal{T}^+$. Then $\lambda_k(\mathbf{V}) < 0$ for $\mathbf{V} \in \mathcal{T}^-$, and $\lambda_k(\mathbf{V}) > 0$ for $\mathbf{V} \in \mathcal{T}^+$. Assume that

$$\nabla_{\mathbf{V}}\lambda_k(A_*, \mathbf{u}_*) \cdot \mathbf{R}_k(A_*, \mathbf{u}_*) > 0 \quad (5.19)$$

in (5.13b). By continuity it will be also positive in some neighborhood of $\mathbf{V}_* = \begin{pmatrix} A_* \\ \mathbf{u}_* \end{pmatrix}$. As the state $\mathbf{V}$ on the 0-wave curve moves towards $\mathbf{V}_*$, $\lambda_k \to 0$ and therefore
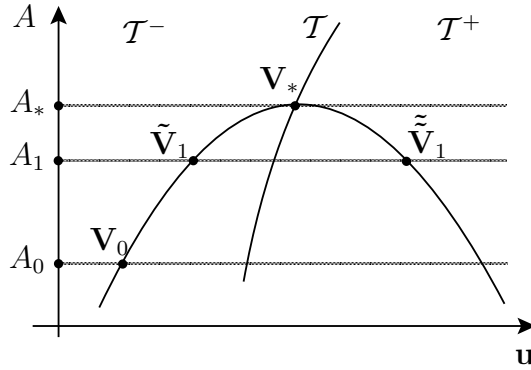
Fig. 5.3. For a given state $\mathbf{V}_0$ in the neighborhood of $\mathbf{V}_*$ there exist two states $\tilde{\mathbf{V}}_1$ and $\tilde{\tilde{\mathbf{V}}}_1$ which can be connected to it by the 0-wave curve.

$\mathbf{R}_0 \to \mathbf{R}_k$, see (5.12), (5.17). By the sign assumption (5.19), the 0-wave curve of $\mathbf{R}_0$ will cross $\mathcal{T}$ from $\mathcal{T}^-$ to $\mathcal{T}^+$, see Fig. 5.2.

For each state $\mathbf{V} \notin \mathcal{T}$, a tangent vector to the integral curve of $\mathbf{R}_0$ is given by (5.16). Observe that its first component is positive in $\mathcal{T}^-$, i.e. $-\lambda_k(\mathbf{V}) > 0$ for $\mathbf{V} \in \mathcal{T}^-$, and negative in $\mathcal{T}^+$, i.e. $-\lambda_k(\mathbf{V}) < 0$ for $\mathbf{V} \in \mathcal{T}^+$. For $\mathbf{V} \to \mathbf{V}_*$ we have $\mathbf{R}_0 \to \mathbf{R}_k$, and $\mathbf{R}_k$ lies in the hyperplane $A = A_*$. Therefore, locally the integral curve of $\mathbf{R}_0$ lies below of $A = A_*$, and touches it at $\mathbf{V}_*$. Note that if we would choose $b_0 = +\lambda_k$ in (5.11), then the integral curve of $\mathbf{R}_0$ would lie above of $A = A_*$, and also touch it at $\mathbf{V}_*$.

Assume that we are given a state $\mathbf{V}_0 = \binom{A_0}{\mathbf{u}_0}$ in a neighborhood of the resonant state $\mathbf{V}_* = \binom{A_*}{\mathbf{u}_*}$, and consider the 0-wave curve (5.12), passing through $\mathbf{V}_0$. Also, consider a hyperplane $A = A_1$ such that $A_1 < A_*$. We are interested in finding a state $\mathbf{V}_1 = \binom{A_1}{\mathbf{u}_1}$, lying on the 0-wave curve described above. Observe that there exist precisely two such states $\tilde{\mathbf{V}}_1$ and $\tilde{\tilde{\mathbf{V}}}_1$ which lie on the different sides of the transition surface $\mathcal{T}$, see Fig. 5.3. In order to choose a relevant state between the states $\tilde{\mathbf{V}}_1$ and $\tilde{\tilde{\mathbf{V}}}_1$, Isaacson and Temple [44] introduce the following criterion.

Definition 5.1 (Isaacson and Temple [44]). *A 0-wave curve (5.12), connecting the states $\mathbf{V}_0$ and $\mathbf{V}_1$, is called **admissible** if it does not cross the transition surface $\mathcal{T}$ between $\mathbf{V}_0$ and $\mathbf{V}_1$.*

Then, for the solution to the Riemann problem (5.6), (5.7) in a neighborhood of the resonant state $\mathbf{V}_*$, this criterion ensures that a total variation in A is not larger than $|A_L - A_R|$.

It is easy to show that the admissibility criterion of Isaacson and Temple [44] is equivalent to the evolutionary criterion (5.8). Indeed, if the 0-wave curve does not intersect $\mathcal{T}$, then it entirely lies either to the left of $\mathcal{T}$, or to the right of it,

i.e. in $\mathcal{T}^-$ or $\mathcal{T}^+$. In these half-spaces $\lambda_k(\mathbf{V}) < 0$ for all $\mathbf{V} \in \mathcal{T}^-$, and $\lambda_k(\mathbf{V}) > 0$ for all $\mathbf{V} \in \mathcal{T}^+$. Therefore, the 0-wave curve will be admissible in the sense of Definition 5.1 if

$$\lambda_k(\mathbf{V}_0) = \lambda_k(\mathbf{V}_1).$$

Since all other λ_i, $i \neq k$ are bounded away from zero, they cannot change their sign as well. But this is exactly the condition (5.8), so the corresponding 0-wave curve is evolutionary.

On the other hand, remember that the evolutionarity criterion, given by Definition 4.3, is valid for an *arbitrary* discontinuity, not necessarily stationary contact. Moreover, the states on the both sides of it do not have to be close to each other. Therefore, the criterion of Isaacson and Temple [44] is a particular case of the evolutionarity criterion, given by Definition 4.3.

It is illuminating to see the resonance effect for the Euler equations in a duct of variable cross section. Consider the Riemann problem (5.6), (5.7) for in this case, i.e. when $\mathbf{u}, \mathbf{f}, \mathbf{h}$ in (5.6) are given by (5.5). The resonance described above occurs when the k-characteristic speed is close to zero, and k-characteristic field is genuinely nonlinear, cf. (5.15). For the Euler equations in a duct, there are only two genuinely nonlinear fields, namely the ones which correspond to $\lambda_1 = v - c$ and $\lambda_3 = v + c$, see Section 2.6. Then the condition that $\lambda_{1,3} \to 0$ means that the gas flow becomes *sonic* near the stationary 0-contact,

$$\mathrm{M} := \frac{v}{c} \to \pm 1,$$

where M is the local signed Mach number. Remember that the Euler equations in a duct of variable cross section can be formally obtained from the BN model of two-phase flows, see Section 2.3.4. Analogous to the sonic case for the BN model, see Section 4.5.2, we can see that such sonic flow will be *unstable*, i.e. a small perturbation at the inlet will cause big jumps at the outlet.

5.3   Weak solution to the Riemann problem

Analogously to the case of the BN model in Section 4.6, we can define a weak solution also for the Riemann problem to Euler equations in a duct of variable cross-section (5.1), (5.2). Note that for this particular case, the non-conservative term $p \, \partial A / \partial x$ in (5.1) plays a role only across the stationary 0-contact wave. In the rest of domain, A is constant and equal to its left or right value,

$$A(x) = \begin{cases} A_L, & x \text{ lies to the left of stationary contact} \\ A_R, & x \text{ lies to the right of it.} \end{cases}$$

Therefore, everywhere away from the stationary contact the system (5.1) reduces to the usual one-dimensional Euler equations

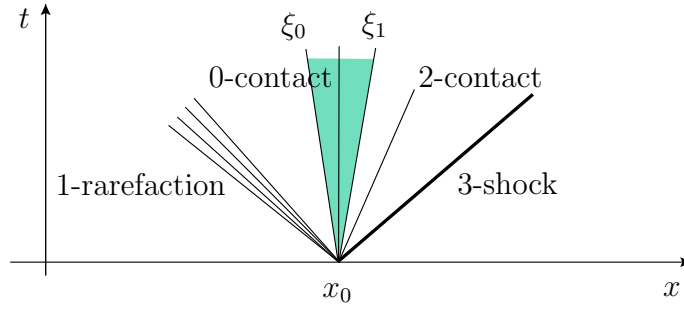$$\mathbf{u}_t + \mathbf{f}(\mathbf{u})_x = 0, \tag{5.20}$$

Fig. 5.4. A typical Riemann problem for the one-dimensional Euler equations in a duct.

where

$$\mathbf{u} = \begin{bmatrix} \rho \\ \rho v \\ \rho E \end{bmatrix}, \quad \mathbf{f}(\mathbf{u}) = \begin{bmatrix} \rho v \\ \rho v^2 + p \\ v(\rho E + p) \end{bmatrix}. \tag{5.21}$$

For the system (5.20), we can define a weak solution in the usual manner.

On the other hand, across the stationary contact, the relations (2.65) hold,

$$\begin{aligned} A\rho v &= \text{const} \\ \eta &= \text{const} \\ \frac{v^2}{2} + \frac{c^2}{\gamma - 1} &= \text{const.} \end{aligned} \tag{5.22}$$

Our main idea is to find a system of equations, which give the relations (5.22) across the stationary contact. In other words, we again, as in Section 4.6, reverse the usual process of obtaining the Rankine–Hugoniot conditions for a system of conservation laws. There, one starts with the system of equations and gets the relations across a discontinuity. Here, we start from the relations across the discontinuity and wish to find the system of equations.

Across the stationary contact the flow is isentropic, see (5.22). As long as some other waves do not coincide with the stationary contact, we can choose a small sector around the stationary contact where the flow is isentropic, see Fig. 5.4 for a typical Riemann problem. Using this fact, we can eliminate the non-conservative momentum equation in the system (5.1). Denote the equations of (5.1) as follows,

$$\begin{aligned} \texttt{<continuity>} &:= (A\rho)_t + (A\rho v)_x \\ \texttt{<momentum>} &:= (A\rho v)_t + (A(\rho v^2 + p))_x - pA_x \\ \texttt{<energy>} &:= (A\rho E)_t + (Av(\rho E + p))_x \end{aligned}$$

Some calculations show that the energy equation `<energy>` $= 0$ is equivalent to the equation

$$\texttt{<entropy>} := \eta_t + v\eta_x = 0.$$

Combining `<continuity>`, `<energy>`, `<entropy>`, we get the dependence

$$\texttt{<momentum>} = \texttt{<energy>} - \left(E + \frac{p}{\rho} - v^2\right)\texttt{<continuity>} - A\rho T\,\texttt{<entropy>}.$$

Therefore, in the left and in the right parts of this sector, the system (5.1) is equivalent to the system

$$
\begin{aligned}
\frac{\partial A}{\partial t} &= 0 \\
\frac{\partial A\rho}{\partial t} + \frac{\partial A\rho v}{\partial x} &= 0 \\
\frac{\partial A\rho E}{\partial t} + \frac{\partial Av(\rho E + p)}{\partial x} &= 0 \\
\frac{\partial \eta}{\partial t} + v\frac{\partial \eta}{\partial x} &= 0.
\end{aligned}
\tag{5.23}
$$

Note that the last equation in (5.23) is trivially satisfied everywhere in the sector, since the flow is isentropic there. Therefore, the system (5.23) may be rewritten as

$$\mathbf{U}_t + \mathbf{F}(\mathbf{U})_x = 0, \tag{5.24}$$

where

$$\mathbf{U} = \begin{bmatrix} A \\ A\rho \\ A\rho E \end{bmatrix}, \quad \mathbf{F}(\mathbf{U}) = \begin{bmatrix} 0 \\ A\rho v \\ Av(\rho E + p) \end{bmatrix}. \tag{5.25}$$

The Rankine–Hugoniot conditions across a stationary discontinuity for this system, augmented with the condition $\eta = \text{const}$, coincide with the relations (5.22). Since the system (5.24) is in divergence form now, we can use the usual definition of a weak solution for it. Note that the approach we have used here is exactly the same as that of Section 4.6.

Consider a system of conservation laws

$$\mathbf{u}_t + \mathbf{f}(\mathbf{u})_x = 0, \tag{5.26}$$

where the pair $(\mathbf{u}, \mathbf{f}(\mathbf{u}))$ are either $(\mathbf{u}, \mathbf{f}(\mathbf{u}))$ in (5.21) or $(\mathbf{U}, \mathbf{F}(\mathbf{U}))$ in (5.25), and let us restrict ourselves to self-similar solutions of it. Then, for the smooth solutions, this system is equivalent to

$$-\mathbf{v}_\xi\,\xi + \mathbf{f}(\mathbf{v})_\xi = 0. \tag{5.27}$$

Consider the Riemann problem for it, i.e. augment (5.27) with constant initial data

$$\mathbf{v}(-\infty) = \mathbf{v}_L, \quad \mathbf{v}(\infty) = \mathbf{v}_R. \tag{5.28}$$

If we multiply (5.27) by a test function $\phi \in C_0^1(]\xi_0, \xi_1[)$ and integrate over all ξ, we get

$$\int_{\xi_0}^{\xi_1} (\mathbf{v}(\phi\,\xi)_\xi - \mathbf{f}(\mathbf{v})\phi_\xi)\, d\xi = 0. \tag{5.29}$$

Now $\mathbf{v}$ does not need to be differentiable anymore, and we can use it to define a weak solution to the Riemann problem (5.27), (5.28). Remember, that *locally* the *non-conservative* system (5.1) can be reduced to a conservative one, either (5.20) or (5.24). Thus, now we can give a definition of a *global* weak solution to the Riemann problem (5.1), (5.2) as a composition of the weak solutions to the conservative systems (5.20) and (5.24).

Definition 5.2. *Consider a sector*

$$S(\xi_0, \xi_1) = \{(x, t) \in \mathbb{R} \ : \ \xi_0 \leq \frac{x}{t} \leq \xi_1\},$$

*bounded by the rays ξ_0 and ξ_1, such that the stationary contact lies in it, and assume that it is the only ray of discontinuity there. Then, a function $\mathbf{v} = \mathbf{v}(\xi) \in L^\infty_{loc}(\mathbb{R})$ is called a **weak solution of the Riemann problem** (5.1), (5.2), if for any small $\epsilon > 0$*

1. *To the left of ξ_0, i.e., $\xi \in]-\infty, \xi_0]$,*

$$\int_{-\infty}^{\xi_0} (\mathbf{v}(\phi\,\xi)_\xi - \mathbf{f}(\mathbf{v})\phi_\xi)\, d\xi = 0, \qquad for\ all\ \ \phi \in C_0^1(]-\infty, \xi_0 + \epsilon[),$$

   $\mathbf{v}(\xi) = \mathbf{u}(x, t)$, $\mathbf{f}(\mathbf{v}) = \mathbf{f}(\mathbf{u})$, *and* $\mathbf{u}$, $\mathbf{f}(\mathbf{u})$ *are given by* (5.21).

2. *To the right of ξ_1, i.e., $\xi \in [\xi_1, \infty[$,*

$$\int_{\xi_1}^{\infty} (\mathbf{v}(\phi\,\xi)_\xi - \mathbf{f}(\mathbf{v})\phi_\xi)\, d\xi = 0, \qquad for\ all\ \ \phi \in C_0^1(]\xi_1 - \epsilon, \infty[),$$

   $\mathbf{v}(\xi) = \mathbf{u}(x, t)$, $\mathbf{f}(\mathbf{v}) = \mathbf{f}(\mathbf{u})$, *and* $\mathbf{u}$, $\mathbf{f}(\mathbf{u})$ *are given by* (5.21).

3. *Inside of the sector, bounded by ξ_0 and ξ_1, i.e., $\xi \in [\xi_0, \xi_1]$,*

$$\int_{\xi_0}^{\xi_1} (\mathbf{v}(\phi\,\xi)_\xi - \mathbf{f}(\mathbf{v})\phi_\xi)\, d\xi = 0, \qquad for\ all\ \ \phi \in C_0^1(]\xi_0 - \epsilon, \xi_1 + \epsilon[),$$

   $\mathbf{v}(\xi) = \mathbf{U}(x, t)$, $\mathbf{f}(\mathbf{v}) = \mathbf{F}(\mathbf{U})$, *and* $\mathbf{U}$, $\mathbf{F}(\mathbf{U})$ *are given by* (5.25).

Remark 5.3. Note that in the sector $S(\xi_0 - \epsilon, \xi_0 + \epsilon)$, the definitions 1 and 3 coincide, and in the sector $S(\xi_1 - \epsilon, \xi_1 + \epsilon)$, the definitions 2 and 3 coincide.
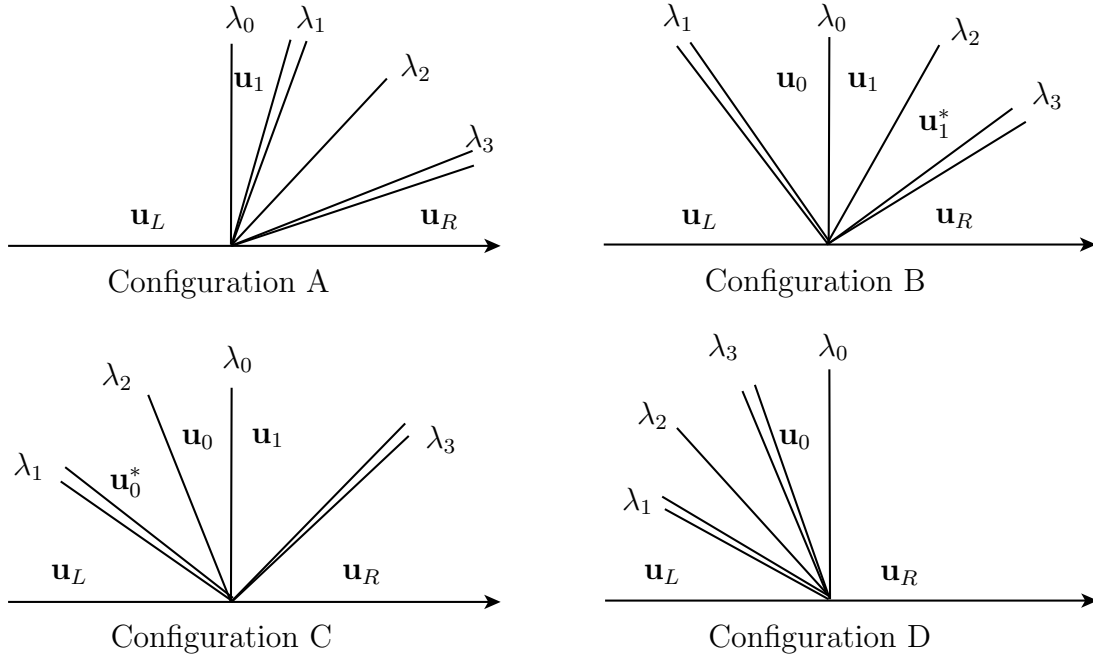
Fig. 5.5. Possible configurations of the Riemann problem.

5.4   Non-uniqueness of the Riemann solution

It appears that the solution to the Riemann problem (5.1), (5.2) is in general non-unique. For the same left and right states $\mathbf{u}_L, \mathbf{u}_R$, one can get completely different Riemann solutions. The reason for this behaviour is that the system (5.1) is *non-strictly* hyperbolic and non-conservaative. For the Riemann problem (5.1), (5.2) it means that the mutual position of the waves, configuration of the Riemann problem, can change, see Fig. 5.5 for the four possible cases. As soon as we fix the configuration, the solution to the Riemann problem is unique. The problem of non-uniqueness arises from the fact that for certain sets of initial data more than one configuration is possible. In this light it makes sense to consider the conditions, which lead to the different configurations of the Riemann problem.

In what follows, we will make extensive use of the wave curves for the Riemann problem (5.1), (5.2). These are the curves in the (v, p)-plane which represent the states which can be connected to $\mathbf{u}_L, \mathbf{u}_R$ by the admissible waves. The shock and rarefaction wave curves will be given by formula (5.54). It can be shown that the 1-curve, shock or rarefaction, is strictly increasing, and the 3-curve is strictly decreasing, see e.g. Godlewski and Raviart [38]. Further, the left and right states of the 2-wave are projected to the same point in the (v, p)-plane. Therefore, the Riemann problem for the usual Euler equations (5.1), (5.2) with $A_L = A_R$ has a unique solution, see e.g. [38, Theorem 3.1, p. 134].

Another wave, which appears in the solution to the Riemann problem (5.1),

(5.2) is the stationary 0-contact wave. Some of its properties are similar to those of the solid contact in the case of the BN model, see Section 4.4. We have shown there that the flow inside of the 0-contact is analogous to the stationary isentropic flow in the converging-diverging nozzle. For convenience, we repeat the main consequences of this fact here:

- The stationary contact can be viewed as a porous film of infinitesimal thickness

- Each pore is a converging-diverging nozzle; the cross-sections on each side of it are A_L and A_R, respectively

- The velocity inside a pore does not change its sign; moreover, if the flow is sub(super)sonic at the inlet, it is also sub(super)sonic at the outlet

- The change of the flow parameters in a pore is given by the following table, where $\uparrow$ stands for increasing and $\downarrow$ for decreasing:

Supersonic	$A \uparrow$	$v \uparrow$	$p \downarrow$	$c \downarrow$	$\rho \downarrow$
	$A \downarrow$	$v \downarrow$	$p \uparrow$	$c \uparrow$	$\rho \uparrow$
Subsonic	$A \uparrow$	$v \downarrow$	$p \uparrow$	$c \uparrow$	$\rho \uparrow$
	$A \downarrow$	$v \uparrow$	$p \downarrow$	$c \downarrow$	$\rho \downarrow$

For a given left state $\mathbf{u}_0$ of the stationary contact we can represent the 0-wave curve parametrically by A as follows,

$$\begin{cases} \rho = \rho(A; \mathbf{u}_0) \\ v = v(A; \mathbf{u}_0) \\ p = p(A; \mathbf{u}_0), \end{cases} \tag{5.30}$$

where the states must satisfy (5.22). The three-dimensional curve (5.30) will be regular if the corresponding derivatives are continuous, therefore locally bounded, and are non-zero simultaneously, i.e. the tangent vector does not vanish,

$$\left(\frac{\partial \rho}{\partial A}, \frac{\partial v}{\partial A}, \frac{\partial p}{\partial A} \right) \neq 0. \tag{5.31}$$

We will formulate the following lemma under these conditions; later on, we will discuss situations when they are violated.

Lemma 5.4. *Consider the Riemann problem* (5.1), (5.2) *with the stiffened gas EOS* (2.5), *and denote the states connected by the 0-wave by* $\mathbf{u}_0$ *and* $\mathbf{u}_1$. *Assume that the conditions* (5.31) *are fulfilled. The flow velocity* v *inside the 0-wave does not change its sign, and is either subsonic, or supersonic everywhere in the flow. Denote its **signed Mach number** by* $\mathrm{M} = \frac{v}{c}$. *Then for the 0-wave curve* (5.30) *the following statements are true*

1. *The 0-wave curve is strictly increasing(decreasing) in p, if $v < 0 (> 0)$.*

2. *The 0-wave curve is convex(concave) with respect to p, if $|\mathrm{M}| > 1 (< 1)$.*

3. *For increasing(decreasing) velocities and pressures in $\mathbf{u}_0$, the velocities and pressures in $\mathbf{u}_1$ also increase(decrease) and vice versa.*

4. *For the states $\mathbf{u}_0$ and $\mathbf{u}_1$,*

$$\left\{ \begin{array}{l} \rho_0 \to \bar{\rho} \\ v_0 \to 0 \\ p_0 \to \bar{p} \end{array} \right. \quad \Longleftrightarrow \quad \left\{ \begin{array}{l} \rho_1 \to \bar{\rho} \\ v_1 \to 0 \\ p_1 \to \bar{p} \end{array} \right.$$

for all $\bar{\rho}, \bar{p} > 0$.

Proof. We take (5.30) and fix $\mathbf{u}_0$, so that ρ, v and p only depend on A. Since the flow inside the 0-wave is analogous to the converging-diverging flow, see Section 4.4, we take the following relations from Courant and Friedrichs [22, (145.05), (145.08)], i.e.

$$\frac{dA}{A} + \frac{d\rho}{\rho} + \frac{dv}{v} = 0 \tag{5.32}$$

$$\frac{dA}{A} = \left(\frac{v^2}{c^2} - 1 \right) \frac{dv}{v}, \tag{5.33}$$

where A is the variable cross-section of a pore (see above), ρ, c, and v are the corresponding parameters of the flow in the pore. Then (5.33) leads to

$$\frac{dv}{dA} = \frac{vc^2}{A(v^2 - c^2)}. \tag{5.34}$$

By the definition of the sound speed

$$\left. \frac{dp}{d\rho} \right|_\eta = c^2, \quad \text{i.e.} \quad \frac{d\rho}{\rho} = \frac{dp}{\rho c^2}.$$

Substituting this into (5.32), we obtain

$$\frac{dp}{dA} = \rho c^2 \left(-\frac{1}{A} - \frac{1}{v} \frac{dv}{dA} \right) = -\frac{\rho v^2 c^2}{A(v^2 - c^2)}. \tag{5.35}$$

Analogously,

$$\frac{d\rho}{dA} = -\frac{\rho v^2}{A(v^2 - c^2)}. \tag{5.36}$$

Now we see when the 0-wave curve will be regular, i.e. the conditions (5.31) will be fulfilled. From (5.34), (5.35), and (5.36) it follows that this will happen when either

$$v \neq 0 \quad \text{or} \quad |v| \neq c. \tag{5.37}$$

From now on, when discussing 0-wave curves, we will always assume that the conditions (5.37) are fulfilled, unless stated otherwise.

Consider the system of ordinary differential equations (5.34), (5.35), (5.36)

$$\frac{d}{dA} \begin{pmatrix} \rho \\ v \\ p \end{pmatrix} = \frac{1}{A(v^2 - c^2)} \begin{pmatrix} -\rho v^2 \\ vc^2 \\ -\rho v^2 c^2 \end{pmatrix} \tag{5.38}$$

with the initial data

$$\begin{cases} \rho(A_0) & = \rho_0 \\ v(A_0) & = v_0 \\ p(A_0) & = p_0 \end{cases}$$

A straightforward calculation shows that under conditions (5.37), the functions on the right-hand side of (5.38) are differentiable for $A > 0$. Then by the existence and uniqueness theorem there exists a unique integral curve of (5.38) as long as the right-hand side is Lipschitz continuous. This curve is nothing else but the 0-wave curve, passing through the point $\mathbf{u}_0$. Note that all states with $v = 0$ are stationary points of the system (5.38). Therefore, the solutions may approach such states only asymptotically.

From (5.34) and (5.35), we obtain

$$\frac{dp}{dv} = -\rho v$$

and thus the statement 1 is proved. Of course, it can be also seen from the table above.

For the proof of the statement 2, we calculate using (5.34) and (5.35)

$$\frac{d^2 p}{dv^2} = -\frac{d\rho}{dv} v - \rho = \rho \left(\frac{v^2}{c^2} - 1 \right),$$

which gives the desired result. The possible 0-waves are presented in Fig. 5.6.

Using $\eta = \frac{p + \pi}{\rho^\gamma}$ in the relations (5.22) across the 0-wave, we get

$$v_1 = v_0 \frac{A_0}{A_1} \left(\frac{p_0}{p_1} \right)^{1/\gamma}$$

$$p_1 = p_0 \left(\frac{A_0 v_0}{A_1 v_1} \right)^\gamma.$$

Note that v_0 and v_1 always have the same sign, cf. (5.22). Differentiating the above equations with respect to v_0 and p_0 respectively, we get

$$\frac{\partial v_1}{\partial v_0} = \frac{A_0}{A_1} \left(\frac{p_0}{p_1} \right)^{1/\gamma} > 0$$

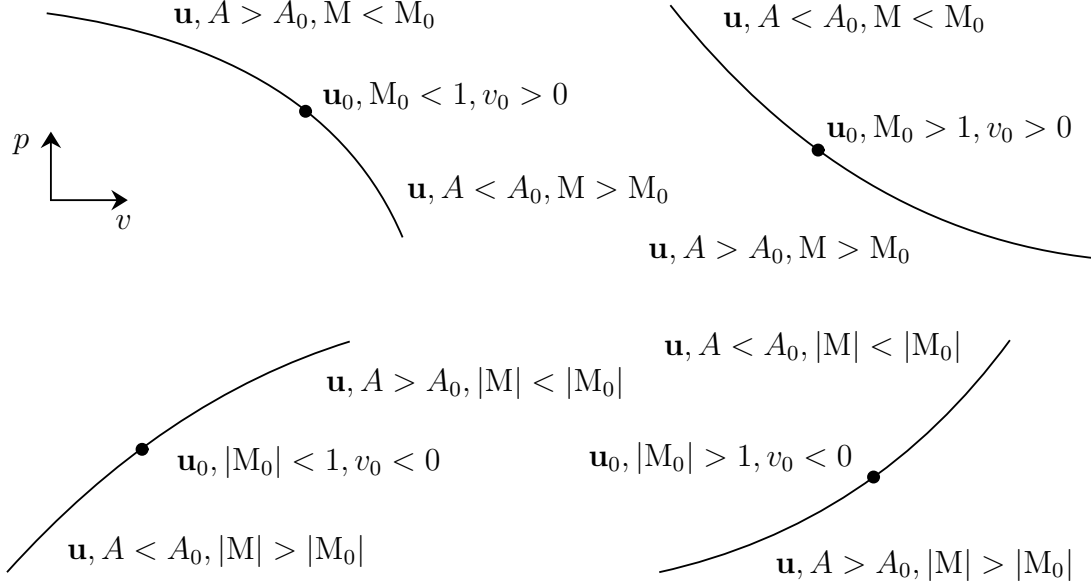$$\frac{\partial p_1}{\partial p_0} = \left(\frac{A_0 v_0}{A_1 v_1} \right)^\gamma > 0,$$

Fig. 5.6. The 0-curves in the (v, p)-plane, parametrized with A, connect the states $\mathbf{u}_0$ and $\mathbf{u}$. Depending on v_0, M_0, the curves exhibit different behaviour.

thus proving the statement 3.

For the statement 4, it is enough to prove only "$\Longrightarrow$", since the statement is symmetric with respect to subscripts 0 and 1. Using $\eta = \frac{p+\pi}{\rho^\gamma}$ and $c^2 = \frac{\gamma(p+\pi)}{\rho}$ in the relations (5.22), we obtain

$$A_0(p_0 + \pi)^{1/\gamma}v_0 = A_1(p_1 + \pi)^{1/\gamma}v_1 \tag{5.39}$$

$$\frac{p_0 + \pi}{\rho_0^\gamma} = \frac{p_1 + \pi}{\rho_1^\gamma} \tag{5.40}$$

$$\frac{v_0^2}{2} + \frac{\gamma\eta^{1/\gamma}(p_0 + \pi)^{1-1/\gamma}}{\gamma - 1} = \frac{v_1^2}{2} + \frac{\gamma\eta^{1/\gamma}(p_1 + \pi)^{1-1/\gamma}}{\gamma - 1}. \tag{5.41}$$

First, let us show that p_1 remains bounded, i.e. $p_1 \nrightarrow \infty$. We prove this by contradiction, i.e. assuming that p_1 is unbounded. Then by statement 1 the pressure p_1 must exceed p_0, $p_1 > p_0$. Using that the left-hand side of (5.41) is bounded, the estimate

$$\frac{v_1^2}{2} + \frac{\gamma\eta^{1/\gamma}(p_1 + \pi)^{1-1/\gamma}}{\gamma - 1} > \frac{\gamma\eta^{1/\gamma}(p_1 + \pi)^{1-1/\gamma}}{\gamma - 1}$$

will give us the desired result that $p_1 < \text{const}$, since γ, π are constants, and η is constant along the 0-curve.

Now the equation (5.39) implies that $v_1 \to 0$. Using this in (5.41), we get $p_1 \to \bar{p}$. Finally, by (5.40) is also $\rho_1 \to \bar{\rho}$, which proves the statement 4. Note
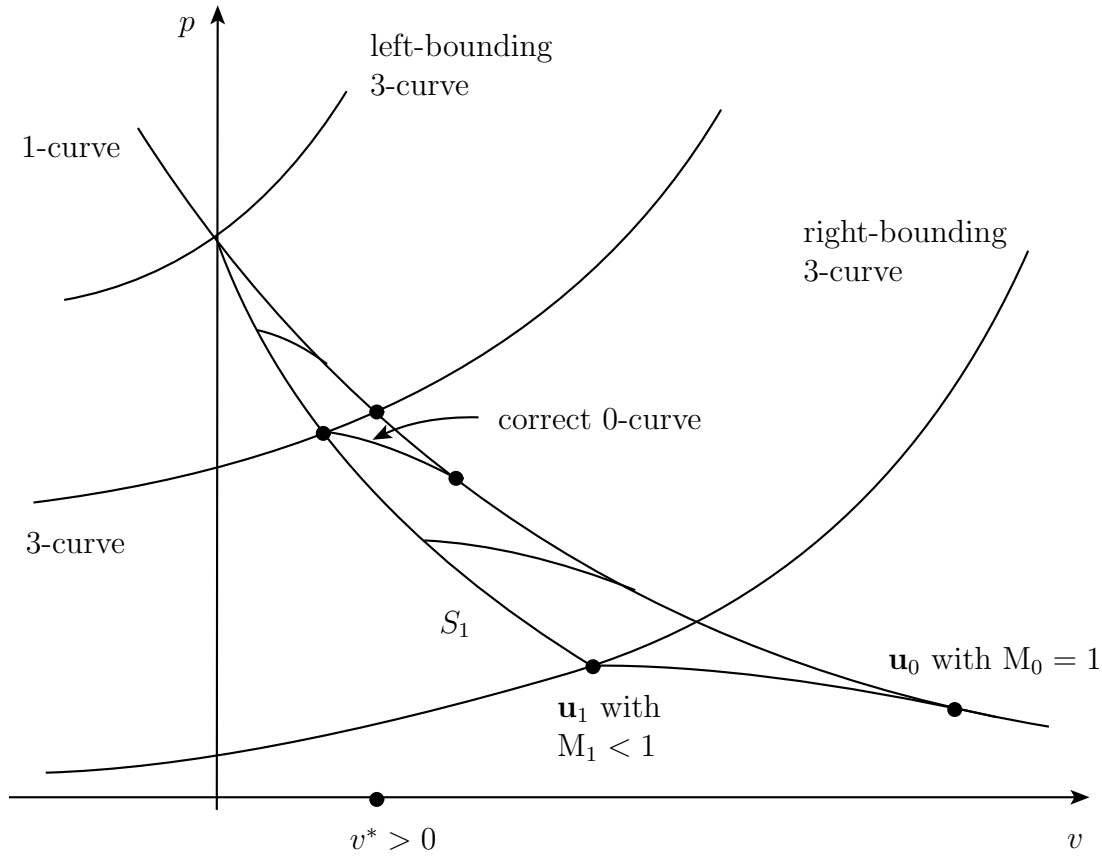
Fig. 5.7. The wave curves for the configuration B with $A_L < A_R$.

that the approach here is exactly the same as in Section 4.5.1, where we have discussed the Riemann problem for the BN model with coinciding contacts of the two phases. □

Let us represent in the (v, p)-plane the possible scenarios of the solution of the Riemann problem (5.1), (5.2), which can lead to a solution in the form of the configuration B, see Fig. 5.5. For this configuration, the 0-wave is next to the 1-wave. In the (v, p)-plane it means that the possible 0-curves necessarily start from the 1-wave curve. The correct 0-wave curve, i.e. the one which gives the solution to the Riemann problem (5.1), (5.2), connects the 1- and 3-curves in the (v, p)-plane. Figs. 5.7, 5.8 represent the wave curves for the configuration B.

Denote the states, connected by the 0-curve, by $\mathbf{u}_0$ and $\mathbf{u}_1$, and let $\mathbf{u}_0$ lie on the 1-curve. Observe that not all states $\mathbf{u}_0$ come into consideration. Indeed, by definition of configuration B, the velocities in the states $\mathbf{u}_0$ and $\mathbf{u}_1$ must be non-negative. In configuration B the 1-wave has a non-positive velocity and therefore the right-hand velocity $v_0 - c_0$ of its characteristic family must also be non-positive, $v_0 - c_0 \leq 0$. In terms of the Mach number, it means that $M_0 \leq 1$.
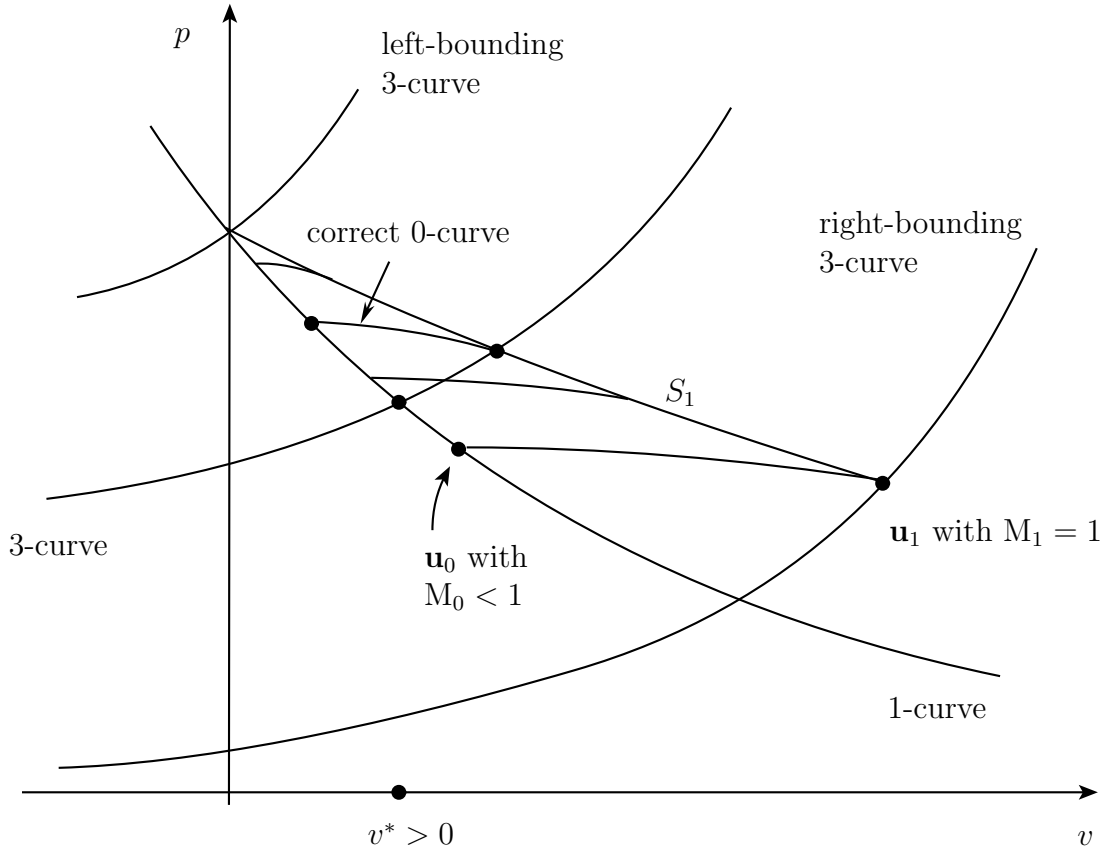
Fig. 5.8. The wave curves for the configuration B with $A_L > A_R$.

Therefore, the candidates for $\mathbf{u}_0$ have necessarily $0 \leq M_0 \leq 1$. This gives rise to the following definition.

Definition 5.5. *Consider the Riemann problem* (5.1), (5.2). *Let us call the 3-curve, crossing the 1-curve in the point with $v = 0$ the **left-bounding 3-curve**. Further,*

1. *If $A_L < A_R$, consider the state $\mathbf{u}_0$ on the 1-curve with $M_0 = 1$, connected with the state $\mathbf{u}_1$ with $M_1 < 1$ by the 0-wave. Let us call the 3-curve passing through $\mathbf{u}_1$ the **right-bounding 3-curve**, see Fig. 5.7.*

2. *If $A_L > A_R$, consider the state $\mathbf{u}_0$ on the 1-curve with $M_0 < 1$, connected with the state $\mathbf{u}_1$ with $M_1 = 1$ by the 0-wave. Let us call the 3-wave, passing through this state $\mathbf{u}_1$, the **right-bounding 3-curve**, see Fig. 5.8.*

Remark 5.6. We cannot use the results of Lemma 5.4 in Definition 5.5, since the parametrization (5.30) of the 0-wave will be singular for $M = 1$, cf. (5.37).

However, taking v as the 0-curve parameter in a neighborhood of sonic points, i.e. replacing (5.38) by the system

$$\frac{d}{dv} \begin{pmatrix} A \\ \rho \\ p \end{pmatrix} = \begin{pmatrix} A(v^2 - c^2)/(vc^2) \\ -\rho v/c^2 \\ -\rho v \end{pmatrix},$$

one can show that the length of the 0-wave curve remains finite.

Now we are ready to establish when the solution to the Riemann problem (5.1), (5.2) in form of configuration B is possible.

Theorem 5.7. *Consider the Riemann problem* (5.1), (5.2) *with the stiffened gas EOS* (2.5)*. If the 1- and 3-curves intersect in the point* (v^*, p^*) *with* $v^* > 0$*, then the following scenarios are possible.*

1. *If the point* (v^*, p^*) *lies between the left- and right-bounding 3-curves of Definition 5.5, then the configuration B is realizable, for all* $\mathbf{u}_L$ *on the 1- and for all* $\mathbf{u}_R$ *on the 3-curve. Moreover, the solution of this kind is unique, and the configuration C for the same Riemann problem is not realizable.*

2. *If the point* (v^*, p^*) *lies to the right of the right-bounding 3-curve, then there exists no solution to the Riemann problem* (5.1), (5.2) *in form of the configuration B.*

3. *If* $\mathrm{M}_L > 1$*, then the configuration A can be realizable.*

4. *If* $\mathrm{M}_R < -1$*, then the configuration D can be realizable.*

Proof. 1. For configuration B the states $\mathbf{u}_0$ must lie on the 1-curve. They are connected to the states $\mathbf{u}_1$ by 0-curves, such that these states $\mathbf{u}_1$ lie between the left- and right-bounding 3-curves, see Figs. 5.7, 5.8. Denote the projection of the set of all $\mathbf{u}_1$ to the (v, p)-plane by

$$S_1 = \{(v_1, p_1) \; : \; \mathbf{u}_1 = (A_1, \rho_1, v_1, p_1)^T\},$$

see Figs. 5.7, 5.8. The set S_1 is defined pointwise, with each point (v_1, p_1) belonging to different integral curves of (5.38). Therefore, S_1 lies on the differentiable integral surface, obtained by taking all integral curves of (5.38), such that $\mathbf{u}_1$ will are between the left- and right-bounding 3-curves.

Let us show that S_1 itself is a differentiable curve. All points $\mathbf{u}_1$ are given implicitly by the system (5.22), which can be rewritten as

$$
\begin{aligned}
F_1 &:= A_1 \rho_1 v_1 - A_0 \rho_0 v_0 = 0 \\
F_2 &:= \frac{p_1 + \pi}{\rho_1^\gamma} - \frac{p_0 + \pi}{\rho_0^\gamma} = 0 \\
F_3 &:= \frac{v_1^2}{2} + \frac{c_1^2}{\gamma - 1} - \frac{v_0^2}{2} - \frac{c_0^2}{\gamma - 1} = 0.
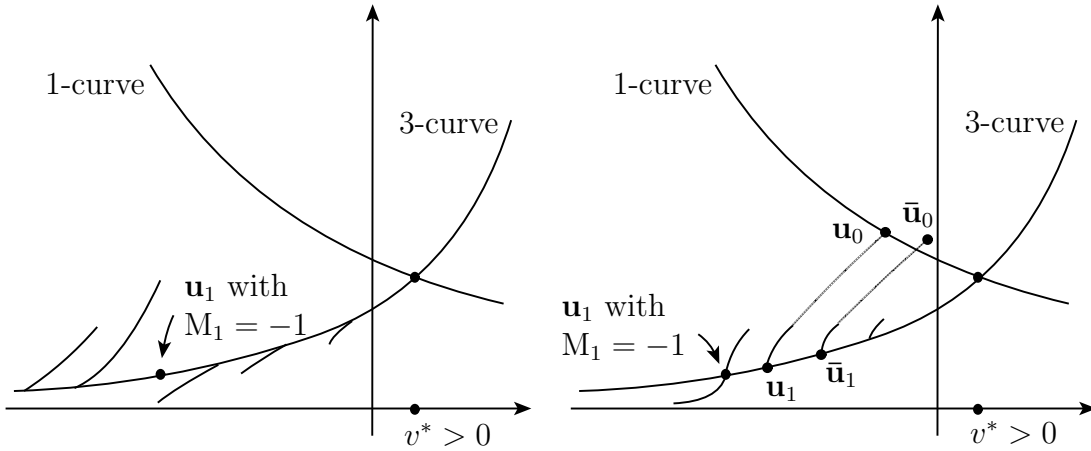\end{aligned}
\tag{5.42}
$$

Fig. 5.9. Configuration C is impossible if the 1- and 3-wave curves intersect in a state with $v^* > 0$. Left: Case $A_L < A_R$. Right: Case $A_L > A_R$.

The functions F_1, F_2, F_3 are differentiable with respect to all their arguments for $\rho > 0$ and the points $\mathbf{u}_0$ lie on the *smooth* 1-wave curve. We can calculate the Jacobian determinant of the system (5.42)

$$J = \left| \frac{\partial(F_1, F_2, F_3)}{\partial(\rho_1, v_1, p_1)} \right| = \frac{A_1}{\rho_1^{\gamma}}(c_1^2 - v_1^2).$$

Note that $J \neq 0$ unless $\mathbf{u}_1$ lies on the right-bounding 3-curve, which is excluded by the assumptions of the theorem. Then, by the implicit function theorem, S_1 will be a differentiable curve locally at every point (v_1, p_1).

From Lemma 5.4 it follows that the mapping $(v_0, p_0) \mapsto (v_1, p_1)$ is one-to-one. Since the points $\mathbf{u}_0$ lie on the strictly decreasing 1-wave curve, S_1 will be also strictly decreasing, see statement 3 of Lemma 5.4. Also, S_1 will approach the point on the 1-curve with $v = 0$ asymptotically, see statement 4 of Lemma 5.4. Since the 3-wave is strictly increasing, there exists a unique intersection point with S_1, see Figs. 5.7 and 5.8. This gives the solution to the Riemann problem (5.1), (5.2) in the framework of the configuration B.

Let us show that the configuration C for the same Riemann problem (5.1), (5.2) is impossible. Consider first the case $A_L < A_R$, see Fig. 5.9 (left). If the configuration C would be realizable, then the 0-wave would be next to the 3-wave, see Fig. 5.5. In the (v, p)-plane, it means that the possible states $\mathbf{u}_1$ must lie on the 3-curve, and the velocities in $\mathbf{u}_1$ would be negative. This follows from the fact that the eigenvalue v_0 for the 2-wave is negative, and sign $v_0 = $ sign v_1. The states $\mathbf{u}_1$ with $M_1 < -1$ are not admissible by the definition of configuration C. Indeed, then we would have $v_1 + c_1 < 0$, so that the 3-wave is either a sonic rarefaction (i.e. there is a sign change in the characteristic speed $v + c$), or a shock with
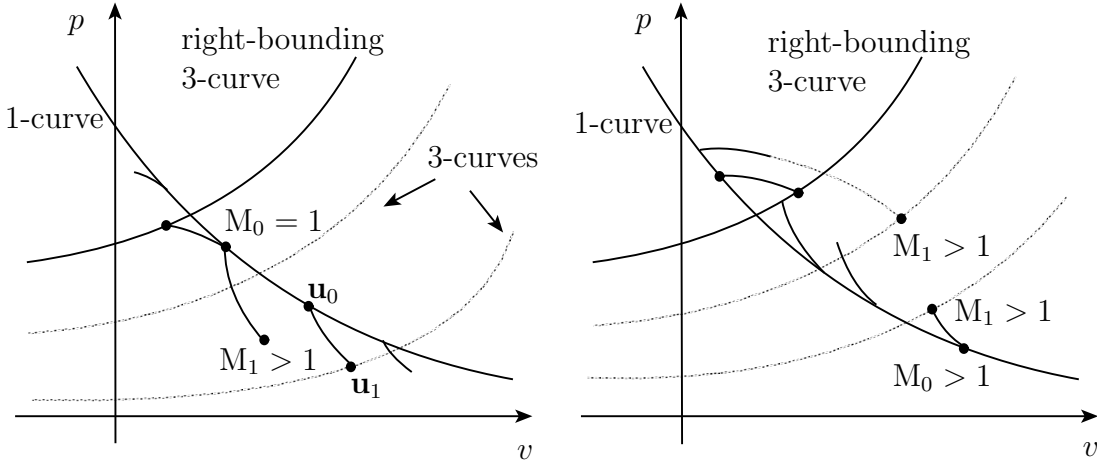
Fig. 5.10. Configuration B is impossible if the 1- and 3-wave curves intersect in a state with $v^* > 0$. Left: Case $A_L < A_R$. Right: Case $A_L > A_R$.

negative speed. These both cases are excluded, see Fig. 5.5. Note that the 0-wave, starting from the $\mathbf{u}_1$ on the 3-wave, can never intersect the 1-wave, since for the case $A_L < A_R$ it points in the opposite direction, see Fig. 5.9 (left).

Now consider the case $A_L > A_R$, see Fig. 5.9 (right). The only possibility for the configuration C to be realizable would be if the state $\mathbf{u}_1$ on the 3-curve with $v_1 < 0$, $|M_1| < 1$ were connected with the 1-curve via the 0-curve. Assume that this is true, i.e. there exists a state $\mathbf{u}_1$ with $v_1 < 0$, $|M_1| < 1$, connected to $\mathbf{u}_0$ with $v_0 < 0$ on the 1-curve. Now let us move this state $\mathbf{u}_1$ towards the p-axis, so that it will become some state $\bar{\mathbf{u}}_1$, connected with $\bar{\mathbf{u}}_0$ by the 0-curve. As we move closer to the p-axis, the length L of the 0-curve, connecting $\bar{\mathbf{u}}_1$ with $\bar{\mathbf{u}}_0$, will remain positive by statement 3 of Lemma 5.4, since we have assumed that the 1- and 3-curves intersect in the point with $v^* > 0$, see Fig. 5.9 (right). This contradicts the statement 4 of Lemma 5.4, which states that L should shrink to zero. Thus, we have a unique way of connecting the 1- and 3-curves in form of configuration B, which is the intersection point of S_1 with the 3-curve.

2. This statement becomes obvious by considering Fig. 5.10. The 3-curve must lie to the right of the right-bounding 3-curve. For the case $A_L < A_R$, the state $\mathbf{u}_0$ on the 1-curve can be connected to a 3-curve only if $M_0 > 1$, see Fig. 5.10 (left). This is impossible by the definition of configuration B. Indeed, in case $M_L < 1$ we would have a sonic rarefaction in the solution of the Riemann problem. However, this is only possible if $A_L = A_R$, see Section 4.5.2. In case $M_L > 1$ we would have configuration A.

For the case $A_L > A_R$, the 0-curve can connect the 1- and 3-curves if either

(i) the 0-curve crosses the right-bounding 3-curve or

(ii) the state $\mathbf{u}_L$ is supersonic with positive velocity, $\mathrm{M}_L > 1$.

For the first case, the 0-curve would connect the subsonic state $\mathbf{u}_0$ with a supersonic one, which is impossible, see the properties of the 0-wave on page 111. For the second case we would have configuration A.

3. We prove this statement by giving several examples. Consider the following Riemann initial data

A_L	ρ_L	v_L	p_L	A_R	ρ_R	v_R	p_R
0.8	0.2069	3.991	0.07	0.3	0.1354	-3.1666	0.0833

$$\tag{5.43}$$

closed with the equation of state (2.5) with $\gamma = 1.4$ and $\pi = 0$. The wave curves for the Riemann problem (5.1), (5.43) are presented in Fig. 5.11 (top). Observe that for these initial data both configurations A and B are possible. The configuration A is realized when the left state $\mathbf{u}_L$ is connected first to the state $\bar{\mathbf{u}}_1$ with the 0-curve, and $\bar{\mathbf{u}}_1$ is then connected with $\bar{\mathbf{u}}^*$ via the 1-shock with speed $s = 0.948 > 0$. Note that if this speed would be negative, then the configuration A with these initial data would be not realizable, cf. Fig. 5.5. Since the intersection point of 1- and 3-curves lies between the left- and right-bounding waves (not shown in Fig. 5.11), the configuration B is also possible. For this configuration, the left state $\mathbf{u}_L$ is connected with $\mathbf{u}_0$ and the latter is connected with $\mathbf{u}_1$. The both wave configurations in (x, t)-plane are shown in Fig. 5.11 (bottom).

However, if we slightly modify the initial data (5.43), we can easily obtain a Riemann problem with a unique solution. For instance, for the Riemann problem (5.1) with the following initial data

A_L	ρ_L	v_L	p_L	A_R	ρ_R	v_R	p_R
0.8	0.2069	3.0	0.2	0.3	0.1354	-3.1666	0.0833

$$\tag{5.44}$$

also closed with the equation of state (2.5) with $\gamma = 1.4$ and $\pi = 0$, only the configuration B is possible. Indeed, consider the wave curves for this Riemann problem in Fig. 5.12. Again, the state $\mathbf{u}_L$ is first connected to the state $\bar{\mathbf{u}}_1$ with the 0-curve; from $\bar{\mathbf{u}}_1$, we draw the 1-curve till the intersection with the 3-curve, passing through $\mathbf{u}_R$. However, the corresponding wave will be a shock with negative speed $s = -0.198$. Therefore, the configuration A is now not possible. The configuration D is not possible for similar reasons. Since the 1- and 3-curves intersect between the corresponding left- and right-bounding 3-curves (not shown in Fig. 5.12), the configuration B is possible for the Riemann problem (5.1), (5.44). The waves in the (x, t)-plane for this Riemann problem are shown in Fig. 5.12 (right).

4. Consider the following Riemann initial data

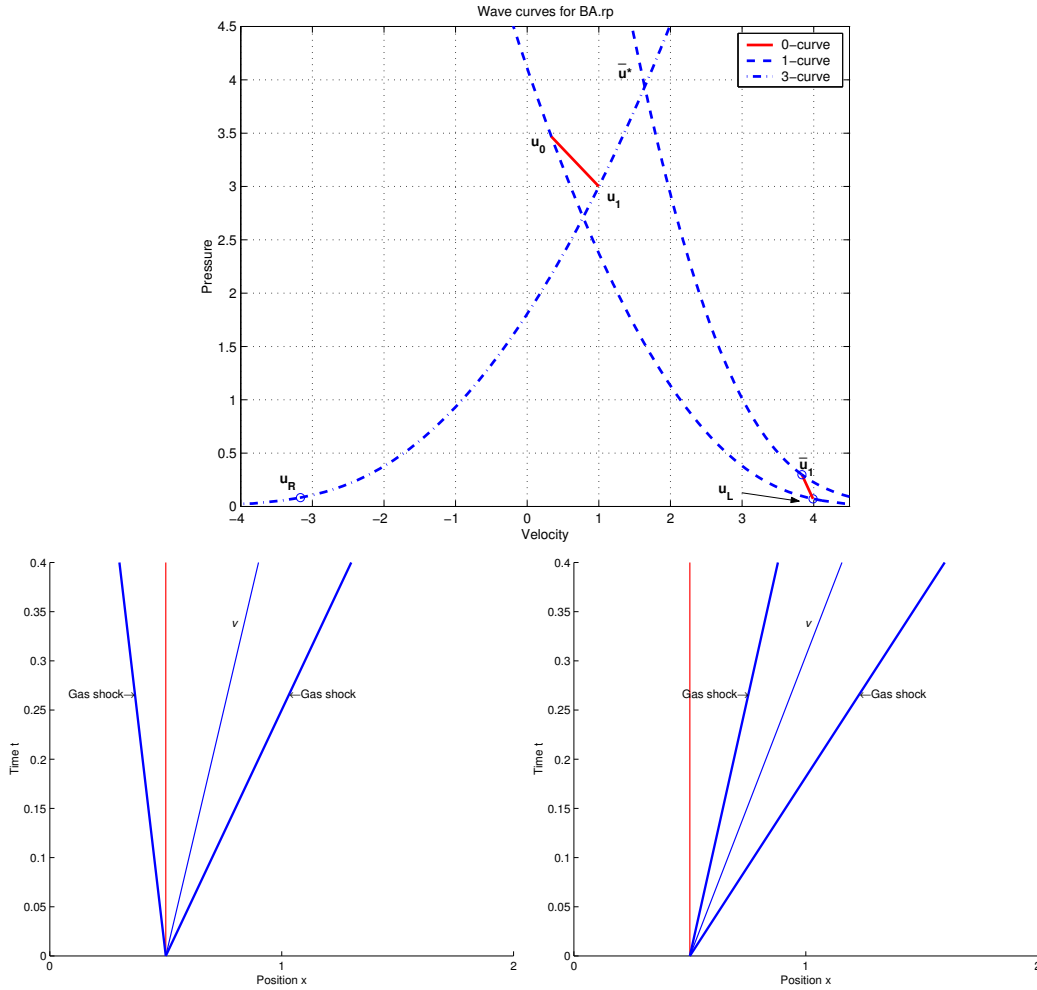| A_L	ρ_L	v_L	p_L	A_R	ρ_R	v_R	p_R
0.3	0.2	3.3	1	0.8	0.2	-4	0.07

$$\tag{5.45}$$

Fig. 5.11. Top: The wave curves for the Riemann problem (5.1), (5.43). Bottom: The corresponding wave configurations B and A in the (x, t)-plane.

Reasoning similar as above, we can show that the Riemann problem (5.1), (5.45), closed with the equation of state (2.5) with $\gamma = 1.4$ and $\pi = 0$, has a non-unique solution in form of either configuration B or configuration D. The wave curves and the wave configurations are shown in Fig. 5.13.

□

For the configuration C, the results are completely analogous. The wave curves are presented in Figs. 5.14 and 5.15. Similarly to how it is done for the configuration B, one can introduce the left- and right-bounding curves.

Definition 5.8. *Consider the Riemann problem* (5.1), (5.2). *Let us call the 1-curve, crossing the 3-curve in the point with $v = 0$ the* **right-bounding 1-curve**.
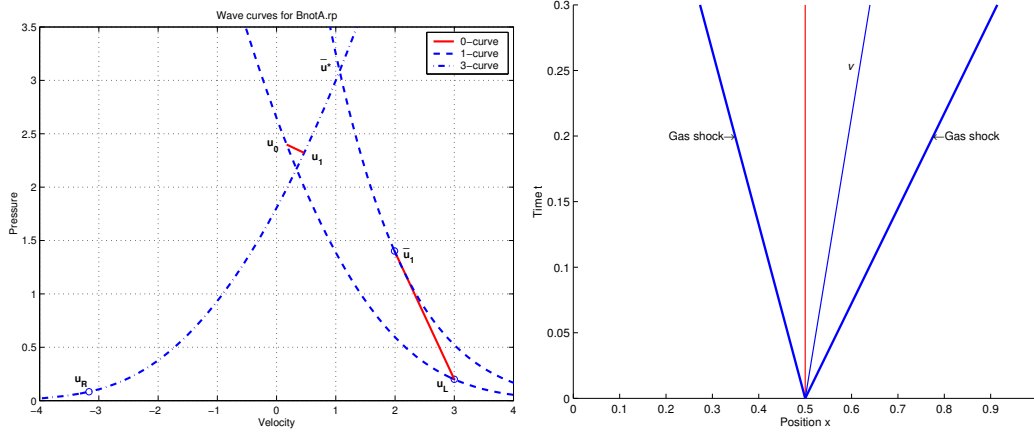
Fig. 5.12. The wave curves for the Riemann problem (5.1), (5.44).

Further,

1. *If $A_L < A_R$, consider the state $\mathbf{u}_1$ on the 3-curve with $|\mathrm{M}_1| < 1$, connected with the state $\mathbf{u}_0$ with $\mathrm{M}_0 = -1$ by the 0-wave. Let us call the 1-curve, passing through this state $\mathbf{u}_0$, the **left-bounding 1-curve**, see Fig. 5.14.*

2. *If $A_L > A_R$, consider the state $\mathbf{u}_1$ on the 3-curve with $\mathrm{M}_1 = -1$, connected with the state $\mathbf{u}_0$ with $|\mathrm{M}_0| < 1$ by the 0-wave. Let us call the 1-curve, passing through $\mathbf{u}_0$ the **left-bounding 1-curve**, see Fig. 5.15.*

Analogously to Theorem 5.7 we have the following result.

Theorem 5.9. *Consider the Riemann problem (5.1), (5.2) with the stiffened gas EOS (2.5). If the 1- and 3-curves intersect in the point (v^*, p^*) with $v^* < 0$, then the following scenarios are possible.*

1. *If the point (v^*, p^*) lies between the left- and right-bounding 1-curves of Definition 5.8, then the configuration C is realizable, for all $\mathbf{u}_L$ on the 1- and all $\mathbf{u}_R$ on the 3-curve. Moreover, the solution of this kind is unique, and the configuration B for the same Riemann problem is not realizable.*

2. *If the point (v^*, p^*) lies to the left of the left-bounding 1-curve, then there exists no solution to the Riemann problem (5.1), (5.2) in form of the configuration C.*

3. *If $\mathrm{M}_L > 1$, then the configuration A can be realizable.*

4. *If $\mathrm{M}_R < -1$, then the configuration D can be realizable.*

Proof. Analogous to the proof of Theorem 5.7.   □
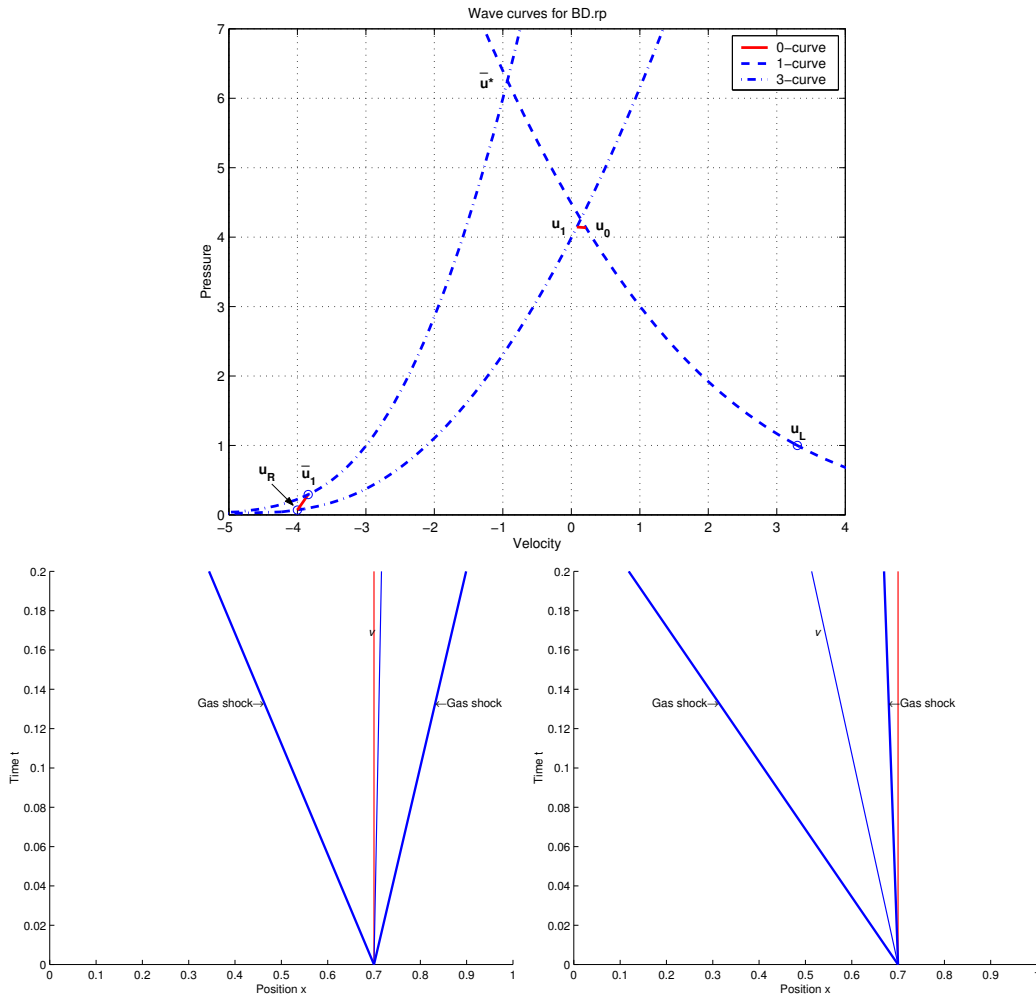
Fig. 5.13. Top: The wave curves for the Riemann problems (5.1), (5.45). Bottom: The corresponding wave configurations B and D in the (x,t)-plane.

5.5 Which solution to take?

To understand the origin of the non-uniqueness of the Riemann solution for the Euler equations in a duct of variable cross-section, it is advantageous to consider analogous situations for other models. An immediate example is given by the usual Euler equations of gas dynamics. They are obtained as the inviscid approximation to, in general viscous, fluid flows. It is well known that this approximation leads to non-unique discontinuous solutions, and therefore to non-unique solutions for Riemann problems. One needs to use an additional criterion, entropy condition, in order to select the physically relevant solution. In fact, one possible way of obtaining an entropy condition is to add a viscous term to the Eu-
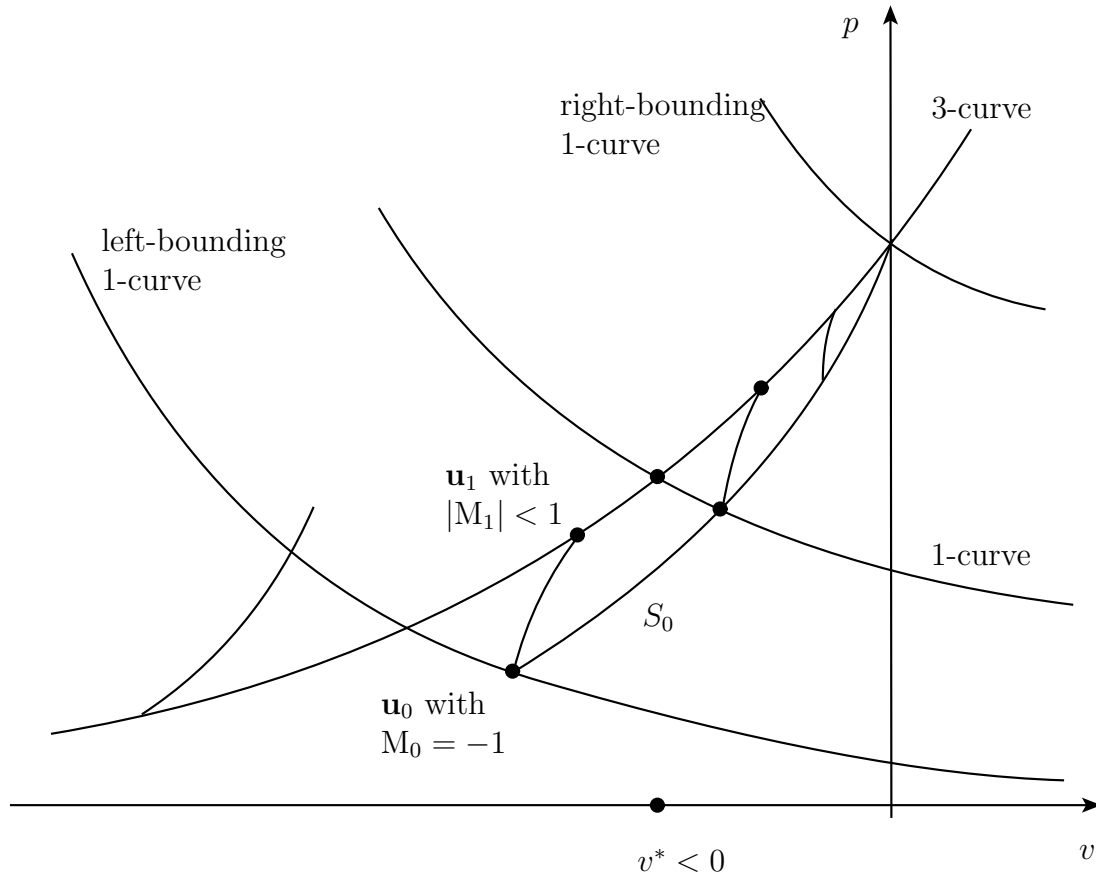
Fig. 5.14. The wave curves for the configuration C with $A_L < A_R$. If the point (v^*, p^*) lies between the left- and right-bounding 1-curves, there exists a unique solution in form of configuration C.

ler equations, i.e. to model the original viscous flow. Then the limit of solutions for vanishing viscosity will yield the physical entropy solution, see e.g. Godlewski and Raviart [38].

For the Euler equations in a duct of variable cross-section, the situation is somewhat analogous. In addition to neglecting viscosity, we have also neglected the multi- (two- or three-) dimensional effects. In this light it is not surprising that we got non-uniqueness of solutions to the Riemann problem. Roughly speaking, we have lost too much information on the truly multi-dimensional flow. However, one might hope to get a criterion for choosing the physically relevant solution by considering multi-dimensional effects, similarly to the limiting procedure for the usual Euler equations. One possible way would be to add some terms to the system of governing equations, which would model these effects. For example, these terms might be obtained using the statistical ensemble averaging techniques in the spirit of recent work of Abgrall and Saurel [3]. This could be an interesting
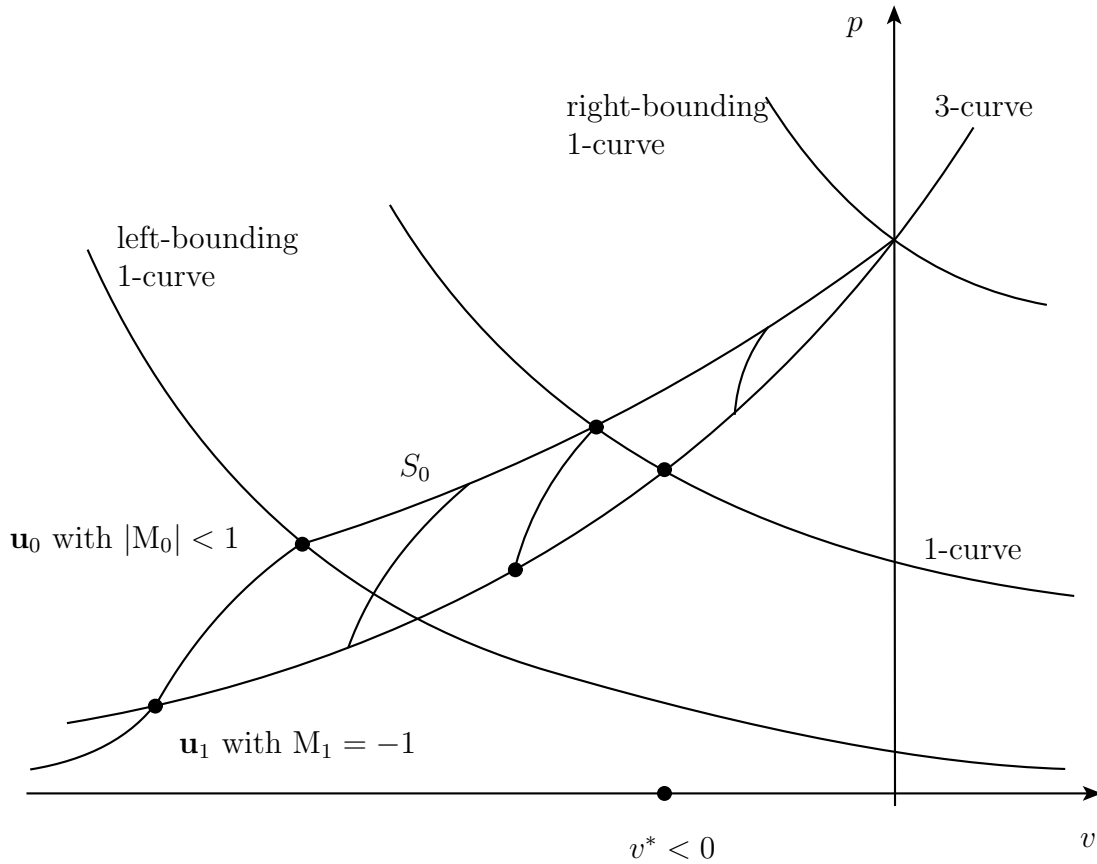
Fig. 5.15. The wave curves for the configuration C with $A_L > A_R$.

topic of future research.

Here, we follow a more straight-forward approach: We compare the results of the quasi-one-dimensional Euler equations in a duct of variable cross-section with multi-dimensional computations of the usual Euler equations in a tube of corresponding geometry. To this end, we employ the popular software package CLAWPACK provided by LeVeque [18, 60]. It is efficient, robust, and simple to use. The basic building block is the user-defined Riemann solver, which is then incorporated in the so-called *wave propagation approach*. It splits the flux difference in the normal direction to the cell interface into two transverse flux differences. Then these differences are used to update the cell averages. Thus the algorithm reflects the fact that waves should propagate in a multi-dimensional manner. As a result, although CLAWPACK uses rectangular meshes, it is able to compute multi-dimensional flows correctly.

Before we start to judge which solution can be considered as physically relevant, we wish to assess the perfomance of the 1D model (5.1) on some well-known test cases. Remember that the Riemann problem for the quasi-one-dimensional
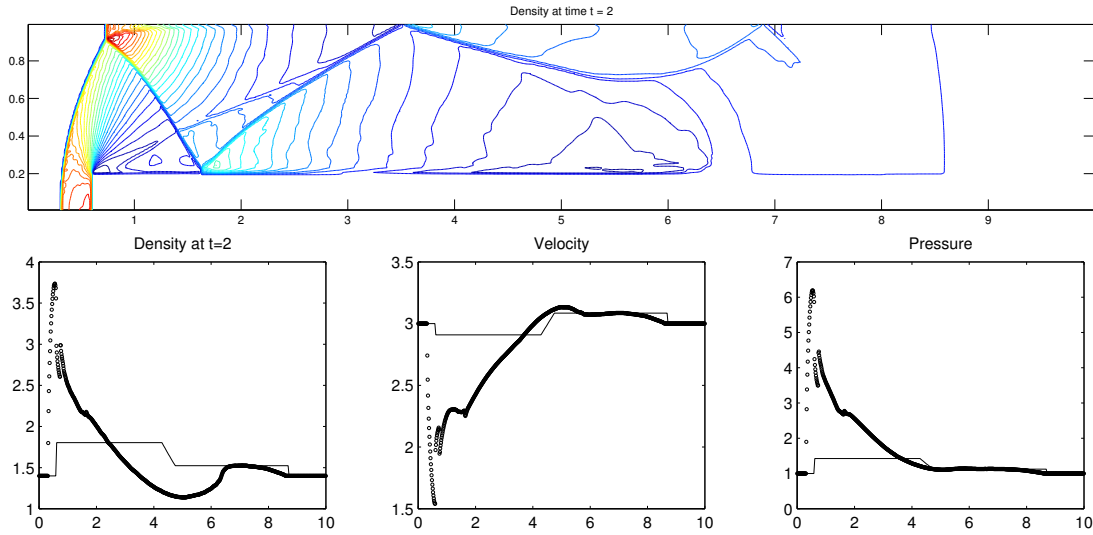
Fig. 5.16. Top: The density contours for the forward-facing step problem. Bottom: The comparison of the averaged 2D solution (dots) with the 1D exact solution (line).

flow in a duct of variable cross-section corresponds to the flow in a duct with a sudden jump in cross-section. There are a number of standard test cases, like the flow around a step (*forward-facing step*) or the diffraction of a shock wave at a corner (*backward-facing step*), which can be seen as the lower half of 2D flow in a duct with a sudden jump in cross-section. Therefore, we first compare the 2D CLAWPACK computations with the exact solution to the corresponding Riemann problem for the 1D model (5.1), and then do the same for the examples of Section 5.4. In order to close both the 2D Euler equations and the 1D model (5.1), we use the stiffened gas EOS (2.5) with $\gamma = 1.4$ and $\pi = 0$. In the calculations below we have used CLAWPACK with a second order method, and Roe's Riemann solver, unless stated otherwise.

5.5.1   Forward-facing step

The forward-facing step is a test case, which is also often referred to as a *Mach 3 wind tunnel with a step*, see e.g. Woodward and Colella [95]. It is intensively used to compare different numerical schemes in 2D, see e.g. [95, 27]. The problem begins with uniform Mach 3 flow in a wind tunnel containing a step. The tunnel is 1 unit wide and the step of 0.2 units high is located 0.6 units to the right from the left-hand end of the tunnel. At the left(right) is an inflow(outflow) boundary condition. At the top and bottom reflecting boundary conditions are used. The unsteady solution consists of a bow shock, which is reflected several times from the upper and lower walls of the tunnel.
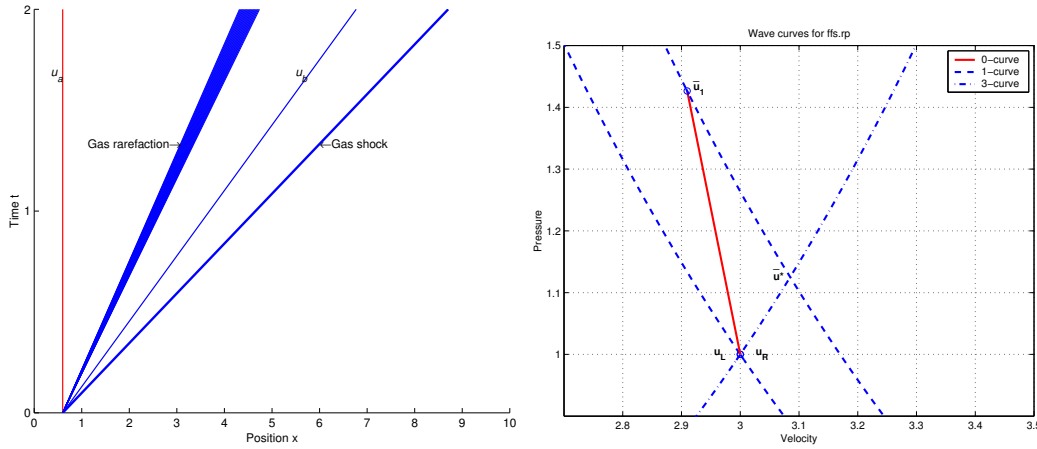
Fig. 5.17. The wave curves and the wave configuration for the 1D forward-facing step problem.

There are several difficulties concerning the numerical solution of this problem. The corner of the step is the center of a rarefaction fan and thus is a singular point of the flow. Due to this rarefaction, the pressures and densities may become negative in the computational cells just behind the corner. Also, the entropy tends to grow behind the corner and then is transported downstream, affecting the solution. To avoid this, one has to apply a special boundary condition at the corner, see [95]. Also, one may have numerical instabilities in the 2D strong almost stationary shocks in front of the corner and at the Mach stem at the upper wall, see again [95].

In our calculations with the Roe solver, we have obtained negative densities and pressures at the corner. To fix them, one can change to the HLLC solver [90, 11] there, which is positivity preserving in 1D. The 2D numerical results for 800×80 grid points are shown in Fig. 5.16 (top).

The corresponding initial data for the quasi-one-dimensional model (5.1) are

$$\begin{array}{|c|c|c|c||c|c|c|c|}
\hline
A_L & \rho_L & v_L & p_L & A_R & \rho_R & v_R & p_R \\
\hline
1 & 1.4 & 3 & 1 & 0.8 & 1.4 & 3 & 1 \\
\hline
\end{array}. \tag{5.46}$$

The configuration of the Riemann problem (5.1), (5.46) and the wave curves for it are presented in Fig. 5.17.

The projections of the states $\mathbf{u}_L$ and $\mathbf{u}_R$ to the (v, p)-plane are represented by the same point, which is also their intersection point (v^*, p^*). Since $v^* = v_L = v_R = 3 > 0$, we are in conditions of Theorem 5.7. Since $\mathrm{M}_L = \mathrm{M}_R = 3$, the 3-curve lies to the right of the right-bounding 3-curve. Therefore, the configuration B in the solution of the Riemann problem (5.1), (5.46) is not realizable. The direct calculation shows that the configuration D is also impossible. The only possible solution in this case is configuration A, see Fig. 5.17. It consists of
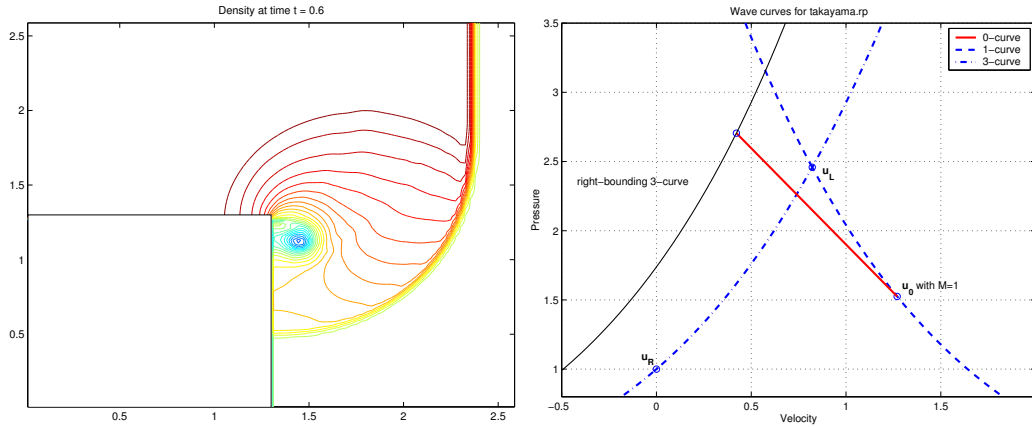
Fig. 5.18. The Takayama's test problem. Left: The 2D solution.
Right: The wave curves for the corresponding Riemann problem (5.1),
(5.47).

the 1-rarefaction, 2-contact, and 3-shock travelling to the right of the stationary
0-contact.

In Fig. 5.16 (bottom), the exact solution to the Riemann problem (5.1), (5.46)
at time $t = 2$ is compared to the averaged 2D calculations. Observe that although
the solutions differ considerably, the position of the 1D 3-shock gives relatively
good approximation for the fastest wave in the averaged 2D solution.

5.5.2   Backward-facing step

Here we consider two shock wave diffraction problems. The first one is described
in Takayama and Inoue [87], and therefore will be referred to as *Takayama's test*.
The shadowgraphs for the second problem were presented by Schardin, see Van
Dyke [93]. This test will be referred to as *Schardin's test*.

Takayama's test   The state behind the shock wave is given by $\rho = 1.862$,
$u = 0.826$, $v = 0$, $p = 2.4583$, and in front of it by $\rho = p = 1$, $u = v = 0$.
Thus, the shock moves with the speed $s = 1.7748$ and its Mach number is 1.5.
The initial position of the shock can be taken at $x = 1.3$, and the computational
domain is $[0, 2.6] \times [0, 2.6]$ without the south-west corner $[0, 1.3] \times [0, 1.3]$. The
2D solution is presented in Fig. 5.18 (left).

The initial data for the corresponding Riemann problem for the quasi-one-
dimensional model (5.1) will be

A_L	ρ_L	v_L	p_L	A_R	ρ_R	v_R	p_R
1.3	1.862	0.826	2.4583	2.6	1	0	1

$$(5.47)$$

The wave curves are presented in Fig. 5.18.

Since the left and right states are connected by a single 3-shock, the projection of the intersection point of the 1- and 3-curves in the (v, p)-plane will coincide with the projection of $\mathbf{u}_L$, so the velocity there will be $v^* = v_L = 0.826 > 0$. We notice immediately that the 3-curve lies to the right of the right-bounding 3-curve, so that the configuration B is not realizable. Since the states $\mathbf{u}_L$, $\mathbf{u}_R$ are subsonic, the configurations A and D are not realizable as well. Therefore, the Riemann problem (5.1), (5.47) does not have a solution. At the same time, the 2D solution of the corresponding problem exists, see Fig. 5.18 (left).

Schardin's test Now the incident shock wave of Mach 1.3 diffracts over the north-west corner in the computational domain $([-6, 12] \times [0, 8]) \setminus ([-6, 1.5] \times [4, 8])$. The state behind the shock wave is given by $\rho = 2.122$, $u = 0.4423$, $v = 0$, $p = 1.805$, and in front of it by $\rho = 1.4$, $u = v = 0$, $p = 1$. The 2D solution is presented in Fig. 5.19 (top left).

The initial data for the corresponding Riemann problem for the quasi-one-dimensional model (5.1) will be

$$
\begin{array}{|c|c|c|c||c|c|c|c|}
\hline
A_L & \rho_L & v_L & p_L & A_R & \rho_R & v_R & p_R \\
\hline
4 & 2.122 & 0.4423 & 1.805 & 8 & 1.4 & 0 & 1 \\
\hline
\end{array}
\tag{5.48}
$$

The wave curves are presented in Fig. 5.19 (top right).

Again, since the left and right states are connected by a single 3-shock, the projection of the intersection point of the 1- and 3-curves in the (v, p)-plane will coincide with the projection of $\mathbf{u}_L$, so the velocity there will be $v^* = v_L = 0.4423 > 0$. The 3-curve now lies between the left- and right-bounding 3-curves, so that the configuration B is realizable now. Since the states $\mathbf{u}_L$, $\mathbf{u}_R$ are subsonic, the configurations A and D are not realizable, so we have a unique solution to the 1D Riemann problem (5.1), (5.48).

In Fig. 5.19 (bottom) we present the comparison between the averaged 2D solution and the exact solution to the 1D Riemann problem (5.1), (5.48). We observe that the 1D model gives more or less correct wave speeds, slightly over-estimating the 3-shock speed. However, the 2D flow is too far away from being one-dimensional, so the 1D solution approximate it very poorly.

5.5.3 Diverse Riemann problems for the 1D model

Non-uniqueness between configurations A and B Consider the 1D Riemann problem (5.1), (5.43), which has already been studied in Section 5.4. This problem has a non-unique solution in form of either configuration A, or configuration B, see Fig. 5.11. With CLAWPACK, we solve the 2D analog of this 1D Riemann problem, i.e., the usual Euler equations in the corresponding 2D computational domain. The 2D solution on the 200×100 grid and the comparison of the averaged 2D solution with the exact solution to the 1D Riemann
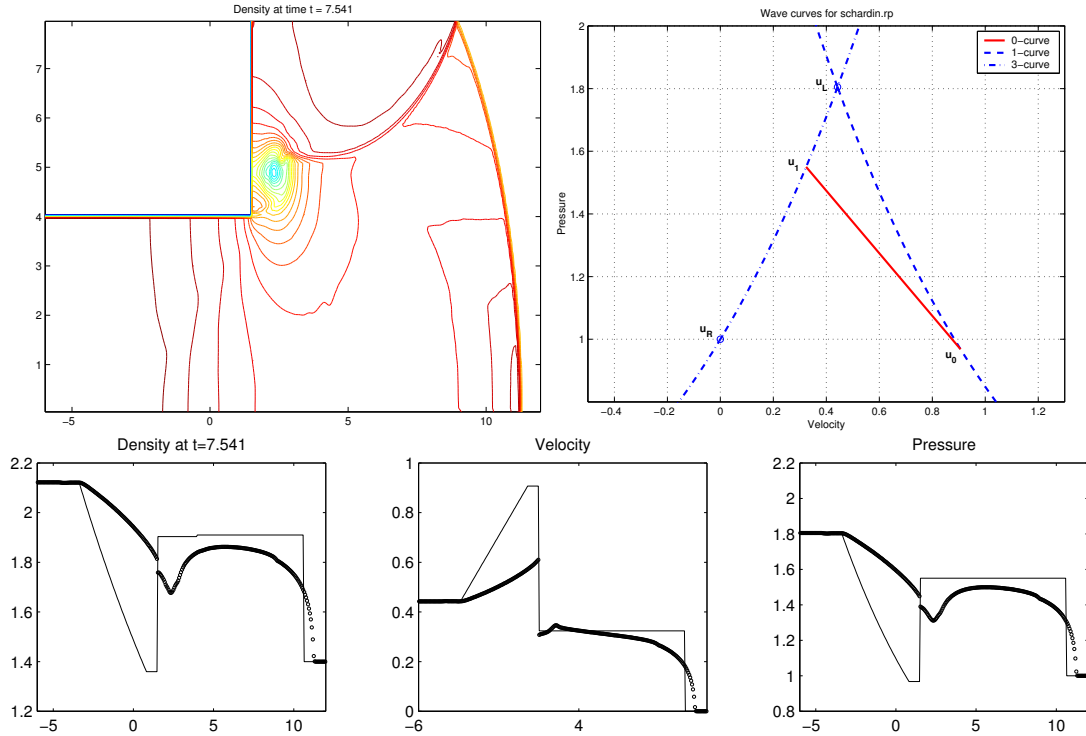
Fig. 5.19. The Schardin's test problem. Top left: The 2D solu-
tion. Top right: The 1D wave curves for the corresponding Riemann
problem (5.1), (5.48). Bottom: The comparison of the averaged 2D
solution (dots) with the 1D exact solution (line).

problem (5.1), (5.43) is shown in Fig. 5.20 (top). We see that the 1D model
slightly over-estimates the 3-shock speed. Also, due to rich 2D motion in the
left section of the domain, the 1D prediction of the position of 1-shock is quite
approximate. The same can be said about the approximation of the flow near
the jump in the cross-section. However, the numerical solution clearly picks up
the configuration B in the 1D solution of the Riemann problem (5.1), (5.43), see
Fig. 5.20.

Unique solution in form of configuration B As we have established in
Section 5.4, the Riemann problem (5.1), (5.44) has a unique solution in form of
configuration B. The comparison of the averaged 2D solution on 100×100 grid
with the exact solution to the 1D Riemann problem is shown in Fig. 5.21. Again,
we observe that the shock speeds are slightly different, however the main features
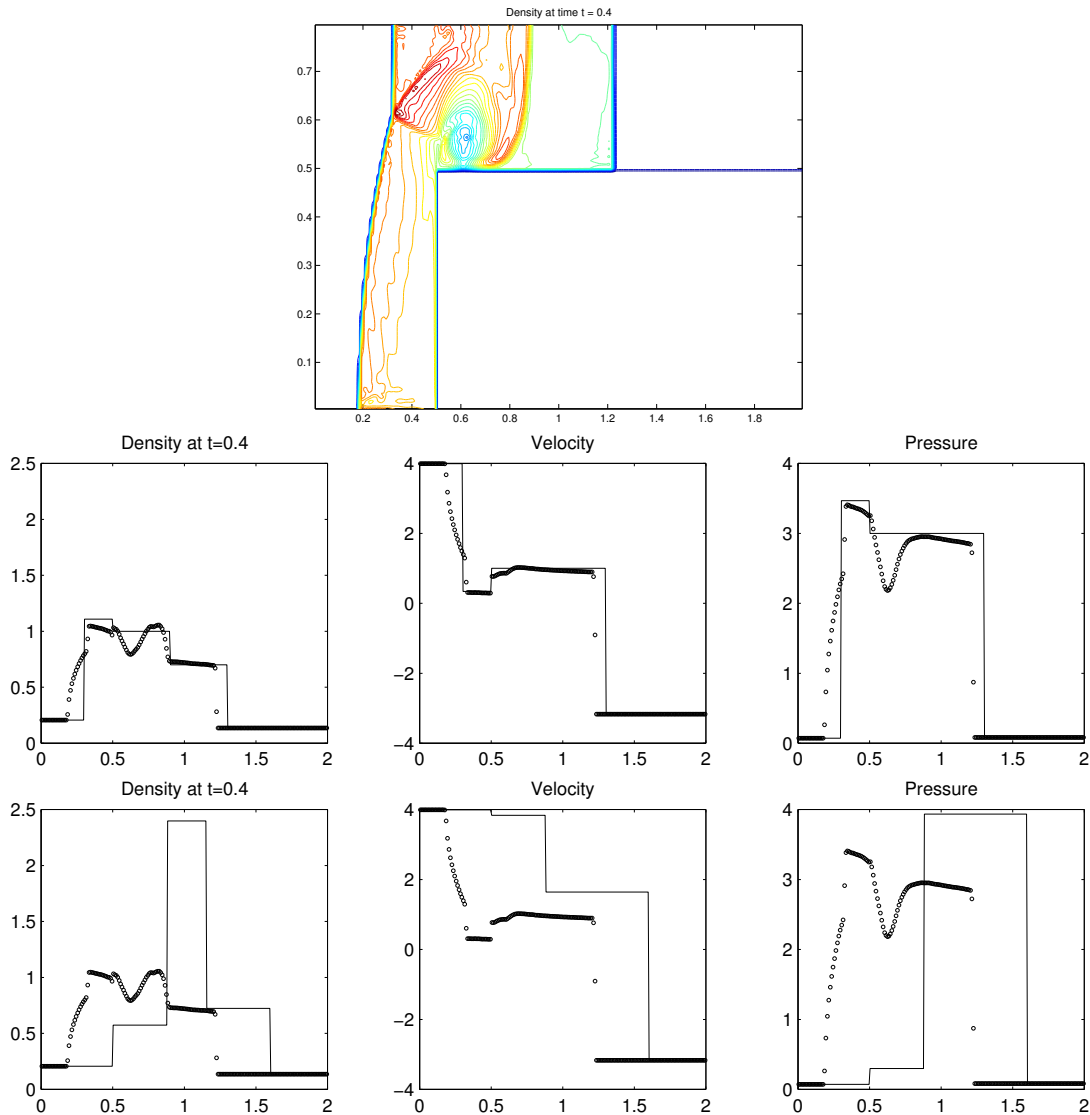of the 2D flow are correctly represented by the 1D model.

Fig. 5.20. Top: The density contours of the 2D solution to the Riemann problem (5.1), (5.43). Middle: The comparison of the averaged 2D solution (dots) with the 1D exact solution in form of configuration B (line). Bottom: The comparison of the averaged 2D solution (dots) with the 1D exact solution in form of configuration A (line).

Non-uniqueness between configurations B and D   The solution to the 1D Riemann problem (5.1), (5.45) is non-unique: It can be either configuration B, or configuration D. Again, we calculate the corresponding 2D problem and obtain the results, shown in Fig. 5.22. We see that the exact 1D solution for the configuration B fits perfectly to the averaged 2D solution. On the other hand,
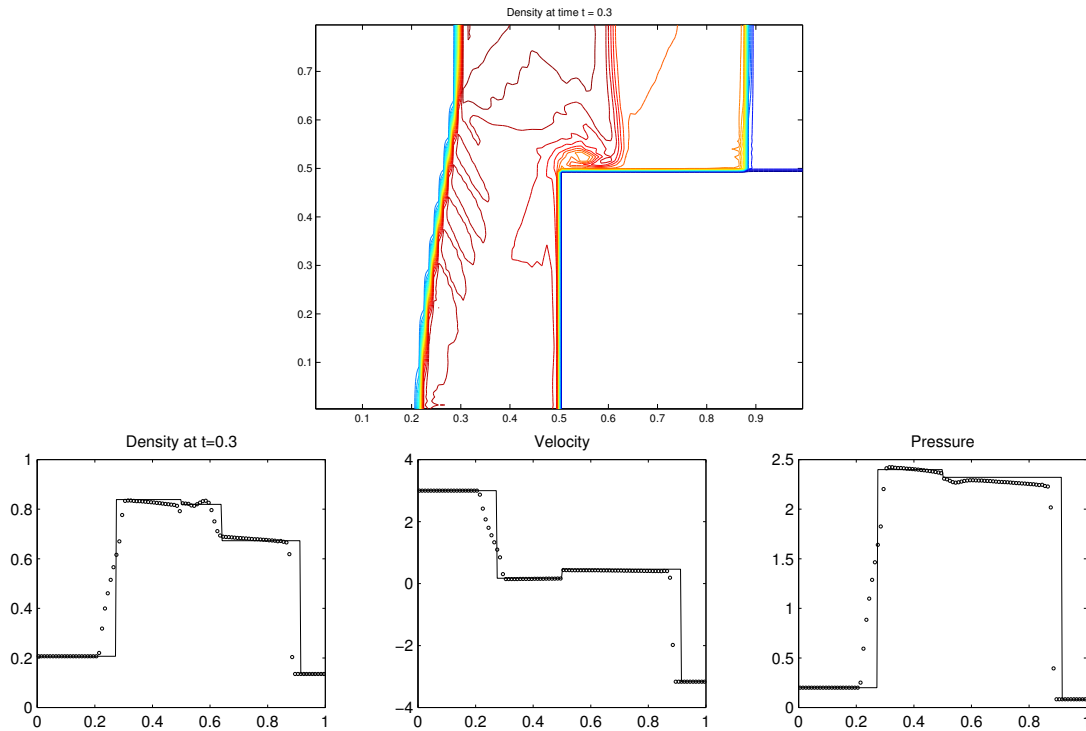
Fig. 5.21. Top: The density contours of the 2D solution to the Riemann problem (5.1), (5.44). Bottom: The comparison of the averaged 2D solution (dots) with the 1D exact solution (line).

the 1D solution for configuration D has nothing in common with it.

5.5.4   A criterion for realizable solution

The preceeding computations show that for all configurations of Riemann problems the 1D solution can differ significantly from the 2D one, see e.g. the results for the forward-facing step on Fig. 5.16 and for Schardin's test on Fig. 5.19. However, if the 1D solution to a Riemann problem is not unique, the 2D calculations clearly pick out one of them. In what follows, we will call the corresponding 1D Riemann solutions *physically relevant*. Let us investigate, what distinguishes these solutions from the physically non-relevant ones.

A classical way to exclude physically irrelevant solutions is to use a notion of entropy. However, one cannot use the entropy inequality used in the theory of conservation laws for the non-conservative system (5.1). In the particular case of the Riemann problem, one can use the approach of Section 5.3 to define it. Note also that *locally* each discontinuity in the solution to the Riemann problems is entropy-satisfying, i.e. the entropy increases across shocks. However, it does not
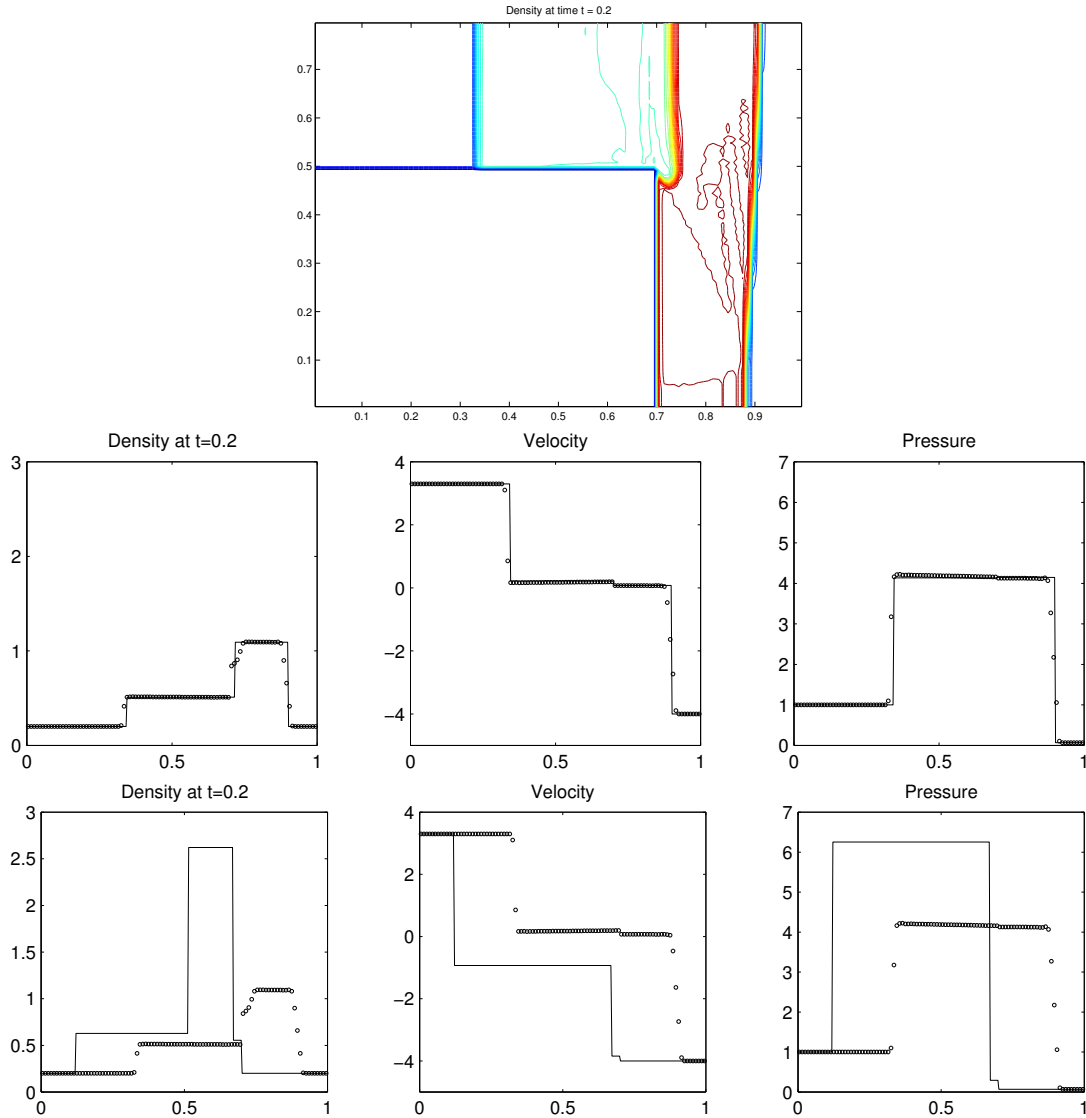
Fig. 5.22. Top: The density contours of the 2D solution to the Riemann problem (5.1), (5.45). Middle: The comparison of the averaged 2D solution (dots) with the 1D exact solution in form of configuration B (line). Bottom: The comparison of the averaged 2D solution (dots) with the 1D exact solution in form of configuration D (line).

help to rule out the physically irrelevant solutions. This suggests an idea of using a *global* entropy condition.

A condition of such kind was proposed by Dafermos [24, 25], who called it the *entropy rate admissibility criterion.* It states that not only should the entropy increase but it should be increasing at the maximum rate. The rigorous definition

of this criterion can be applied for the conservation laws only. However, we can use the general idea for the non-conservative system (5.1) as well.

As a measure of the entropy increase rate, we use the jump in the isentrope $\eta = \frac{p+\pi}{\rho^\gamma}$ across shocks. These jumps are always positive. Then, our calculations show that physically relevant solutions, i.e. the ones picked out by 2D calculations, indeed have the maximal increase in entropy in comparison with the other solutions. This may be seen as an analogy of the entropy rate admissibility criterion of Dafermos [24].

Since the Euler equations in a duct can be formally obtained from the governing equations for the Baer–Nunziato model of two-phase flows [10], the solution to the Riemann problem for it will be in general also not unique. Therefore, the analysis of the Euler equations for a duct of variable cross-section and in particular the above criterion can help in investigating the properties of the governing equations for the Baer–Nunziato model.

5.6 The solution to the Riemann problem

Consider the Riemann problem for the system of the Euler equations in a duct of variable cross-section (5.1), (5.2), and let us look for an exact solution to it. Analogously to the case of the Baer–Nunziato model of two-phase flows [10], we can introduce the notion of the "inverse" solution to the Riemann problem, see Section 4.1. Instead of starting with the end states $\mathbf{u}_L$, $\mathbf{u}_R$, and looking for the intermediate states in the solution of the Riemann problem, i.e. the "usual", or "direct" solution of the Riemann problem, we have fixed some intermediate state in the Riemann solution, prescribed the configuration of the Riemann problem, and looked for the end states $\mathbf{u}_L$, $\mathbf{u}_R$, which can be connected to this intermediate state by the prescribed waves, "inverse" solution.

Remember that the system (5.1) can be formally obtained from the governing equations for the Baer–Nunziato model of two-phase flows, see Section 2.3. Therefore, we can use the procedure of the "inverse" solution which we have introduced in Section 4.1, to construct exact solutions to the Riemann problems (5.1), (5.2). This procedure is implemented in the package CONSTRUCT [5]. It is designed for the Riemann problem for the Baer–Nunziato model of two-phase flows. For CONSTRUCTing exact solutions to the Euler equations in a duct of variable cross-section, one has to set the solid velocity equal to zero, and consider only the gas waves in the solution of the Riemann problem. The gas volume fraction then corresponds to the variable cross-section. Using CONSTRUCT, one can build numerical tests for assessing the accuracy of numerical methods of interest.

Now let us obtain the "direct" solution to the Riemann problem (5.1), (5.2). To do so, we remember that there are 4 possible configurations of this Riemann problem, see Fig. 5.5. Then, we solve the Riemann problem by examining if either of configurations A, B, C, or D is possible.

It is easy to check if the configurations A or D are realizable. Let us start with the configuration A. Since $\mathbf{u}_L$ is given, we can find $\mathbf{u}_1$ from the relations (5.22). To the right of the stationary contact, the system (5.1) reduces to the Euler equations. Now, we solve the Riemann problem for the Euler equations to the right of the stationary contact with the initial data $\mathbf{u}_1$ and $\mathbf{u}_R$. If the slowest wave speed in the solution of this Riemann problem is positive, then the configuration A is possible. Note that if the 1-wave is a rarefaction, and the last 1-characteristic speed is equal to zero, i.e. the 1-rarefaction touches the stationary contact from the right, then the parabolic degeneracy occurs, see Section 2.5. We do not consider this complicated case further.

We can treat the configuration D analogously. From $\mathbf{u}_R$, we can find $\mathbf{u}_0$. Next, we solve the Riemann problem to the left of the stationary contact with the initial data $\mathbf{u}_L$ and $\mathbf{u}_0$. Again, if the fastest wave speed is negative, then the configuration D is realizable. If the 3-wave is the rarefaction and it touches the stationary contact from the left, then the parabolic degeneracy occurs.

Checking for the configurations B and C is not so straightforward. Let us rewrite the relations (5.22) in the following way

$$\frac{p_0 + \pi}{\rho_0^\gamma} = \frac{p_1 + \pi}{\rho_1^\gamma} \tag{5.49}$$

$$A_0 \rho_0 v_0 = A_1 \rho_1 v_1 \tag{5.50}$$

$$\frac{\gamma(p_0 + \pi)}{\rho_0(\gamma - 1)} + \frac{v_0^2}{2} = \frac{\gamma(p_1 + \pi)}{\rho_1(\gamma - 1)} + \frac{v_1^2}{2}. \tag{5.51}$$

On the other hand,

$$v_0 = F_L(p_0) \tag{5.52}$$

$$v_1 = F_R(p_1), \tag{5.53}$$

where F_k, $k = L, R$ depends on wave type, i.e. if it is a shock or rarefaction,

$$F_k(p) = \begin{cases} v_k \pm (p - p_k) \left(\frac{A_k}{p + B_k} \right)^{\frac{1}{2}}, & \text{if } p > p_k \text{ (shock)} \\ v_k \pm \frac{2c_k}{\gamma - 1} \left(\left(\frac{p + \pi}{p_k + \pi} \right)^{\frac{\gamma - 1}{2\gamma}} - 1 \right), & \text{if } p \le p_k \text{ (rarefaction)}. \end{cases} \tag{5.54}$$

Here the upper sign corresponds to the 3-wave, the lower to the 1-wave,

$$A_k = \frac{2}{\rho_k(\gamma + 1)}, \qquad B_k = \frac{p_k(\gamma - 1)}{\gamma + 1} + \frac{2\gamma\pi}{\gamma + 1}.$$

The equations (5.49)-(5.53) give the system of 5 equations for determining the 6 unknowns $\rho_0, v_0, p_0, \rho_1, v_1, p_1$. For the configurations B and C the closure is done in a different way. For the configuration B, we use

$$\rho_0 = R_L(p_0), \tag{5.55}$$

and for the configuration C

$$\rho_1 = R_R(p_1), \tag{5.56}$$

where

$$R_k(p) = \begin{cases} \rho_k \dfrac{\frac{p}{p_k} + \frac{\gamma-1}{\gamma+1} + \frac{2\gamma\pi}{p_k(\gamma+1)}}{\frac{p(\gamma-1)}{p_k(\gamma+1)} + 1 + \frac{2\gamma\pi}{p_k(\gamma+1)}}, & \text{if } p > p_k \text{ (shock)} \\[2em] \rho_k \left(\dfrac{p + \pi}{p_k + \pi} \right)^{\frac{1}{\gamma}}, & \text{if } p \le p_k \text{ (rarefaction)}, \end{cases}$$

and $k = L, R$. Putting all together, we have the nonlinear algebraic system for determining the states $\mathbf{u}_0$ and $\mathbf{u}_1$. We can rewrite it as

$$\mathcal{F}(\mathcal{W}) = 0, \tag{5.57}$$

where

$$\mathcal{W} = \begin{bmatrix} \rho_0 \\ v_0 \\ p_0 \\ \rho_1 \\ v_1 \\ p_1 \end{bmatrix}, \qquad \mathcal{F} = \begin{bmatrix} \frac{p_0+\pi}{\rho_0^\gamma} - \frac{p_1+\pi}{\rho_1^\gamma} \\ A_0\rho_0 v_0 - A_1\rho_1 v_1 \\ \frac{\gamma(p_0+\pi)}{\rho_0(\gamma-1)} + \frac{v_0^2}{2} - \frac{\gamma(p_1+\pi)}{\rho_1(\gamma-1)} - \frac{v_1^2}{2} \\ v_0 - F_L(p_0) \\ v_1 - F_R(p_1) \\ f_6 \end{bmatrix}, \tag{5.58}$$

and

$$f_6 = \begin{cases} \rho_0 - R_L(p_0) & \text{for configuration B} \\ \rho_1 - R_R(p_1) & \text{for configuration C}. \end{cases} \tag{5.59}$$

We solve the system (5.57) with the Newton method,

$$\mathcal{W}^{(n+1)} = \mathcal{W}^{(n)} - \mathcal{M}^{-1}(\mathcal{W}^{(n)})\,\mathcal{W}^{(n)}, \tag{5.60}$$

where

$$\mathcal{M} = \begin{bmatrix} -\dfrac{\gamma(p_0+\pi)}{\rho_0^{\gamma+1}} & 0 & \dfrac{1}{\rho_0^\gamma} & \dfrac{\gamma(p_1+\pi)}{\rho_1^{\gamma+1}} & 0 & -\dfrac{1}{\rho_1^\gamma} \\ A_0 v_0 & A_0\rho_0 & 0 & -A_1 v_1 & -A_1\rho_1 & 0 \\ -\dfrac{\gamma(p_0+\pi)}{\rho_0^2(\gamma-1)} & v_0 & \dfrac{\gamma}{\rho_0(\gamma-1)} & \dfrac{\gamma(p_1+\pi)}{\rho_1^2(\gamma-1)} & -v_1 & \dfrac{\gamma}{\rho_1(\gamma-1)} \\ 0 & 1 & -F_L'(p_0) & 0 & 0 & 0 \\ 0 & 0 & 0 & 0 & 1 & -F_R'(p_1) \\ m_{61} & m_{62} & m_{63} & m_{64} & m_{65} & m_{66} \end{bmatrix},$$

and the last row of $\mathcal{M}$ depends on the configuration,

$$\mathcal{M}_6 = \begin{cases} \begin{bmatrix} 1 & 0 & -R_L'(p_0) & 0 & 0 & 0 \end{bmatrix} & \text{for configuration B} \\ \begin{bmatrix} 0 & 0 & 0 & 1 & 0 & -R_R'(p_1) \end{bmatrix} & \text{for configuration C} \end{cases} \tag{5.61}$$

It is well known that the convergence of the Newton method (5.60) depends strongly on the initial guess $\mathcal{W}^{(0)}$. Denote it by

$$\mathcal{W}^{(0)} = \left[\rho_0^{(0)}, v_0^{(0)}, p_0^{(0)}, \rho_1^{(0)}, v_1^{(0)}, p_1^{(0)}\right]^T, \tag{5.62}$$

so the starting guesses for the states on the both sides of the 0-wave will be $\mathbf{u}_i^{(0)} = \left[(\rho_i^{(0)}, v_i^{(0)}, p_i^{(0)}\right]^T$, $i = 0, 1$. From Section 5.4 we know which configuration (B or C) will be realizable for the particular Riemann problem, if it will be realizable at all, see Theorems 5.7, 5.9. From these theoremes it is clear that the correct states $\mathbf{u}_0$ and $\mathbf{u}_1$ on the both sides of the 0-wave lie close to the state $\mathbf{u}^*$, obtained by the intersection of the 1- and 3-curves in the (v, p)-plane. Therefore, we choose this state as the starting guess for both $\mathbf{u}_i^{(0)}$, $i = 0, 1$. With this choice, some tens of iterations in the Newton method (5.60) were needed in solving the Riemann problems of Sections 5.4 and 5.5.

There are several further options in implementing the Newton method for solving Riemann problems to (5.1). Since the solution across the stationary contact is not unique, cf. the analysis of Section 4.1, one could force $\mathbf{u}_0, \mathbf{u}_1$ to be the admissible states by solving the system of equations (5.22) for them at each Newton iteration. Also, it is possible that the densities and pressures become negative after some iteration. In this case, we simply set them to small positive values.

5.7 The Godunov-type method

Using the exact Riemann solver described above, one can develop a Godunov-type method for the non-conservative system (5.1) on its basis. Consider the system of the Euler equations in a duct (5.1), subject to the prescribed initial data $\mathbf{u}(x, 0)$. Assume we have an equally spaced grid, associated with the cell $I_j = [x_{j-1/2}, x_{j+1/2}]$, $x_{j+1/2} = j\Delta x$. At time $t^n = n\Delta t$, for each cell I_j, we define a cell average by

$$\mathbf{u}_j^n = \frac{1}{\Delta x} \int_{x_{j-1/2}}^{x_{j+1/2}} \mathbf{u}(x, t^n)\, dx. \tag{5.63}$$

Our key observation is that the cross-section A_j^n has a jump only across the cell boundary $x_{j+1/2}$ and is constant inside the cell I_j. Consequently, the non-conservative term $p\, \partial A/\partial x$ disappears in I_j and we are left with the *conservation law* there,

$$\mathbf{u}_t + \mathbf{f}(\mathbf{u})_x = 0, \tag{5.64}$$

where $\mathbf{u}, \mathbf{f}(\mathbf{u})$ are given by (5.3). Integrating (5.64) over $[x_{j-1/2}, x_{j+1/2}] \times [t^n, t^{n+1}]$ and using (5.63), we get

$$\mathbf{u}_j^{n+1} = \mathbf{u}_j^n - \frac{1}{\Delta x} \left[\int_{t^n}^{t^{n+1}} \mathbf{f}(\mathbf{u}(x_{j+1/2}, t))\, dt - \int_{t^n}^{t^{n+1}} \mathbf{f}(\mathbf{u}(x_{j-1/2}, t))\, dt\right]. \tag{5.65}$$
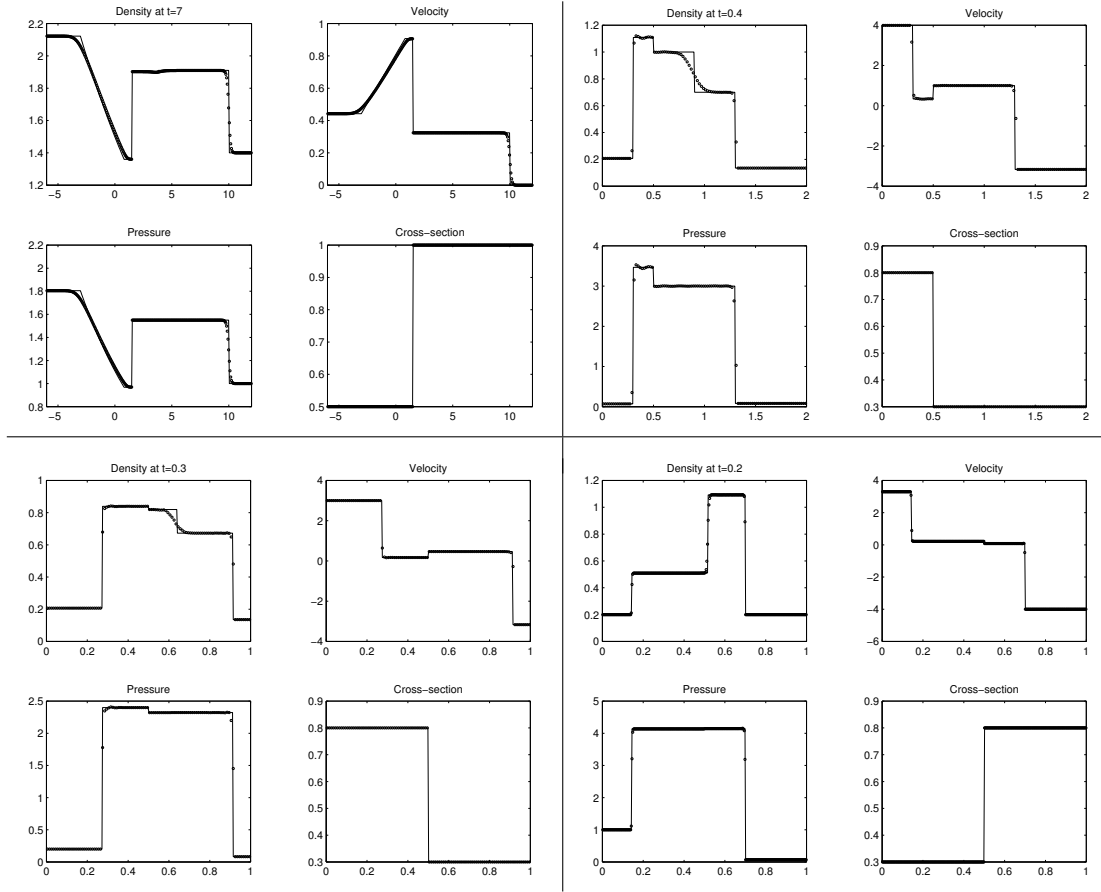
Fig. 5.23. Numerical results for the Godunov-type scheme (5.66). Top left: the Riemann problem (5.1), (5.48). Top right: the Riemann problem (5.1), (5.43). Bottom left: the Riemann problem (5.1), (5.44). Bottom right: the Riemann problem (5.1), (5.45).

In the spirit of the classical Godunov method, we solve the Riemann problem at each cell boundary $x_{j+1/2}$ exactly, using the Newton method (5.60). Remember that the solution of this Riemann problem is self-similar, $\mathbf{u} = $ const along each ray $(x - x_{j+1/2})/t = $ const. In general, $\mathbf{u}$ has a jump across the stationary contact $\lambda_0 = 0$. Denote the values to the left and to the right of it by $\mathbf{u}^-$ and $\mathbf{u}^+$, respectively. Using this in (5.65), the Godunov-type method reads

$$\mathbf{u}_j^{n+1} = \mathbf{u}_j^n - \frac{\Delta t}{\Delta x} \left[\mathbf{f}(\mathbf{u}_{j+1/2}^-) - \mathbf{f}(\mathbf{u}_{j-1/2}^+) \right]. \tag{5.66}$$

The above formula is valid as long as the CFL condition is fulfilled,

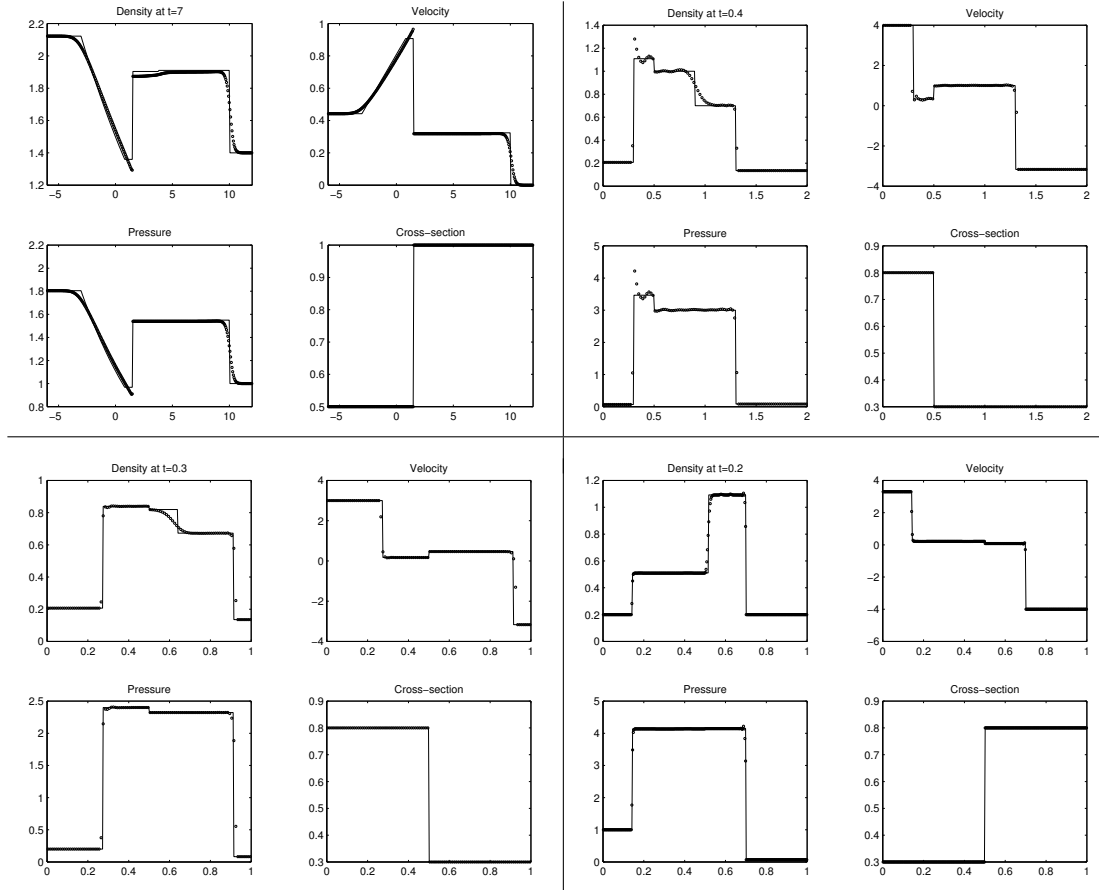$$\frac{\Delta t}{\Delta x} \max |\lambda_i| \leq 1. \tag{5.67}$$

Fig. 5.24. Numerical results for the VFRoe scheme. Top left: the Riemann problem (5.1), (5.48). Top right: the Riemann problem (5.1), (5.43). Bottom left: the Riemann problem (5.1), (5.44). Bottom right: the Riemann problem (5.1), (5.45).

It guarantees that the $\mathbf{u}_{j+1/2}^{\pm}$ remain constant on each cell boundary $x_{j+1/2}$. The scheme (5.66) can be extended to second order via the MUSCL approach.

To test the Godunov-type method (5.66), we have solved several test cases of Sections 5.4 and 5.5. In Fig. 5.23, we present the first-order results, which were obtained on 300 mesh cells with a CFL number of 0.9. In general, the main features of the flow are correctly resolved. However, some shortcomings of the method are obvious. Firstly, the contact discontinuities are extensively smeared, which is typical for a first-order scheme. The second-order version of the scheme behaves significantly better for the contact discontinuities. Secondly, there are small oscillations in the vicinity of some shocks in Fig. 5.23, consider e.g. the 1-shock for the Riemann problem (5.1), (5.43) in Fig. 5.23. For this Riemann problem, the 1-shock is slow, i.e. the ratio of the shock speed to the

Initial data	VFRoe	Godunov
(5.48)	1.83	3.33
(5.43)	0.30	0.42
(5.44)	0.38	0.55
(5.45)	3.34	3.65

Table 5.1. User CPU time in sec as given by the UNIX command `time` on HP 9000 workstation.

maximum wave speed is about 0.1. The problem of correct computation of slowly moving shocks for the nonlinear systems with shock capturing schemes has been reported before, see e.g. [9, 49, 72]. The oscillations are generated already by first-order schemes, and become more pronounced in higher-order schemes due to their lower numerical dissipation. In course of time, these oscillations are transported downstream.

Let us compare the performance of the Godunov-type scheme (5.66) with the VFRoe method, presented in Section 3.2. We solve the problems, presented in Fig. 5.23, with VFRoe using the same run parameters, i.e. the first-order scheme, 300 mesh cells, and CFL = 0.9. The results are shown in Fig. 5.24. For some problems, the VFRoe scheme behaves quite reasonably, e.g. for the Riemann problems (5.1), (5.44) or (5.1), (5.45). However, we observe huge oscillations in the solution of the Schardin's test and the Riemann problem (5.1), (5.43). We have already witnessed such behaviour of the VFRoe scheme in Section 4.7 when discussing its perfomance for the Baer–Nunziato model of two-phase flows.

An obvious advantage of VFRoe over the Godunov-type scheme (5.66) is its speed. The CPU time needed for the solution of the problems, presented in Figs. 5.23 and 5.24, is given in Table 5.1. As we see, the VFRoe scheme is on average about 40% faster than the Godunov-type scheme (5.66). The reason for this is the presence of three iterative procedures in the Godunov-type scheme:

 (i) Exact solution to the Riemann problem for usual Euler equations

 (ii) Exact solution behind the stationary contact

(iii) Newton's method (5.60).

Note that for the particular case of a *Riemann problem*, i.e., the problems considered above, we employ Newton's method (5.60) only for the one local Riemann problem per time step, namely in the position of the initial discontinuity, the jump in cross-section is *stationary*. For more complicated problems, e.g. when the cross-section varies in the whole computational domain, we expect even bigger differences in speed for the VFRoe and Godunov-type methods.

Chapter 6

Outlook

In this thesis, we studied several models of the generic homogenized model of two-phase flows. All these models are given by non-strictly hyperbolic systems of equations. A crucial issue about these systems is they all are non-conservative, i.e. they cannot be written in divergence form. This fact causes major difficulties in both mathematical investigation of the models, and their numerical solution.

In Section 3.2, we have proposed a simple method for the generic non-conservative model, the VFRoe method. We studied our method on several test problems and observed that the quality of the numerical solution can differ significantly from problem to problem. The numerical results of Section 3.3 show good accuracy of the method for a wide range of complicated physical problems. However, we have witnessed that the method can produce spurious oscillations in case of coinciding wave speeds in the solution of Riemann problems. Moreover, these oscillations do not dissapear as the mesh is refined. The reason for such behaviour is clear: We have obtained the discretization for the non-conservative terms under the assumption that velocity and pressure are constant. Obviously it is not true e.g. across shocks. Therefore, one has to look for some other discretization principle.

In dealing with the system of governing equations, the VFRoe method discussed above essentially separates the conservative part, i.e. the two sets of the Euler equations for both phases, and the non-conservative terms. Roughly speaking, given a discretization of the conservative part, we look for a corresponding discretization of the non-conservative terms. An alternative approach would be to consider the hyperbolic system *as a whole*. This is the idea behind the Godunov-type scheme proposed in Section 5.7. Since the wave in the solution of local Riemann problems, along which the non-conservative terms act, is always *stationary*, we get a *conservation law* inside a cell. Then, we are able to integrate it *exactly*, in the spirit of the classical Godunov method. The resulting method exhibits high accuracy but is quite slow due to several iterative procedures involved.

It is difficult to solve a more complicated Riemann problem, say for the Baer–

Nunziato model, exactly. One would have to consider a lot of different cases in the Riemann solution. As a result, one would get a big nonlinear system of algebraic equations. Its solution with some iterative method will also not be easy. All in all, such a procedure for finding an exact solution will be extremely inefficient computationally. Therefore, this approach does not seem to be a good candidate for a practical numerical method.

In looking for such a method, one may try to determine *a priori* the position of the wave in the solution to local Riemann problems, along which the non-conservative terms act. Then, to the left and to the right of this wave, we would have a conservation law. Integrating it exactly, we would obtain a Godunov-type conservative method. An alternative approach could be based on the definition of a weak solution to the non-conservative Riemann problem, given in Sections 4.6 and 5.3.

There are several open questions connected with the notion of an evolutionary discontinuity, given in Section 4.2. We have established that for a general non-strictly hyperbolic conservation law, the Lax shock condition is possibly not equivalent to the evolutionarity condition. It would be very interesting to investigate this issue in more detail. Also, the notion of evolutionarity can be a promising stand point for discussing overcompressive shocks and related issues.

The problem of nonlinear resonance occuring in the hyperbolic systems have been studied for more than 20 years now and traces back to the works of T.-P. Liu. In Section 5.4, we have seen that such resonant behaviour is typical for the "transitional" points in the flow, i.e. the points which separate distinct types of solution. Indeed, the left- and right-bounding curves, introduced in Section 5.4, by definition pass through these points. The position of the initial data with respect to these bounding curves determine whether we will have a solution or not, and whether the solution will be unique or not. A detailed investigation of these questions can be a interesting field of research.

Finally, there are a number of questions connected to the non-uniqueness of the Riemann solution, studied in Section 5.4. We were able to obtain only partial results, concerning the existence and uniqueness of the solution to the Riemann problem. However, the *origin* of this non-uniqueness is still not clear. The solution to the Riemann problem for the usual Euler equations is unique; by averaging of these equations we arrive at the non-conservative Euler equations in a duct, for which the solution to the Riemann problem is not unique anymore. The question is now what additional constraints one has to pose on the solution to guarantee its uniqueness and how it is related to the range of applicability of the model.

Bibliography

[1] R. Abgrall, How to prevent pressure oscillations in multicomponent flow calculations: a quasi conservative approach, *J. Comput. Phys.* **125**, 150-160 (1996).

[2] R. Abgrall and S. Karni, Computations of compressible multifluids, *J. Comput. Phys.* **169**, 594-623 (2001).

[3] R. Abgrall and R. Saurel, Discrete equations for physical and numerical compressible multiphase mixtures, *J. Comput. Physics* **186**, 361-396 (2003).

[4] D. M. Anderson, G. N. McFadden, and A. A. Wheeler, Diffuse-interface methods in fluid mechanics, *Annu. Rev. Mech.* **30**, 139-165 (1998).

[5] N. Andrianov, *CONSTRUCT: a collection of MATLAB routines for constructing the exact solution to the Riemann problem for the Baer-Nunziato model of two-phase flows.* Available at http://www-ian.math.uni-magdeburg.de/home/andriano/CONSTRUCT

[6] N. Andrianov, R. Saurel, and G. Warnecke, A simple method for compressible multiphase mixtures and interfaces, *Int. J. Numer. Meth. Fluids* **41**, 109-131 (2003).

[7] N. Andrianov and G. Warnecke, The Riemann problem for the Baer-Nunziato model of two-phase flows, submitted. Available at http://www.math.ntnu.no/conservation/2002/048.html

[8] N. Andrianov and G. Warnecke, On the solution to the Riemann problem for the compressible duct flow, submitted. Available at http://www.math.ntnu.no/conservation/2003/019.html.

[9] M. Arora and P. L. Roe, On postshock oscillations due to shock capturing schemes in unsteady flows, *J. Comput. Phys.* **130**, 25-40 (1997).

[10] M.R. Baer and J. W. Nunziato, A two-phase mixture theory for the deflagration-to-detonation transition (DDT) in reactive granular materials, *Int. J. Multiphase Flows*, **12**, 861-889 (1986).

[11] P. Batten, N. Clarke, C. Lambert, and D. M. Causon, On the choice of wavespeeds for the HLLC Riemann solver, *SIAM J. Sci. Comput.* **18**, 1553-1570 (1997).

[12] J. B. Bdzil, R. Menikoff, S. F. Son, A. K. Kapila, D. S. Stewart, Two-phase modeling of deflagration-to-detonation transition in granular materials: A critical examination of modeling issues, *Phys. Fluids* **11** (2), 378-402 (1999).

[13] D. Bestion, The physical closure laws in the CATHARE code, *Nucl. Eng. and Des.* **124**, 229 (1990).

[14] G. Boillat, Chocs caractéristiques, *C. R. Acad. Sci. Paris Sér. I* **274**, 1018-121 (1972).

[15] T. Buffard, T. Gallouët and J.-M. Hérard, A sequel to a rough Godunov scheme. Applications to real gas flows, *Computers and Fluids* **29** (7), 813-847 (2000).

[16] G. G. Cherny, *Gas dynamics,* Nauka, Moscow, 1988. (In Russian)

[17] A. Chinnayya, E. Daniel and R. Saurel, Computation of detonation waves in heterogeneous energetic materials. Submitted to *J. Comput. Phys.* (2001)

[18] CLAWPACK software, available at
http://www.amath.washington.edu/~claw/

[19] F. Coquel, K. El Amine, E. Godlewski, B. Perthame, and P. Rascle, A numerical method using upwind schemes for the resolution of two-phase flows, *J. Comput. Phys.* **136**, 272-288 (1997).

[20] M. G. Crandall and P.-L Lions, Viscosity solutions of Hamilton-Jacobi equations, *Trans. Amer. Math. Soc.* **277** (1), 1-42 (1983).

[21] M. G. Crandall, L. C. Evans, and P.-L Lions, Some properties of viscosity solutions of Hamilton-Jacobi equations, *Trans. Amer. Math. Soc.* **282** (2), 487-502 (1984).

[22] R. Courant and K. O. Friedrichs, *Supersonic flow and shock waves,* Springer, New York, 1999.

[23] C. Crowe, M. Sommerfeld, and Y. Tsuji, *Multiphase flows with droplets and particles,* CRC Press, Boca Raton, 1998.

[24] C. Dafermos, The entropy rate admissibility criterion for solutions of hyperbolic conservation laws, *J. Diff. Eqs.* **14**, 202-212 (1973).

[25] C. Dafermos, *Hyperbolic conservation laws in continuum physics*, Springer, Berlin, 2000.

[26] G. Dal Maso, P. G. LeFloch, and F. Murat, Definition and weak stability of nonconservative products, *J. Math. Pures Appl.* **74**, 483-548 (1995).

[27] R. Donat and A. Marquina, Capturing shock reflections: An improved flux formula, *J. Comput. Phys.* **125**, 45-58 (1996).

[28] D. A. Drew and S. L. Passman, *Theory of multicomponent fluids*, Springer, New York, 1999.

[29] V. G. Dulov, Decay of an arbitrary initial discontinuity of the gas parameters across a jump-discontinuity in the cross-sectional area, *Vestnik Leningrad. Univ.* **19** (4), 76-99 (1958). (in Russian)

[30] B. Einfeldt, C. D. Munz, P. L. Roe, and B. Sjögreen, On Godunov-type methods near low densities, *J. Comput. Phys.* **92**, 273-295 (1991).

[31] P. Embid and M. Baer, Mathematical analysis of a two-phase continuum mixture theory, *Continuum Mech. Thermodyn.* **4**, 279-312 (1992).

[32] R. Fedkiw, B. Merriman, and S. Osher, Simplified discretization of systems of hyperbolic conservation laws containing advection equations, *J. Comput. Phys.* **157**, 302-326 (2000).

[33] T. Gallouët and J.-M. Masella, Un schéma de Godunov approché, *C. R. Acad. Sci. Paris Sér. I* **323**, 77-84 (1996).

[34] T. Gallouët, J.-M. Hérard and N. Seguin, Some recent finite volume schemes to compute Euler equations using real gas EOS, preprint 00-21 of the Centre de Mathématiques et d'Informatique, Université de Provence, 2000.

[35] T. Gallouët, J.-M. Hérard and N. Seguin, Some approximate Godunov schemes to compute shallow water equations with topography. On the use of symmetrizing variables to deal with vacuum, preprint 00-32 of the Centre de Mathématiques et d'Informatique, Université de Provence, 2000.

[36] T. Gallouët, Rough schemes for complex hyperbolic systems, in *Finite Volumes for Complex Applications*, F. Benkhaldoun and R. Vilsmeier (eds.), Hermes, Paris, 1996, 1-10.

[37] S. Gavrilyuk and R. Saurel, A compressible multiphase flow model with microinertia, *J. Comput. Phys.* **175**, 326-360 (2002).

[38] E. Godlewski and P.-A. Raviart, *Numerical approximation of hyperbolic systems of conservation laws,* Springer, New York, 1996.

[39] S. K. Godunov, A difference scheme for numerical computation of discontinuous solutions of equations of gas dynamics, *Math. Sb.* **47**, 271-306 (1959).

[40] A. Harten, High resolution schemes for hyperbolic conservation laws, *J. Comput. Phys.* **49**, 357-393 (1983).

[41] A. Harten and J. M. Hyman, Self-adjusting grid methods for one-dimensional hyperbolic conservation laws, *J. Comput. Phys.* **50**, 235-269 (1983).

[42] G. F. Hewittt (ed.) *International encyclopedia of heat and mass transfer,* CRC Press, Boca Raton, 1997.

[43] T. Y. Hou, P. Rosakis, and P. LeFloch, A level-set approach to the computation of twinning and phase-transition dynamics, *J. Comput. Phys.* **150**, 302-331 (1999).

[44] E. Isaacson and B. Temple, Nonlinear resonance in systems of conservation laws, *SIAM J. Appl. Math.* **52**, 1260-1278 (1992).

[45] E. Isaacson and B. Temple, Convergence of the 2×2 Godunov method for a general resonant nonlinear balance law, *SIAM J. Appl. Math.* **55**, 625-640 (1995).

[46] M. Ishii, *Thermo-fluid dynamic theory of two-phase flow,* Eyrolles, Paris, 1975.

[47] A. K. Kapila, S. F. Son, J. B. Bdzil, R. Menikoff, and D. S. Stewart, Two-phase modeling of DDT: structure of the velocity-relaxation zone, *Phys. Fluids* **9** (12), 3885-3897 (1997).

[48] A. K. Kapila, R. Menikoff, J. B. Bdzil, S. F. Son, and D. S. Stewart, Two-phase modeling of deflagration-to-detonation transition in granular materials: Reduced equations, *Phys. Fluids* **13** (10), 3002-3024 (2001).

[49] S. Karni and S. Čanić, Computations of slow moving shocks, *J. Comput. Phys.* **136**, 132-139 (1997).

[50] B. Keyfitz and H. C. Kranzer, A viscosity approximation to a system of hyperbolic conservation laws with no classical Riemann solution, in *Nonlinear hyperbolic problems*, Carasso *et al.* (eds.), Lecture notes in mathematics **1402**, 185-198 (1988).

[51] D. Kröner, *Numerical schemes for conservation laws*, John Wiley & Sons, Chichester, 1997.

[52] A. G. Kulikovskii, N. V. Pogorelov, and A. Yu. Semenov, *Mathematical aspects of numerical solution of hyperbolic systems,* CRC Press, Boca Raton, 2001.

[53] R. T. Lahey, L. Y. Cheng, D. A. Drew and J. E. Flaherty, The effect of virtual mass on the numerical stability of accelerating two-phase flows, *Int. J. Multiphase Flow,* **6**, 281-294 (1980).

[54] R. T. Lahey and D. A. Drew, *The three dimensional time and volume averaged conservation equations of two-phase flow*, Advances in Nuclear Science and Technology, vol. 20, 1-69, 1988.

[55] L. D. Landau and E. M. Lifschitz, *Fluid mechanics,* Pergamon Press, Oxford, 1987.

[56] M.-H. Lallemand and R. Saurel, Pressure relaxation procedures for multiphase compressible flows, *INRIA Rapport de recherche n^0 4038*, available at http://www.inria.fr/rrrt/rr-4038.html.

[57] P. D. Lax, Hyperbolic systems of conservation laws II, *Comm. Pure Appl. Math.* **10**, 537-566 (1957).

[58] P. LeFloch, *Hyperbolic Systems of Conservation Laws: The theory of classical and nonclassical shock waves*, Birkhäuser, Basel, 2002.

[59] R. J. LeVeque, *Numerical methods for conservation laws,* Birkhäuser Verlag, Basel, 1992.

[60] R. J. LeVeque, Wave propagation algorithms for multi-dimensional hyperbolic systems, *J. Comp. Phys.* **131**, 327-353 (1997).

[61] T.-P. Liu, Nonlinear stability and instability of transonic flows through a nozzle, *Commun. Math. Phys.* **83**, 243-260 (1982).

[62] T.-P. Liu, Nonlinear resonance for quasilinear hyperbolic equation, *J. Math. Phys.* **28**, 2593-2602 (1987).

[63] S. P. Marsh, *LASL shock Hugoniot data,* Univ. of California Press, Berkeley, 1980.

[64] J.-M. Masella, I. Faille, and T. Gallouët, On an approximate Godunov scheme, *Int. J. Comput. Fluid Dyn.* **12**, 2, 133-149 (1999).

[65] J. Massoni, R. Saurel, B. Nkonga and R. Abgrall, Proposition de méthodes et modèles Eulériens pour les problèmes à interfaces entre fluides compressibles en présence de transfert de chaleur, *Int. J. Heat Mass Transfer* **45**, 1287-1307 (2002).

[66] R. Menikoff and B. J. Plohr, The Riemann problem for fluid flow of real materials, *Rev. Mod. Phy.* **61** (1), 75-130 (1989).

[67] C.-D. Munz, A tracking method for gas flow into vacuum based on the vacuum Riemann problem *J. Math. Methods Appl. Sci.* **17**, 597-612 (1994).

[68] C.-D. Munz, On Godunov-type schemes for Lagrangian gas dynamics, *J. SIAM J. Numer. Anal.* **31**, 17-42 (1994).

[69] R. I. Nigmatulin, *Dynamics of multiphase media,* Hemisphere, New York, 1991.

[70] S. Osher and R. Fedkiw, Level set methods: An overview and some recent results, *J. Comput. Phys.* **169**, 463-502 (2001).

[71] V. H. Ransom, Numerical benchmark tests, in *Multiphase Science and Technology*, vol. 3, G. F. Hewitt, J. M. Delhaye, N. Zuber (eds). Hemisphere, Washington, 1987.

[72] T. Roberts, The behaviour of flux difference splitting schemes near slowly moving shock waves, *J. Comput. Phys.* **90**, 141-160 (1990).

[73] P. L. Roe, Approximate Riemann solvers, parameter vectors, and difference schemes, *J. Comput. Phys.* **43**, 357-372 (1981).

[74] S. Roller and C.-D. Munz, A low Mach number scheme based on multiscale asymptotics, *Comput. Vis. Sci.* **3**, 85-91, (2000).

[75] R. Saurel and R. Abgrall, A multiphase Godunov method for compressible multifluid and multiphase flows, *J. Comput. Phys.* **150**, 425-467 (1999).

[76] R. Saurel and O. LeMetayer, A multiphase model for compressible flows with interfaces, shocks, detonation waves and cavitation, *J. Fluid Mech.* **431**, 239-271 (2001).

[77] R. Scardovelli and S. Zaleski, Direct numerical simulation of free-surface and interfacial flow, *Annu. Rev. Mech.* **31**, 567-603 (1999).

[78] D. Serre, *Systems of conservation laws*, Cambridge Univ. Press, Cambridge, 1999.

[79] L. A. S. Shieh, R. Krishnamurty and V. H. Ransom, Stability, accuracy, and convergence of the numerical methods in RELAP5/MOD3, *Nucl. Sci. Eng.* **116**, 227 (1994).

[80] J. A. Sethian, *Level set methods,* Cambridge Univ. Press, Cambridge, 1996.

[81] J. Smoller, *Shock waves and reaction–diffusion equations,* Springer, New York, 1983.

[82] H. Städtke, G. Franchello and B. Worth, Numerical simulation of multi-dimensional two-phase flow based on flux vector splitting, *Nucl. Eng. and Des.* **177**, 199-213 (1997).

[83] H. B. Stewart and B. Wendroff, Two-phase flow: models and methods, *J. Comput. Phys.* **56**, 363-409 (1984).

[84] G. Strang, On the construction and comparison of difference schemes, *SIAM J. Num. Anal.* **5**, 506-517 (1968).

[85] E. Tadmor, Numerical viscosity and the entropy condition for conservative difference schemes, *Math. Comput.* **43**, 369-381 (1984).

[86] E. Tadmor, Numerical viscosity of entropy stable schemes for systems of conservation laws, *Math. Comput.* **49**, 91-103 (1987).

[87] K. Takayama and O. Inoue, Shock wave diffraction over a 90 degree sharp corner, *Shock Waves* **1**, 301-312 (1991).

[88] I. Tiselj and S. Petelin, Modeling of two-phase flow with second-order accurate scheme, *J. Comput. Phys.* **136**, 503-521 (1997).

[89] E. F. Toro, *Riemann solvers and numerical methods for fluid dynamics*, Springer, Berlin, 1999.

[90] E. F. Toro, M. Spruce, and W. Spears, Restoration of the contact surface in the HLL Riemann solver, *Shock Waves* **4**, 25-34 (1994).

[91] *TRAC PF-1, An advanced best estimate computer program for pressurized water reactor analysis,* Los Alamos National Laboratory report (1983).

[92] G. Tryggvason, B. Bunner, A. Esmaeeli, D. Juric, N. Al-Rawahi, W. Tauber, J. Han, S. Nas, and Y.-J. Jan, A front-tracking method for the computations of multiphase flow, *J. Comput. Phys.* **169**, 708-759 (2001).

[93] M. Van Dyke, *An album of fluid motion*, Parabolic Press, 1982.

[94] M. Vinokur, An analysis of finite-difference and finite-volume formulations of conservation laws, *J. Comput. Phys.* **81**, 1-52 (1989).

[95] P. Woodward and P. Colella, The numerical simulation of two-dimensional fluid with strong shocks, *J. Comput. Phys.* **54**, 115-173 (1984).

[96] I. K. Yaushev, Decay of an arbitrary discontinuity in a channel with a jump in the cross-sectional area, *Izv. Sibirsk. Akad. Nauk SSSR* **8** (2), 109-120 (1967). (in Russian)

[97] M. J. Zucrow, J. D. Hoffman, *Gas dynamics,* vol. 2, John Wiley & Sons, 1977.